

DISS. ETH N° 27325

MATHEMATICAL MODELS FOR ANALYSING
THE IMMUNE RESPONSE TO INFLUENZA VACCINATION
IN A PATIENT POPULATION

A dissertation submitted to attain the degree of
DOCTOR OF SCIENCES of ETH ZURICH
(Dr. sc. ETH Zurich)

presented by

JANINA ESTHER LINNIK

Dipl.-Biochem.
Free University of Berlin
born on 23 April 1990
citizen of Germany

accepted on the recommendation of

Prof. Dr. Jörg Stelling, examiner
Prof. Dr. Adrian Egli, co-examiner
Prof. Dr. Thomas Höfer, co-examiner
Prof. Dr. Marloes Maathuis, co-examiner

2021

Janina Esther Linnik

*Mathematical models for analysing the immune response
to influenza vaccination in a patient population*

© 2021

ABSTRACT

Influenza viruses cause respiratory infections and spread in yearly outbreaks worldwide, causing up to 650 thousand deaths every year. Vaccination can induce protective antibodies against influenza viruses and is the most successful strategy to prevent influenza infections. Unfortunately, influenza viruses rapidly evolve and escape immunity established in previous vaccinations. Frequent updates of the influenza vaccine formulation and continuous evaluation of vaccine efficacy in large populations are necessary. A detailed molecular characterization of vaccine responses is experimentally very difficult and often unfeasible in larger populations. Instead, the hemagglutination inhibition (HI) antibody titer is commonly used as an easily accessible measure for the potency of influenza vaccine responses.

In this thesis, we present three mathematical models for analysing HI titers and propose how they can be used in conjunction to characterize the vaccine response in a patient population based on easily accessible measurements and medical record information. Specifically, we apply the models to patients after hematopoietic stem cell transplantation (HSCT), a high-risk group eliciting heterogeneous vaccine responses that are not well understood.

We first identify patient factors associated with HI titers for three different influenza strains. We show that sequential regression models are superior to the commonly used binary regression on conventional cut-offs (seroconversion/seroprotection) for inferring associations between patient factors and HI titers. Both approaches have a similar interpretation and yield consistent results, but sequential regression models infer associations with higher precision.

Next, we present a biophysical model of the HI assay that establishes a quantitative relationship between antibody concentration, antibody avidity (binding strength) and HI titer. We apply the model to infer antibody avidities in HSCT patients from antibody concentrations and HI titers, and experimentally validate our predictions. The model predicts that influenza vaccination mostly induced an increase in antibody concentration but not in avidity. Because the model links antibody concentrations and avidities to HI titers, it enables to connect mathematical models of the immune response to HI titers assessed in vaccine studies.

Finally, we integrate the identified most important patient factors into a dynamic model of the vaccine response in HSCT patients and combine it with the biophysical measurement model of the HI assay to infer patient-specific differences in immune response mechanisms. Specifically, we infer differences in memory B cells and germinal center (GC) processes that are potentially modulated by the investigated patient factors. The model predicts that vaccination induced antibody production by both plasma B cells from GCs and reactivated memory B cells. The heterogeneity in HI titer responses was well described by memory B cells and only a few patient factors that potentially affect the GC response (lymphocyte count and IFN- λ genotype). The study demonstrates how dynamic modelling of the immune response can be combined with clinical patient information and statistical inference to characterize the vaccine response based on HI titers.

ZUSAMMENFASSUNG

Influenzaviren verursachen Atemwegsinfektionen und verbreiten sich in jährlichen Ausbrüchen mit weltweit bis zu 650 Tausend Todesfällen pro Jahr. Eine Impfung kann schützende Antikörper gegen Influenzaviren induzieren und ist die wirksamste Methode Influenzainfektionen zu verhindern. Leider verändern sich Influenzaviren sehr schnell und entziehen so sich der Immunität, die in bisherigen Impfungen etabliert wurde. Daher müssen Influenza-Impfstoffe häufig angepasst und der Impfschutz durch regelmäßiges Impfen aufrecht erhalten werden. Um die Effektivität von Influenza-Impfstoffen zu überwachen, müssen die Impfstoffe kontinuierlich evaluiert und in klinischen Studien bewertet werden. Die molekulare Charakterisierung der Impfstoffreaktionen experimentell sehr aufwändig und daher in Studien mit größeren Fallzahlen oft nicht durchführbar. Stattdessen wird häufig der Anti-Hämagglutinin (HA) Antikörper-Titer Test zur Evaluierung von Influenza-Impfstoffen verwendet.

In dieser Arbeit stellen wir drei mathematische Modelle zur Analyse von HA Antikörper-Titern vor und zeigen wie sie zur Charakterisierung der Impfantwort auf Grundlage von Daten aus Krankenakten und einfachen Experimenten in Studien mit großen Fallzahlen verwendet werden können. Wir wenden unsere Modelle auf die Impfantwort von Patienten nach einer Stammzelltransplantation (SZT) an — eine Risikogruppe die eine heterogene und noch schlecht verstandene Impfantwort zeigt.

Zuerst identifizieren wir die wichtigsten Patientenfaktoren die mit HA-Titern für drei verschiedene Influenzastämme zusammenhängen. Wir zeigen, dass sich mit sequentiellen Regressionsmodellen Assoziationen besser inferieren lassen als mit der üblicherweise verwendeten binären Regression von traditionellen Schwellenwerten (Serokonversion/Seroprotektion). Beide Regressionsmodelle können ähnlich interpretiert werden, aber sequentiellen Modelle inferieren Assoziationen mit höherer Präzision.

Als nächstes behandeln wir ein biophysikalisches Modell des HA-Antikörper-Titer Tests, das die Abhängigkeit von HA-Titer zu Antikörperkonzentration und Antikörper-Avidität (Bindungsstärke) zeigt. Wir wenden das Modell auf Antikörperkonzentrationen und HA-Titer der SZT-Patienten an um Aviditäten zu inferieren und validieren die Vorhersagen experimentell. Das Modell zeigt, dass die Grippeimpfung in den meisten SZT-Patienten nur einen Anstieg in der Antikörperkonzentration, aber nicht in der Avidität induzierte. Da das Modell die Abhängigkeit des HA-Titers von Antikörperkonzentration und Aviditäten beschreibt, ermöglicht es mathematische Modelle der Immunantwort mit HA-Titern aus Impfstudien zu verbinden.

Schließlich integrieren wir die wichtigsten Patientenfaktoren in ein dynamisches Modell der Impfantwort in SZT-Patienten, um Unterschiede in der Immunantwort zu untersuchen. Wir inferieren aus den beobachteten HA-Titern die Anzahl der aktivierten B-Gedächtniszellen und Unterschiede in Keimzentrumsprozessen, welche potentiell durch die untersuchten Patientenfaktoren verursacht werden. Das Modell sagt voraus, dass sowohl Plasmazellen aus der Keimzentrumsreaktion als auch B-Gedächtniszellen durch die Impfung aktiviert werden und zur Antikörperantwort beitragen.

Die Heterogenität der HA-Titer-Antworten wird durch Unterschiede in B-Gedächtniszellen und durch einige wenige Patientenfaktoren, die die Keimzentrumsreaktion möglicherweise beeinflussen (Anzahl der Lymphozyten und IFN- λ -Genotyp), gut beschrieben. Diese Studie zeigt, wie ein dynamisches Modell der Immunantwort mit Patientendaten und statistischer Inferenz kombiniert werden kann, um die Impfantwort basierend auf HA-Titern zu charakterisieren.

ACKNOWLEDGEMENTS

I would like to thank Jörg Stelling for giving me the opportunity to work on this thesis and to follow my interests, for supporting me whenever I asked for help, for his encouragement and enthusiasm, and for his creativity in solving problems. Thank you, Jörg, for all the support throughout the years, all the valuable guidance and scientific freedom.

I would like to thank Adrian Egli for his essential support in realizing the projects presented in this thesis and for always having an open ear for problems. Thank you, Adrian, for engaging in the adventure of this interdisciplinary PhD project — having me as one of the first PhD students circulating between the D-BSSE and the Department of Biomedicine, thank you for introducing me to immunology and for giving me the chance to learn so much over the last years.

I thank my closest collaborator Yaseen Syedbasha for his great work, his tremendous help and kindness, and for teaching me all the Tips and Tricks in the lab — together, we went through ups and downs that are so characteristic to the research process — it was great fun to work together, to discuss results that faced us sometimes as mysterious puzzles, to design new experiments, shape projects, and support each other.

I would like to thank Michael Kaltenbach for introducing me to categorical regression, his encouragement and mentorship throughout the years, his immense help in understanding problems and shaping projects, his ability to shed light on difficult aspects, and countless discussions that were of great importance to this thesis.

I thank Claudia Stühler for always having an open ear for immunological questions and for helping me to orient through the wealth of immunological literature. I thank Fabian Rudolf for asking the right questions, his encouragement, and for helping me with establishing the avidity measurements. I thank Lukas Kaufmann and Dominik Vogt for their great work with managing and measuring patient samples, which were of such importance for this thesis. I would like to thank Debora Marks for inviting me to visit her lab and for many valuable discussions, and I thank her and Chris Sander for their warm hospitality and the inspiring time I had during my visit.

I thank the past and current members of the Computational Systems Biology group for all the discussions, emotional support, great work environment and friendships. I also thank the past and current members of the Applied Microbiology Research group for always being extremely welcoming, supportive and also for providing a great work environment.

Finally, I would like to thank my high school teacher Hermann Henne, who enabled me to visit a summer school on *Simulations as the Third Pillar of Science*, which sparked my fascination for modelling living systems and greatly influenced my path. I would like to acknowledge the support of the German Academic Scholarship Foundation during my undergraduate studies, which enabled me to study at three different universities and to follow my interests. And I would like to thank SystemsX for supporting interdisciplinary research and organizing wonderful retreats for PhD students.

CONTENTS

1	INTRODUCTION	1
1.1	The influenza virus	2
1.2	The immune response to influenza vaccination	3
1.2.1	The adaptive immune response	3
1.2.2	Vaccination aims at inducing high levels of neutralizing antibodies	4
1.2.3	Evaluation of antibody responses to influenza vaccination	4
1.2.4	Analysis of hemagglutination inhibition (HI) titers	5
1.2.5	The vaccine response is orchestrated by various cell types	6
1.2.6	What factors influence the vaccine response?	7
1.3	Mathematical models help to decipher immune responses	10
1.4	Contributions of this thesis	11
2	ASSOCIATION OF HOST FACTORS WITH ANTIBODY RESPONSE TO INFLUENZA VACCINATION IN HSCT PATIENTS	13
2.1	Summary	13
2.2	Abstract	13
2.3	Introduction	14
2.4	Methods	16
2.4.1	Ethics and regulatory requirements	16
2.4.2	Study design, participants and data collection	16
2.4.3	Vaccine composition	17
2.4.4	Genotyping	17
2.4.5	Hemagglutination inhibition assay	18
2.4.6	Data analysis	18
2.5	Results and Discussion	21
2.5.1	Patient characteristics	21
2.5.2	HSCT patients show high variability in antibody titers	23
2.5.3	HSCT patients benefited from booster shot	25
2.5.4	Cross-reactivity between influenza strains	25
2.5.5	Regression analysis of HI titers yields higher precision in estimated effects	26
2.5.6	Association of host factors with vaccine response and baseline titers in HSCT patients	28
2.5.7	Patients with local side effects show stronger vaccine response	34
2.6	Conclusion	34
2.7	Supplementary Tables	36
2.8	Supplementary Figures	39
2.9	Supplementary Methods	49
2.9.1	Sequential models for regression of influenza antibody titers	49

3	MODEL-BASED INFERENCE OF NEUTRALIZING ANTIBODY AVIDITIES AGAINST INFLUENZA VIRUS	53
3.1	Introduction	53
3.2	Results	54
3.2.1	Model of the hemagglutination inhibition (HI) assay	54
3.2.2	The model quantitatively relates IgG concentration and avidity to HI titer	58
3.2.3	Inference of neutralizing antibody avidities in HSCT patients	59
3.2.4	Inferred avidities correlate with experimentally determined avidities	60
3.2.5	Detection of vaccine-induced affinity maturation in HSCT patients	62
3.2.6	Association with criteria for compromised immune response	62
3.3	Discussion	64
3.4	Methods	66
3.4.1	Ethics statement	66
3.4.2	Patient sera	66
3.4.3	Vaccine composition	68
3.4.4	HI assay	68
3.4.5	ELISA for influenza-specific IgG detection	68
3.4.6	Urea elution assay to measure IgG avidities	68
3.4.7	Reference serum	69
3.4.8	Model derivation	69
3.4.9	Model implementation	72
3.4.10	Model parameters and initial conditions	72
3.4.11	Inference of neutralizing antibody avidities	74
3.4.12	Identification of patients with increase in avidity and increase in non-neutralizing IgG	75
3.4.13	Sensitivity analysis	76
3.4.14	Statistical analysis	76
3.4.15	Data and software availability	77
3.4.16	Conflict of interests	77
3.4.17	Author contributions	77
3.4.18	Acknowledgments	78
3.5	Supplementary Figures	79
4	INFERRING DIFFERENCES IN IMMUNE RESPONSE DYNAMICS FROM INFLUENZA VACCINE-INDUCED ANTIBODY TITERS IN IMMUNOCOMPROMISED PATIENTS	85
4.1	Abstract	85
4.2	Introduction	85
4.3	Results	87
4.3.1	Vaccine response model	87
4.3.2	Sensitivity to GC reaction parameters	89
4.3.3	Mapping of patient factors to GC reaction parameters	92
4.3.4	Estimation and quality of fit	95

4.3.5	Differences in vaccine responses can be explained by differences in GC reaction processes and differences in preexisting memory B cells	97
4.4	Discussion	100
4.5	Methods	102
4.5.1	Vaccine response model	102
4.5.2	Sobol sensitivity analysis	105
4.5.3	Patient data	106
4.5.4	Linking IgG antibody concentrations to HI antibody titers	106
4.5.5	Inference	107
4.5.6	Data and code availability	110
4.6	Author contributions	110
4.7	Acknowledgments	110
4.8	Supplementary Tables	111
4.9	Supplementary Figures	113
5	CONCLUDING REMARKS AND OUTLOOK	117
5.1	Sequential models for titer regression	117
5.2	A mechanistic model for HI assays	118
5.3	Towards a better understanding of immune response dynamics in patient populations	118
5.4	New correlates of protection	119
	BIBLIOGRAPHY	123

ABBREVIATIONS

AG antigen

APC antigen-presenting cell

BAFF B-cell activating factor

BIC Bayesian information criterion

CI confidence interval

DC dendritic cell

ELISA enzyme-linked immunosorbent assay

FDC follicular dendritic cell

GC germinal center

GVHD graft-versus-host disease

HA hemagglutinin

HI hemagglutination inhibition

HLA human leukocyte antigen

HSCT hematopoietic stem cell transplantation

IFN interferon

IL interleukin

IQR interquartile range

LF lymphoid follicle

MHC major histocompatibility complex

NA neuraminidase

ODE ordinary differential equation

OR odds ratio

RBC red blood cell

SHM somatic hypermutation

SNP single nucleotide polymorphism

TIV trivalent influenza vaccine

INTRODUCTION

Parts of this chapter are published in: J. E. Linnik and A. Egli. Impact of host genetic polymorphisms on vaccine induced antibody response. *Human Vaccines & Immunotherapeutics*, 12(4):907–915, 2016. <https://doi.org/10.1080/21645515.2015.1119345>.

It is not possible to step twice into the same river according to Heraclitus, or to come into contact twice with a mortal being in the same state.

— Plutarch

When the pre-Socratic philosopher Heraclitus meditated on his famous *panta rhei* (everything flows) principle, he probably not have thought about the adaptive immune system and might not have expected that, more than two millennia later, his idea speaks to scientists concerned with the ever-changing state of mortal beings and their environment. We are surrounded by microorganisms that evolve on a shorter time scale than our own evolution. Exposure to new pathogens, such as viruses, bacteria, fungi and parasites, can cause diseases. Nevertheless, our body is able to adapt to new pathogens and protect us from illness thanks to the adaptive immune system. The adaptive immunity can be interpreted as a fast Darwinian process within our body that quickly reacts to new pathogens and gives rise to highly adapted immune cells and antibodies necessary to fight pathogenic invaders, clear infections and keep us healthy and safe (Victora and Nussenzweig, 2012). In contrast to the *innate* immune response, which is unspecific and provides the first line of defence against pathogens, the *adaptive* immune response can result in immunological memory, a phenomenon describing life-long protection against reinfection with the same pathogen (Murphy and Weaver, 2016).

Already Heraclitus' contemporaries documented that people who survived a disease, such as smallpox, were immune to subsequent infections (Fenner et al., 1988). In Europe, the first attempts to immunize individuals were described in the 18th century, more than one century before Robert Koch proved that microorganisms cause infectious diseases. Children and adults were intentionally exposed to cowpox to immunize them against the often deadly smallpox (Gross and Sepkowitz, 1998; Riedel, 2005). In 1796, Edward Jenner reported that the inoculation with cowpox could protect against smallpox and called this procedure *vaccination* (Jenner, 1800). As of today, we use this term to describe the immunization with attenuated disease-causing agents to protect from diseases, which – without previous immunization – could overwhelm our organism and lead to severe illness or even death. In the last century, vaccines have become the primary preventive strategy against many infectious diseases and have saved millions of lives (Andre et al., 2008).

One of the most notorious pathogens that frequently challenges our immunity and our public health systems is the influenza virus. Influenza viruses cause respiratory infections and spread in yearly outbreaks worldwide, causing around 1 billion infections, 3–5 million cases of severe illness, and 300–650 thousand deaths every year (Krammer et al., 2018; Paget et al., 2019). The

influenza vaccine formulation has to be updated annually to ensure a match with circulating influenza strains. Continuous evaluation and assessment of vaccination efficacy in large populations is crucial to monitor vaccination success and guide vaccine development (Paules and Fauci, 2019). Unfortunately, individuals at high risk for developing influenza-related complications show lower vaccine response rates (Paules and Subbarao, 2017), such as very young children and the elderly (Siegrist and Aspinall, 2009), pregnant women (Faucette et al., 2015), as well as patients with chronic diseases and comorbidities, e.g., diabetes (Association et al., 2004), autoimmune diseases (Gelinck et al., 2007; van Assen et al., 2010), or patients after transplantation (Kunisaki and Janoff, 2009; Manuel et al., 2011; Ljungman, 2012). A better understanding of the influenza vaccine response, especially in heterogeneous high-risk populations, will help to improve current vaccination strategies and to develop novel types of vaccines (Germain, 2010; Hagan et al., 2015; Wooden and Koff, 2018).

This thesis presents three mathematical models and their application to analyse influenza vaccine-induced immune responses in a population of immunocompromised patients after blood (hematopoietic) stem cell transplantation — a high-risk group showing highly heterogeneous and poorly understood vaccine responses (Ljungman and Avetisyan, 2008). In the following sections, we briefly introduce the relevant background on influenza viruses and the immune response to influenza vaccination, followed by an overview of available methods for analysing vaccine responses and their limitations. Finally, we conclude with the goals and contributions of this thesis.

1.1 THE INFLUENZA VIRUS

Influenza in humans is caused by influenza A and B viruses that occur globally as seasonal epidemics (caused by influenza A and B), as well as sporadically as pandemics (caused by influenza A) (Krammer et al., 2018). Influenza A viruses are classified into subtypes based on their surface proteins, hemagglutinin (HA) and neuraminidase (NA). In total, 18 HA and eleven NA subtypes of influenza A viruses have been identified in birds or bats — most of them in wild birds, which are the primary reservoir of influenza A viruses (Tong et al., 2013). A similar animal reservoir has not been found for influenza B viruses; these are classified into two antigenically distinct lineages based on their HA protein, the Victoria and the Yamagata lineage (Paules and Subbarao, 2017).

Influenza viruses gradually accumulate mutations in their HA and NA proteins, a process called *antigenic drift* (Bouvier and Palese, 2008). This antigenic drift makes it necessary to update the influenza vaccine frequently (Boni, 2008). Importantly, substantial antigenic drift can be introduced by very few or even a single amino acid substitution in the globular head domain of HA (Koel et al., 2013). The globular head domain is the part of the HA receptor that binds to sialic acids on surface glycoproteins of mammalian cells and mediates virus entry (Skehel and Wiley, 2000). In addition to antigenic drift, there is also *antigenic shift* in influenza A viruses; this describes a drastic change in HA proteins (sometimes also in NA) caused by an exchange of viral RNA segments during a co-infection with antigenically diverse strains.

In the last century, four influenza pandemics have occurred: in 1918 (caused by H1N1), 1957 (H3N2), 1968 (H3N2), and 2009 (H1N1). The pandemic H1N1 strain in 2009 differed substantially from the circulating seasonal H1N1 strains and caused their extinction (Krammer et al., 2018).

Since 2009, the strains derived from the 2009 H1N1 pandemic strain co-circulate with influenza A H3N2 and influenza B strains. Due to the small number of documented influenza pandemics, we are currently not able to predict the next pandemic influenza strain (Neumann and Kawaoka, 2019).

1.2 THE IMMUNE RESPONSE TO INFLUENZA VACCINATION

Vaccination is the most successful method to prevent influenza infections (Houser and Subbarao, 2015). There are currently three types of licensed influenza vaccines: inactivated and live attenuated virus vaccines (mostly manufactured in embryonated chicken eggs) and recombinant hemagglutinin vaccines (Grohskopf et al., 2014). The current seasonal influenza vaccines include antigens from both circulating influenza A subtypes (pandemic H1N1 and seasonal H3N2) along with either one (trivalent vaccine) or both (quadrivalent vaccine) influenza B lineages. Vaccines are evaluated in randomized controlled trials (to determine *efficacy*) and in observational studies involving vaccinated and unvaccinated individuals (to determine *effectiveness*). If the vaccine matches the circulating strains well, meta-analyses show that efficacy rates of 50–60% and effectiveness rates of 60–90% can be achieved (Osterholm et al., 2012). Unfortunately, influenza vaccine effectiveness is often lower (Paules and Fauci, 2019): between 2004 – 2018, the influenza vaccine effectiveness against medically attended laboratory-confirmed illness in the United States ranged from 10–60%. In comparison, the measles vaccine has an effectiveness of 97%. In this respect, more effective influenza vaccination strategies are needed, especially in high-risk groups that show reduced vaccine effectiveness also when vaccine and circulating strains match well (Paules and Subbarao, 2017).

1.2.1 The adaptive immune response

We distinguish two types of adaptive immune responses, the humoral and the cell-mediated response (Murphy and Weaver, 2016). The humoral immune response describes the production of antibodies that are released into the fluid component of blood or plasma (serum) and extracellular fluids (once called *humors*). Human antibodies are glycoproteins, called *immunoglobulins* (Ig), released by B lymphocytes and occur as IgA, IgD, IgE, and IgG isotypes. IgG antibodies constitute approximately 75% of all antibodies in serum and have a major role in the immunity against influenza, along with IgA (15% of serum antibodies) and IgM (10%) (Schroeder and Cavacini, 2010; Krammer et al., 2018). The cell-mediated response is orchestrated by T lymphocytes. Cytotoxic T cells (CD8 T cells) control infections by destroying infected cells, while effector (helper) T cells (CD4 T cells) are essential regulators of B cells. Supported by T cell help, B cells can differentiate to antibody-secreting plasma cells or memory B cells, which do not secrete antibodies but can be reactivated upon a second exposure to the same antigen. Activated memory B cells quickly differentiate to plasma cells, inducing a faster and stronger antibody response compared to a naive response (Siegrist, 2008; Akkaya et al., 2020).

1.2.2 Vaccination aims at inducing high levels of neutralizing antibodies

Currently licensed influenza vaccines aim at inducing potent antibody responses against the influenza HA surface protein, which mediates viral entry (**Figure 1.1**). Antibodies that can bind the globular head domain of HA have been early identified (and later confirmed) as important correlates of protection against influenza (Smith et al., 1933; Ohmit et al., 2011; Benoit et al., 2015). Because these antibodies block the interaction between the virus and host cells, either through steric hindrance or direct blocking of the receptor binding site, they can also inhibit binding of influenza viruses to red blood cells (RBCs) *in vitro*, described as hemagglutination inhibition (HI), and can neutralize viruses in cell cultures. The lack of such neutralizing antibodies in a population is considered the main driving factor for the rapid spread of a virus in a pandemic (Krammer, 2019).

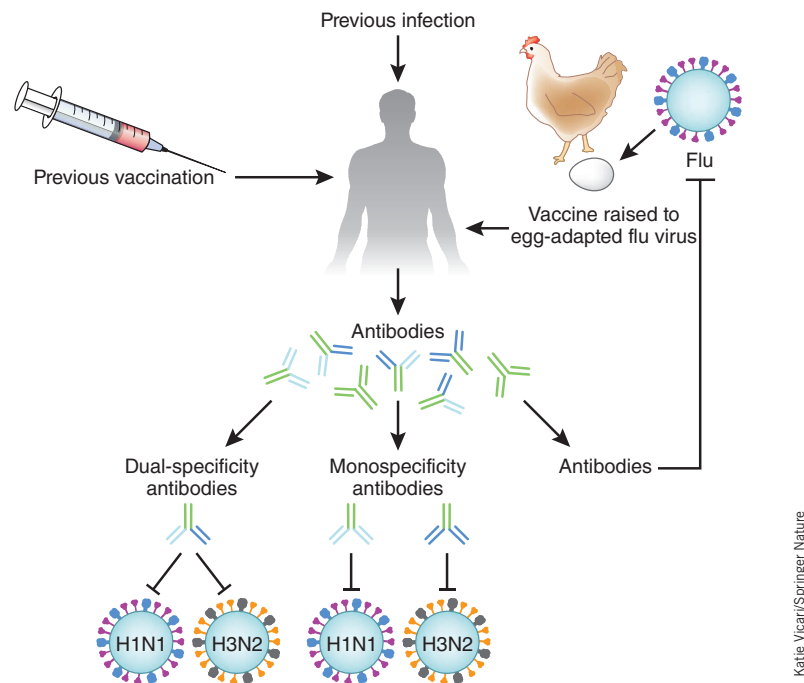


Figure 1.1. Influenza vaccination induces antibodies against viral surface proteins. The antibody response depends on preexisting memory B cells acquired in previous vaccinations or infections. Influenza vaccine-induced antibodies mostly target the surface protein hemagglutinin (HA) and can be specific to a single influenza strain or to multiple strains (cross-reactivity) (Lee et al., 2016; Angeletti et al., 2017). Image reprinted from Webby (2016) with permission by *Springer Nature*.

1.2.3 Evaluation of antibody responses to influenza vaccination

Two important parameters determine the potency of an antibody response: the antibody *concentration* and the antibody *avidity* (Groth, 1963). Avidity describes the overall binding strength of all

antibody binding sites to an antigen (here the viral surface protein HA) — in contrast to *affinity* that describes the binding strength of one antibody binding site (monovalent vs. multivalent binding). For instance, IgG antibodies have two binding sites, IgAs have four, and IgMs have ten. Thus, it is not sufficient to only measure antibody concentration, as the detected antibodies could potentially have low avidity and poor virus-neutralizing activity. While concentrations are relatively easy to measure, e.g., in enzyme-linked immunosorbent assay (ELISA) experiments, the determination of avidities is experimentally delicate. Avidity measurements require either highly sensitive, expensive equipment that requires long calibration times, such as surface plasmon resonance (SPR) systems, or ELISA-based experiments with chaotropic agents, such as urea, that are time-consuming and difficult to establish because the optimal protocol can vary substantially for different antigens and serums samples (Underwood, 1993; Olsson et al., 2019).

To evaluate the influenza-specific antibody response in larger populations, the hemagglutination inhibition (HI) assay has established itself because it allows quantifying the neutralizing activity of a serum sample relatively fast and easy as an *HI titer* (Hirst, 1941; Kaufmann et al., 2017). To determine the HI titer, a serum sample with an unknown antibody concentration is serially diluted, and a constant amount of influenza virus and RBCs is added to each dilution. The dilution factor of the last serum dilution that is still able to fully inhibit hemagglutination is, by definition, the HI titer (WHO, 2002). Thus, the HI titer is a coarse-grained measure of influenza-inhibiting antibodies in a serum sample, whose values are restricted to the considered serum dilutions. Importantly, the HI titer has been established as a correlate of protection in individuals, and regulatory agencies widely accept HI titers as a readout in vaccine efficacy trials (Hobson et al., 1972; Haaheim and Katz, 2011; Ohmit et al., 2011; Couch et al., 2013). However, since the HI titer measures the combination of both antibody concentration and avidity, an increase in antibody concentration can not be distinguished from an increase in antibody avidity (and the other way around). The relationship between HI titer, serum antibody concentration, and avidity has not yet been established. To fill this gap, we present in Chapter 3 (Linnik et al., 2020) a biophysical model of the HI assay that disentangles the contribution of IgG concentration and IgG avidity to the HI titer and allows to infer the difficult-to-measure IgG avidities from easy-to-measure IgG concentrations and HI titers.

1.2.4 Analysis of hemagglutination inhibition (HI) titers

HI titers are traditionally evaluated based on conventional cut-offs (Hobson et al., 1972; Beyer et al., 2004): individuals showing at least a four-fold increase in HI titer are considered to be *seroconverted*, meaning they responded to the vaccination. HI titers greater or equal to 1:40 are considered to be *seroprotective*, which means they are assumed to reduce the risk of infection by 50%. However, this dichotomous surrogate endpoint has only been tested in a limited number of individuals with a limited number of influenza strains and is probably not generally applicable (Cagigi et al., 2016). Moreover, when the research question at hand is to compare vaccination outcomes between different groups, the dichotomization into seroconverted/seroprotected individuals is a loss of information that can lead to undetected effects, especially when the sample size is small (Scott et al., 1997; Capuano et al., 2007). It has been demonstrated that *ordinal* regression on the full range of observed HI titers has superior power compared to dichotomization approaches (Capuano et al., 2007).

Ordinal regression models take into account that the analysed HI titers have an intrinsic order (McCullagh, 1980, 2018), but neglect that titers can only be reached successively step-by-step in a *sequential* process (Cox, 1988; Tutz, 1991). As of today, most studies utilize the conventional cut-offs to analyse HI titers, either by binary logistic regression or contingency table analysis (Beyer et al., 2004). Only a few influenza vaccine studies apply ordinal regression models (e.g., Hung et al. (2010)), and the application of sequential regression models (Tutz, 1991) for analysing HI titers has not yet been reported. In Chapter 2, we apply sequential models to investigate associations between patient characteristics and HI titers and show that sequential logistic regression on HI titers and binary logistic regression on seroconversion/seroprotection categories yield qualitatively similar results, but sequential models infer associations with higher precision.

1.2.5 *The vaccine response is orchestrated by various cell types*

Although vaccine trials mostly consider HI titers to evaluate vaccine responses, the vaccine-induced immune response is far more complex and involves various types of specialized immune cells and signalling molecules (Plotkin et al., 2012). The injected vaccine antigen is recognized by dendritic cells (DCs) through pattern-recognition receptors, in particular Toll-like receptors (TLRs) (Kawai and Akira, 2010). Activated TLRs initiate the expression of inflammatory genes, leading to the production of additional cell surface receptors and release of signalling molecules, such as cytokines and chemokines (Honda and Taniguchi, 2006). Activated DCs mature to antigen-presenting cells (APCs) and migrate to lymph nodes, where they present vaccine epitopes to T cells through human leukocyte antigen (HLA) molecules on their cell surface (Chen and Flies, 2013). This, in turn, initiates the maturation of naive CD4 T cells to effector T cells. Helper T cells of type 1 mainly support the cytotoxic immune response and secrete cytokines such as interleukin (IL)-2, interferon (IFN)- γ , while helper T cells of type 2 secrete different cytokines, such as IL-4, IL-6, and IL-10, and support B cell activation (Randolph et al., 1999). Follicular helper T cells are located in the follicle of lymph nodes and directly control B cell differentiation (Bentebibel et al., 2013; Spensieri et al., 2013; Gavillet et al., 2015).

B cells are the main workhorses of the adaptive immune system. Naive and memory B cells are activated if they recognize the vaccine antigen either in soluble form or on the surface of APCs with their B cell receptor (Pape et al., 2007). Activated B cells internalize the antigen and present antigen epitopes on their cell surface to cognate helper T cells to receive additional activation signals (Katikaneni and Jin, 2019). This B-T cell interaction is mediated by major histocompatibility complex (MHC) II molecules displayed on B cells. A fraction of activated naive B cells rapidly differentiate into short-lived plasmablasts, which produce IgM antibodies and later IgG or IgA after Ig isotype *class switching*. Plasmablasts produce the first wave of antibodies, but these antibodies are not yet perfectly adapted to the antigen. Another fraction of activated B cells migrate to follicles in the secondary lymphoid tissue to undergo a *germinal center* (GC) reaction (**Figure 1.2**). In the *dark zone* of GCs, B cells rapidly proliferate and diversify by acquiring mutations in their B cell receptor, which recognizes the same antigen as the later released antibodies. This process is called *somatic hypermutation* (SHM) and is coordinated by the enzyme activation-induced cytidine deaminase (AID). During SHM, mutation rates are about 10^6 -fold higher than the background

mutation rate in other genes, enabling a tremendous antibody diversity (Martin and Scharff, 2002). Subsequently, B cells compete for antigen presented on follicular DCs (FDCs) and move to the *light zone* of the GC for interaction with follicular helper T cells. Only B cells that acquire antigen from FDCs and successfully present it to follicular helper T cells survive the GC reaction (Heesters et al., 2014; Mesin et al., 2016). This survival of the "fittest" B cells results in the expansion of B cells with highly adapted B cell receptors. Moreover, B cells can *recycle* to the dark zone to undergo several rounds of proliferation and selection, resulting in a successive increase in the binding avidity of the B cell receptor, a process called *affinity maturation*. Eventually, selected B cells class-switch, exit the GC reaction and bifurcate into memory B cells and plasma cells that secrete high-avidity IgG antibodies. Importantly, plasma cells can migrate to the bone marrow, where they can survive for several months or even years, maintaining high levels of protective antibodies in serum. Memory B cells remain in the periphery for surveillance, and once reactivated, they rapidly proliferate and differentiate to plasma cells (Lau et al., 2017; Moran et al., 2018). In addition, activated memory B cells can also re-enter GCs, and it is thought that less somatically mutated memory B cells are more likely to re-engage in a GC reaction to undergo additional rounds of mutation and selection (Dogan et al., 2009; Pape et al., 2011; Zuccarino-Catania et al., 2014; Mesin et al., 2020; Turner et al., 2020).

The GC reaction depends on the antigen and on its environment and is by far not fully understood (Turner et al., 2018). Because of its outstanding importance to adaptive immunity, the GC reaction is intensely investigated. Sequencing and *in vivo* imaging techniques, in conjunction with mathematical models of GC dynamics, greatly advanced our understanding of GC processes in recent years, especially of GC formation, B cell diversity, T-cell dependent selection, recycling, and affinity maturation (Schwickert et al., 2007; Victora et al., 2010; Schwickert et al., 2011; Zhang et al., 2013; Meyer-Hermann et al., 2012; Wang et al., 2015; Tas et al., 2016; Kuraoka et al., 2016; Papa et al., 2017; Firl et al., 2018; Murugan et al., 2018; Pikor et al., 2020). A recent experimental study detected influenza-specific GC B cells after influenza vaccination in the draining lymph nodes of healthy adults (n = 8 investigated individuals) and provided the first direct evidence that influenza vaccination can trigger GCs in humans (Turner et al., 2020). However, little is known about the dynamics of influenza vaccine-induced GCs and how GC processes vary in a population (Kuraoka et al., 2016; Kil et al., 2019). In Chapter 4, we apply our current understanding of GC dynamics and adaptive immunity to model the antibody response to influenza vaccination in a patient population.

1.2.6 What factors influence the vaccine response?

First of all, the vaccine response is highly influenced by previous influenza infections or vaccinations. Especially the first immune responses to an antigen is thought to influence subsequent responses, a phenomenon described as *original antigen sin* or *imprinting* (Francis, 1960; Fonville et al., 2014; Gostic et al., 2016). Antibody titers against influenza strains encountered in early life increase over time, probably due to (at least partial) recall immune responses (Li et al., 2013; Krammer, 2019). Repeated vaccination against influenza viruses can lead to reduced vaccine effectiveness, especially when high basal antibody levels prevent broadly protective B cell responses (Andrews et al., 2015; Thompson et al., 2016). However, vaccine effectiveness is still better in repeatedly vaccinated

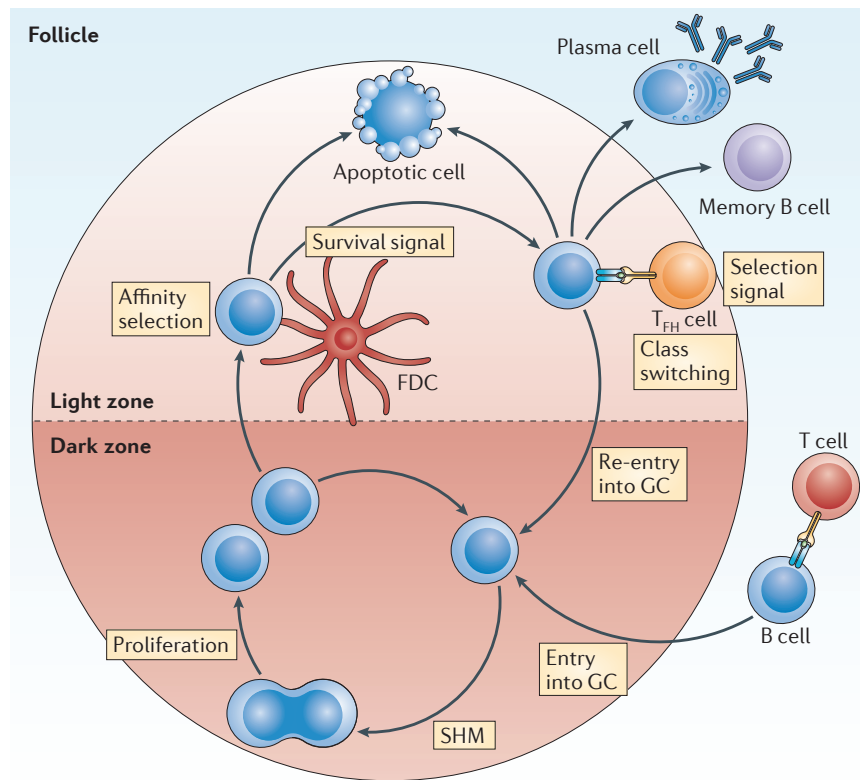


Figure 1.2. B cells evolve in germinal centers. Activated B cells that present antigen to helper T cells can enter germinal centers (GCs) where they rapidly proliferate and diversify their B cell receptor through somatic hypermutation (SHM). After several rounds of proliferation, they compete for antigen displayed on follicular dendritic cells (FDCs) and for T cell help. Only B cells that are able to present antigen to follicular helper T cells survive the GC reaction. Selected B cells bifurcate into antibody-secreting plasma cells and memory B cells or re-enter the GC reaction for additional rounds of proliferation and selection. Image reprinted from Heesters et al. (2014) with permission by *Springer Nature*.

individuals than in individuals not vaccinated at all (Khurana et al., 2019; Martínez-Baz et al., 2017). The immune response to repeated vaccinations is highly heterogeneous, and mechanisms and magnitude of recall responses as well as their impact on antibody production and affinity maturation are still poorly understood (Belongia et al., 2017). Since influenza viruses circulate regularly, and most of us encounter them already in childhood, recall responses are most likely always involved in influenza vaccine responses. The ultimate goal of influenza vaccination would be to induce a broad, highly diverse immune response and not only boosting preexisting immunity. Therefore, we have to better understand the non-naïve immune response, especially in high-risk groups, which are recommended to receive influenza vaccinations regularly (Lewnard and Cobey, 2018).

Second, the vaccine response depends on the antigen, type of vaccine and vaccine administration. Natural influenza infection usually induces longer-lived immunity and more diverse antibodies than influenza vaccination, but the mechanisms behind durable immunity remain unclear (Chiu et al., 2014; Krammer et al., 2018). The current understanding of B cell dynamics and the interaction of the various B cell subsets with DCs and T cells is still rudimentary and does not

allow to rationally influence B cell fate during vaccination (Krammer, 2019). To better understand the generation of durable immunity and guide vaccine development, additional correlates for protection, e. g., affinity maturation and antigen-specific memory B cells, need to be investigated and integrated into vaccine assessment (Cagigi et al., 2016; Wooden and Koff, 2018). Because the detection of antigen-specific B cell subsets requires high experimental effort (Buisman et al., 2009), vaccine studies in larger populations usually focus only on antibodies in serum. Methods that indirectly infer preexisting memory B cells from antibody response kinetics could help to better understand how (repeated) vaccination affects this important B cell subset. The current approach to vaccine development is mostly empirical, and common strategies to improve vaccine-induced protection in poorly responding groups include administration of higher doses of vaccine antigen in the elderly (Lee et al., 2018), adding immunologic adjuvants, such as aluminum salts or organic compounds (Tregoning et al., 2018), or the administration of a second dose (booster vaccination) in immunocompromised patients (de Lavallade et al., 2011). However, the benefit of booster vaccinations in immunocompromised populations is under debate, and several studies report conflicting results (Gueller et al., 2011; Engelhard et al., 2011; de Lavallade et al., 2011; Karras et al., 2013). The evaluation of vaccines in immunocompromised patients is particularly challenging as randomized studies are often unfeasible. More studies analysing booster responses in immunocompromised patients are needed to optimize vaccination schedules in this high-risk group.

And finally, the vaccine response is associated with various host-related factors affecting the immune system, such as sex, age, diseases, medical treatment, and genetic background (Franco et al., 2013; Linnik and Egli, 2016; Paules and Subbarao, 2017). The mechanisms behind these associations are not fully understood and focus of ongoing research. The effect of increasing age on the immune system (immunosenescence) is linked to several processes, e.g., thymic involution, decline in innate immunity, and impaired B cell development (Aw et al., 2007). Sex differences occur in both innate and adaptive immunity, are conserved across species, and have been linked to hormones and sex chromosome genes (Klein and Flanagan, 2016). In general, women show stronger antibody responses, have higher antibody basal levels, and greater B cell numbers (Abdullah et al., 2012; Furman et al., 2014). Chronic diseases, such as diabetes, autoimmune diseases, or chronic graft-versus-host disease (cGVHD) in transplant recipients have been reported to affect the influenza vaccine response (Gelinck et al., 2007; van Assen et al., 2010; Ljungman, 2012). Since these patients usually receive various medical treatments and often have comorbidities, such patient populations are highly heterogeneous and difficult to study. To disentangle associations between host factors and antibody response, relevant host factors have to be included and corrected for in the analysis. Moreover, differences in genotypes involved in antigen processing (especially HLA) and signalling (e.g., IFN- λ) have been proposed to alter the vaccine-induced antibody response (Haralambieva et al., 2011; Kennedy et al., 2012; Franco et al., 2013; Pulendran, 2014; Linnik and Egli, 2016). The genetic background may be especially important in immunocompromised individuals where compensating mechanisms are potentially impaired as studies on IFN- λ genotypes in immunocompromised transplant patients suggest (Egli et al., 2014a,b).

Understanding the mechanism of how differences in immune cells, proteins and signalling molecules affect the vaccine response is experimentally extremely challenging. Experiments in mice can

lead to wrong conclusions due to important differences between the human and mouse immune system (Shultz et al., 2012; Tao and Reese, 2017). For instance, human B cells carry the IFN- λ receptor, while mouse B cells lack it (Wack et al., 2015; de Groen et al., 2015; Syedbasha and Egli, 2017; Syedbasha et al., 2020). *In vitro* experiments with human immune cells try to mimic the natural environment by adding relevant signalling molecules. However, due to the complexity of the adaptive immune system and many unknowns, *in vitro* systems can not fully reflect the *in vivo* situation. In addition, host factors may bias the results. Mathematical models allow to investigate mechanistic hypothesis in a precisely defined environment and have proved themselves as valuable assistants in understanding immune response mechanisms and explaining experimental results (Meyer-Hermann et al., 2012; Zhang et al., 2013; Wang et al., 2015; Hauser et al., 2007; Murugan et al., 2018; Buchauer and Wardemann, 2019). A model that connects different data types via mechanistic hypotheses, such as immunobiological results and host-related factors, could check their compatibility with clinical observations, raise new hypotheses, and guide future experiments.

1.3 MATHEMATICAL MODELS HELP TO DECIPHER IMMUNE RESPONSES

Mathematical models of the adaptive immune response are derived from our mechanistic understanding of the interaction and kinetics of critical components, such as lymphocytes (B and T cells), antibodies, antigen, and signalling molecules. In 1970, Bell presented an ordinary differential equation (ODE) model of the antigen-dependent B cell expansion and laid the theoretical base for understanding clonal selection and affinity maturation (Bell, 1970). In subsequent years, ODE models of GC B cell dynamics predicted key processes of the GC reaction that have been later confirmed experimentally, such as recycling of GC B cells (Kepler and Perelson, 1993; Oprea and Perelson, 1997; Allen et al., 2007b; Schwickert et al., 2007), and feedback by secreted antibodies that mask antigen in GCs (Iber and Maini, 2002; Zhang et al., 2013). ODE models enable to concisely describe dynamic systems, but they assume that the simulated entities are homogeneously distributed. When spatial distribution has to be taken into account, agent-based models are frequently applied to model immune responses (Bauer et al., 2009), and have successfully predicted that B cell selection depends not only on the competition for antigen on FDCs but also on the competition for limited T cell help (Meyer-Hermann et al., 2006; Victora et al., 2010).

The first GC models focused on modelling a single GC to investigate the driving processes, such as proliferation, recycling, and selection. Since activated GCs may be connected, e. g., via secreted antibodies, and respond in a coordinated manner (Schwickert et al., 2007; Zhang et al., 2013), models of GC populations have been developed to describe affinity maturation during infection (Childs et al., 2015; Murugan et al., 2018). A model of several GC reactions in parallel was able to explain reduced affinity maturation during malaria infection (Murugan et al., 2018). However, little is known on how GC reactions could vary between vaccinated individuals and how these differences relate to host factors associated with poor vaccine response. Since studying GC processes is associated with high experimental effort (Turner et al., 2020), GC responses in patient populations are not well characterized. In Chapter 4, we investigate whether our current understanding of GC dynamics can explain the heterogeneous antibody response to influenza vaccination in hematopoietic stem cell transplant (HSCT) patients. We infer differences in preexisting memory B cells and GC

processes directly from observed HI antibody titers using a model that combines our understanding of GC B cell dynamics with important patient factors via mechanistic hypotheses about how these factors might modulate the GC response.

1.4 CONTRIBUTIONS OF THIS THESIS

The goal of this thesis was to establish novel methods for analysing HI antibody titers that could improve the evaluation of the influenza vaccine response in larger populations, where detailed molecular analysis of influenza-specific B cell subsets and antibodies is unfeasible, and to apply them to investigate the vaccine response in a population of HSCT patients. The thesis demonstrates how different mathematical models can be used in conjunction to characterize the vaccine response in a patient population from easy-to-establish measurements (**Figure 1.3**).

Chapter 4

Inferring differences in immune response dynamics

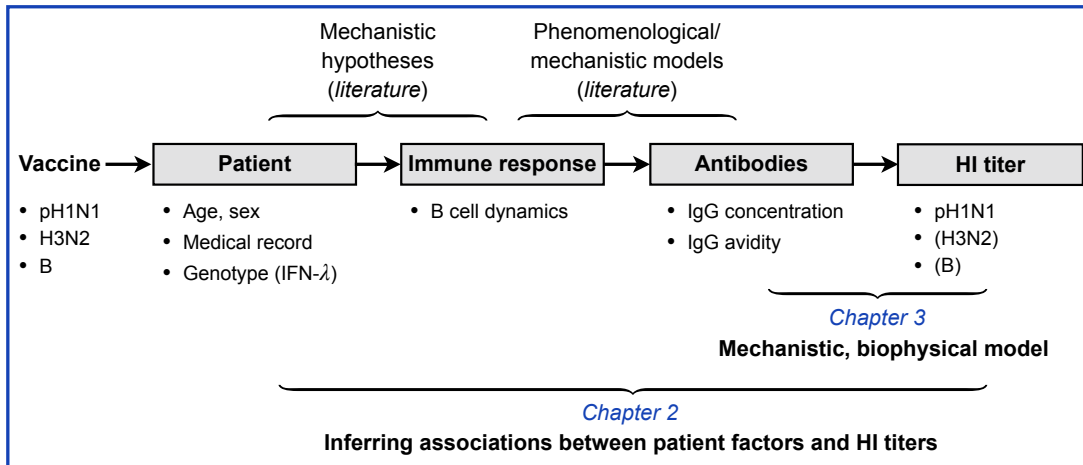


Figure 1.3. Thesis overview. We investigate the immune response to seasonal influenza vaccination (against pandemic H1N1, H3N2, and B influenza strains) in hematopoietic stem cell transplant (HSCT) patients. In Chapter 2, we infer associations between patient factors and HI antibody titers. In Chapter 3, we present a biophysical model of the HI assay that establishes the relationship between IgG concentration, avidity, and HI titer for influenza H1N1. In Chapter 4, we combine the HI assay model from Chapter 3 with a model of the vaccine-induced B cell response and antibody production to describe HI titer responses in HSCT patients. We integrate important patient factors associated with the antibody response (identified in Chapter 2) into the model and infer differences in memory B cells and GC processes associated with the investigated patient factors.

In Chapter 2, we identify the most important patient factors associated with HI baseline titers and HI titer responses against three different influenza strains (pandemic H1N1, H3N2, B). We perform a multivariable regression analysis with sequential models and show that the inferred effects have a similar interpretation as the commonly used binary regression on seroprotection/seroconversion but that our approach estimates effects with higher precision. Furthermore, we show that HSCT

patients benefit from the booster vaccination and elicit similar average responses after two influenza vaccinations as healthy individuals after one.

In Chapter 3, we derive from first principles a biophysical model of the HI assay for influenza H1N1 and establish a mechanistic link between IgG concentration, avidity, and HI titer. We apply the model to infer IgG avidities from ELISA-detected IgG concentrations and HI titers in HSCT patients and experimentally validate our predictions in independent avidity measurement. Our model predicts that vaccination induced affinity maturation in only a few patients and that the observed HI titer increases are mostly explained by an increase in IgG concentration. Because the model links IgG concentrations and avidities to HI titers, it closes the gap between immunobiological models and vaccination outcomes in vaccine studies that apply HI titers.

In Chapter 4, we combine the lessons learned from the previous chapters with literature knowledge to develop an ODE model of the vaccine-induced B cell dynamics, antibody production, and HI titer response in HSCT patients. We apply the model to infer differences in preexisting memory B cells and GC reaction processes that are potentially modulated by the investigated patient factors (identified in Chapter 2). The model predicts that both newly generated plasma cells and reactivated memory B cells contribute to the observed increase in HI titers, and that the heterogeneity in HI titer responses is well described by preexisting memory B cells and only a few patient-specific factors that potentially modulate the GC reaction, such as absolute lymphocyte count in the blood and IFN- λ genotype. Our analysis suggests that an increase in lymphocyte count is associated with an increase in the number of successfully established GCs and potentially affects additional GC processes leading to stronger antibody responses.

ASSOCIATION OF HOST FACTORS WITH ANTIBODY RESPONSE TO INFLUENZA VACCINATION IN HSCT PATIENTS

This chapter is an Author's Original Version (AOV) of an article that has been accepted for publication in *The Journal of Infectious Diseases* published by Oxford University Press: J. Linnik, M. Syedbasha, H.-M. Kaltenbach, D. Vogt, Y. Hollenstein, L. Kaufmann, N. Cantoni, S. Ruosch-Girsberger, A. M. S. Müller, U. Schanz, T. Pabst, G. Stüssi, M. Weisser, J. Halter, J. Stelling, and A. Egli. Association of host factors with antibody response to seasonal influenza vaccination in allogeneic hematopoietic stem cell transplant (HSCT) patients. *The Journal of Infectious Diseases*, 08 2021. <https://doi.org/10.1093/infdis/jiab391>.

2.1 SUMMARY

Influenza causes increased morbidity and mortality in patients after allogeneic hematopoietic stem cell transplantation (HSCT). Therefore, HSCT patients are recommended to receive influenza vaccination regularly. However, vaccination efficacy is reduced compared to healthy individuals, and factors determining vaccination outcomes are still poorly understood. We identified host factors associated with the antibody response to seasonal influenza vaccination in a multivariable regression analysis of hemagglutination inhibition (HI) antibody titers and seroconversion/seroprotection categories. We show that both approaches yield consistent results, but that regression on HI titers infers association with higher precision. HSCT patients showed a highly heterogeneous vaccine response and required two vaccine doses to achieve average responses comparable to a single dose in healthy volunteers. Pre-vaccination titers were strongly associated with the time after transplantation, confirming that HSCT patients can elicit potent vaccine responses and can acquire durable antibody levels over the years after transplantation. However, we identified several common host factors that reduce the odds of responding, such as treatment with calcineurin inhibitors, an unrelated donor, and absolute lymphocyte counts below the normal range. Moreover, mycophenolate treatment and a donor mismatch in HLA class II negatively affected pre-vaccination titers. Patients belonging to such poorly responding groups might benefit from additional preventive strategies.

2.2 ABSTRACT

Patients after allogeneic hematopoietic stem cell transplantation (HSCT) are at high risk for severe influenza infections. Influenza is a vaccine-preventable disease, but vaccination efficacy is reduced after HSCT, and patient factors influencing vaccine response are still poorly understood.

In this observational multicenter cohort study, we enrolled 135 HSCT patients and 69 healthy volunteers (HVs) in 2014/15 and 2015/16. HVs received one dose of the seasonal influenza vaccine, patients two doses at a 30-day interval. Antibody response was assessed by hemagglutination inhibition (HI) assays. Effects of vaccination and patient-factor associations with pre- and post-vaccination titers were investigated in a multivariable regression analysis on HI titers

against A/California/2009/H1N1, A/Texas/2012/H3N2, and B/Massachusetts/2012. For comparison, associations were also inferred by binary logistic regression on seroprotection (HI titer ≥ 40) and seroconversion (HI titer fold-change ≥ 4). Both approaches yielded consistent results, but regression on titers estimated effects with higher precision. Patients showed higher odds for HI titer increase after the second dose compared to the first (95% confidence interval (CI) OR = 1.03 – 1.54) and achieved after two doses a response comparable to a single dose in HVs. Pre-vaccination titers were positively associated with the time after transplantation (OR = 2.47 – 5.99 for 4 years post-HSCT) and negatively with mycophenolate treatment (OR = 0.30 – 0.78) and donor mismatch in HLA class II (OR = 0.25 – 0.79). Important negative factors for vaccine response were an unrelated donor (OR = 0.44 – 0.71) and intake of calcineurin inhibitors (OR = 0.25 – 0.53 for cyclosporine A, OR = 0.34 – 0.65 for tacrolimus), while lymphocyte count (OR = 1.23 – 1.49 per doubling), and, surprisingly, chronic graft-versus-host-disease (OR = 1.34 – 1.74 per grade) were positively associated.

In conclusion, regression on titers should be preferred over dichotomization approaches. Patients' vaccine responses are highly heterogeneous, but overall, patients benefited from the booster shot and can acquire seroprotective antibody baseline levels over the years. However, an unrelated donor and calcineurin inhibitors, a frequent immunosuppressive treatment, lower the odds of responding, urging to investigate additional preventive strategies for HSCT patients.

2.3 INTRODUCTION

Influenza is a major cause of morbidity and mortality in high-risk populations such as the elderly, pregnant women, and patients after hematopoietic stem cell transplantation (HSCT) (Kunisaki and Janoff, 2009; Ljungman et al., 2011; Schuster et al., 2017). Before stem cell transplantation, patients receive chemotherapy, radiation therapy, or both, to destroy malignant cells, permit engraftment, and prevent rejection, leaving patient's immune cells depleted for months or even years (Storek et al., 2008; Williams and Gress, 2010). Once the immune system reconstitutes, HSCT patients often remain immunocompromised and require life-long immunosuppressive treatment to prevent or treat graft-related complications such as graft-versus-host disease (GVHD) (Copelan, 2006; Mackall et al., 2009). Therefore, community-acquired viruses, such as influenza, pose a high risk for HSCT patients, with reported case fatalities of up to 20–30% for seasonal and pandemic influenza (Kunisaki and Janoff, 2009). Vaccination is the primary intervention to protect from influenza, but vaccine effectiveness is lower in HSCT patients than in healthy individuals (Ljungman and Avetisyan, 2008; Beck et al., 2012). To develop better vaccination strategies for HSCT patients and to identify patients at high risk for a higher morbidity and even fatal outcome, it is important to understand which host factors influence the vaccine response.

Several studies investigated the response to influenza vaccination in HSCT patients (reviewed in (Ljungman and Avetisyan, 2008)). Most studies agree that time post HSCT (transplantation-to-vaccination interval), especially within the first year (Engelhard et al., 1993; Avetisyan et al., 2008; Mohty et al., 2011; Fukatsu et al., 2017), and immunosuppressive treatment with calcineurin inhibitors or monoclonal antibodies (Gueller et al., 2011; Roll et al., 2012; Nazi et al., 2013; Fukatsu et al., 2017) are important factors determining vaccination outcomes. However, there are

mixed results on the effect of chronic GVHD (Pauksen et al., 2000; Mohty et al., 2011; Issa et al., 2011; Gueller et al., 2011; Roll et al., 2012; Dhédin et al., 2014; Fukatsu et al., 2017), and little is known on the effect of donor relationship and mismatch (Engelhard et al., 2011). One of the main strategies to improve vaccine efficacy is administering a second dose (booster shot), but there is also conflicting data on the benefit of booster shots for HSCT patients (Gueller et al., 2011; Engelhard et al., 2011; de Lavallade et al., 2011; Karras et al., 2013).

In recent years, host genetic factors have been proposed to influence the vaccine-induced antibody response in children and adults (Haralambieva et al., 2011; Kennedy et al., 2012; Pulendran, 2014; Linnik and Egli, 2016). An association between the interferon(IFN)- λ genotype and influenza vaccine response has also been observed in immunosuppressed organ transplant patients (Egli et al., 2014b). Genetic factors may be especially important in immunocompromised populations where compensating mechanisms are potentially impaired, but so far, genetic factors have not been investigated in HSCT patients.

Understanding the vaccine response in HSCT patients is particularly challenging. Controlled studies are unethical or unfeasible, and the number of patients in observational studies is usually low, which hampers statistical power and can introduce bias in the estimated effects (Greenland et al., 2016). Moreover, HSCT patients are highly heterogeneous, e.g., in medication and comorbidities, which further complicates the comparison of published studies. Many host factors are not independent of each other. For instance, donor mismatch can increase the risk for GVHD, which in turn requires increased immunosuppression. Therefore, adjustment for relevant patient factors, such as multivariable regression analysis, is crucial to disentangle host factor associations. Besides, vaccine responders and non-responders are commonly classified based on conventional cut-off values such as seroprotection and seroconversion, and statistical analysis is performed on dichotomized outcomes instead of the full data, which can further decrease statistical power (Capuano et al., 2007; Fedorov et al., 2009).

Here, we performed a multivariable regression analysis directly on the observed antibody titers to investigate the association of patient and transplant characteristics with vaccination outcomes in allogeneic HSCT patients, including IFN- λ genotypes that were reported to be associated with vaccine response (Haralambieva et al., 2011; Kennedy et al., 2012; Egli et al., 2014b). We assessed the antibody response against three different influenza types (H1N1, H2N3, B), which enabled us to study strain-specific differences, and, more importantly, to investigate strain-independent host factors associated with vaccine response. We compared patients' vaccine responses to healthy volunteers, who received two doses of the seasonal influenza vaccine instead of one. In addition, we investigated the association of local side effects with vaccine response. Our results obtained by titer regression are consistent with results obtained by the commonly used binary logistic regression on seroconversion and seroprotection categories but our approach yields higher precision in the estimated effects.

2.4 METHODS

2.4.1 Ethics and regulatory requirements

The study was conducted following the Declaration of Helsinki and approved by the Ethics committee northwest and central Switzerland (EKNZ identifier 2014-141). All participants signed informed consent. The study was registered under the ClinicalTrials.gov identifier NCT03467074.

2.4.2 Study design, participants and data collection

In this prospective observational multicenter cohort study, we recruited patients at six hematological centers in Switzerland (at the University Hospitals in Basel, Bern, and Zurich, the Cantonal Hospitals in Aarau and Lucerne, and at Ospedale San Giovanni in Bellinzona) from October 2014 to January 2015 and October 2015 to January 2016 (**Figure 2.1**). Only adult patients (at least 18 years old) who received allogeneic hematopoietic stem cells at least one year ago (time post HSCT ≥ 1 year) and without known vaccine intolerance, such as egg protein allergy or vaccine-associated adverse events, were eligible for participation. Patients received two doses of non-adjuvanted seasonal influenza vaccine (see section Vaccine composition). The second dose (booster shot) was given 30 days after the first, following the standard of care for HSCT patients. Serum samples and peripheral blood mononuclear cells (PBMCs) were collected before the first vaccination (d0) and afterward (d7, d30, d60, d180) and stored in aliquots at -80°C .

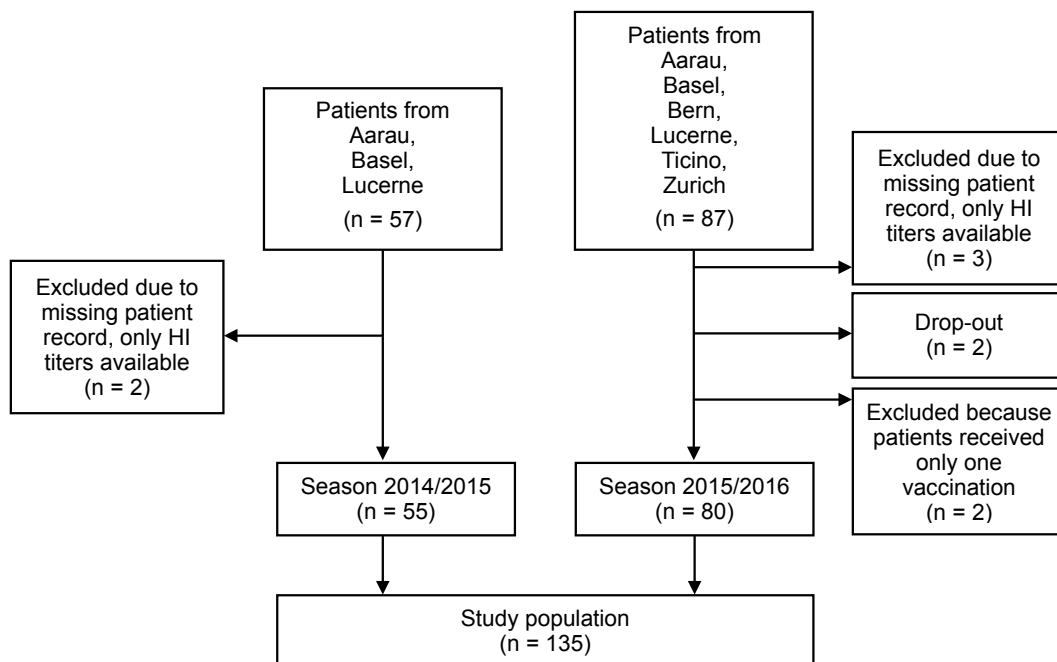


Figure 2.1. Overview of patient recruitment.

The study team documented patients' medication and the grade of chronic GVHD (cGVHD) at the time of inclusion according to the NIH consensus criteria (Filipovich et al., 2005). Patients were asked to document side effects on d7 and d37 in a questionnaire. Absolute lymphocyte counts were available from routine laboratory tests from the same day or the same week of the first vaccination, except for one patient in season 2014/15 and seven patients in season 2015/16 for which the lymphocyte counts were measured at a later/earlier time point. The genotype of the transplanted stem cells (the donor's genotype) was determined from blood samples using TaqMan quantitative real-time PCR assays (see section Genotyping). Patients were advised to consult a physician in case of influenza-like illness and influenza infections were confirmed by PCR.

In addition, we collected serum samples from vaccinated healthy volunteers (d0, d7, d30, d60, and d180 after vaccination) during the same influenza seasons for comparison (25 in 2014/15 and 44 in 2015/16, 69 volunteers in total). In contrast to HSCT patients, healthy volunteers received only one dose of the seasonal influenza vaccine.

2.4.3 Vaccine composition

In 2014/15, all participants received a non-adjuvanted trivalent influenza vaccine (Agrrippal, Novartis, Switzerland) against the following strains: A/California/7/2009, A/Texas/50/2012 (H3N2), and B/Massachusetts/2/2012 (Yamagata lineage). In 2015/16, participants received a non-adjuvanted quadrivalent vaccine (Fluarix Tetra, GSK, UK) against A/California/7/2009 (H1N1), A/Switzerland/9715293/2013 (H3N2), B/Phuket/3073/2013 (Yamagata lineage), and B/Brisbane/60/2008 (Victoria lineage). Both vaccines comprised inactivated, subunit influenza viruses with 15 µg HA antigen of each vaccine strain. Vaccines were administered by intramuscular injection. We measured HI titers against all vaccine strains from both seasons except for B/Phuket/3073/2013.

2.4.4 Genotyping

We investigated SNPs that were reported to be associated with vaccination outcome and antiviral immune response (Thomas et al., 2009; Tanaka et al., 2009; Ge et al., 2009; Suppiah et al., 2009; Jiménez-Sousa et al., 2013; Egli et al., 2014b). Specifically, we genotyped three SNPs near the *IFNL3* gene locus (rs8099917, rs12979860, rs10853727) and one SNP within the 3' UTR region of the interferon-λ receptor gene *IFNLR1* (rs10903035). In addition, we determined the genotype of three SNPs in other cytokine genes (*IFNA1*, *IL4*, and *IL6*), which have been suggested in genome-wide association studies to be associated with measles vaccine-induced antibody response (Haralambieva et al., 2011; Kennedy et al., 2012).

All SNPs were genotyped using TaqMan Real-Time PCR assay kits by Applied Biosystems as previously described (Thomas et al., 2014; Egli et al., 2014a; da Silva Conde et al., 2014). To differentiate the major and minor alleles, we used the probe sets for rs8099917 (T>G, #C__11710096_10), rs12979860 (C>T, #C__7820464_10), rs10853727 (T>C, #C__7820456_10), rs10903035 (A>G, #C__68976_10), rs28383797 (G>A, #C__59380188_10), rs2243248 (T>G, #C__16176227_10), and rs2069824 (T>C, #C__383639_10).

The genomic DNA of the donor was isolated from EDTA blood (QIAamp DNA Blood Mini Kit by Qiagen, #51106), as described by the manufacturer. In brief, 5 μ L of 2X TaqMan genotyping master mix (Applied Biosystems, #4371355), 0.5 μ L of 20X combined primers and probes mix, and 1 μ L of DNA (1-20 ng) were added to 3.5 μ L nuclease-free water in a total volume of 10 μ L. We used the 7500 Fast real-time PCR system (Applied Biosystems) with the following cycle conditions: 50 cycles of denaturation at 92°C for 15s and annealing at 60°C for 60s. Samples and positive controls were run in duplicates. SNP genotypes were determined by automated genotype calling in conjunction with the allelic discrimination plot using the Applied Biosystems TaqMan Genotyper Software.

2.4.5 Hemagglutination inhibition assay

Antibody levels were determined as hemagglutination inhibition (HI) titers. We performed HI assays according to the WHO manual (WHO, 2002) using a previously published protocol (Kaufmann et al., 2017). In both influenza seasons, we measured HI titers against viruses in the vaccine and circulating viruses: A/California/7/2009, A/Texas/50/2012 (H3N2), A/Switzerland/9715293/2013 (H3N2), B/Massachusetts/2/2012 (Yamagata lineage), and B/Brisbane/60/2008 (Victoria lineage).

2.4.6 Data analysis

Patient information, HI assay results, and SNP genotypes were collected in Excel worksheets, and all data were preprocessed and analysed using in-house scripts in R (R Core Team, 2019).

2.4.6.1 Investigated endpoints and regression analysis of HI titers

Primary endpoints were investigating the association of patient and transplant characteristics with (i) vaccine-induced antibody response in terms of relative HI titer increase and seroconversion (HI titer fold change ≥ 4), and (ii) pre-vaccination antibody levels, i.e., HI titer level and seroprotection (HI titer ≥ 40) on d0. Secondary endpoints were (i) investigating the association of local side effects with vaccine response in HSCT patients, and (ii) comparing vaccine responses between HSCT patients and healthy volunteers (HVs).

For analysing HI titers, we used a generalized linear regression model for ordered data where response categories are reached successively step-by-step, known in the literature as the sequential model, continuation-ratio model, or stopping-ratio model (here referred to as titer regression, see **Supplementary Methods** for details) (Tutz, 1991; Agresti, 2003; Yee et al., 2010). To investigate associations with vaccine response, we pooled post-vaccination titers from d30 and d60; we corrected for strain-specific baseline levels (titers on d0) and time point to account for differences between d30 and d60 (effect of booster shot). To estimate the average effect of vaccination, we performed a regression over all time points encoding each time point after vaccination (d7, d30, d60, d180) as a binary variable with d0 as the reference level. Using this model, we estimated the odds ratio for HI titer increase (increase by at least one titer level) on d7/d30/d60/d180 compared to d0 in HSCT patients and HVs. Models were fitted using maximum likelihood estimation implemented

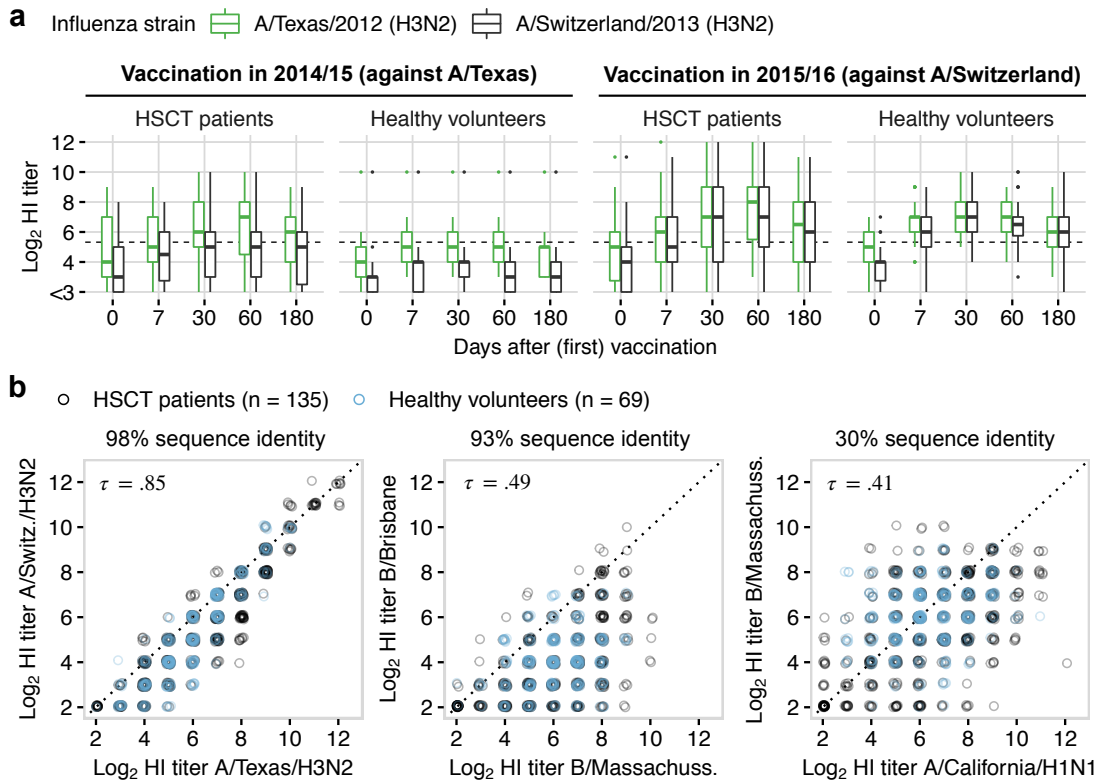


Figure 2.2. Cross-reactivity between influenza strains. (a) HI titers against the two H3N2 strains A/Texas/2012 and A/Switzerland/2013 by influenza season. In 2014/15, the A/Texas strain was part of the vaccine composition, while in 2015/16, A/Switzerland replaced it. (b) Correlation in HI titers between influenza strains. Sequence identity refers to hemagglutinin protein sequences provided on GISAID. Correlations were quantified using Kendall’s rank correlation coefficient τ for ordinal outcomes.

in the R package VGAM (Yee et al., 2010). Adjacent titer categories were grouped together, when observations per category were too sparse, which affected the lowest titer and very high titers. We corrected for experimental batches, inclusion center, influenza strain, and season in all performed analyses.

We compared the effects estimated from HI titers by the sequential logistic model to the commonly used binary regression on seroconversion/seroprotection categories. We performed the same inference on the pooled seroconversion on d30 and d60, and on seroprotection on d0 using the glm function for binary logistic regression in R (R Core Team, 2019).

More specifically, we pooled the data for three different influenza types, namely pandemic A/California/2009 (H1N1), seasonal A/Texas/2012 (H3N2), and B/Massachusetts/2012 (Yamagata lineage) collected during the two flu seasons. HI titers against B/Brisbane/2008 (Victoria lineage) had to be excluded due to low immunogenicity (Figure S2.3). HI titers against A/Switzerland/2013 (H3N2) were highly correlated with HI titers against A/Texas/2012 (H3N2) (Figure 2.2b, Kendall’s $\tau = 0.85$, $P < 10^{-15}$), and we chose the titers against the A/Texas strain to study H3N2-response because unlike the A/Switzerland titers, they showed a strong response in both seasons (Figure 2.2a).

2.4.6.2 Patient variables

We included the patient and transplant characteristics summarized in Table 3.2 in our multivariable regression analysis, except for the patient's underlying disease.

Patient variables were encoded as follows: Time after transplantation in years (continuous variable), total lymphocyte count in cells per μL (log-transformed continuous variable), treatment with rituximab within the previous six months before vaccination (binary variable), treatment with cyclosporine A, tacrolimus, mycophenolate mofetil/sodium or prednisone at the time of inclusion (all as binary variables), transplant source (bone marrow vs peripheral blood, binary variable), disease state (complete remission vs recurrence, binary variable), family relationship with donor (related vs unrelated, binary variable), HLA mismatch (fully matched vs at least one mismatch, where we distinguished between mismatch in HLA class I, HLA class I or haploidentical transplantation – all encoded as binary variables). We included the grade of cGVHD as an ordered categorical variable (with 0 for no cGVHD, 1–3 for cGVHD grade), and added interaction effects between cGVHD grade and donor mismatch to investigate potential synergistic effects since HLA mismatching is one of the main risk factors for cGVHD (Woolfrey et al., 2011; Petersdorf et al., 2013). We adjusted for sex (binary variable) and age in years (continuous variable) as well as for PCR-confirmed influenza A or B infection during the considered flu season, encoded as a binary variable with 0 for no infection and 1 for A or B infection.

We encoded each genotype as a binary variable with 0 for homozygous major allele carriers and 1 for minor allele carriers. Specifically, we included the *IFNL3* genotype in rs8099917 (T>G) and rs12979860 (C>T) as well as the *IFNL1* genotype in rs10853727 (A>C). We excluded the SNP rs10853727 due to small sample size and because no patients carried the homozygous minor allele (CC); only 24/135 patients (18%) carried the heterozygous minor allele (CT), and almost all patients carrying the rs10853727 minor allele also had the rs12979860 minor allele (n=23/24). For the three SNPs in the other cytokine genes (*IFNA1*, *IL4* and *IL6*) we also mostly observed the major allele (95%, 84%, 81%) and only 1% of the study population carried the homozygous minor allele (**Table S2.1**). Therefore, we also excluded these SNPs from further analysis.

We detected no interaction effects between host factors and influenza strains according to the Bayesian information criterion (BIC), confirming that the inferred effects were not significantly different across the investigated strains and that the observed strain-specific differences in post-vaccination titers were mostly explained by differences in pre-vaccination titers (**Figure 2.3a**). Finally, we also tested whether continuous variables (lymphocyte count, time post HSCT, age) have a significant quadratic term, needed for capturing saturation effects.

2.4.6.3 Missing data

The collected data had only a few missing values (**Table S2.3**) except for the influenza infection state (27% missing), disease state (25% missing), and absolute lymphocyte count (9% missing). We used multiple imputation in conjunction with several sensitivity analyses to ensure that the missing data do not affect the interpretation of our results.

Assuming a Missing At Random (MAR) process, we generated 50 imputed data sets from an imputation model that included all patient variables, HI titers, and other necessary factors that might

explain the missing data, such as influenza season, inclusion center, and interaction effects. Results were combined using Rubin's rule (Little and Rubin, 2019). Imputed data sets were generated using the function `aregImpute` of the R package `Hmisc` that uses bootstrapping to approximate the process of drawing predicted values from a full Bayesian predictive distribution (Harrell Jr et al., 2019). Imputation R^2 were 0.96 or higher for all missing HI titers and 0.71–0.95 for the remaining missing variables, indicating overall a suitable imputation procedure (**Table S2.3**).

In addition, we performed the same analysis as on the imputed data ($n = 135$) on four different data subsets: (i) data complete in lymphocyte count ($n = 123$), (ii) data complete in disease state ($n = 101$), (iii) data complete in influenza infection state ($n = 99$), and as an extreme case, (iv) data complete in lymphocyte count, influenza infection state and disease state ($n = 85$) (**Figure S2.5** and **Figure S2.9**).

2.4.6.4 Sensitivity analyses

We compared the results obtained by the full regression model, which included all patient variables described above, with four reduced models excluding (i) donor family relationship, (ii) donor mismatch (both to investigate whether this influences the effect of mismatch/donor relationship), (iii) lymphocyte count (as this variable is often not available), and (iv) the interaction effect between cGVHD and donor mismatch (**Figure S2.6** and **Figure S2.10**).

To investigate the stability of the inferred effects, we fitted the full model to ten data subsets ($n = 108$), where 20% of patients were randomly excluded (**Figure S2.7** and **Figure S2.11**). Note that patients with rituximab treatment ($n = 3$) and a haploidentical donor ($n = 1$) had to be included in all data subsets because of the small sample size.

2.4.6.5 Data and code availability

Data and results are available in a machine-readable format on GitLab along with R scripts for reproducing: <https://gitlab.com/csb.ethz/hsct-study> (will be made public upon publication).

2.5 RESULTS AND DISCUSSION

2.5.1 Patient characteristics

HSCT patient characteristics are summarized in **Table 3.2**. The two cohorts (from influenza seasons 2014/15 and 2015/16) showed similar distributions in age, sex, and transplant characteristics. There were slightly more patients suffering from cGVHD in the first cohort than in the second (64% vs 50%), accompanied by a slightly higher fraction of patients receiving immunosuppressive drug treatment (**Table 3.2**). The distribution of immunosuppressive treatment stratified by cGVHD grade is shown in **Figure S2.1**.

Table 2.1. Patient characteristics. Columns refer to two consecutive influenza seasons. Abbreviations: IQR: interquartile range; GVHD: graft-versus-host disease

		2014/2015	2015/2016	All
Total		55	80	135
Age	Median, IQR, range (years)	55, 44-64, 22-72	54, 47-63, 24-74	54, 46-64, 22-74
	≥ 65 years	13 (24%)	18 (22%)	31 (23%)
Sex	Female	26 (47%)	32 (40%)	58 (43%)
	Male	29 (53%)	48 (60%)	77 (57%)
Underlying disease	Acute myeloid leukemia (AML)	21 (38%)	29 (36%)	50 (37%)
	Acute lymphoblastic leukemia (ALL)	10 (18%)	12 (15%)	22 (16%)
	Multiple myeloma (MM)	6 (11%)	8 (10%)	14 (10%)
	Chronic myeloid leukemia (CML)	6 (11%)	6 (8%)	12 (9%)
	Chronic lymphocytic leukemia (CLL)	6 (11%)	0	6 (4%)
	Myelodysplastic syndromes (MDS)	3 (5%)	8 (10%)	11 (8%)
	Non-Hodgkin lymphoma (NHL)	1 (2%)	6 (8%)	7 (5%)
	Myeloproliferative neoplasms (MPN)	1 (2%)	5 (6%)	6 (4%)
	Other	1 (2%)	6 (8%)	7 (5%)
Time after transplantation	Median, IQR, range (years)	4, 2-8, 1-25	4, 2-7, 1-22	4, 2-7, 1-25
	1-2 years	19 (35%)	33 (41%)	52 (39%)
	3-5 years	15 (27%)	21 (26%)	36 (27%)
	> 5 years	21 (38%)	26 (33%)	47 (35%)
Lymphocyte count	Median, range (10 ⁹ cells/L)	1.5, 0.3-7.5	1.7, 0.5-5.5	1.7, 0.3-7.5
Disease state	Remission	51 (93%)	40 (50%)	91 (67%)
	Recurrence	4 (7%)	6 (8%)	10 (7%)
	Unknown	0	34 (43%)	34 (25%)
Transplant source	Peripheral blood stem cells	49 (89%)	74 (92%)	123 (91%)
	Bone marrow	6 (11%)	6 (8%)	12 (9%)
Donor source	Matched donor	45 (82%)	60 (75%)	105 (78%)
	Matched unrelated donor	19 (35%)	26 (33%)	45 (33%)
	Mismatched donor	10 (18%)	20 (25%)	30 (22%)
	Mismatched unrelated donor	8 (15%)	12 (15%)	20 (15%)
	HLA class I mismatch	5 (9%)	6 (8%)	11 (8%)
	HLA-A, -B, -C	3, 0, 2	4, 1, 1	7, 1, 3
	HLA class II mismatch	4 (7%)	10 (13%)	14 (10%)
	HLA-DP, -DQ, -DR	2, 2, 0	5, 1, 4	7, 3, 4
	HLA-haploidentical donor	1 (2%)	0	1 (1%)
	Not available mismatch type	0	4 (5%)	4 (3%)
Immunosuppressive treatment ^a	None	25 (45%)	45 (56%)	70 (52%)
	Tacrolimus	16 (29%)	14 (18%)	30 (22%)
	Prednisone	13 (24%)	16 (20%)	29 (22%)
	Mycophenolate ^b	9 (16%)	11 (14%)	20 (15%)
	Cyclosporine A ^c	5 (9%)	13 (16%)	18 (13%)
	Rituximab ^d	3 (5%)	0	3 (2%)
Chronic GVHD	None	20 (36%)	40 (50%)	60 (44%)
	Mild (grade 1)	12 (22%)	16 (20%)	28 (21%)
	Moderate (grade 2)	12 (22%)	6 (8%)	18 (13%)
	Severe (grade 3)	11 (20%)	14 (18%)	25 (19%)
	Not available	0	4 (5%)	4 (3%)
<i>IFNL3</i> genotype	rs809917 (GT/GG)	23 (42%)	27 (34%)	50 (37%)
	rs12979860 (CT/TT)	35 (64%)	40 (50%)	75 (56%)
<i>IFNL1</i> genotype	rs10903035 (AG/GG)	25 (46%)	44 (55%)	69 (51%)
Influenza infection ^e	Influenza A	5 (9%)	1 (1%)	6 (4%)
	Influenza B	3 (5%)	0	3 (2%)

^aBefore vaccination (documented at the time of inclusion),

^bMycophenolate Mofetil (CellCept[®]) or Mycophenolate Sodium (Myfortic[®]),

^cSandimmun Neoral[®],

^dMabThera[®] within the previous six months,

^ePCR-confirmed influenza infection during flu season.

Chronic GVHD were similarly distributed among patients with an unrelated/related donor, as well as among fully matched/mismatched patients (**Table S2.2**). In total, 105 patients had a fully matched donor (matched in 10/10 HLA loci), 25 patients a 9/10 matched donor, and only one patient a haploidentical donor (5/10 matched). The type of mismatch was not available for four mismatched patients.

All determined genotypes are summarized in **Table S2.1** and the distribution of investigated genotypes is shown in **Figure S2.2**. Importantly, all patients carrying the rs8099917 minor allele (GT/GG) also carried the minor allele in rs12979860 (CT/TT) ($n = 50$, 37%); 25 of 75 patients carrying the rs12979860 minor carried the rs8099917 major allele (**Figure S2.2**). Consequently, we could not distinguish whether a potential association of rs8099917 with vaccination outcome is due to the rs8099917 genotype or due to an interaction effect between rs8099917 and rs12979860 genotypes.

The fractions of seroprotected patients on d0 (HI titer ≥ 40) in the first/second season was 47%/38% for A/California (H1N1), 35%/41% for A/Texas (H3N2), and 38%/26% for B/Massachusetts; for comparison, the d0 seroprotection rates in healthy volunteers (HVs) were 28%/53% for A/California (H1N1), 16%/50% for A/Texas (H3N2) and 64%/50% for B/Massachusetts (for all strains and time points see **Table S2.4**).

2.5.2 HSCT patients show high variability in antibody titers

HSCT patients showed a more diverse vaccine response for all measured influenza strains and over the whole study period compared to HVs (**Figure 2.3a** and **Figure 2.3b**). However, HVs showed larger differences in HI titer levels between strains and seasons. Seroconversion (HI titer fold change ≥ 4) rates on d30 were similar or even higher in HSCT patients compared to HVs, ranging from 24–59% in patients and 12–73% in HVs for the respective vaccine strains. Seroprotection rates on d30 ranged from 53–70% in patients and 35–98% in HVs, and were higher in HSCT patients at all time points for A/California (H1N1) and A/Texas/H3N2 in the first season, but otherwise, always higher in HVs than in patients (**Table S2.4**). The number of non-responders, defined as no seroprotection on d0 and no HI titer increase on d7, d30 or d60 after vaccination, ranged from 2–18% in HSCT patients and 0–12% in HVs, and were higher in HSCT patients for all vaccine strains except for the A/California (H1N1) strain in the first season, where 9% of patients ($n = 5$) and 12% of HVs ($n = 3$) were non-responders (**Table S2.4**).

To compare the average effect of vaccination between HSCT patients and HVs, we estimated the odds ratios for showing higher HI titers (increase by at least one titer level) on d7, d30, d60, and d180 compared to d0 over both seasons and all influenza types (see **Methods**). Healthy volunteers showed a stronger response on d7 and d30, while responses were comparable on d60 and d180 (**Figure 2.3c**), even though HSCT patients received two vaccine doses (on d0 and d30) and HVs received just one (d0). The difference was largest on d7, suggesting that many HVs responded with a rapid antibody production by memory B cells. Thus, the slower and weaker antibody response in HSCT patients might be partially explained by a lower number of memory cells for the investigated influenza strains, and partially by the compromised immune system. Moreover, healthy volunteers were younger than HSCT patients — with a median age of 37 yrs (IQR 32–49 yrs) compared to

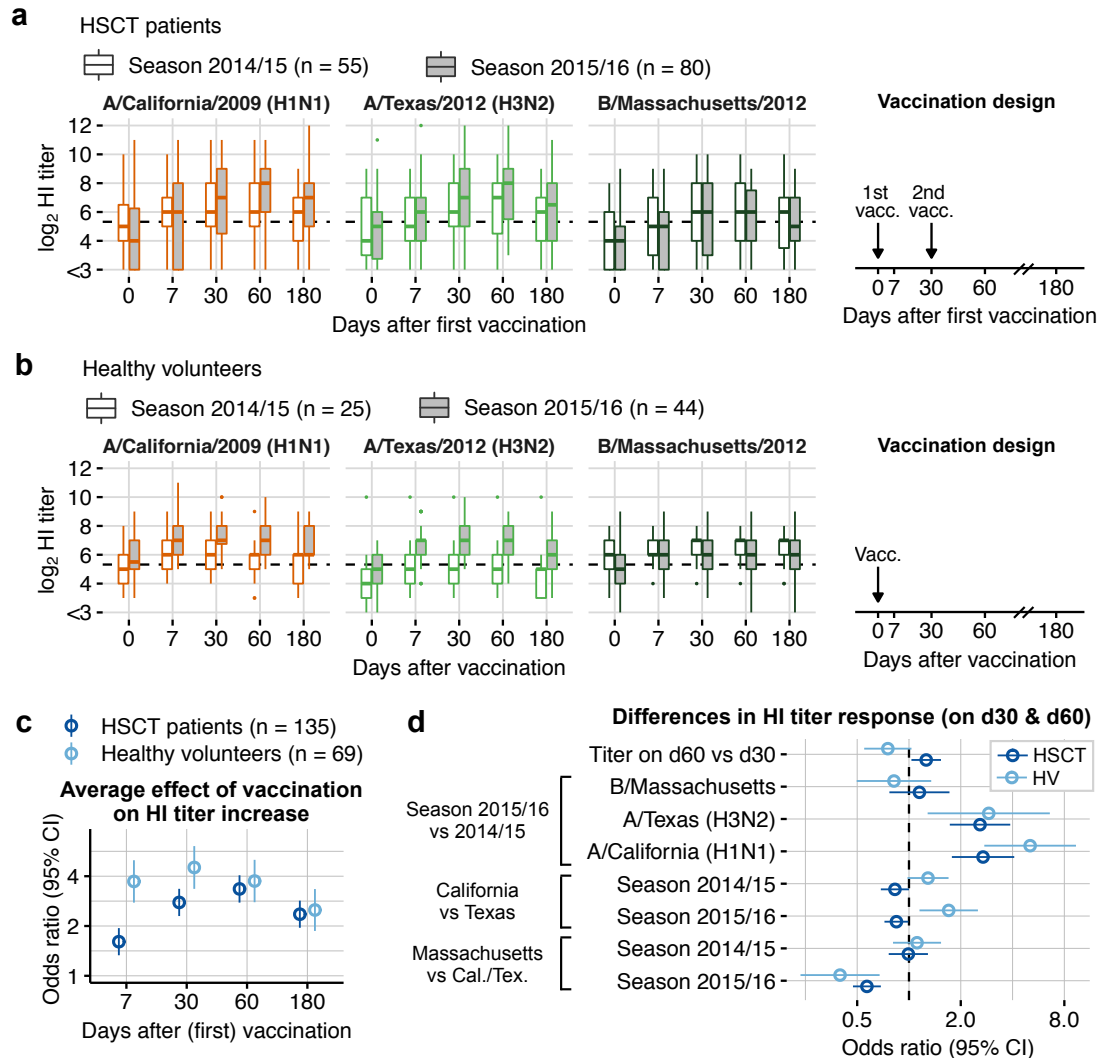


Figure 2.3. Antibody titers in hematopoietic stem cell transplant (HSCT) patients and healthy volunteers. (a) Hemagglutination inhibition (HI) titers against three different influenza strains in HSCT patients from two consecutive flu seasons. (b) As (a) but in healthy volunteers from the same seasons. (c) Average effect of vaccination on HI titer increase (relative to influenza strain- and season-specific baseline levels) in HSCT patients and healthy volunteers. Effects are expressed as the odds ratio for an increase in at least one titer level on d7/d30/d60/d180 compared to d0. (d) Estimated differences in vaccine response between time points, season and influenza strains. Effects are expressed as the odds ratio for an HI titer increase by at least one level compared to the reference, specifically, d60 vs d30, season 2015/16 vs 2014/15 (by strain), A/California titers vs A/Texas titers and B/Massachusetts titers vs others (by season).

54 yrs (IQR 46–64 yrs) — and influenza vaccine efficacy in adults decreases with increasing age (Goodwin et al., 2006; Smetana et al., 2018).

In summary, the vaccine response in HSCT patients is highly heterogeneous. While some patients showed no response or a weaker response than HVs, others showed a stronger response. However, the differences in pre-vaccination titers and potential differences in vaccination history (unknown in this study) hamper the comparison between HSCT patients and HVs.

2.5.3 HSCT patients benefited from booster shot

The results in **Figure 2.3c** suggest that HSCT patients showed a stronger vaccine response on d60 (OR = 3.35, 95% CI = [2.77, 4.05], $P < 10^{-12}$) compared to d30 (OR = 2.78 [2.30, 3.36], $P < 10^{-12}$). Consistent with these estimates, slightly more patients were seroconverted on d60 than d30 across all strains in both seasons (**Table S2.4**). On average, 11% of seroconverted patients (range 5–19%, 1–5 patients) were seroconverted on d60 but not on d30. Moreover, although HSCT patients showed a weaker response on d7 and d30 compared to HVs, both groups showed a similar response on d60 and d180, suggesting that the booster shot had a compensating effect (**Figure 2.3c**). We quantified the effect of the booster shot by estimating the odds ratio for showing an increase in HI titer by at least one titer level on d60 compared to d30, adjusting for relevant patient and experimental factors using our multivariable regression model (see **Methods**). Indeed, patients had higher odds for showing HI titer increase on d60 compared to d30 with an estimated OR = 1.26 (95% CI = [1.03, 1.54], $P = 0.022$). In comparison, HVs showed lower odds for HI titer increase on d60 than d30, although not significantly lower (OR = 0.75 [0.55, 1.03], $P = 0.080$). Nevertheless, the estimated odds ratios were significantly different from each other (Welch's test on log-transformed OR, $P < 10^{-3}$, see also **Figure 2.3d**). In summary, this suggests that the booster shot helped the patients in our study population to mount a stronger antibody response.

Whether HSCT patients benefit from a second influenza vaccine dose is still under debate. A significant booster effect has been observed for an AS03-adjuvanted H1N1 vaccine in 17 (Gueller et al., 2011) and in 26 HSCT patients (de Lavallade et al., 2011). For the same adjuvanted H1N1 vaccine, another study reported responses in 65 HSCT patients with two doses comparable to 138 healthy adults with a single dose (Mohty et al., 2011). A randomized trial in 65 HSCT patients vaccinated with a non-adjuvanted quadrivalent influenza vaccine did not detect a significant effect (Karras et al., 2013). However, the median time after transplantation was only one year (IQR 0.3–2 yrs) in this trial, while complete B-cell reconstitution can take up to two years (Williams and Gress, 2010; Ogonek et al., 2016). For comparison, our patient population had a median time after transplantation of four years (IQR 2–7 yrs). Taking these observations together suggests that the effect of a booster shot depends on both patient- and vaccine-specific factors.

2.5.4 Cross-reactivity between influenza strains

Both HSCT patients and HVs showed a significantly stronger vaccine response for influenza A/California (H1N1) and A/Texas (H3N2) in 2015/16 compared to the participants in 2014/15 (**Figure 2.3d**). It is unlikely that this effect is due to a higher fraction of patients under immuno-

suppressive treatment in 2014/15 since we corrected for immunosuppressants and observed this effect also in HVs. More likely, participants were primed by the vaccination in the previous season. However, we did not observe significantly different responses in B/Massachusetts titers between the two seasons (**Figure 2.3d**).

The stronger response in A/Texas titers in the first season compared to the second is surprising. A/Texas/50/2012 (H3N2) was part of the vaccine in 2014/15 but not in 2015/16, where it has been replaced with A/Switzerland/9715293/2013 (H3N2), suggesting a strong cross-reactivity between these two strains (**Figure 2.2a**). A/Texas/50/2012 and A/Switzerland/9715293/2013 differ in only 9-14 amino acids in their HA protein sequence ($\sim 98\%$ sequence identity according to GISAID sequences) (Kaufmann et al., 2017) and we observed a strong correlation between the respective HI titers (**Figure 2.2b**, Kendall's $\tau = 0.85$, $P < 10^{-15}$). Interestingly, vaccination with A/Texas in 2014/15 did not induce a comparable response in HI titers against A/Switzerland, but vaccination with A/Switzerland in 2015/16 induced similar or even higher HI titers against A/Texas (**Figure 2.2a**). Potentially, the seasonal vaccines differed in immunogenicity and cross-reactivity, or participants showed a stronger response for A/Texas in 2015/16 due to the priming effect.

In 2014/15, A/Switzerland-like and not A/Texas-like H3N2 strains dominated the Northern Hemisphere (European Centre for Disease Prevention and Control, 2016; D'Mello et al., 2015). The mismatch in vaccine composition and the antigenic difference between A/Texas and A/Switzerland resulted in low vaccine effectiveness and caused a comparably severe influenza season in 2014/15 (Chambers et al., 2015; European Centre for Disease Prevention and Control, 2016). In line with previous reports, we observed 80% of influenza A infections in 2014/15 and only 20% in 2015/16 (Table 3.2), which were all A/Switzerland (H3N2) infections.

We also observed some cross-reactivity between B/Massachusetts/2/2012 and B/Phuket/3073/2013 (both from the Yamagata lineage, $\sim 98\%$ HA sequence identity). Although B/Massachusetts was part of the vaccine in 2014/15 but not in 2015/16, where B/Phuket replaced it, there was no significant difference in the B/Massachusetts response between the two seasons for both HSCT patients and HVs (**Figure 2.3d**). Since we did not measure HI titers against B/Phuket, we could not investigate the correlation in HI titers between these two strains. However, the similar antibody response in both seasons suggests some cross-reactivity.

2.5.5 Regression analysis of HI titers yields higher precision in estimated effects

To investigate associations of patient factors with vaccine response (vaccine-induced increase in HI titers on d30/d60) and baseline titers (pre-vaccination titers on d0), we fitted a multivariable sequential regression model directly to the observed HI titer levels (see **Methods** and **Supplementary Methods** for details). HI titers were available for 135 patients against the three different influenza types (H1N1, H3N2, B), resulting in 405 baseline titers (pre-vaccination titers on d0), and 810 response titers (post-vaccination titers on d30 and d60). Since most influenza vaccine studies perform binary logistic regression on seroprotection and seroconversion cut-offs, we compared the results obtained by titer and binary regression.

An illustrative comparison between the binary and titer regression model is shown in **Figure 2.4a**. The effects inferred from binary logistic regression can be interpreted as an odds ratio between

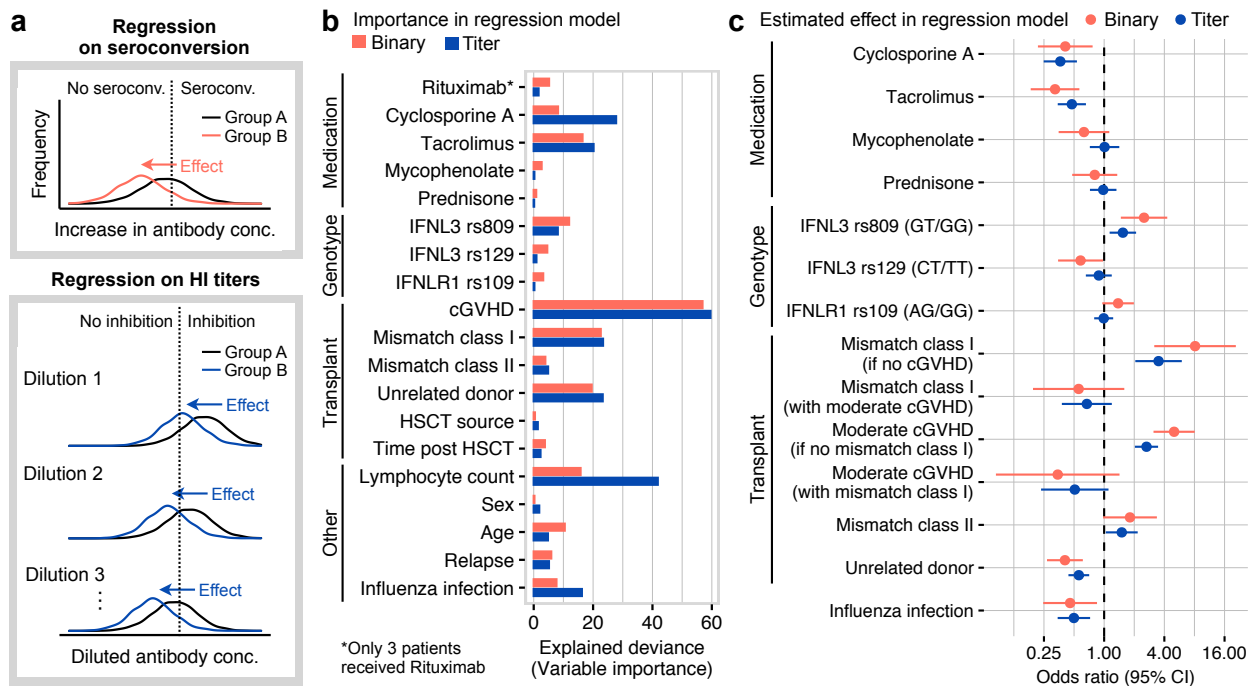


Figure 2.4. Host factors associated with vaccine response in HSCT patients.

(a) Illustrative explanation of the compared models: the commonly used binary regression model for seroconversion vs the sequential regression model for HI titers. An effect inferred from binary logistic regression can be interpreted as the odds ratio between groups A and B for showing seroconversion. In contrast, an effect inferred by the sequential regression model used in this study can be interpreted as the odds ratio for showing hemagglutination inhibition when hemagglutination inhibition has also been observed in all preceding dilution steps (i.e., increase in HI titer by at least one level). Alternatively, effects can also be interpreted as a shift in the underlying antibody concentration between the compared subpopulations. Since all patient serum samples are diluted equally, this shift is the same at all dilution steps (see **Supplementary Methods**). (b) Variable importance in terms of contribution to explained residual deviance of all investigated host factors. Results can only be compared within each model but not across models. (c) Estimated effects for important host factors. All inferred effects are shown in **Figure S2.5**.

an exposed (group A) and an unexposed population (group B) to show seroconversion (or seroprotection) (**Figure 2.4a**). For the titer regression model used here (Tutz, 1991), estimated effects are the odds ratio for hemagglutination inhibition at the same dilution step between groups A and B, when hemagglutination inhibition has also been observed in all preceding dilution steps, or in other words, for showing at least one level higher HI titers. Note that we corrected for baseline titers when analysing post-vaccination titers since we want to infer effects on the relative HI titer increase, which means that we compare patients with the same baseline titer levels. In general, in the multivariable setting, an inferred effect gives the odds ratio between groups A and B for showing a higher HI titer/seroconversion/seroprotection when all the other variables are held constant. Importantly, effects inferred by both models can also be interpreted as a shift in the underlying antibody concentration (**Figure 2.4a**) that gives rise to the observed HI titer or seroconversion/seroprotection category, respectively (see **Supplementary Methods**) (Agresti, 2003).

Consistent with the interpretation of both models, binary and sequential regression models yielded qualitatively similar results in all our analyses (**Figure 2.4b** and **Figure S2.8**). It has been previously

suggested that regression over titer categories using ordinal regression models (McCullagh, 1980, 2018) increases the power of serological studies compared to the regression on dichotomized outcomes (Capuano et al., 2007). Ordinal models account for the intrinsic order of the titer categories, but neglect that titers can only be reached successively step-by-step in a sequential process. In our study, titer regression with sequential models estimated effects with higher precision (**Figure 2.4c**, **Figure S2.6**, **Figure S2.10**) due to the higher resolution in patient's underlying antibody level, and the effects inferred by both approaches can be interpreted similarly, i.e., as a positive or negative shift in antibody concentration.

2.5.6 Association of host factors with vaccine response and baseline titers in HSCT patients

Finally, we identified the most important host factors determining vaccine response and baseline titers. We compared each host factor's contribution to the residual deviance in the respective multivariable regression model, which reflects how much this variable is needed to explain the observed variability in HI titers (**Figure 2.4b** and **Figure S2.8**).

The most important negative factors for vaccine response were an unrelated donor, an influenza infection, as well as cyclosporine A and tacrolimus treatment (**Figure 2.4c**, for all results see **Figure S2.5**). Interestingly, important positive factors were cGVHD and a donor mismatch in human leukocyte antigen (HLA) class I loci. In addition, increasing absolute lymphocyte counts were highly associated with stronger response.

For baseline titers, the time after transplantation was the most dominant association (**Figure 2.5a**). We also observed a positive association with lymphocyte count and negative associations for mycophenolate mofetil/sodium treatment, HLA class II mismatch, increasing age, and influenza infection (**Figure S2.9**).

In the following, we discuss the estimated effects of the various host factors separately.

2.5.6.1 Immunosuppressive treatment

Patients receiving calcineurin inhibitors, specifically cyclosporine A (OR = 0.36 [0.24, 0.53], $P = 2 \cdot 10^{-7}$) and tacrolimus (OR = 0.48 [0.34, 0.66], $P = 7 \cdot 10^{-6}$), showed lower odds for vaccine-induced HI titer increase. Calcineurin inhibitors suppress T-cell activation and have been previously reported to negatively affect influenza vaccine response in HSCT patients (Gueller et al., 2011; Roll et al., 2012; Fukatsu et al., 2017).

For mycophenolate mofetil/sodium, another immunosuppressive treatment to prevent graft rejection, we observed no significant effect on response but on baseline titers (OR = 0.49 [0.30, 0.78], $P = 0.003$). Mycophenolate inhibits the proliferation of T- and B-lymphocytes and suppresses cell-mediated immune responses (Allison and Eugui, 2005). Thus, mycophenolate treatment potentially affected the production of long-lived B cells in our patient population, needed for long-term production of antibodies. In general, treatment with mycophenolate mofetil (MMF) is a known risk factor for hypogammaglobulinemia (antibody counts below the normal range) (Arai et al., 2014). A previous study in 82 HSCT patients observed less seroprotection among patients receiving MMF, but the effect was not significant, perhaps due to small sample size or dichotomization (Issa et al., 2011).

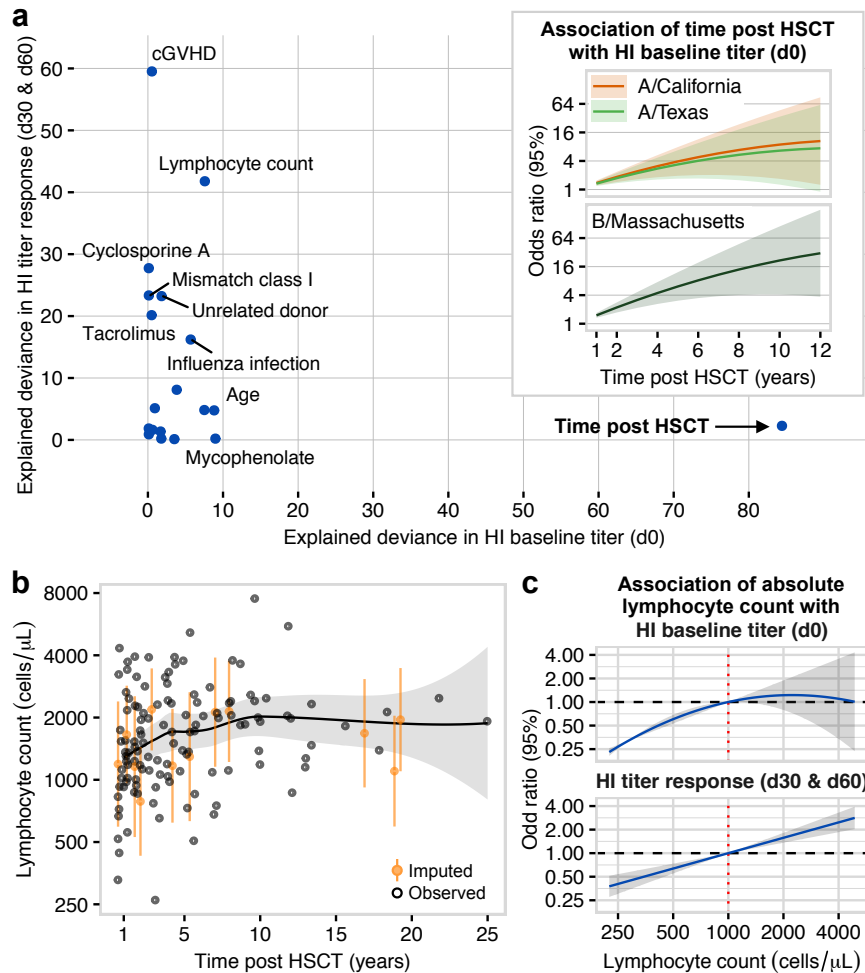


Figure 2.5. Association of time after HSCT and absolute lymphocyte count with vaccination outcomes. (a) Comparison of variable importance for explaining HI baseline titers (d0) vs HI titer response (d30 & d60). While multiple host factors affected vaccine response, baseline titers were mostly explained by the time post HSCT. The association of time post HSCT was significantly stronger for HI titers against B/Massachusetts compared to the influenza A strains ($P = 0.001$). There was no significant difference between A/California (H1N1) and A/Texas (H3N2) ($P = 0.340$). (b) Scatterplot showing lymphocyte counts by time after transplantation for the investigated HSCT patient population. For patients with missing values, data show the mean and standard deviation of imputed values. Data were fitted by a smoothing spline. (c) Association of absolute lymphocyte count with response and baseline titers. Normal lymphocyte counts range from 1000–4800 cells per μ L blood. Shaded area indicates 95% CI in all figures.

We detected no effect of prednisone on vaccine response, a corticosteroid suppressing inflammation, used to treat GVHD. However, our data indicate to a small positive association with baseline titers (OR = 1.54 [0.98, 2.42], $P = 0.060$). Previous HSCT studies reported a protective role of steroid use in influenza acquisition (Machado et al., 2005) and progression (Nichols et al., 2004). The authors hypothesized that steroid use could help patients restore local immunity (Machado et al., 2005). Additional studies with larger sample size are needed to confirm this positive effect. We were not able to investigate the effect of rituximab, a monoclonal anti-CD20 antibody targeting B cells. Only three patients received rituximab, in conjunction with other immunosuppressants (**Figure S2.1**).

2.5.6.2 *Time after transplantation*

The time after transplantation was not significantly associated with vaccine response, probably because we included only patients who received hematopoietic stem cells at least one year ago. Previous studies that observed a significant association also included patients with two (Mohty et al., 2011), three (Avetisyan et al., 2008), and six months (de Lavallade et al., 2011; Issa et al., 2011) post HSCT, whereas another study with a time-post-HSCT distribution like ours detected no significant effect (Fukatsu et al., 2017).

However, the time after transplantation was the most important predictor for pre-vaccination titer levels (**Figure 2.5a**). The association was significantly stronger for titers against B/Massachusetts compared to the influenza A strains (A/California and A/Texas (**Figure 2.5a**). Importantly, the average effect on HI titer increase of four years post HSCT (OR = 3.84 [2.47, 5.99], **Figure 2.5a**) was comparable to the average effect of vaccination on d60 (OR = 3.35 [2.77, 4.05], **Figure 2.3b**). Thus, HSCT patients can acquire seroprotective antibody levels over the years, probably by repeated influenza vaccinations.

2.5.6.3 *Absolute lymphocyte count*

Our patient population showed a large variability in absolute lymphocyte count (B, T, and NK lymphocytes) ranging from ~250–7500 cells per μL blood (**Figure 2.5b**). Patients with lymphocyte count below 1000 cells per μL showed both lower response and baseline titers. In contrast, patients with lymphocyte count above 1000 cells per μL showed a stronger response but not significantly different baseline titers (**Figure 2.5c**). Similarly, Engelhard et al. reported a significant association of absolute lymphocyte count with both seroconversion and seroprotection after vaccination in allogeneic HSCT patients vaccinated with an adjuvanted A/California (H1N1) vaccine (Engelhard et al., 2011).

In healthy adults, lymphocyte counts range from 1000–4800 cells per μL blood and correlate with absolute counts of B and T-helper cells, which are necessary for a potent antibody response (Valiathan et al., 2014). After HSCT, the innate immunity, including NK lymphocytes, recovers first (within weeks or months), whereas adaptive immunity, consisting of B and T lymphocytes, can take several years (Storek et al., 2008). Although B and T cells often reach normal counts within 1–2 yrs, the adaptive immunity can stay impaired for longer, e.g., due to slow recovery of the B- and T-cell repertoires and impaired cell-cell communication (Williams and Gress, 2010; Ogonek et al.,

2016). However, patients' vaccine responses were strongly associated with absolute lymphocyte count and not with the time after transplantation in our study population.

All other estimated effects were very similar when we excluded lymphocyte count from the multivariable regression model (**Figure S2.6**), showing that the other host-factor associations were statistically independent of lymphocyte count.

2.5.6.4 HLA mismatch

Surprisingly, we found a positive association with vaccine response for mismatch in HLA class I, but in conjunction with a strong negative interaction effect with cGVHD (OR = 0.44 [0.30, 0.65] per cGVD grade, $P = 4 \cdot 10^{-5}$). Thus, patients with a class I mismatch showed a stronger vaccine response than fully matched patients (OR = 3.50 [2.05, 5.98], $P = 4 \cdot 10^{-6}$), but only if they did not suffer from cGVHD (**Figure 2.4c**). The effect was weaker and not significant when we removed the interaction effect (OR = 1.44 [0.99, 2.04], $P = 0.059$), suggesting that this association highly depends on the patient's cGVHD state. However, only eleven patients in our study population had a class I mismatch, of which four had no cGVHD, and these small case numbers potentially introduce upward bias in the estimated effect (Greenland et al., 2016). We did not detect a significant interaction between cGVHD and class II mismatch (OR = 0.78 [0.56, 1.09], $P = 0.139$, $n = 5/14$ without cGVHD). Class II mismatch showed a weak positive association with response (OR = 1.50 [1.04, 2.17], $P = 0.030$) and a strong negative association with pre-vaccination titers (OR = 0.45 [0.25, 0.79], $P = 0.006$). However, both effects were unstable in our sensitivity analysis (**Figure S2.7**), suggesting that patients showed high heterogeneity in antibody titers that was not explained by our model. All associations were only marginally affected when we did not correct for an unrelated donor (**Figure S2.6**).

HLA class I and class II proteins are expressed on different cell types: while class I is expressed on all cells (except for red blood cells), class II is limited to antigen-presenting cells, such as B- and T-lymphocytes, macrophages and dendritic cells. Previous vaccine studies in HSCT patients mostly neglected the role of mismatch, probably due to the immense complexity and small study sizes. There is a consensus that a mismatch in one of the HLA class I loci (A, B, C) or in the class II locus DRB1 negatively affects transplantation outcomes (Petersdorf, 2013; Fürst et al., 2013; Tiercy, 2016). Class I mismatched patients have twice the mortality risk compared to fully matched patients (Passweg et al., 2015). In contrast, a mismatch in class II has either no significant or weaker effect, depending on the loci (Passweg et al., 2015). Our data suggest that class I vs class II mismatched patients are differently affected by cGVHD and might respond to vaccination differently. However, the classification of mismatches into only two categories does not fully capture the biological diversity, and additional donor factors, such as donor's age (Kollman et al., 2016), might also influence the patient's immune state. Studies with significantly larger sample sizes are needed to distinguish HLA mismatch effects on vaccine response.

2.5.6.5 Chronic GVHD

In contrast to the mismatch effect, the positive association with cGVHD was also significant without the interaction effect (OR = 1.63 [1.43, 1.86], $P = 7.7 \cdot 10^{-13}$ with mismatch interaction, OR =

1.53 [1.34, 1.75], $P = 1.6 \cdot 10^{-10}$ without). Our sensitivity analyses confirmed that this effect was very stable compared to the other effects (**Figure S2.5** and **Figure S2.7**).

The robust, positive association of cGVHD with vaccine response is puzzling. It raises the question of whether patients suffering from cGVHD have an overstimulated immune system that can boost vaccine response under certain circumstances. Several studies showed that patients with cGVHD show disturbed B-cell homeostasis and persistent B-cell activation (Sarantopoulos et al., 2007, 2009; Greinix et al., 2008; Jacobson et al., 2014). Vaccine studies reported mixed results, with either no significant effect of cGVHD (Pauksen et al., 2000; Issa et al., 2011; Engelhard et al., 2011; Gueller et al., 2011; Fukatsu et al., 2017), or a negative effect (Mohty et al., 2011; Dhédin et al., 2014; Roll et al., 2012). However, the results are not directly comparable: A study that determined active GVHD (acute GVHD of grade ≥ 2 or chronic extensive GVHD) as the main, negative determinant for vaccine response accounted for the time after transplantation and lymphocyte counts in a multivariable regression analysis, but not for immunosuppressive drug treatment (Mohty et al., 2011). In general, studies showing a negative effect investigated HSCT patients with a shorter transplantation-to-vaccination interval than in our patient population (Mohty et al., 2011; Dhédin et al., 2014; Roll et al., 2012). Another study with a time-post-HSCT distribution like ours detected no significant effect in a multivariable regression analysis. Thus, the effect of cGVHD might depend on the time after transplantation. In our study, cGVHD might also be confounded with repeated vaccinations, because patients with cGVHD are recommended to receive yearly influenza vaccination (Hilgendorf et al., 2011). However, patients with cGVHD did not show significantly higher baseline titers than patients without cGVHD (**Figure S2.10**). Since the patient's vaccination history was not available, we were not able to test this hypothesis.

In summary, the effect of cGVHD is probably modulated by other host factors. Future studies could try to resolve the reported conflicting results by investigating interaction effects for cGVHD, for instance, with time after transplantation or donor mismatch.

2.5.6.6 *Unrelated donor*

Having an unrelated donor was an important negative factor for vaccine response as previously reported (Engelhard et al., 2011). This effect was statistically independent of HLA mismatch (OR = 0.55, 95% = [0.44, 0.71], $P = 1.7 \cdot 10^{-6}$ when adjusted for mismatch, OR = 0.62 [0.50, 0.78], $P = 4.0 \cdot 10^{-5}$ when unadjusted).

The definition of HLA matching depends on the resolution of HLA typing. The gold standard is matching in 10 HLA loci (10/10 match). However, more than 14,000 HLA alleles have been identified accounting for >10,000 HLA proteins, making histocompatibility matching extremely challenging (Tiercy, 2016). Our and previous results suggest that the diversity in HLA proteins has negative consequences for the vaccine response in HSCT patients with an unrelated donor (Engelhard et al., 2011).

2.5.6.7 *Disease state and HSCT source*

Patients with relapse showed a significantly weaker vaccine response than patients in complete remission (OR = 0.68 [0.47, 0.99], $P = 0.043$). However, the effect was small and unstable

(**Figure S2.5**), indicating that the missing entries on the disease state in 25% of the patients hampered the analysis.

There was no significant association with transplant source (peripheral blood stem cells vs bone marrow), but only twelve patients (9%) received bone marrow stem cells.

2.5.6.8 Sex and age

Consistent with previous studies (Issa et al., 2011; Gueller et al., 2011), sex and age played only a minor role for vaccination outcomes in our patient population (**Figure 2.4b** and **Figure S2.8**). Nevertheless, we observed some weak associations. Female patients showed slightly higher odds for vaccine-induced HI titer increase, although not significantly higher (OR = 1.30 [0.96, 1.77], $P = 0.092$). In healthy adults, females often have significantly stronger immune responses to vaccination and infection (Furman et al., 2014; Klein and Flanagan, 2016), but sex differences in HSCT patients have not yet been reported. Increasing age was negatively associated with pre-vaccination titers (OR = 0.81 [0.71, 0.93] for a 10-year difference in age, $P = 0.002$). Immunosenescence affects the adaptive immune system, particularly B cells (Aw et al., 2007; Siegrist and Aspinall, 2009). While the effect of age on vaccine response is well studied in healthy adults (Goodwin et al., 2006; Smetana et al., 2018), it has not yet been reported for HSCT patients.

2.5.6.9 Donor's *IFNL3* genotype

Interestingly, we observed a positive association of the *IFNL3* rs8099917 minor allele (GT/GG) with response (OR = 1.54 [1.13, 2.09], $P = 0.006$) and baseline titers (OR = 1.55 [1.00, 2.40], $P = 0.050$). The other investigated genotypes showed no significant associations (**Figure 2.4c**). However, since all patients carrying the rs8099917 minor allele also carried the *IFNL3* rs12979860 minor allele (CT/CC), the positive association could also be due to an interaction effect between these two genotypes.

Both rs8099917 and rs12979860 genotypes gained prominence in recent years because several studies reported an association with IFN- α treatment and spontaneous clearance of hepatitis C virus (HCV) (Thomas et al., 2009; Tanaka et al., 2009; Ge et al., 2009; Suppiah et al., 2009; Sheahan et al., 2014; Bruening et al., 2017). A study in solid organ transplant patients demonstrated that patients carrying the *IFNL3* rs8099917 minor-allele had lower IFN- λ expression and were more likely to be seroconverted after influenza vaccination (Egli et al., 2014b). Recent studies showed that IFN- λ directly modulates B-cell proliferation (Syedbasha et al., 2020) and has adjuvant effects in mice for influenza vaccination (Ye et al., 2019). However, the mechanistic role of IFN- λ in vaccine response is still unknown.

2.5.6.10 Influenza infection

There were only nine patients with a PCR-confirmed influenza infection. Nevertheless, we observed a stable and significant negative association with both response (OR = 0.50 [0.34, 0.72], $P = 3 \cdot 10^{-4}$) and baseline titers (OR = 0.55 [0.32, 0.94], $P = 0.030$), confirming that low antibody levels increase the risk for influenza infection.

2.5.7 Patients with local side effects show stronger vaccine response

No serious adverse events were reported. Patients from all centers except from Bern documented the occurrence of local side effects one week after each vaccination (**Table 2.2**). In total, 46/118 (39%) patients reported any side effect on d7 and 41/118 (35%) on d37. The most frequent event was pain, followed by swelling, redness and warm skin (**Table 2.2**). Patients reporting any local side effect on d7 had a stronger HI titer increase on d30 compared to patients without side effects (OR = 1.72 [1.26, 2.35], $P = 7 \cdot 10^{-4}$ for imputed data; OR = 1.72 [1.24, 2.40], $P = 0.001$ for complete case analysis), and analogously, patients with any side effect on d37 showed stronger response on d60 (OR = 1.66 [1.23, 2.25], $P = 0.001$ for imputed data; OR = 1.81 [1.30, 2.52], $P = 5 \cdot 10^{-4}$ for complete case analysis).

Table 2.2. Reported local side effects by HSCT patients (n = 118). Questionnaires on side effects were not available for patients from Bern.

Side Effect	Count on day 7	Count on day 37
Pain	38 (32%)	32 (27%)
Swelling	26 (22%)	16 (14%)
Warm skin	21 (18%)	14 (12%)
Redness	20 (17%)	16 (14%)
Restricted arm movement	11 (9%)	12 (10%)
Itching	9 (8%)	11 (9%)
Any	46 (39%)	41 (35%)

We investigated the association of each side effect in a multivariable regression analysis to identify the best predictors (**Figure S2.4**). Our results suggest that patients experiencing redness and pain on d7 or d37 might respond more on d30 or d60, respectively (**Figure S2.4**). However, only the association for redness on d37 was significant (OR = 1.98 [1.22, 3.21], $P = 0.005$), probably because our sample size was too small.

2.6 CONCLUSION

HSCT patients show a highly heterogeneous influenza vaccine response that can be partially explained by easily accessible host factors, such as absolute lymphocyte count or the type of immunosuppressive treatment. Factors related to the donor, such as family relationship, mismatch, and IFN- λ genotype, are potentially additional modulating factors that have not been sufficiently investigated yet. Additionally, the conflicting results on the effect of cGVHD suggest that interaction effects between host factors might need to be taken into account in future studies. However, since HSCT patients are rare, pooled studies are probably needed to reach adequate sample sizes for the investigation of such interactions.

This study shows that sequential regression models for HI titers are a compelling alternative to the commonly used binary regression on seroconversion/seroprotection for identifying determinants of serological outcomes. The gain in precision of estimated effects is particularly large for small case numbers per treatment or other exposure categories, frequently the case for HSCT patients or other heterogeneous patient populations. Therefore, we hope to encourage future studies to apply sequential regression models directly on HI titers. However, if observations for some titer categories are sparse, adjacent titer categories need to be grouped together. Both approaches, binary and titer regression, can suffer from the sparse data bias, and additional strategies, such as penalization, might be required in extreme cases (Greenland et al., 2016; Mansournia et al., 2018).

On average, HSCT patients benefited from the booster shot and showed comparable responses after two vaccine doses as healthy volunteers after one. Importantly, the strong association of the time after transplantation with pre-vaccination titers shows that HSCT patients can acquire durable antibody levels over the years. However, lymphocyte counts below the normal range, an unrelated donor, or calcineurin inhibitors — frequently used to prevent GVHD — lower the odds of responding. Moreover, treatment with mycophenolate or a mismatch in HLA class II seem to reduce long-term antibody production. Thus, although the current standard of care approach induces potent vaccine responses in some HSCT patients, patients belonging to the poorly responding groups might benefit from additional, more targeted preventive strategies.

CONFLICT OF INTERESTS

None.

AUTHOR CONTRIBUTIONS

Study design and conceptualization: AE, JS, JH. Funding acquisition: AE, JS. Experiments: MS, DV, LK. Data management and data curation: DV, YH, AMSM, JL. Methodology and formal analysis: JL, HMK. Code implementation: JL. Administration and resources: AE, JS, JH, NC, SR, US, TP, GS, MW. Supervision: JS, AE, HMK. Writing the first draft: JL. Reviewing and editing: all.

ACKNOWLEDGMENTS

We thank all participants for their support and participation. We thank Kathrin Ullrich for her technical support with patient samples. AE was supported by SNSF Ambizione Score (PZ00P3_154709), Forschungsfond University of Basel, Bangerter-Rhyner Stiftung, and Stiftung Infektionskrankheiten Basel. AE, JS and JL acknowledge support by an iPhD fellowship of the SystemsX program evaluated by the Swiss National Science Foundation (9th call).

2.7 SUPPLEMENTARY TABLES

Table S2.1. Overview of genotypes in the investigated HSCT patient population (n = 135). The respective homozygous major allele is highlighted in gray. Only the first three SNPs were included in the final analysis.

Gene	SNP ID	Allele	2014/15	2015/16	All
<i>IFNL3/4</i>	rs8099917	TT	32 (58%)	53 (66%)	85 (63%)
		GT	22 (40%)	16 (20%)	38 (28%)
		GG	1 (2%)	11 (14%)	12 (9%)
<i>IFNL3/4</i>	rs12979860	CC	20 (36%)	40 (50%)	60 (44%)
		CT	32 (58%)	31 (39%)	63 (47%)
		TT	3 (5%)	9 (11%)	12 (9%)
<i>IFNLR1</i>	rs10903035	AA	30 (55%)	36 (45%)	66 (49%)
		AG	20 (36%)	32 (40%)	52 (39%)
		GG	5 (9%)	12 (15%)	17 (13%)
<i>IFNL3/4</i>	rs10853727	TT	46 (84%)	65 (81%)	111 (82%)
		CT	9 (16%)	15 (19%)	24 (18%)
		CC	0	0	0
<i>IFNA1</i>	rs28383797	GG	51 (93%)	77 (96%)	128 (95%)
		AG	2 (4%)	3 (4%)	5 (4%)
		AA	2 (4%)	0	2 (1%)
<i>IL4</i>	rs2243248	TT	46 (84%)	68 (85%)	114 (84%)
		GT	9 (16%)	11 (14%)	20 (15%)
		GG	0	1 (1%)	1 (1%)
<i>IL6</i>	rs2069824	TT	46 (84%)	63 (79%)	109 (81%)
		CT	9 (16%)	15 (19%)	24 (18%)
		CC	0	2 (2%)	2 (1%)

Table S2.2. Number of patients with cGVHD by donor relationship/mismatch.

	With cGVHD	Without cGVHD	NA	Total
Related donor	32	35	3	70
Unrelated donor	28	36	1	65
Fully matched	47	54	4	105
Mismatched	13	17	0	30
Total	60	71	4	135

Table S2.3. Overview of missing data in the investigated HSCT patient population (n = 135). HI titers on d0 were available for all patients and all influenza strains.

Variable	Missing entries	Imputation R ²
Patient variables		
Influenza infection	36 (27%)	0.83
Remission state	34 (25%)	0.84
Lymphocyte count	12 (9%)	0.78
cGVHD grade	4 (3%)	0.85
Mycophenolate treatment	1 (1%)	0.71
Mismatch type	4 (3%)	0.95
HI titers		
California titer on d30	1 (1%)	0.97
Massachusetts titer on d30	1 (1%)	0.98
Texas titer on d30	1 (1%)	0.99
California titer on d60	5 (4%)	0.96
Massachusetts titer on d60	5 (4%)	0.98
Texas titer on d60	5 (4%)	0.99
Side effects*		
Restricted arm movement on d7	14 (12%)	0.97
Pain on d7	14 (12%)	0.96
Reddness on d7	13 (11%)	0.98
Swelling on d7	13 (11%)	0.98
Warm skin on d7	13 (11%)	0.99
Itching on d7	13 (11%)	0.97
Restricted arm movement on d37	16 (14%)	0.91
Pain on d37	15 (13%)	0.88
Reddness on d37	15 (13%)	0.99
Swelling on d37	15 (13%)	1.00
Warm skin on d37	15 (13%)	0.95
Itching on d37	15 (13%)	0.95

*n = 118, patients from Bern excluded.

Table S2.4. Seroprotection (SP) and seroconversion (SC) in HSCT patients and healthy volunteers.

Patients received two doses of the seasonal influenza vaccine (on d0 and d30), healthy volunteers only one (on d0). Non-responders are defined as being not seroprotected on d0 (HI titer < 40) and showing no increase in HI titer on d7, d30 or d60.

HSCT patients										
	Season 2014/15					Season 2015/16				
	d0	d7	d30	d60	d180	d0	d7	d30	d60	d180
Total	55	52	55	55	55	80	71	79	75	74
A/California/2009 (H1N1)										
SP	26 (47%)	30 (58%)	36 (65%)	37 (67%)	33 (60%)	30 (38%)	37 (52%)	54 (68%)	57 (76%)	50 (68%)
SC	0 (0%)	6 (12%)	13 (24%)	14 (25%)	5 (9%)	0 (0%)	12 (17%)	35 (44%)	40 (53%)	32 (43%)
Non-responder: 5 (9%)					Non-responder: 7 (9%)					
B/Massachusetts/2012 (Yamagata lineage)										
SP	21 (38%)	23 (44%)	32 (58%)	33 (60%)	32 (58%)	21 (26%)	32 (45%)	42 (53%)	42 (56%)	36 (49%)
SC	0 (0%)	9 (17%)	19 (35%)	21 (38%)	17 (31%)	0 (0%)	13 (18%)	29 (37%)	34 (45%)	25 (34%)
Non-responder: 10 (18%)					Non-responder: 11 (14%)					
A/Texas/2012 (H3N2)										
SP	19 (35%)	24 (46%)	33 (60%)	36 (65%)	31 (56%)	33 (41%)	43 (61%)	55 (70%)	57 (76%)	46 (62%)
SC	0 (0%)	8 (15%)	21 (38%)	24 (44%)	18 (33%)	0 (0%)	18 (25%)	41 (52%)	43 (57%)	34 (46%)
Non-responder: 6 (11%)					Non-responder: 2 (2%)					
A/Switzerland/2013 (H3N2)										
SP	7 (13%)	14 (27%)	21 (38%)	22 (40%)	19 (35%)	17 (21%)	34 (48%)	51 (65%)	54 (72%)	42 (57%)
SC	0 (0%)	6 (12%)	17 (31%)	21 (38%)	19 (35%)	0 (0%)	21 (30%)	47 (59%)	50 (67%)	42 (57%)
Non-responder: 9 (16%)					Non-responder: 4 (5%)					
B/Brisbane/2008 (Yamagata lineage)										
SP	4 (7%)	5 (10%)	8 (15%)	9 (16%)	7 (13%)	3 (4%)	4 (6%)	17 (22%)	15 (20%)	21 (28%)
SC	0 (0%)	2 (4%)	7 (13%)	6 (11%)	3 (5%)	0 (0%)	8 (11%)	23 (29%)	25 (33%)	25 (34%)
Non-responder: 25 (45%)					Non-responder: 26 (32%)					
Healthy volunteers										
	Season 2014/15					Season 2015/16				
	d0	d7	d30	d60	d180	d0	d7	d30	d60	d180
Total	25	25	25	25	25	44	44	44	44	44
A/California/2009 (H1N1)										
SP	7 (28%)	13 (52%)	13 (52%)	13 (52%)	14 (56%)	26 (59%)	43 (98%)	43 (98%)	43 (98%)	37 (84%)
SC	0 (0%)	4 (16%)	5 (20%)	5 (20%)	4 (16%)	0 (0%)	14 (32%)	15 (34%)	11 (25%)	6 (14%)
Non-responder: 3 (12%)					Non-responder: 0					
B/Massachusetts/2012 (Yamagata lineage)										
SP	16 (64%)	20 (80%)	20 (80%)	19 (76%)	19 (76%)	22 (50%)	32 (73%)	33 (75%)	31 (70%)	26 (59%)
SC	0 (0%)	2 (8%)	3 (12%)	3 (12%)	2 (8%)	0 (0%)	6 (14%)	5 (11%)	6 (14%)	1 (2%)
Non-responder: 3 (12%)					Non-responder: 3 (7%)					
A/Texas/2012 (H3N2)										
SP	4 (16%)	8 (32%)	9 (36%)	7 (28%)	5 (20%)	22 (50%)	38 (86%)	39 (89%)	38 (86%)	35 (80%)
SC	0 (0%)	4 (16%)	5 (20%)	3 (12%)	3 (12%)	0 (0%)	16 (36%)	24 (55%)	20 (45%)	11 (25%)
Non-responder: 2 (8%)					Non-responder: 0					
A/Switzerland/2013 (H3N2)										
SP	1 (4%)	1 (4%)	1 (4%)	1 (4%)	1 (4%)	6 (14%)	36 (82%)	38 (86%)	35 (80%)	30 (68%)
SC	0 (0%)	4 (16%)	6 (24%)	3 (12%)	1 (4%)	0 (0%)	22 (50%)	32 (73%)	30 (68%)	21 (48%)
Non-responder: 9 (36%)					Non-responder: 0					
B/Brisbane/2008 (Yamagata lineage)										
SP	0 (0%)	0 (0%)	0 (0%)	0 (0%)	0 (0%)	3 (7%)	7 (16%)	11 (25%)	9 (20%)	7 (16%)
SC	0 (0%)	1 (4%)	0 (0%)	0 (0%)	0 (0%)	0 (0%)	11 (25%)	16 (36%)	10 (23%)	5 (11%)
Non-responder: 17 (68%)					Non-responder: 9 (20%)					

2.8 SUPPLEMENTARY FIGURES

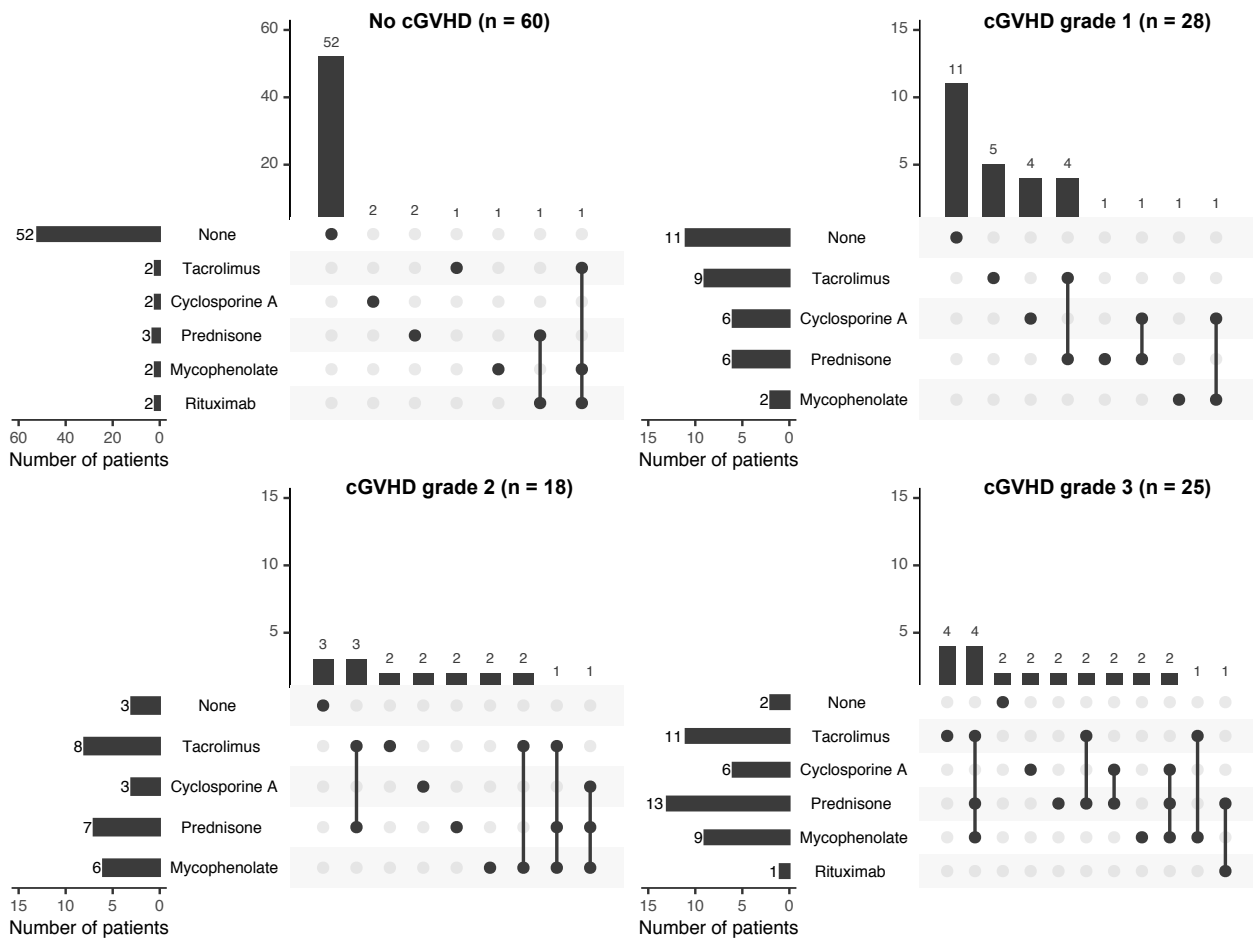


Figure S2.1. Number of patients with immunosuppressive drug treatment stratified by cGVHD grade. Numbers on top of the barplots show the number of patients in each intersection/subset that is specified by the diagram below.

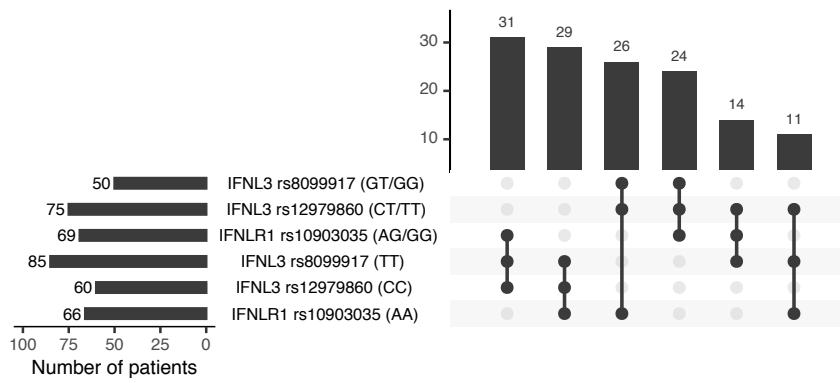


Figure S2.2. Distribution of investigated SNPs in the study population.

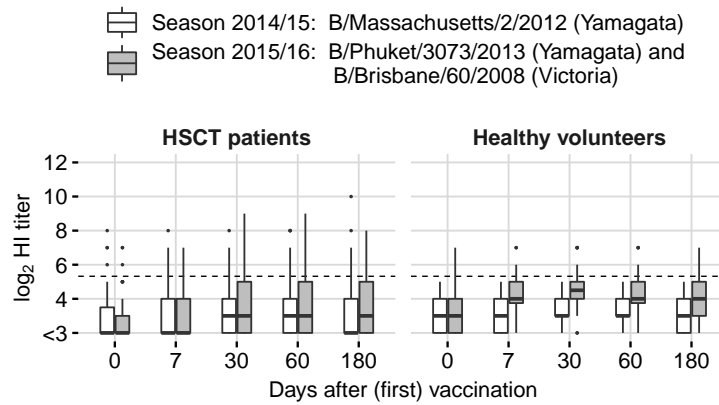


Figure S2.3. HI titers against B/Brisbane/60/2008. HI titers were low in both seasons, even though the vaccine comprised the B/Brisbane strain in the second season.

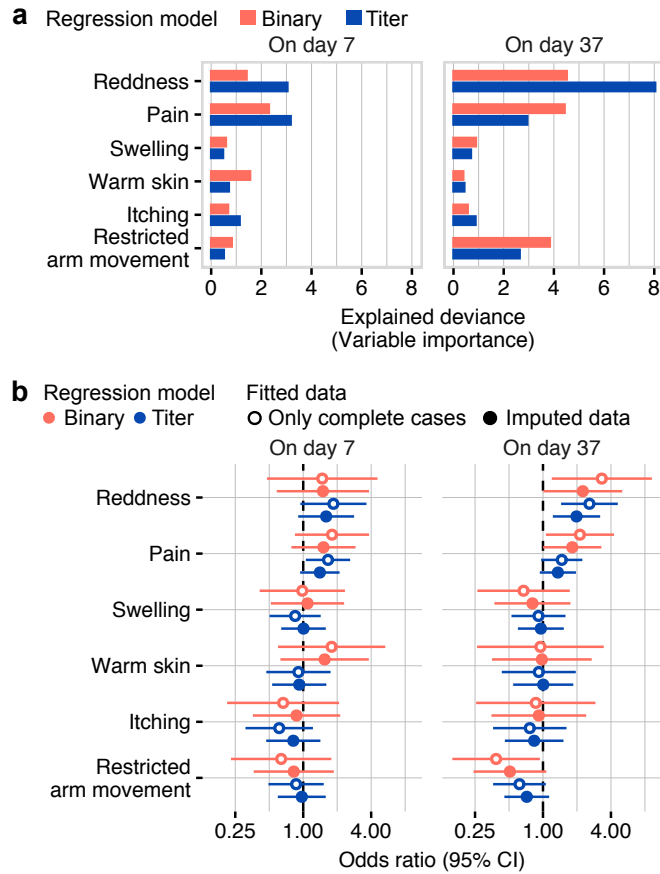


Figure S2.4. Association of local side effects with vaccine response. Side effects were documented one week after each vaccination (d7, d37), and associations were investigated with HI titer increase (titer regression) and seroconversion (binary regression) on d30 and d60, respectively. **(a)** Contribution of each side effect to the explained deviance. Results can only be compared within each model but not across models. **(b)** Estimated associations inferred from all data with imputed missing values ($n = 118$) and only from complete cases ($n = 103/102$ on d7/d37).

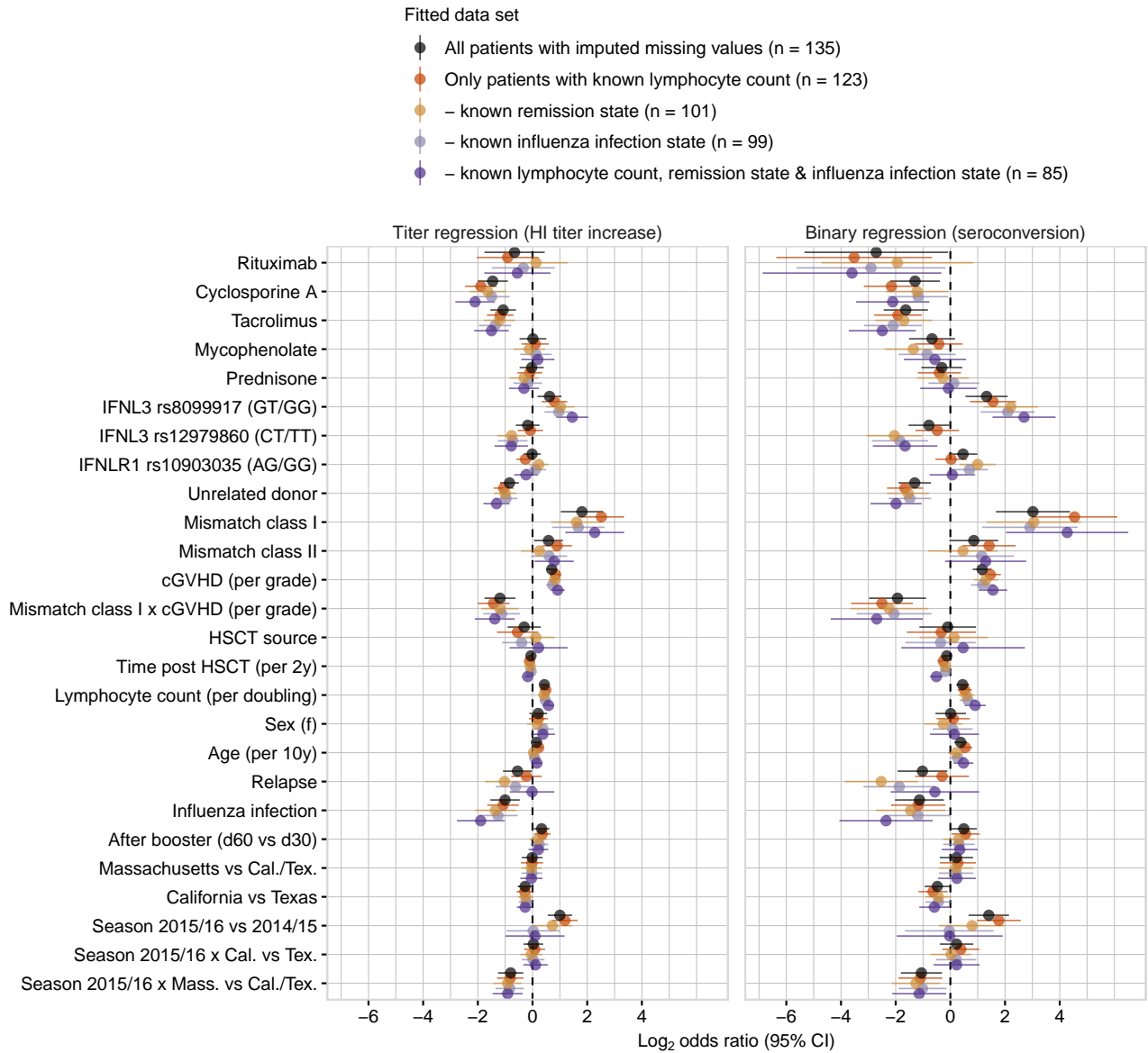


Figure S2.5. Comparison between estimated effects inferred from imputed vs complete data for the pooled HI titer response/seroconversion on d30 and d60 (vaccine response).

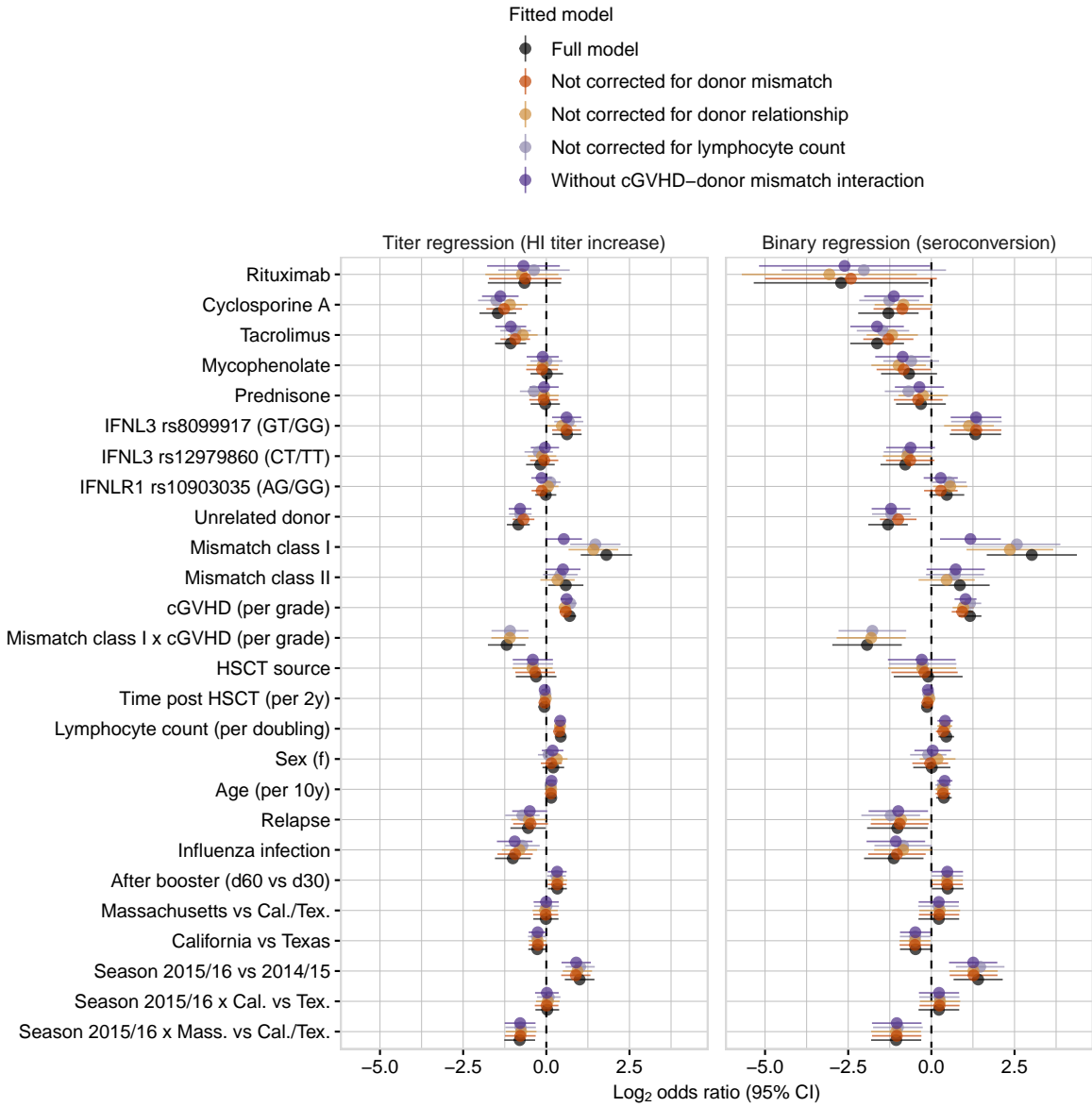


Figure S2.6. Comparison between estimated effects inferred by the full vs reduced models for vaccine response.

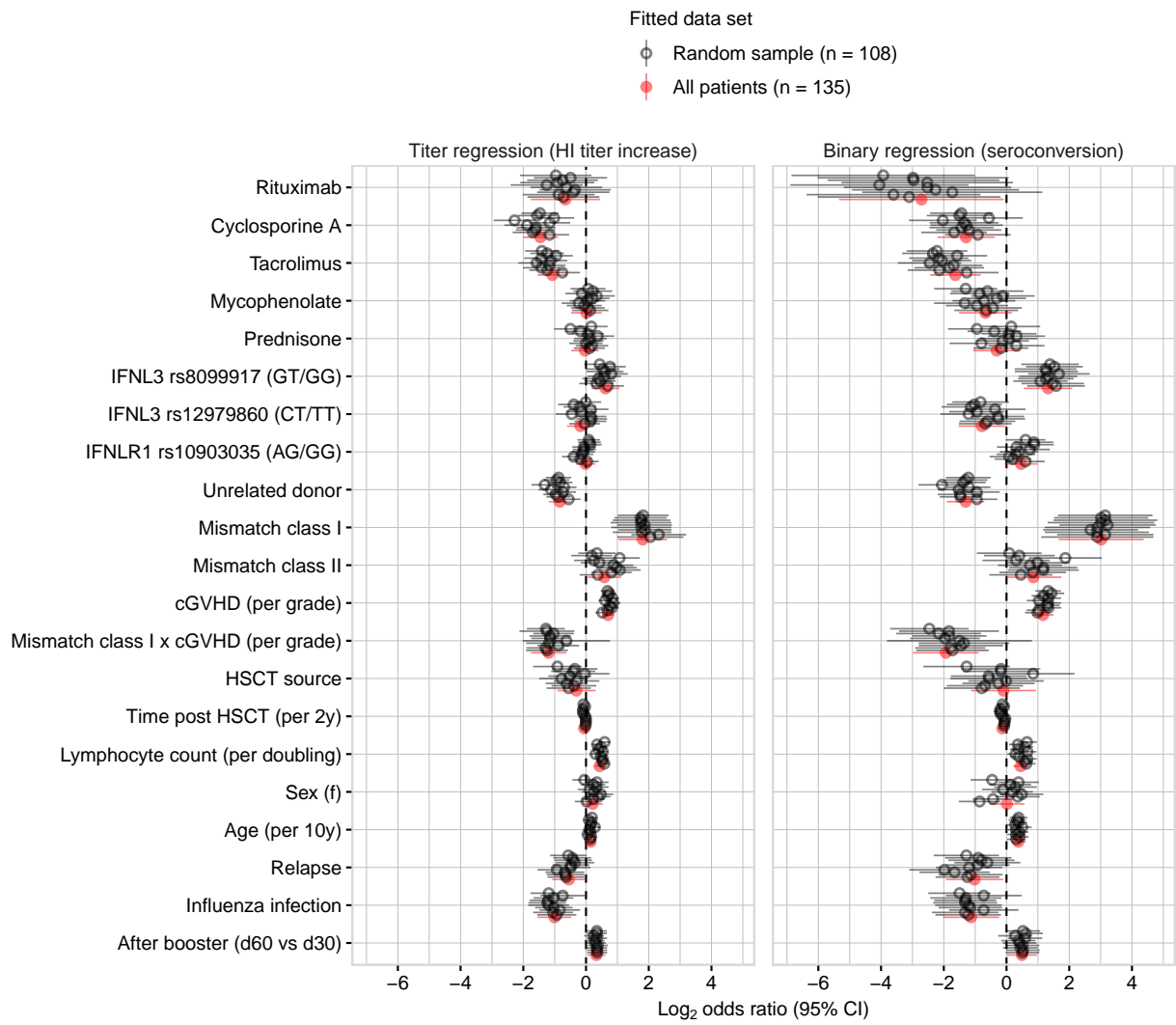


Figure S2.7. Sensitivity analysis to investigate the stability of estimated effects on vaccine response.

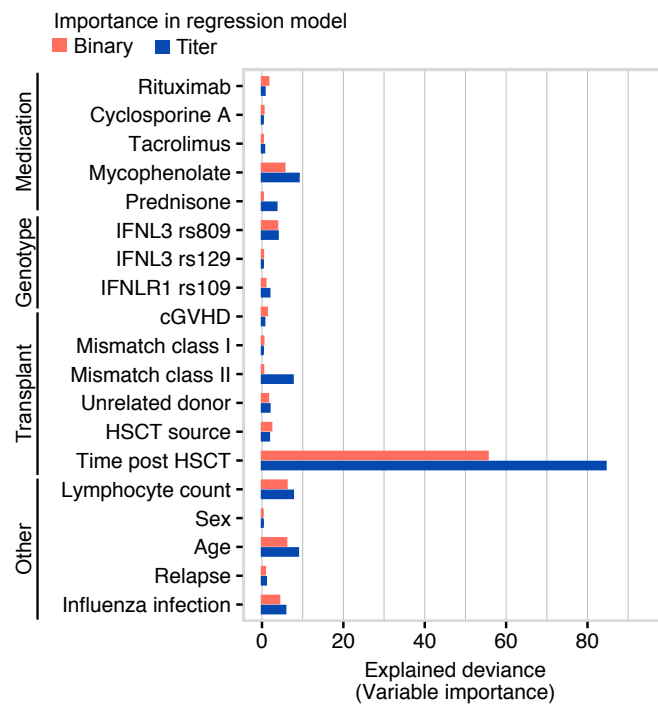


Figure S2.8. Explained deviance by investigated host factors for HI baseline titers (titer regression) and seroprotection on d0 (binary regression). Results can only be compared within each model but not across models.

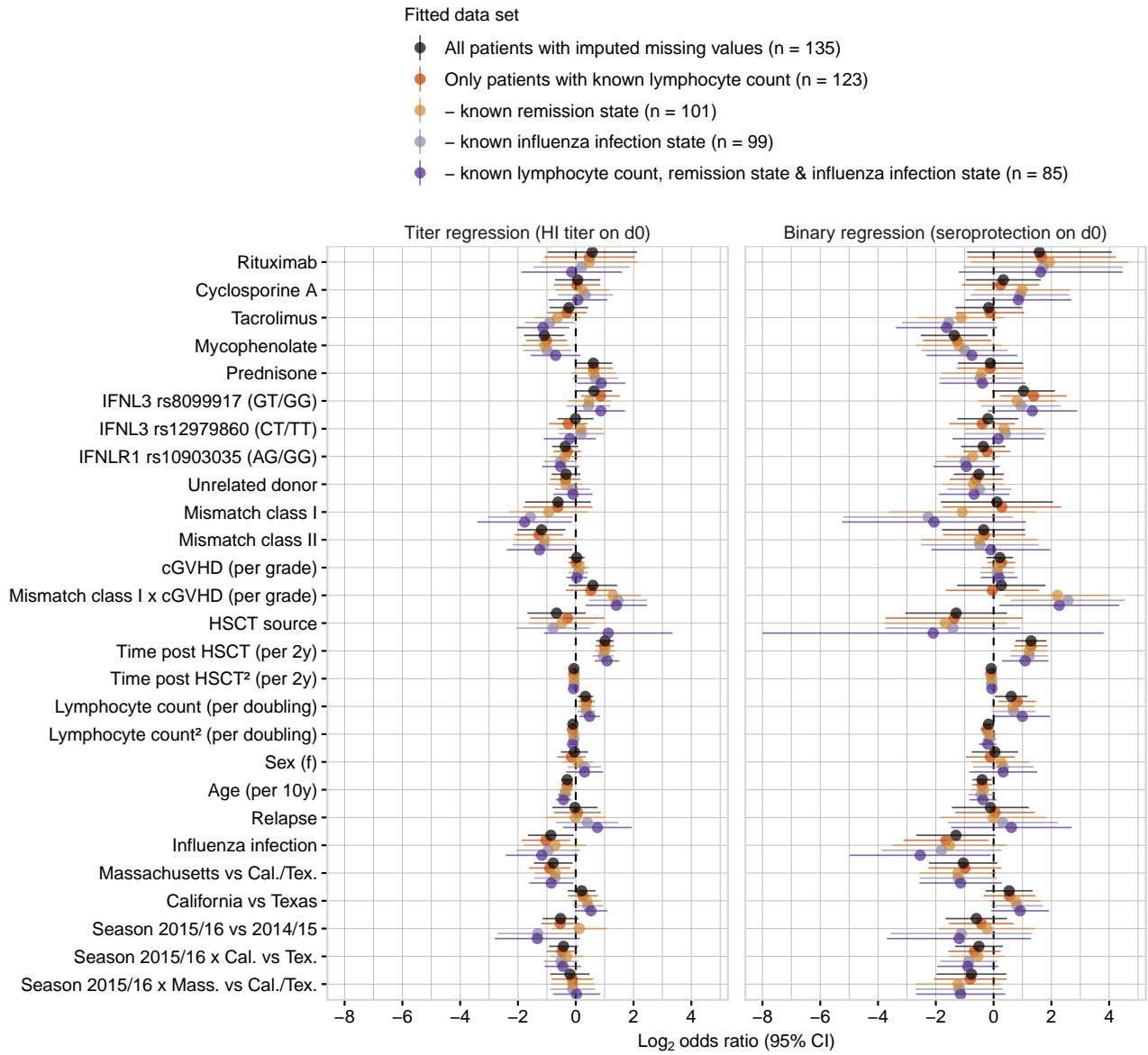


Figure S2.9. Comparison between estimated effects inferred from imputed vs complete data for baseline titers.

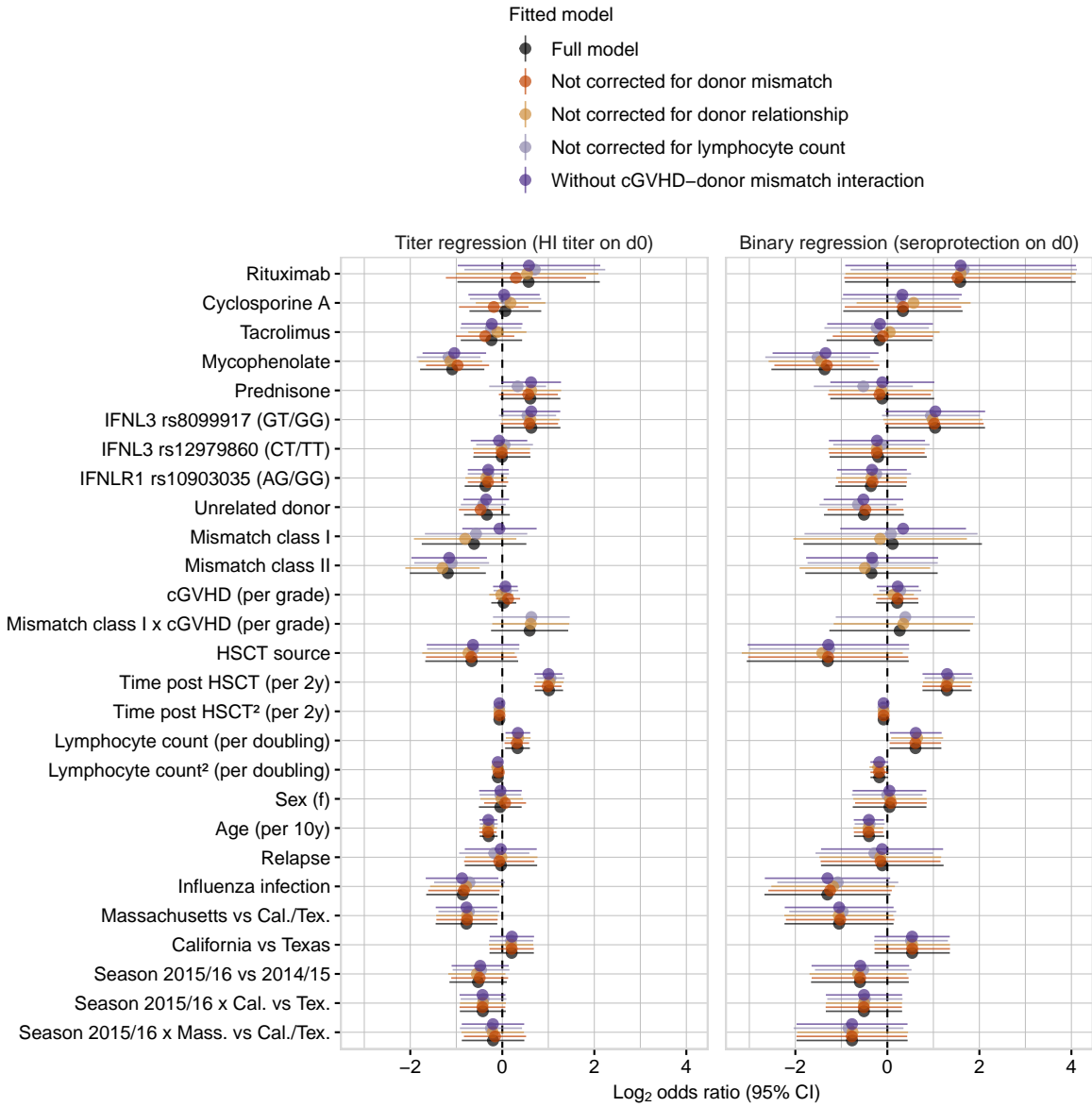


Figure S2.10. Comparison between estimated effects inferred by the full vs reduced models for baseline titers.

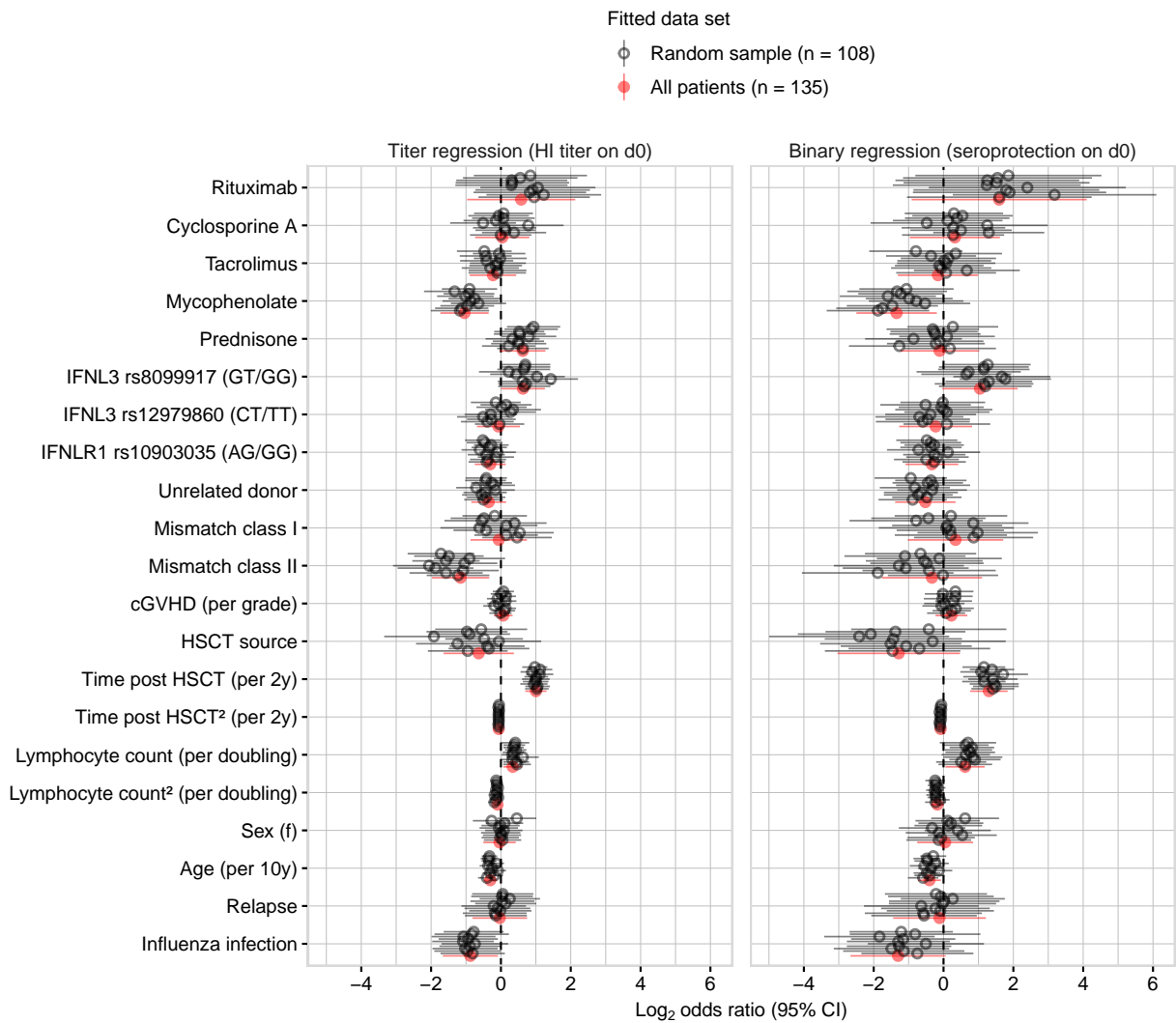


Figure S2.11. Sensitivity analysis to investigate the stability of estimated effects for baseline titers.

2.9 SUPPLEMENTARY METHODS

2.9.1 *Sequential models for regression of influenza antibody titers*

Sequential models have been introduced in categorical regression to model response categories that are reached successively step-by-step (Cox, 1988; Tutz, 1991). Since then, sequential models have been applied in social sciences, e.g., to model educational levels or career development (Liu et al., 2011). In biology and medicine, these models remain largely unknown, although serial dilution data obtained in biological assays and many clinical response categories can be explained by an underlying sequential process, for instance, by an increase in concentration.

Antibody titers serve as a coarse-grained measure of antibody abundance in serum samples. In general, titers are obtained from serial dilution experiments and correspond to the minimal dilution of antibodies that is still able to perform certain biological functions, for instance, virus neutralization or hemagglutination inhibition. As of today, the standard approach to analyse antibody titers is based on dichotomization using predefined cut-off values that classify outcomes in responders and non-responders, such as seroconversion or seroprotection. It has been demonstrated that this loss of information can lead to undetected effects, especially when the sample size is small (Scott et al., 1997; Capuano et al., 2007). For optimal cut-off values, regression on dichotomized outcomes can perform similarly to regression on the full information (Fedorov et al., 2009). However, since cut-offs are chosen by convention, they might not achieve optimal power (Armstrong and Sloan, 1989). The ordinal logistic regression model (also known as the proportional odds model or cumulative odds model) (McCullagh, 1980; Agresti, 2003) has been previously proposed to analyse antibody titers for swine influenza and has been shown to have superior power compared to binary logistic regression (Capuano et al., 2007). The ordinal model takes into account that the analysed categories have an intrinsic order but neglects the underlying sequential process, i. e., that titer categories can only be reached successively. The application of sequential models in titer regression has not yet been reported, although it captures the measurement process more accurately. Therefore, we briefly illustrate how sequential models can be interpreted in antibody titer regression.

2.9.1.1 *The measurement process*

Antibody titers against influenza virus are commonly determined in hemagglutination inhibition (HI) assays (WHO, 2002). This assay is based on the observation that influenza viruses can cross-link red blood cells (RBCs) to macroscopic aggregates (Hirst, 1941). This process is called hemagglutination. If a sufficient amount of influenza-binding antibodies is present, hemagglutination is inhibited. To determine the HI titer, a serum sample with an unknown antibody concentration is serially diluted, normally two- or ten-fold, and a constant amount of influenza virus and RBCs is added to each dilution. By definition, the dilution factor of the last serum dilution that is still able to fully inhibit hemagglutination is the HI titer (WHO, 2002). Thus, the HI titer is a coarse-grained measure of influenza-binding antibodies, whose values are restricted to the considered serum dilutions.

In the following, we derive a regression model for HI titers based on the assumption that the unobserved antibody concentration gives rise to the observed antibody titer.

2.9.1.2 Regression model

The HI assay can be interpreted as follows: At each serum dilution step, there is a certain probability that hemagglutination inhibition occurs. We assume that the main factor that drives this process is the amount of influenza-binding antibodies in the considered serum sample. Factors related to the experimental design, such as the amount of virus, RBCs, or temperature, are ideally constant over all measurements, or we can correct for them (batch effects). We aim at identifying factors that are associated with the antibody concentration in the investigated sera, such as the type of vaccine or the vaccine antigen, and patient-specific factors such as age, gender, or medical treatment.

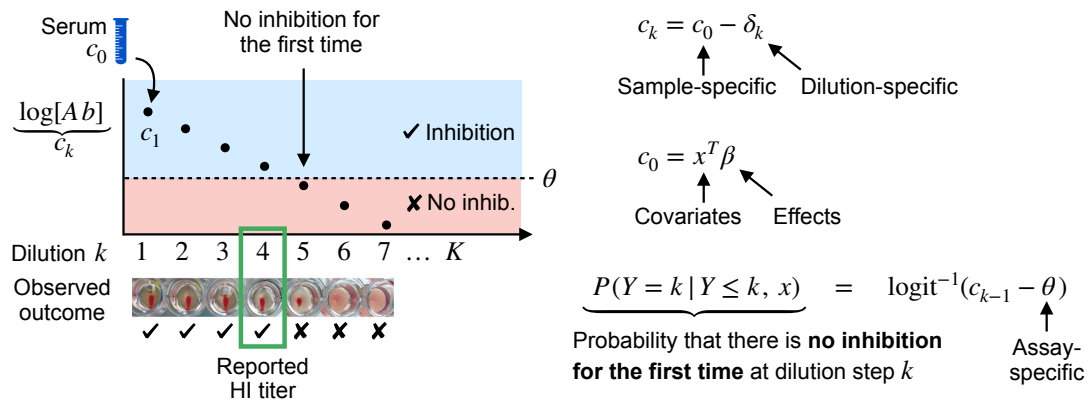


Figure S2.12. Overview of the HI assay and the regression model for HI antibody titers.

Let c_0 denote the logarithm of the undiluted and unobserved antibody concentration that gives rise to the observed HI titer, and let $x^T = (x_1, \dots, x_p)$ denote a vector of explanatory variables that determine the antibody concentration. We assume that c_0 is related to x through a linear model of the form $c_0 = x^T \beta$, where β is a vector of parameters $\beta^T = (\beta_1, \dots, \beta_p)$. To determine the HI titer, a dilution series of the antibody concentration c_0 is performed and each dilution is tested for hemagglutination inhibition. Let c_k denote the logarithm of the diluted antibody concentration at dilution step $k = 1, \dots, K$. With each dilution step, c_0 decreases by a dilution-specific factor δ_k :

$$c_k = c_0 - \delta_k. \quad (2.1)$$

We assume that hemagglutination inhibition occurs at dilution step k if c_k is above an unknown threshold θ that is specific to the assay (**Figure S2.12**):

$$\begin{aligned} &\text{Inhibition if } c_k > \theta, \\ &\text{No inhibition if } c_k \leq \theta. \end{aligned}$$

The assay stops when no hemagglutination inhibition occurs for the first time and the dilution factor of the preceding dilution is reported as the HI titer (**Figure S2.12**). We observe no inhibition for

the first time at dilution step k if $c_k \leq \theta$ and $c_{k-1} > \theta$. Let $Y \in \{1, \dots, K\}$ denote the dilution steps where the assay can stop. The probability that the assay stops at dilution step k and not before relates to c_{k-1} still being above the threshold θ via a logistic function:

$$P(Y = k | Y \leq k) = \frac{\exp(c_{k-1} - \theta)}{1 + \exp(c_{k-1} - \theta)} = \text{logit}^{-1}(c_{k-1} - \theta), \quad k = 2, \dots, K.$$

We substitute c_{k-1} with Equation 2.1 and the linear model for c_0 and obtain the following linear predictor:

$$c_{k-1} - \theta = c_0 - \delta_{k-1} - \theta = x^T \beta - \underbrace{\delta_{k-1} - \theta}_{:=\theta_{k-1}}.$$

We combine the dilution-specific factors δ_k with the assay-specific threshold θ to a set of unknown threshold parameters θ_k . This yields a model that is also known as the reverse stopping ratio model (Tutz, 1991; Yee et al., 2010):

$$P(Y = k | Y \leq k) = \text{logit}^{-1}(x^T \beta - \theta_{k-1}), \quad k = 2, \dots, K. \quad (2.2)$$

For each patient i with explanatory variables x_i , the probability that the assay stopped at dilution step k is given by the probability that the assay stops for the first time at dilution k and not in the preceding dilutions:

$$P(Y_i = k) = \text{logit}^{-1}(x_i^T \beta - \theta_{k-1}) \prod_{l=2}^{k-1} \left(1 - \text{logit}^{-1}(x_i^T \beta - \theta_{l-1})\right), \quad k = 2, \dots, K,$$

and

$$P(Y_i = 1) = 1 - \sum_{l=2}^K P(Y_i = l).$$

The parameters β and θ_k are estimated over all patients $i = 1, \dots, n$. Let p_{ik} denote the probabilities $P(Y_i = k)$, and let y_{ik} be a binary indicator of the response of patient i that takes the value 1 if the assay stopped at dilution step k and 0 otherwise. Then, the full likelihood is given by the following product (Agresti, 2003):

$$\prod_{i=1}^n \prod_{k=1}^K p_{ik}^{y_{ik}}.$$

An overview of the binary, ordered, and sequential logistic models along with an illustrative comparison of the latent variable interpretation for each regression model is shown in **Figure S2.13** (Cox, 1988; Tutz, 1991; Agresti, 2003; McCullagh, 2018).

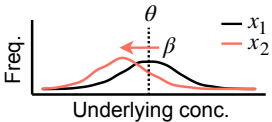
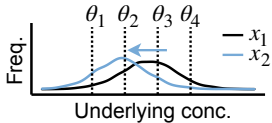
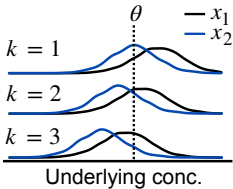
Model	Categories	Likelihood	Interpretation
Binary logistic	Responder vs. Nonresponder	$\prod_{i=1}^n p_i^{y_i} (1 - p_i)^{1 - y_i}, \quad p_i = \text{logit}^{-1} (x_i^T \beta - \theta)$	
Ordered logistic	Titer levels (K dilutions)	$\prod_{i=1}^n \prod_{k=1}^K p_{ik}^{y_{ij}}, \quad p_{ik} = \underbrace{\text{logit}^{-1} (x_i^T \beta - \theta_k)}_{P(Y \geq k x_i)} - \underbrace{\text{logit}^{-1} (x_i^T \beta - \theta_{k+1})}_{P(Y \geq k+1 x_i)}$	
Sequential logistic	Titer levels (K dilutions)	$\prod_{i=1}^n \prod_{k=1}^K p_{ik}^{y_{ij}}, \quad p_{ik} = \underbrace{\text{logit}^{-1} (x_i^T \beta - \delta_{k-1} - \theta)}_{P(Y=k Y \leq k, x_i)} \prod_{l=2}^{k-1} \underbrace{\left(1 - \text{logit}^{-1} (x_i^T \beta - \delta_{l-1} - \theta) \right)}_{P(Y=l Y \leq l, x_i)}$	

Figure S2.13. Comparison between binary, ordered, and sequential logistic regression models.

MODEL-BASED INFERENCE OF NEUTRALIZING ANTIBODY AVIDITIES AGAINST INFLUENZA VIRUS

This chapter is to be submitted as: J. Linnik, M. Syedbasha, Y. Hollenstein, J. Halter, A. Egli, and J. Stelling. "Model-based inference of neutralizing antibody avidities against influenza virus."

ABSTRACT

To assess the response to vaccination, quality (avidity) and quantity (concentration) of neutralizing antibodies are the most important parameters. Specifically, an increase in avidity indicates germinal center (GC) formation, which is required for establishing long-term protection. For influenza, the classical hemagglutination inhibition (HI) assay, however, quantifies the combination of both and to separately determine avidity requires high experimental effort. Here, we present a biophysical model that infers avidities from measured HI titers and IgG concentrations. We applied our model to infer serum IgG avidities against influenza A/California/7/2009 (H1N1) in vaccinated hematopoietic stem cell transplantation patients ($n = 45$) and validated our results with independent avidity measurements. The model predicted that increased IgG concentrations mainly contribute to observed HI titer increases and that immunosuppressive treatment is associated with lower baseline avidities. Because the model requires only easy-to-establish measurements as input, we anticipate that it will help to disentangle causes for poor vaccination outcomes also in larger vaccine studies.

3.1 INTRODUCTION

To prevent influenza epidemics, it is crucial to annually develop effective vaccines against circulating influenza strains. To assess influenza vaccine efficacy, hemagglutination inhibition (HI) titers are traditionally used as a surrogate for the influenza-neutralization capacity of vaccine-induced antibodies in serum (Palache et al., 2003; Benoit et al., 2015). The HI assay makes use of the phenomenon that influenza viruses bind with their surface receptor hemagglutinin (HA) to red blood cells (RBCs) and can cross-link them to macroscopic cell aggregates in a process called hemagglutination (Hirst, 1941). In the presence of influenza-binding antibodies that block RBC binding sites, hemagglutination is inhibited. This allows quantifying the neutralization capacity of serum antibodies in dilution experiments: the highest serum dilution that fully inhibits hemagglutination is determined, and its dilution factor is reported as the HI titer (WHO, 2002). The HI titer measures a combination of both antibody concentration and avidity, where avidity quantifies the overall strength of a multivalent antibody binding to hemagglutinin epitopes involved in virus-RBC interaction (neutralizing binding). When assessing vaccine response, however, it is important to distinguish between antibody concentration and avidity. In particular, no increase in avidity following vaccination indicates a hampered formation of germinal centers (GCs) where B cells undergo affinity maturation and proliferate to long-lived B cells, providing long-term protection (Shlomchik and Weisel, 2012; De Silva and Klein, 2015).

Avidity measurements of serum antibodies are time-consuming and costly. Commonly used techniques are surface plasmon resonance (SPR) and elution experiments with chaotropic agents (such as urea) based on enzyme-linked immunosorbent assays (ELISAs). While SPR experiments require special equipment and long calibration, elution assays are very sensitive to experimental conditions, and optimal protocols might vary substantially for different samples (Underwood, 1993; Olsson et al., 2019). In comparison, measurements of HI titers and serum IgG concentrations are faster to establish and simpler to perform (Kaufmann et al., 2017). HI assays are considered the gold standard and routinely performed in vaccine studies; they proved to be fast, cheap, and reliable. IgG concentrations can be determined in standardized ELISA experiments. These are suitable for large-scale serological studies because they can be fully automated and yield highly reproducible results. Therefore, estimation of avidities from HI titers and IgG concentrations would facilitate influenza vaccine studies in larger populations.

Here, we present a biophysical model of the HI assay that mechanistically describes the relationship of neutralizing IgG concentration and avidity to the resulting HI titer, and enables the inference of neutralizing IgG avidities from HI titers and ELISA-detected IgG concentrations. We applied our approach to vaccinated hematopoietic stem cell transplantation (HSCT) patients, focusing on IgG antibodies specific to pandemic influenza A/California/7/2009 (H1N1pmd09). Despite available vaccines, the case fatality rate for influenza infection is 17–29% in these patients (Kunisaki and Janoff, 2009). HSCT patients are commonly immunocompromised due to post-transplant immune reconstitution and immunosuppressive treatment against graft rejection. Since patients with low antibody avidities are at risk for fatal infections, we investigated the association of inferred avidities with three indicators of immunocompromised status as defined by CDC (Brunette et al., 2015), known to be associated with immune cell proliferation, affinity maturation and antibody production (Ogonek et al., 2016): first two years post transplantation, immunosuppressive treatment, and chronic graft-versus-host disease (cGVHD) grade according to NIH criteria (Filipovich et al., 2005). Our model detected that immunosuppressive treatment is associated with lower baseline avidities, but we did not detect a significant association with cGVHD or the time after transplantation. In addition, our model suggests that vaccination induced affinity maturation of neutralizing antibodies in only a few patients.

3.2 RESULTS

3.2.1 *Model of the hemagglutination inhibition (HI) assay*

We extended and combined existing models of antibody-virus interaction (Groth, 1963) and cell-cell agglutination (Dolgosheina et al., 1992) to a model that mechanistically captures the key processes of the HI assay (**Figure 3.1**). The HI assay is performed in three consecutive steps (WHO, 2002): (i) Serial dilution of patient serum and 30 min incubation with influenza virus, (ii) addition of RBCs followed by 30 min incubation, and (iii) determination of the HI titer based on the presence or absence of hemagglutination inhibition in each serum dilution (**Figure 3.1**, top). We represent these steps separately: the model output of one step serves as input for subsequent steps (**Figure 3.1**, bottom).

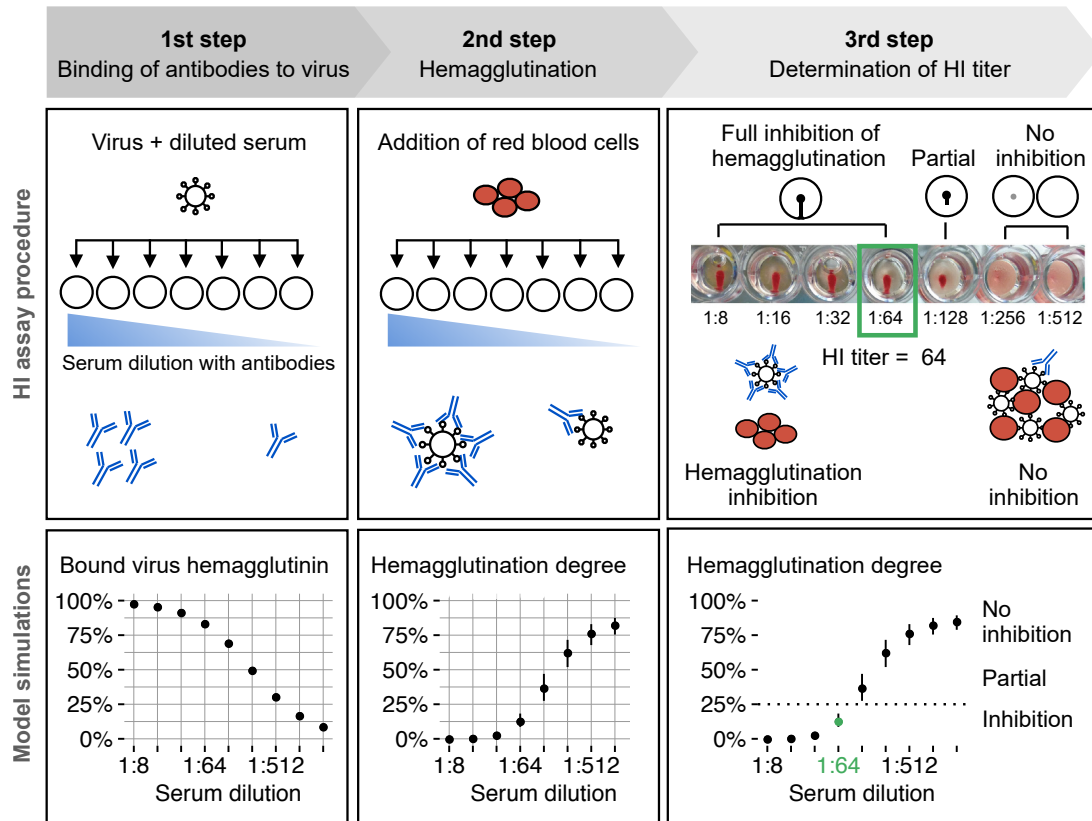


Figure 3.1. Overview of the hemagglutination inhibition (HI) assay (top) and illustrative simulation results (bottom). First step: patient serum is serially diluted and incubated with a constant amount of influenza virus. The model computes the amount of antibody-bound viral hemagglutinin (HA) for each serum dilution. Second step: red blood cells (RBCs) are added to each dilution and virus particles with free HA binding sites cross-link RBCs to cell aggregates. The model predicts a switch-like increase in agglutinated RBCs with decreasing antibody concentration. Third step: the plate is tilted by 90 degrees to detect full hemagglutination inhibition. If none/few RBCs are agglutinated, sedimented RBCs flow down to the rim. By definition, those wells show full hemagglutination inhibition. The reciprocal of the maximal inhibitory dilution is the HI titer. We classify our simulation results into inhibition and no inhibition by setting a threshold at 25% hemagglutination. Simulation results show median and interquartile range indicating the uncertainty due to experimental conditions (RBC concentration, virus concentration, readout time) and model parameters (summarized in **Table 3.1**) for an IgG serum concentration of 25 nM (4 $\mu\text{g}/\text{mL}$) and $K_D^{\text{app}} = 0.1$ nM.

Step 1 (binding of antibodies to virus): We modeled the binding of IgG antibodies to virus hemagglutinin (HA) as a diffusion-controlled reversible reaction between IgG molecules and virus particles (see **Methods** for all details). Each homotrimeric HA receptor has three identical binding sites for monoclonal IgG, but we assume that an HA trimer accommodates at most one IgG molecule due to steric hindrance (Taylor et al., 1987; Pountourios et al., 1990; Otterstrom et al., 2014). Serum contains a mixture of polyclonal IgG antibodies. Thus, after the addition of influenza virus to serum, HA-specific IgG clones form a mixture of IgG-HA complexes according to their individual dissociation constants (avidities). We assume that any other interactions are negligible because serum samples are pretreated with proteases to limit unspecific binding. Without information on the individual concentrations or avidities of each IgG clone, we consider the total concentration of HA-specific serum IgG and the apparent dissociation constant K_D^{app} . This constant is proportional to the ratio of free HA-specific IgG molecules over all formed IgG-HA complexes at equilibrium. Importantly, the inverse $1/K_D^{\text{app}}$ is interpreted as the apparent avidity of HA-specific serum IgG. We compute the fraction of antibody-bound virus at binding equilibrium for each serum dilution (**Figure 3.1**, left) as input for step 2 because 30 min incubation suffices to reach binding equilibrium.

Step 2 (hemagglutination): When RBCs are added, virus particles bind reversibly with free HA binding sites to sialic acid (SA) linked receptors on RBCs. We assume that IgG antibodies and SA-linked receptors do not compete for HA binding sites because the affinity of SA to HA is in the mM range (Sauter et al., 1989, 1992; Weinhold and Knowles, 1992), far below the affinity of HA-specific IgGs in the nM range (Lee et al., 2016). The tight binding of the virus to RBCs results from binding multiple SA moieties simultaneously (Takemoto et al., 1996). The virus-RBC interactions will eventually induce hemagglutination. We model it as a coagulation process (Von Smoluchowski, 1917), where RBCs stick together whenever they collide such that virus particles can cross-link them. Only when a free SA linked receptor on an RBC meets a free HA on a virus particle that is simultaneously bound to another RBC, the collision leads to a successful cross-link. We define a degree of hemagglutination that takes the value 0% without any hemagglutination (not a single cross-link), and 100% when all RBCs form a single aggregate. The model predicts a switch-like increase in the degree of hemagglutination with decreasing antibody concentration, consistent with the experimentally observed switch-like behavior of the assay (**Figure 3.1**, middle).

Step 3 (determination of HI titer): After another 30 min incubation, each serum dilution is inspected for hemagglutination inhibition and the reciprocal of the maximal dilution that shows full inhibition is the HI titer (**Figure 3.1**, right). To model this binary decision (inhibition or no inhibition), we classify the outcome by setting a threshold at 25% hemagglutination because we define 50% hemagglutination as partial inhibition and our model predicts for ≥ 1 HA unit virus a hemagglutination degree of $\geq 75\%$. By definition, this is interpreted as full inhibition (**Figure S3.1**), suggesting that differences in hemagglutination degree below 25% or above 75% cannot be distinguished by eye. We extracted parameters from literature for IgG, chicken RBCs and the virus strain to make the model specific for H1N1pdm09 (**Table 3.1**). In addition, we established the agglutination rate parameter from experiments with reference serum (see **Methods**). Here, avidity is defined as the inverse of the apparent dissociation constant of the IgG-hemagglutinin complex, $1/K_D^{\text{app}}$: the lower the K_D^{app} value, the tighter the binding and thus the higher the avidity.

Table 3.1. Model parameters and variables. Abbreviations are: IgG, Immunoglobulin G; RBC, red blood cell; HA, hemagglutinin; HAU, HA unit; SA, sialic acid.

Description	Symbol	Value	Distribution in sensitivity analysis	Reference
Serum IgG concentration	A_0	Sample-specific	Unif(0, 2800) nM (0 – 420 $\mu\text{g}/\text{mL}$)	Eidem et al. (2015)
Apparent IgG dissociation constant	K_D^{app}	Sample-specific	Unif(0.001, 300) nM	Lee et al. (2016)
Initial virus concentration	V_0	$1.3 \cdot 10^{-4}$ nM (4 HAU)	Unif($0.9 \cdot 10^{-4}$, $2.3 \cdot 10^{-4}$) nM (3 – 7 HAU)	WHO (2002)
Initial RBC concentration	RBC_0	$3.1 \cdot 10^{-5}$ nM	Unif($1.6 \cdot 10^{-5}$, $6.3 \cdot 10^{-5}$) nM	WHO (2002)
Number of HA receptors per virus	r	400	Discrete Unif(300,500)	Ruigrok et al. (1984); Harris et al. (2013)
Number of epitopes per HA receptor	e	3	Fixed at 3	Wilson et al. (1981); Jackson et al. (1991)
Number of shaded epitopes per bound IgG	e^*	3	Bernoulli(0.5) with $e^* \in \{3, 6\}$	Otterstrom et al. (2014)
Number of SA receptors per RBC	b	$4.5 \cdot 10^5$	Discrete Unif($4 \cdot 10^5$, $5 \cdot 10^5$)	Aich et al. (2011); Aoki (2017)
Number of shaded SA receptors per bound virus	b^*	34	Sampled from model	See Methods
SA-HA association rate constant	$k_{\text{ass}}^{\text{RBC}}$	$2 \cdot 10^{-6} \text{ s}^{-1}$	Lognorm($\log(2 \cdot 10^{-6})$, 0.2^2) s^{-1}	Takemoto et al. (1996)
SA-HA dissociation rate constant	$k_{\text{diss}}^{\text{RBC}}$	$2 \cdot 10^{-4} \text{ nM}^{-1} \text{ s}^{-1}$	Lognorm($\log(2 \cdot 10^{-4})$, 0.2^2) $\text{nM}^{-1} \text{ s}^{-1}$	Takemoto et al. (1996)
RBC agglutination rate constant	k_{agg}	$2 \cdot 10^6 \text{ s}^{-1}$	Unif($0.4 \cdot 10^6$, $13 \cdot 10^6$) s^{-1}	Estimated from data

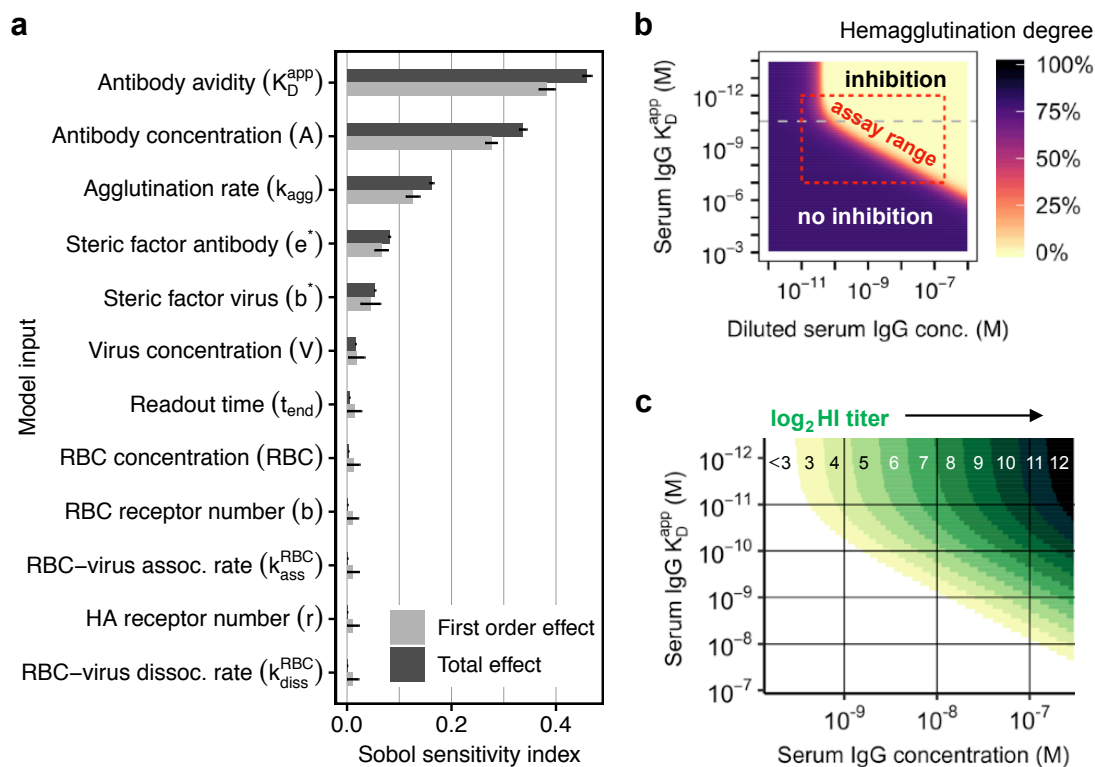


Figure 3.2. Model sensitivity and resolution of the hemagglutination inhibition assay for influenza H1N1pdm09. (a) Sensitivity analysis using Sobol indices. First-order effects show only the linear contribution to the total variance in hemagglutination degree (they sum up to 1), whereas total effects consider also interactions (see **Methods** for details). (b) Predicted degree of hemagglutination for different IgG concentrations and apparent dissociation constants K_D^{app} (avidity). The red box indicates the usual assay range, bounded by the biological range of $K_D^{app} = 0.001 - 100$ nM, and the gray dashed line indicates $K_D^{app} = 0.03$ nM. (c) Predicted HI titers for the biological range of influenza-specific serum IgG and avidity. Colored areas correspond to titers shown on top.

3.2.2 The model quantitatively relates IgG concentration and avidity to HI titer

To infer antibody avidities accurately, the model needs to be sensitive to the experimental data used as inputs. However, it should not be sensitive to other experimental factors and uncertainties in model parameters. To evaluate the model in this respect, we used Sobol sensitivity analysis (Saltelli et al., 2004), which attributes variance in model output (here hemagglutination degree) to the individual model input factors. The more influential the input factor is, the higher is its contribution to the variance in hemagglutination degree. We considered the ranges for all model input factors summarized in **Table 3.1**. Specifically, for IgG concentration and avidity the ranges match the experimentally observed ranges for H1N1pdm09-specific IgG after vaccination in adults (Eidem et al., 2015; Lee et al., 2016). For experimental conditions, we aimed to generously cover experimental variability. For model parameters, we considered measurement uncertainty and biological variability as described in the literature.

Sensitivity analysis showed that avidity and serum IgG concentration are the most influential factors for the model's output (**Figure 3.2a**). Variability in RBC and virus concentration, as well as in

readout time, contribute very little to the total variance. The model is also robust to uncertainty in all model parameters except for the kinetic agglutination rate of RBCs, which we varied within the 95% highest probability density interval estimated from our calibration data (see **Methods**). Other relevant factors were the ability of IgG to bind two HA receptors simultaneously and the number of RBC receptors that are covered by one bound virion. Hence, the model's predictions are dominated by the measured input quantities, despite uncertainties in experimental conditions, mechanisms, and parameters.

The model predicts a clear separation between hemagglutination inhibition and no inhibition — partial inhibition occurs only within a small range of IgG concentration and avidity (**Figure 3.2b**). Thus, the well-known binary nature of the assay is captured. Using an initial virus concentration of 4 HA units as defined by WHO ensures both high sensitivity and robustness, whereas 8 HA units or more increase robustness but lower sensitivity (**Figure S3.1e**). The model predicts also a yet unknown property of the HI assay: for avidities $K_D^{\text{app}} \geq 0.03$ nM, hemagglutination quantifies a combination of IgG concentration and avidity, but for very high avidities $K_D^{\text{app}} < 0.03$ nM, the assay only detects changes in IgG concentration (**Figure 3.2b**).

Within the linear range for $K_D^{\text{app}} \geq 0.03$ nM, a doubling in IgG concentration or avidity results in a doubling of the predicted HI titer (**Figure 3.2c**). In other words, a two-times lower antibody avidity can be compensated by a two-times higher antibody concentration. However, this only applies to the linear range and the exact relationship depends on the considered avidity and concentration ranges (**Figure 3.2c**). The model also suggests why HI titers above 8192 (= 13 in \log_2) are rarely observed. Even for a high serum IgG concentration of 1000 nM (150 $\mu\text{g}/\text{mL}$), such high titers require antibody avidities in the fM range, but influenza-specific antibody affinities in vaccinated healthy adults lie in the nM range (Lee et al., 2016).

In summary, we conclude that the model yields robust predictions in the applicable assay range, and reveals new quantitative aspects of the HI assay.

3.2.3 Inference of neutralizing antibody avidities in HSCT patients

Next, we applied our model to infer avidities from ELISA-detected serum IgG concentrations and HI titers in HSCT patients (patient characteristics are summarized in **Table 3.2**). We used a Bayesian approach that accounts for uncertainties due to ELISA measurement error and discretization in HI titers (see **Methods** for details). Model parameters were fixed for all serum samples (**Table 3.1**), assuming that differences in HI titer arise mostly from differences in IgG concentration and avidity as suggested by our sensitivity analysis (**Figure 3.2a**). All patients received two doses of non-adjuvanted trivalent seasonal influenza vaccine on d0 and d30 (see **Methods**). Measurements were available from 45 patients at five time points before (d0) and after (d7, d30, d60, d180) the first vaccination with 221 serum samples in total. HI titers and IgG concentrations were significantly correlated (Kendall's $\tau = 0.69$, $P < 10^{-15}$, rank correlation for ordinal data; **Figure 3.3a**). However, especially moderate HI titer values of 32 and 64 (\log_2 HI titer 5 and 6) showed a large spread in serum IgG, indicating variable antibody avidities.

For serum samples with HI titers below assay resolution (HI titer < 8), we could only infer an upper bound for the avidity (it could be lower, but not higher). This affected 23 serum samples

from seven patients (12% of inferred avidities). Analogously, for serum samples with $K_D^{\text{app}} \leq 0.03$ nM, we could, in principle, only report a lower bound, but all inferred avidities for our patient cohort exceeded this threshold. In 24 samples, inferred K_D^{app} -values showed very large uncertainty (approximately $\pm 100\%$) due to large measurement error in ELISA measurements; we excluded these samples from further analysis. In the remaining samples, posterior distributions were log-normally distributed (**Figure S3.2**) and we determined the uncertainty intervals due to discretized HI titer measurements and ELISA measurement error by sampling, yielding an average uncertainty in K_D^{app} -values of approximately $\pm 30\%$ (range 20–57%, interquartile range (IQR) 25–30%). In summary, we were able to reliably infer 197 avidities from in total 43 patients (89% of analysed samples). The inferred avidities ranged from $K_D^{\text{app}} = 0.1$ nM to ≥ 22 nM (upper bound), with a median of 1.7 nM and IQR 0.9–2.5 nM. Inferred avidities and HI titers were significantly correlated (Kendall’s $\tau = 0.56$, $P < 10^{-15}$), although the correlation was weaker than for IgG concentration (**Figure 3.3a**).

3.2.4 *Inferred avidities correlate with experimentally determined avidities*

We validated our model with experimental measurements of 59 serum samples from 12 patients. We performed ELISA-based elution assays that quantify the fraction of IgG remaining bound after 3h incubation with 4M urea, yielding a measure for the overall binding strength of serum IgG to H1N1pmd09 in the form of an avidity index between 0 (low avidity) and 1 (high avidity).

The inferred and the experimentally determined avidities were significantly correlated (Pearson’s $\rho = 0.54$, 95% CI = [0.31, 0.70], $P < 10^{-4}$, **Figure 3.3b**). We detected one outlier patient (standardized residuals ≈ 3) whose serum did not show HI activity at any time point (**Figure 3.3b**), suggesting that the ELISA detected non-neutralizing IgG in this patient. Experimental and inferred avidities distinguished different types of patient responses, for example, where both IgG concentration and avidity increased after vaccination (patient 1 in **Figure 3.3c**) or where an increase in HI titer was mostly explained by an increase in IgG concentration (patient 2). We identified one patient that produced non-neutralizing IgG (patient 3): Here, the ELISA detected an increase in IgG concentration that leads to HI titer doubling according to our model predictions. However, the HI titer did not increase at any time point (**Figure 3.3c**), suggesting that the ELISA-detected IgGs had no HI activity. The inferred K_D^{app} -value refers to neutralizing IgG-virus interactions only, and its value is biased towards lower avidity if the measured IgG concentration also includes non-neutralizing IgGs. Nevertheless — in contrast to patient 11 who did not show HI activity at any time point (**Figure 3.3b**) — the inferred avidities for patient 3 approximately mirrored the experimentally determined avidity indices, probably because this patient showed high HI titer and serum IgG levels before vaccination and only a small increase in non-neutralizing IgGs after vaccination, indicating that previously acquired neutralizing IgGs dominated the avidity measurements (**Figure 3.3c**).

Thus, apparent serum avidities inferred by our model-based approach were in good accordance with experimentally determined avidities. However, if non-neutralizing IgG dominates in serum, the results are not directly comparable because the inferred avidity refers to neutralizing IgG with HI activity.

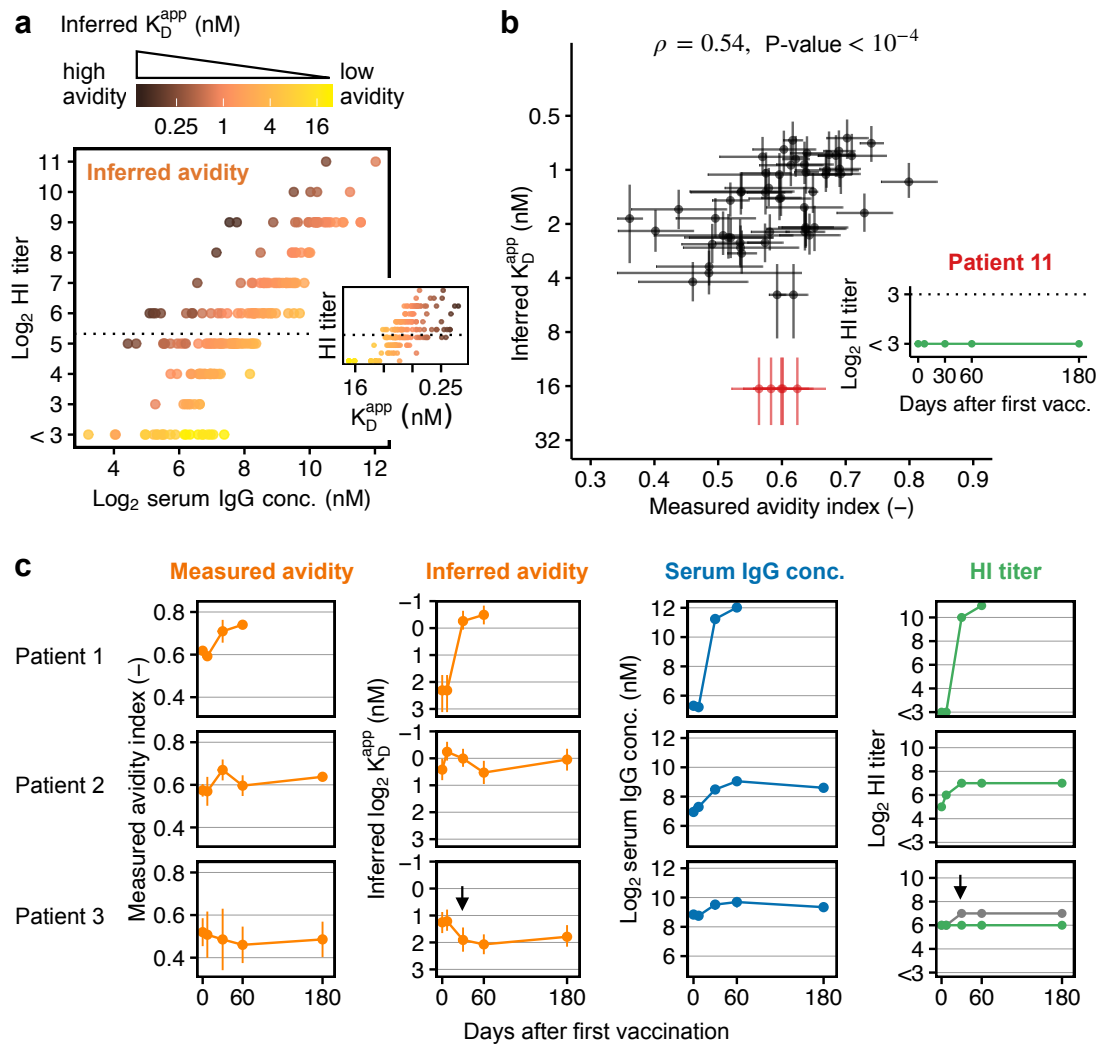


Figure 3.3. Inference of antibody avidities in HSCT patients. (a) ELISA-detected anti-H1N1pmd09 serum IgG concentration, HI titers and corresponding inferred apparent dissociation constants K_D^{app} from 197 serum samples from 43 HSCT patients. The dashed line indicates the seroprotection threshold (HI titer ≥ 40). (b) Correlation of inferred and experimentally determined avidities in 59 serum samples from 12 HSCT patients (Pearson's $\rho = 0.54$, 95% CI = [0.31, 0.70]). Data show mean and standard deviation for avidity indices from two experiments (each performed in duplicates) and the median of the posterior distribution with the uncertainty range due to discretized HI titer measurements and ELISA measurement error for inferred K_D^{app} -values (see **Methods** for details on inference and **Figure S3.2** for posterior distributions). Avidity indices correspond to the fraction of H1N1pmd09-specific serum IgG remaining bound after 4M urea treatment. Patient 11 was identified as an outlier, probably because ELISA detected non-neutralizing IgG; the patient showed no HI activity at any time point. For this patient, the measured avidity index is plotted against the estimated upper bound for the inferred avidity and the uncertainty interval reflects the estimated uncertainty of the upper bound due to discretized HI titer measurements and ELISA measurement error. (c) Example patients with different types of responses to vaccination. In patient 3, we detected an increase in non-neutralizing IgG on d30. The predicted HI titer for the observed increase in IgG (shown in grey) is twice as high as the actually observed titer (green). For all 12 patients with experimentally determined avidities see **Figure S3.3**.

3.2.5 Detection of vaccine-induced affinity maturation in HSCT patients

Next, we compared the vaccine-induced increase in inferred avidities in all investigated HSCT patients and identified candidates for successful GC formation and affinity maturation (**Figure 3.4**). Since the establishment of GCs takes approximately seven days (De Silva and Klein, 2015), we considered an increase in IgG concentration and avidity on d30 or d60 as indicative for GC formation (patients were vaccinated on d0 and d30; see **Methods**).

The response characteristics of the patient cohort are shown in **Figure 3.4a**. Given the uncertainty in inferred K_D^{app} -values, we could detect fold changes in avidity of approximately >1.5 or <0.5 (except for samples below assay resolution with HI titer <8) (**Figure S3.4a**). Eight patients showed a detectable increase in avidity on d30 and/or d60, of which only one showed no increase in serum IgG (**Figure 3.4b**). This suggests that vaccination induced GC formation and affinity maturation in seven patients (including patient 1 in **Figure 3.3c**). Serum avidity returned back to baseline on d180 in most of these patients, suggesting that vaccination failed to induce a sustained production of high-avidity antibodies. Over all patients showing a detectable increase in avidity at any time point after vaccination (n=11), we observed a time-dependent increase with the largest increase on d60, i.e., after the booster dose (**Figure 3.3c**), consistent with our understanding of GC dynamics (De Silva and Klein, 2015). We could not detect a significant increase in avidity in 24 patients, although 15/24 patients showed an increase in serum IgG on d30 or d60 (such as patient 2 in **Figure 3.3c**).

In summary, although 30 patients showed an increase in serum IgG concentration on d30 and/or d60, only 7/30 patients (23%) are candidates for vaccine-induced affinity maturation, and 6/30 patients (20%) showed vaccine-induced production of non-neutralizing IgG (such as patient 3 in **Figure 3.3c**). We excluded 4/45 patients as they showed too large measurement uncertainty in ELISA-detected IgG concentration on several time points (see above).

3.2.6 Association with criteria for compromised immune response

Finally, we investigated associations between inferred avidities, IgG concentration and HI titers with time post HSCT ≤ 2 years, intake of immunosuppressive drugs quantified by immunosuppression grade ranging from 0 (none) to 3 (severe), and cGVHD grade with the same range (**Figure 3.4d**). We investigated effects on baseline (levels before vaccination) and response (relative increase) in a multivariable regression analysis with patient-specific random intercepts and controlling for sex and age. Regression was performed on log₂-transformed values using models for continuous data for avidity/concentration and models for sequential ordinal data for HI titers (Tutz, 1991). When analysing the vaccine-induced increase in avidity, we excluded non-neutralizing IgG responders (n=6) because their inferred avidities are not indicative of affinity maturation.

Early transplant patients (time post HSCT ≤ 2 years) showed significantly lower baseline levels in IgG concentration (-1.92 ± 0.46 , $P = 1.8 \cdot 10^{-4}$) and HI titer (log odds ratio -0.96 ± 0.25 , $P = 1.2 \cdot 10^{-4}$) than patients with HSCT >2 years (**Figure 3.4d**). At the time of this study, the annual influenza vaccine contained H1N1pmd09 already for five years. Therefore, it is likely that patients with HSCT >2 years acquired durable H1N1pmd09-neutralizing antibodies in previous seasons. Yet,

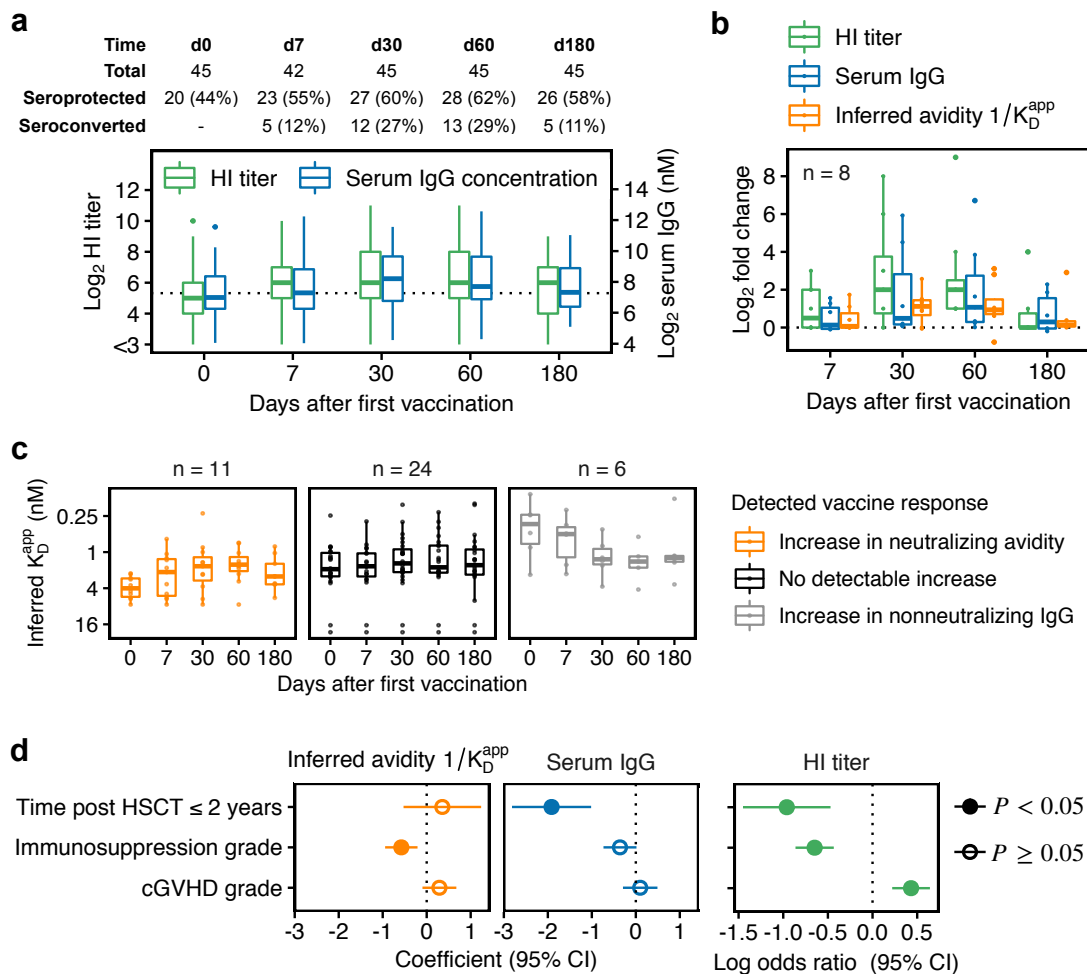


Figure 3.4. Response to influenza vaccination against H1N1pmd09 in HSCT patients. (a) HI titers and ELISA-detected serum IgG concentrations in the investigated patient population. Patients were vaccinated on d0 and d30 with a non-adjuvanted trivalent influenza vaccine. Seroprotection corresponds to HI titer ≥ 40 and seroconversion to a four-fold HI titer increase compared to d0. (b) Fold changes in HI titer, serum IgG and inferred avidity ($1/K_D^{\text{app}}$) in all patients with a detectable increase in inferred avidity on d30 and/or d60. (c) Comparison of inferred avidities between patients with a detectable increase in avidity at any time point after vaccination (left), patients with no detectable increase (middle), and patients with a detectable increase in non-neutralizing IgG (right). We excluded 4/45 patients as they showed too large measurement uncertainty in IgG concentration on several time points. (d) Estimated effects on baseline levels of criteria for compromised immune response. Effects were estimated in a multivariable regression analysis on log2-transformed values controlling for sex and age. Time after HSCT was encoded as a binary variable (1 for HSCT ≤ 2 years and 0 for HSCT > 2 years). Immunosuppression grade and cGVHD grade ranging from 0 (no immunosuppression/cGVHD) to 3 (severe immunosuppression/cGVHD) were encoded as ordered categorical variables with grade 0 as reference (see **Methods** for details).

early transplant patients did not show significantly different baseline avidities compared to patients with HSCT>2 years (0.36 ± 0.45 , $P = 0.43$), potentially because previous vaccinations did not induce (detectable) affinity maturation. Patients under immunosuppression showed significantly lower baseline avidities with an estimated effect size of -0.58 ± 0.19 per immunosuppression grade ($P = 4.0 \cdot 10^{-3}$). This means, that patients with immunosuppression grade 2 showed approximately two-fold lower baseline avidities than patients without immunosuppression, while patients with immunosuppression grade 3 showed three- to four-fold lower baseline avidities (see also **Figure S3.5**). Most patients in our cohort under immunosuppression received cell division inhibitors such as prednisone or mycophenolate mofetil (MMF) and calcineurin inhibitors such as tacrolimus or cyclosporine A that lower T cell activity, while a few patients received rituximab, an anti-CD20 antibody that leads to B-cell depletion (**Table 3.2**). Since we did not know the patients' medical history, we could not investigate whether the low baseline levels are explained by immunosuppressive drug treatment or an underlying disease during a former encounter with H1N1pmd09. For instance, patients might have suffered from GVHD in previous seasons, which required treatment with immunosuppressive drugs. In the current season, we could not detect any effects on the vaccine-induced increase in serum IgG or avidity, probably due to lack of power. We also did not detect a significant effect of cGVHD on avidity or serum IgG, but we detected a positive effect on HI baseline titers (log odds ratio 0.43 ± 0.11 , $P = 6.2 \cdot 10^{-5}$).

3.3 DISCUSSION

The HI assay is a well-established gold standard method, and yet, little is known on the relationship between HI titer, serum antibody concentration, and avidity. Mathematical models of cell agglutination by antibody cross-linking have been previously reported (Ming et al., 1965; Dolgosheina et al., 1992) and applied to guide the design of immunoassays (Kylilis et al., 2019). We presented an extension to a three-component system consisting of antibodies, viruses, and cells. Our model captures known properties of the HI assay and provides a biophysical explanation for why the HI assay has become the gold standard in serological studies. First, the assay is equally sensitive to both antibody concentration and avidity. Only for extremely high avidities ($K_D^{\text{app}} < 0.03$ nM), it detects only changes in concentration. Second, the assay is robust to pipetting errors or other experimental variability in RBC and virus concentration.

The model allows the inference of neutralizing serum avidities from ELISA-detected IgG concentrations and HI titers, which are simpler, faster, and cheaper to measure than antibody avidities, especially in larger populations. In our experimental setup where HI titers were determined in two-fold serial dilutions, we were able to estimate avidities with a precision of approximately $\pm 30\%$. A limitation of our approach is that we cannot distinguish whether HI titers below assay resolution (here: HI titer<8) correspond to non-neutralizing IgG (which could potentially have high avidity but not to HA) or to neutralizing IgG below assay resolution (with low avidity or low concentration). In addition, the detection of both neutralizing and non-neutralizing IgG can bias our results towards lower avidities; this possibility could be evaluated with SPR or calorimetry measurements. We also neglected IgM antibodies because IgMs show lower serum concentration than IgGs (Gonzalez-Quintela et al., 2008). When IgM concentration is high while IgG's low, for

example on d7 after vaccination in naive subjects, modeling the contribution of IgM to the HI titer may be necessary.

Regarding our experimental assays, we note that most influenza-specific IgG antibodies bind to the immunodominant HA globular domain (part of HA1) that harbors the SA binding site and attaches the virus to host cells (Wilson et al., 1981; Gerhard et al., 1981). Although we used whole-virus for ELISA coating, we observed a similar correlation between ELISA-detected serum IgG and HI titers as previous studies for HA and HA1 coating (Li et al., 2014; Trombetta et al., 2018). This is in line with studies on immunodominance showing that antibody response to influenza is dominated by HA-specific neutralizing IgG, and the HA globular domain is favored over the HA stalk domain, neuraminidase or other proteins on influenza (Altman et al., 2015; Angeletti et al., 2017).

Only a few patients showed a vaccine-induced increase in avidity, potentially because the number of responders was low or because the increase was below our detection limit (fold change < 1.5). However, we observed consistent effects: among 32 (13) patients with an increase in serum IgG on d30 or d60 (seroconversion on d60), we identified only seven (five) candidates for vaccine-induced affinity maturation. Thus, vaccine-induced increases in HI titer were mostly explained by increased IgG concentration. These results might not apply to other populations, especially because hampered affinity maturation is likely in HSCT patients (Ogonek et al., 2016). The precision of our inference was also sufficient to detect differences in baseline avidities between patients with and without immunosuppression. Excluding the two patients without HI activity at any time point from our analysis only slightly affects the detected association between immunosuppression grade and avidity (-0.39 ± 0.16 , $P = 0.02$). HI titers were negatively associated with immunosuppression grade as well, but positively with cGVHD grade. Patients with cGVHD show disturbed B cell homeostasis, persistent B cell activation, and elevated levels of B-cell activating factor (BAFF), which promotes survival and differentiation of activated B cells (Sarantopoulos et al., 2007, 2009; Greinix et al., 2008; Jacobson et al., 2014). However, several studies reported no significant effect of cGVHD on vaccine response to H1N1pmd09 (Issa et al., 2011; Engelhard et al., 2011; Gueller et al., 2011) or a negative effect (Roll et al., 2012; Mohty et al., 2011). Information on the patients' vaccination history, medication and disease state at the time of previous vaccinations would be required to better understand this positive association.

We inferred serum avidities for our HSCT patient cohort because serum avidities serve as markers for GC formation and affinity maturation in vaccine studies in general (Khurana et al., 2011, 2012; Eidem et al., 2015; Khurana et al., 2019). For example, it has been shown that in response to influenza A, the average HA-specific affinity of GC B cells is correlated with the HA-specific apparent avidity of serum antibodies (Frank et al., 2015) and that avidity of serum antibodies is important for protection (Olszewska et al., 2000; Polack et al., 2003). However, it is unknown to which extent vaccination against H1N1pmd09 induces affinity maturation in HSCT patients and it is currently under debate whether poor vaccine-induced affinity maturation is responsible for the poor effectiveness of seasonal influenza vaccines (Ellebedy, 2018; Arevalo et al., 2020). Previous studies in healthy adults showed that serum avidity against HA1 peaks at 21–28d after vaccination and decreases almost back to baseline on d180 (Eidem et al., 2015; Khurana et al., 2019). We observed a similar behavior among those HSCT patients that showed a detectable increase in avidity, although, in contrast to healthy subjects, HSCT patients received a booster dose on d30. We observed the

largest increase in avidity on d60, suggesting that the booster dose might enhance vaccine-induced affinity maturation.

Interestingly, all patients identified as non-neutralizing IgG producers showed relatively high HI titers (geometric mean titer=128, range=32–1024) and high neutralizing avidities before vaccination (**Figure 3.4c**). Even if we detected both neutralizing and non-neutralizing IgG on d0 in these patients, this would bias the inferred K_D^{app} -values towards lower avidities, which means that the actual neutralizing baseline avidities could be even higher. This observation supports computer simulations suggesting that preexisting antibodies that mask immunodominant epitopes, such as the RBC-binding HA head domain, lead to the production of antibodies against less accessible epitopes such as the HA stalk domain (Meyer-Hermann, 2019). This might be important for the generation of broadly neutralizing antibodies targeting the HA stalk domain, which show high potential *in vivo* despite poor neutralization activity *in vitro* (Krammer, 2016, 2019). Further studies might investigate whether preexisting antibodies with high avidities against the HA head domain favor the production of HA-stalk antibodies.

Overall, we argue that our biophysical model of the HI assay not only generates detailed insights and hypotheses on influenza vaccine responses in small patient cohorts as here. Because the model requires only easy-to-establish measurements as inputs, we anticipate that it can also refine the analysis in larger vaccine studies.

3.4 METHODS

3.4.1 Ethics statement

The study was conducted in accordance with the Declaration of Helsinki and approved by the Ethic committee northwest and central Switzerland (EKNZ ID 2014-141). All patients signed informed consent.

3.4.2 Patient sera

Adult patients that received allogeneic hematopoietic stem cell transplantation (HSCT) at least one year before were recruited in a multicenter cohort study in Switzerland (at the University Hospital Basel and the Cantonal Hospitals in Aarau and Lucerne) between October 2014 and January 2015. Only patients without known vaccine intolerance such as egg protein allergy or vaccine-associated adverse events were eligible for participation. In total, 57 patients were recruited; we included 45 of them in the present study based on the availability of serum samples. Following the standard of care for HSCT patients, each patient received two doses of the seasonal non-adjuvanted trivalent influenza vaccine (TIV), where the second dose was given 30 days after the first. Serum samples were collected prior to first vaccination (d0) and after vaccination (d7, d30, d60, d180) and stored in aliquots at -80°C. Almost all patients were in complete remission (42/45, 93%), and no patient showed progression. Patient characteristics is summarized in **Table 3.2**.

Table 3.2. Characteristics of allogeneic hematopoietic stem cell transplant patients (all patients and subset of patients with experimentally determined avidities for validation of inferred avidities).

		All	Validation subset
Total		45	12
Age	Median, IQR (years)	58, 44–64	45, 43–67
	≥ 65 years	11 (25%)	4 (33%)
Sex	Male	23 (51%)	4 (33%)
	Female	22 (49%)	8 (67%)
Underlying disease	Acute myeloid leukemia (AML)	17 (38%)	6 (50%)
	Acute lymphoblastic leukemia (ALL)	8 (18%)	2 (17%)
	Chronic myeloid leukemia (CML)	5 (11%)	1 (8%)
	Chronic lymphocytic leukemia (CLL)	5 (11%)	1 (8%)
	Multiple myeloma (MM)	5 (11%)	1 (8%)
	Plasma cell leukemia (PCL)	1 (2%)	0
	Myeloproliferative neoplasms (MPN)	1 (2%)	1 (8%)
	Myelodysplastic syndromes (MDS)	2 (4%)	0
	Non-Hodgkin lymphoma (NHL)	1 (2%)	0
Time after transplantation	median, IQR (years)	4, 2–8	6, 3–8
	1–2 years	16 (36%)	2 (17%)
	3–5 years	13 (29%)	3 (25%)
	>5 years	16 (36%)	7 (58%)
Transplant source	Peripheral blood	40 (89%)	11 (92%)
	Bone marrow	5 (11%)	1 (8%)
Donor source	Matched related donor	16 (36%)	5 (42%)
	Matched unrelated donor	21 (47%)	5 (42%)
Disease status ^a	Complete remission	42 (93%)	12 (100%)
	Stable	1 (2%)	0
	Recurrence	2 (4%)	0
	Progressive	0	0
Immunosuppression ^a	None	18 (40%)	2 (17%)
	Mild (grade 1)	6 (13%)	2 (17%)
	Moderate (grade 2)	14 (31%)	6 (50%)
	Severe (grade 3)	7 (16%)	2 (17%)
Immunosuppressive treatment ^a	Prednisone	13 (29%)	5 (42%)
	Tacrolimus	14 (31%)	7 (58%)
	Mycophenolate ^b	9 (20%)	3 (25%)
	Cyclosporine A ^c	4 (9%)	0
	Rituximab ^d	3 (7%)	0
Chronic GVHD	None	15 (33%)	0
	Mild (grade 1)	9 (20%)	4 (33%)
	Moderate (grade 2)	10 (22%)	6 (50%)
	Severe (grade 3)	11 (24%)	2 (17%)

Abbreviations: IQR: interquartile range; GVHD: graft-versus-host disease.

^aBefore vaccination, ^bCellCept[®] or Myfortic[®], ^cSandimmun[®], ^dMabThera[®] within the previous six months.

3.4.3 *Vaccine composition*

Patients received two doses of the non-adjuvanted TIV from 2014/2015 (A/grippal, Novartis, Switzerland), comprising inactivated subunit influenza virus with 15 µg HA antigen of each vaccine strain: A/California/7/2009 (H1N1pdm09), A/Texas/50/2012 (H3N2) and B/Massachusetts/2/2012 (Yamagata lineage).

3.4.4 *HI assay*

HI assays were performed according to the WHO manual (WHO, 2002). Sera were pre-treated with receptor destroying enzyme (RDE) (Sigma-Aldrich, C8772) and two-fold serially diluted, covering dilutions from 1:8 to 1:2048. A 0.75% (v/v) suspension of chicken RBCs (Cedarlane, CLC8800) and 4 HA units of influenza H1N1pdm09 virus (NYMC-X181) were used to perform the assay. The reported HI titer is the dilution factor of the highest serum dilution that showed full hemagglutination inhibition. The protocol has been published in detail (Kaufmann et al., 2017).

3.4.5 *ELISA for influenza-specific IgG detection*

ELISA 96-well plates (Thermo Scientific, 442404) were coated with 0.5 µg/mL whole virus H1N1pdm09 (NYMC-X181, 45 µg HA/mL) at 4°C overnight. Plates were blocked with 5% bovine serum albumin (BSA) in PBS for 1h at room temperature (RT). Patient serum samples were 1:4000 diluted in 0.5% BSA in PBS. Reference serum was 1:1000 diluted (top dilution of calibration curve) and then six times four-fold serially diluted, yielding a calibration curve with seven measurements. After blocking and washing with 0.05% TWEEN 20 in PBS, 100 µL/well of diluted serum samples were added and incubated for 2h at RT. Unbound serum antibodies were removed by washing the plates four times, and bound serum IgG was detected by 70 µL/well of 1:3000 diluted rabbit anti-human IgG antibody linked to horseradish peroxidase (Agilent, P021402-2) incubated for 2h at RT. After washing, plates were developed with 100 µL/well TMB substrate solution (BD, 555214) for 15 min and stopped with 50 µL/well 2N H₂SO₄. Absorbance was measured at 450 and 620 nm. Measurements were background- and blank-corrected. To obtain a calibration curve, reference measurements were fitted using a four-parameter logistic equation (log concentration vs log absorbance). All measurements were performed in duplicates.

3.4.6 *Urea elution assay to measure IgG avidities*

The ELISA described above was adapted to measure serum IgG avidities against influenza H1N1pdm09. Each serum was accordingly diluted to obtain a final concentration within the linear range of the calibration curve. After incubation with serum and washing as described above, each well was incubated for an additional 3h at RT with either 100 µL/well 4M urea (treated) or 100 µL/well PBS (untreated). The concentration of bound IgG was determined using a calibration curve as described above. The fraction of IgG remaining bound after urea treatment compared to

the untreated wells is reported as the avidity index. Avidities were determined in two experiments, each performed in duplicates.

3.4.7 Reference serum

The concentration of H1N1pdm09-specific IgG antibodies was determined in ELISA experiments relative to a reference serum collected from a healthy volunteer on day 7 after vaccination with 2014/2015 TIV (Arippal, Novartis, Switzerland), showing an HI titer of 512. Since the absolute reference concentration could only be determined by mass spectrometry, which was not feasible in this study, we estimated the concentration based on reported H1N1pdm09-specific IgG concentrations in vaccinated healthy adults with similar HI titers (Eidem et al., 2015). We set the reference concentration to 100 $\mu\text{g}/\text{mL}$ (670 nM), yielding an estimated avidity for the reference serum of 0.4–0.8 nM, consistent with observed affinities for post-vaccination serum IgG for H1N1pdm09 in healthy adults (Lee et al., 2016).

3.4.8 Model derivation

3.4.8.1 Assay step 1: binding of antibodies to virus

We model the formation of antibody-epitope complexes, denoted by C , as a diffusion-controlled reaction between viruses and antibodies, following the model of antibody-virus interaction proposed by Groth (1963). For complex formation, free antibodies, A , need to successfully collide with free influenza virus particles, V . In addition, antibody-epitope complex formation depends on the probability of epitopes being unbound, denoted by ϕ . The dynamics of complex formation is thus given by:

$$\frac{dC(t)}{dt} = k_{\text{ass}} \cdot A(t) \cdot V(t) \cdot \phi(t) - k_{\text{diss}} \cdot C(t),$$

where k_{ass} and k_{diss} are kinetic rate constants for association and dissociation, respectively. Note that some IgG antibodies bind bivalently to hemagglutinin, resulting in higher antibody affinities compared to their monovalent Fab fragments due to lower macroscopic dissociation rates (Edwards and Dimmock, 2000; Williams et al., 2018). This antibody valency is lumped into the macroscopic dissociation constant k_{diss} .

The total number of epitopes is proportional to the total virus concentration $V_{\text{tot}1}$ (where '1' indicates the first step of the assay), the average number of hemagglutinin receptors per virus, r , and the number of identical binding sites per hemagglutinin, e ($e = 3$ since hemagglutinin is a homotrimer). With e^* being the number of epitopes bound or shaded by one antibody molecule, the fraction of unbound epitopes is:

$$\phi(t) = \frac{e \cdot r \cdot V_{\text{tot}1} - e^* \cdot C(t)}{e \cdot r \cdot V_{\text{tot}1}}.$$

We assume that cross-linking of virus particles by antibodies is rare for the considered concentrations, such that the concentration of virus particles V remains approximately the same during the

experiment, i.e., $V \approx V_{\text{tot}_1}$. In addition, the mass balance for antibodies is $A_{\text{tot}_1} = A(t) + C(t)$. Substituting into the dynamics of complex formation leads to:

$$\frac{dC(t)}{dt} = \frac{k_{\text{ass}}}{e \cdot r} \cdot [A_{\text{tot}_1} - C(t)] \cdot [e \cdot r \cdot V_{\text{tot}_1} - e^* \cdot C(t)] - k_{\text{diss}} \cdot C(t).$$

Since the average number of epitopes per virus particle $e \cdot r$ is constant, the dynamics is equivalent to a reversible bimolecular reaction following mass action kinetics with apparent dissociation constant $K_{\text{D}}^{\text{app}} = e \cdot r \cdot \frac{k_{\text{diss}}}{k_{\text{ass}}}$. We assume that antibody-virus binding is fast, such that after the incubation time the system is at steady-state. At steady-state, the complex concentration C^{eq} fulfills

$$0 = [A_{\text{tot}_1} - C^{\text{eq}}] \cdot [e \cdot r \cdot V_{\text{tot}_1} - e^* \cdot C^{\text{eq}}] - K_{\text{D}}^{\text{app}} \cdot C^{\text{eq}}.$$

We exploit the analytic solution to this quadratic equation in C^{eq} to compute the fraction of covered hemagglutinin epitopes at equilibrium, θ , defined as:

$$\theta = \frac{e^* \cdot C^{\text{eq}}}{e \cdot r \cdot V_{\text{tot}_1}}$$

to obtain:

$$\theta = \frac{erV_{\text{tot}_1} + e^*A_{\text{tot}_1} + K_{\text{D}}^{\text{app}}}{2erV_{\text{tot}_1} + \sqrt{e^2r^2V_{\text{tot}_1}^2 + (K_{\text{D}}^{\text{app}})^2 + e^{*2}A_{\text{tot}_1}^2 - 2erV_{\text{tot}_1}e^*A_{\text{tot}_1} + 2K_{\text{D}}^{\text{app}}erV_{\text{tot}_1} + 2K_{\text{D}}^{\text{app}}e^*A_{\text{tot}_1}}}{2erV_{\text{tot}_1}} \quad (3.1)$$

3.4.8.2 Assay step 2: hemagglutination

When RBC suspension is added to the system, two processes happen simultaneously: viruses bind to SA-linked receptors on RBCs with their free hemagglutinin binding sites, and RBCs stick together and form aggregates whenever they collide such that virus particles are able to cross-link them.

For virus binding to SA-linked receptors, we assume mass-action kinetics, leading to:

$$\frac{dV(t)}{dt} = -k_{\text{ass}}^{\text{RBC}} \cdot \underbrace{(1 - \theta) \cdot r \cdot V(t)}_{\text{free virus sites}} \cdot \underbrace{[1 - \rho(t)] \cdot b \cdot \text{RBC}_{\text{tot}_2}}_{\text{free RBC sites}} + k_{\text{diss}}^{\text{RBC}} \cdot \underbrace{\frac{b}{b^*} \cdot \rho(t) \cdot \text{RBC}_{\text{tot}_2}}_{\text{bound RBC sites}}. \quad (3.2)$$

Kinetic constants for association and dissociation are denoted as $k_{\text{ass}}^{\text{RBC}}$ and $k_{\text{diss}}^{\text{RBC}}$. We assume $e = e^* = 3$ (Poumbourios et al., 1990) to define the contribution of the concentration of hemagglutinin receptors that are not covered by antibodies (free virus sites) to the association rate. Association further depends on the amount of RBC binding sites that are not yet covered by virus, defined by the fraction of covered sites, $\rho(t)$, the average number of SA-linked surface receptors each RBC carries, b , and the total concentration of RBCs in step 2 of the assay, $\text{RBC}_{\text{tot}_2}$. For the dissociation term, we assume that one virus particle covers on average b^* binding sites, since influenza virus particles are approximately 60-times smaller than RBCs (see below). The correction by b^* reflects

the definition of the fraction of covered RBC binding sites (making the term for bound RBS sites equivalent to the concentration of bound virus, $V_{\text{tot}_2} - V(t)$):

$$\rho(t) = \frac{b^* \cdot [V_{\text{tot}_2} - V(t)]}{b \cdot RBC_{\text{tot}_2}}. \quad (3.3)$$

To capture RBC aggregation, let B_k denote the concentration of agglutinating particles (individual RBCs and RBC aggregates) consisting of k cells, with a maximum aggregate size N . To describe the dynamics, we use the Smoluchowski coagulation equation (Von Smoluchowski, 1917), where the rate of agglutination is proportional to an agglutination rate constant k_{agg} and the number of available cross-linking sites $\rho(t)(1 - \rho(t))(1 - \theta)^2$, which is proportional to the number of mutual pairs of free binding sites on colliding RBCs and can be interpreted as a cross-linking probability:

$$\frac{dB_k(t)}{dt} = k_{\text{agg}}\rho(t)(1 - \rho(t))(1 - \theta)^2 \left(\frac{1}{2} \sum_{i+j=k} K_{ij}B_i(t)B_j(t) - B_k(t) \sum_{i=1}^N K_{ik}B_i(t) \right)$$

For the special case $K_{ij} = K_{ik} = K$, where the kernel is independent of the particle size, there is a simple analytical solution for the discrete size distribution of aggregates. Let $\sum_{i=1}^N B_i(t) = B_N(t)$ denote the total concentration of particles, and $B_N(t = 0) = RBC_{\text{tot}_2}$ the concentration of particles before agglutination. In addition, from mass conservation follows: $\sum_{k=1}^N kB_k(t) = RBC_{\text{tot}_2}$. Summing over all values of k then yields:

$$\begin{aligned} \frac{dB_N(t)}{dt} &= k_{\text{agg}}\rho(t)(1 - \rho(t))(1 - \theta)^2 \left[\left(\frac{K}{2}\right) \cdot RBC_{\text{tot}_2}^2 - K \cdot RBC_{\text{tot}_2}^2 \right] \\ &= -k_{\text{agg}}\rho(t)(1 - \rho(t))(1 - \theta)^2 \left(\frac{K}{2}\right) \cdot RBC_{\text{tot}_2}^2. \end{aligned}$$

Integrating once gives:

$$B_N(t) = \frac{RBC_{\text{tot}_2}}{1 + \left(\frac{k_{\text{agg}}}{2}\right) \rho(t)(1 - \rho(t))(1 - \theta)^2 RBC_{\text{tot}_2} t}. \quad (3.4)$$

Here, we set $K = 1$ such that the effect of K is lumped into k_{agg} because we estimated k_{agg} from data (see below).

3.4.8.3 Assay step 3: determination of HI titer

We define the degree of hemagglutination as:

$$h(t) = \left(1 - \frac{B_N(t)}{RBC_{\text{tot}_2}} \right) \cdot 100, \quad (3.5)$$

such that it takes values between 0% and 100%. If there is no hemagglutination, the concentration of agglutinated particles is the same as the initial concentration of RBCs ($B_N(t) = RBC_{\text{tot}_2}$) and the degree of hemagglutination is 0%. If all RBCs are agglutinated, there is only one agglutinating

particle in the system and $B_N(t) = 1/N_A \cdot 10^9$ nM, where N_A is Avogadro's number. Since $N_A \approx 6 \cdot 10^{23}$, $B_N \approx 10^{-15} \approx 0$ nM such that $h(t) = 100\%$.

3.4.9 Model implementation

To obtain the degree of hemagglutination $h(t)$ in Equation 3.5, we compute θ from Equation 3.1, $\rho(t)$ for any time point t in assay step 2 from Equations 3.2 and 3.3, and the corresponding $B_N(t)$ from Equation 3.4.

In addition, the total concentration of antibodies is given by

$$A_{\text{tot}_1} = 0.5 \cdot d_p \cdot d^j \cdot A_0,$$

where A_0 is the initial serum antibody concentration, d_p is the serum predilution factor, d the serial dilution factor and j the considered dilution step. The total concentrations of virus are

$$V_{\text{tot}_1} = 0.5 \cdot V_0 \text{ and } V_{\text{tot}_2} = 0.5 \cdot V_{\text{tot}_1},$$

because each assay step involves adding equal volumes of solution; V_0 is the initial virus concentration. Analogously,

$$RBC_{\text{tot}_2} = 0.5 \cdot RBC_0,$$

where RBC_0 is the initial concentration of RBCs.

The model is implemented in the R package `himodel` (<https://gitlab.com/csb.ethz/himodel>).

3.4.10 Model parameters and initial conditions

All model parameters and initial conditions could be either extracted or derived from literature (summarized in **Table 3.1**), except for the agglutination rate of RBCs (k_{agg}), which we estimated from data as described below.

3.4.10.1 RBC concentration (RBC_0)

Following the WHO protocol (WHO, 2002), a 0.75% (v/v) suspension of chicken RBCs is used to measure HI titers against H1N1pdm09. This corresponds approximately to $1.875 \cdot 10^6$ cells/mL (Tyrrell and Valentine, 1957). Given that 1 mol corresponds to $6.022 \cdot 10^{23}$ cells, the molar concentration is approximately $RBC_0 = 3.1 \cdot 10^{-5}$ nM. To determine the effect of pipetting errors, we set the RBC concentration range in the sensitivity analysis to 0.375%–1.5% (v/v) suspension, which corresponds to approximately $1.6 \cdot 10^{-5}$ – $6.3 \cdot 10^{-5}$ nM.

3.4.10.2 Number of sialic acid-linked receptors on RBC (b)

Influenza hemagglutinin binds to SA-linked surface receptors of RBCs. Human H1 influenza viruses bind preferentially to $\alpha 2 \rightarrow 6$ linked SA (Rogers and D'Souza, 1989), which occurs on the surface of chicken RBCs mainly in N-linked glycans (Aich et al., 2011; Aoki, 2017). Chicken RBCs

contain a mixture of $\alpha 2 \rightarrow 3$ and $\alpha 2 \rightarrow 6$ -linked glycans in a ratio of approximately 60:40–50:50 (Aich et al., 2011). The total number of N-glycan on RBCs has been estimated to be $1 \cdot 10^6$ (Aoki, 2017). Thus, we assume that the average number of receptors that can interact with hemagglutinin is $0.45 \cdot 10^6$. Chicken RBCs also have SA-linked O-glycans such as glycoporphins (Duk et al., 2000) on their surface, but most of them contain $\alpha 2 \rightarrow 3$ -linked SA. Therefore, we neglect them.

3.4.10.3 Steric virus factor (b^*): number of sialic acid-linked receptors covered by bound virions

Influenza virions are approximately 60-times smaller than RBCs (Harris et al., 2006). To model the binding of virions to RBCs, we need to take into account that bound virions cover multiple SA-linked receptors. We estimated the average number of covered $\alpha 2 \rightarrow 6$ SA-linked receptors, b^* , from simple geometry. We assume that SA-linked receptors are uniformly distributed on RBCs. Their estimated surface area ranges from 140–160 μm^2 and we assume an average surface area of $A_{\text{RBC}} = 150 \cdot 10^6 \text{ nm}^2$ (Ballas, 1987; Movassaghian and Torchilin, 2015). The virus-covered area is determined by the virus' diameter. Most influenza virions are spherical with a diameter ranging from 84–170 nm and mean diameter $d = 120 \text{ nm}$ (Harris et al., 2006). We estimate the shaded area from the circle area, which yields:

$$b^* = \frac{\pi(d/2)^2}{A_{\text{RBC}}} \cdot b \approx 34. \quad (3.6)$$

In the sensitivity analysis, we sample b^* assuming $d \sim \text{Unif}(84, 170)$, $A_{\text{RBC}} \sim \text{Unif}(130 \cdot 10^6, 170 \cdot 10^6)$, and $b \sim \text{Unif}(0.4 \cdot 10^6, 0.5 \cdot 10^6)$, where d has unit nm, A_{RBC} has unit nm^2 and b is unitless.

3.4.10.4 Virus concentrations (V_0)

To ensure the reproducibility of the HI assay, the same amount of virus particles must be used in each experiment. Therefore, virus concentration is measured in HA units, an operational unit that is determined in the so called HA titration assay, where virus is titrated against a constant amount of RBCs (same amount as used in the HI assay, i.e. 50 μL of 0.75% (v/v) RBC suspension are added to 50 μL serum-virus dilution). The amount of virus that agglutinates an equal volume of standardized RBC suspension is defined as 1 HA unit (WHO, 2002). Electron microscopy data show that partial hemagglutination occurs at 1:1 binding (on average, one virus particle binds to one RBC) (Tyrrell and Valentine, 1957). We assume that full hemagglutination requires at least 2:1 binding. We used the rate equation for virus-RBC binding (Equation 3.2) to determine the virus concentration that leads to 2:1 binding with $0.5 \cdot 3.1 \cdot 10^{-5} \text{ nM}$ RBC (**Figure S3.1a**): $3.2 \cdot 10^{-5} \text{ nM}$. Assuming that this virus concentration corresponds to 1 HA unit in our model simulations, 4 HA units are approximately $V_0 = 1.3 \cdot 10^{-3} \text{ nM}$. In the sensitivity analysis, we varied V_0 in the range of 3–7 HA units.

3.4.10.5 Agglutination rate (k_{agg})

We inferred the agglutination rate of RBCs from HI titer and serum IgG concentration of the reference serum using the inference procedure described in the next section. We used a broad

uniform prior for $k_{\text{agg}} \sim \text{Uniform}(10^5, 10^9)$, set the coagulation kernel K to 1 and fixed all remaining parameters to the values in **Table 3.1**. The k_{agg} posterior distribution was approximately log-normal (centered at around $2 \cdot 10^6 \text{ s}^{-1}$ with 95% credibility interval of approximately $0.4 \cdot 10^6 - 13 \cdot 10^6 \text{ s}^{-1}$) with slightly heavier tail towards larger k_{agg} values since hemagglutination reaches saturation at approximately 30 min (**Figure S3.1b**). Data at earlier time points would be needed to infer k_{agg} with higher precision. We set $k_{\text{agg}} = 2 \cdot 10^6 \text{ s}^{-1}$; the precision suffices as we are interested in hemagglutination at ≥ 30 min.

3.4.11 Inference of neutralizing antibody avidities

Given a measured IgG antibody concentration A_i of serum sample i (with estimated log mean $\mu_{A,i}$ and log standard deviation $\sigma_{A,i}$) and the corresponding HI titer determined in an HI assay with $j = 1, \dots, J$ dilution steps, serum predilution factor d_p , and serial dilution factor d , the generative model to infer the posterior distributions for $K_{D,i}^{\text{app}}$ is defined as follows:

$$\begin{aligned} K_{D,i}^{\text{app}} &\sim \text{Lognormal}(\mu_K, \sigma_K^2) \\ A_i &\sim \text{Lognormal}(\mu_{A,i}, \sigma_{A,i}^2) \\ A_{0,ij} &= A_i \cdot d_p \cdot d^j \\ \theta_{ij} &= f_\theta(A_{0,ij}, K_{D,i}^{\text{app}}) \\ \rho_{ij} &= f_\rho(\theta_{ij}) \\ h_{ij} &= f_h(\rho_{ij}, \theta_{ij}) \\ p_{ij} &= \text{logit}^{-1}(\alpha(h_{ij} - h_0)) \\ y_{ij} &\sim \text{Bernoulli}(p_{ij}). \end{aligned}$$

Here, $A_{0,ij}$ is the final concentration of diluted serum IgG at dilution step j . It gives rise to sample- and dilution-specific θ_{ij} , ρ_{ij} , and h_{ij} as defined by Equations 3.1, 3.3 and 3.5 (here abbreviated for convenience with f_θ , f_ρ and f_h and with time dependencies dropped).

To specify the HI titer of serum sample i , each serum dilution j is inspected for hemagglutination inhibition and the minimal dilution that shows full inhibition is determined. We treat the binary decision at each dilution step (inhibition/no inhibition) as a Bernoulli process with inhibition probability p_{ij} , a shorthand notation for $P(y_{ij} = 1 \mid h_{ij})$. The indicator variable y_{ij} takes the value 0 if the hemagglutination degree h_{ij} is above a certain threshold h_0 (no inhibition) and 1 otherwise (inhibition):

$$y_{ij} = \begin{cases} 0, & \text{if } h_{ij} > h_0 \text{ (no inhibition),} \\ 1, & \text{if } h_{ij} \leq h_0 \text{ (inhibition).} \end{cases} \quad (3.7)$$

This binary decision is modelled by a logistic function with steepness parameter α and inflection point h_0 . The conditional likelihood for $\mathbf{y}_i^T = (y_{i1}, y_{i2}, \dots, y_{ij})$ over all J dilutions is then given by a product of Bernoulli likelihoods:

$$P(\mathbf{y}_i | K_{D,i}^{\text{app}}, A_i) = \prod_{j=1}^J p_{ij}^{y_{ij}} \cdot (1 - p_{ij})^{(1-y_{ij})} \quad (3.8)$$

and the full posterior is:

$$P(K_{D,i}^{\text{app}}, A_i | \mathbf{y}_i) = \frac{P(K_{D,i}^{\text{app}}) P(A_i) P(\mathbf{y}_i | K_{D,i}^{\text{app}}, A_i)}{P(\mathbf{y}_i)}. \quad (3.9)$$

We sampled posterior distributions using the Metropolis-Hastings algorithm (Brooks et al., 2011) with 6000 samples, burn-in size of 1000 samples, and 5 chains. We used a broad log-normal prior for $K_{D,i}^{\text{app}}$ centered at 1 nM with log mean $\mu_k = 0$ and log standard deviation $\sigma_k = 4$. To define the value of h_0 , we investigated the relationship between HA units and hemagglutination degree in our HA titration simulations. The model predicted that the hemagglutination degree is $> 75\%$ for ≥ 1 HA unit (**Figure S3.1c**), which by definition corresponds to full hemagglutination. Thus, assuming symmetry, we consider $h_0 = 25\%$ a reasonable estimate, also assuming that differences below 25% cannot be distinguished by eye. However, a different value for h_0 does not affect the interpretation of our results: it would only shift the estimates of all samples either towards lower avidities (for larger h_0) or higher avidities (for smaller h_0). Steepness parameter α affects only the width of the posterior distribution. Here, we set $\alpha = 15$ and then investigated the relationship between posterior distribution and resulting HI titer by sampling. We sampled 500 times from the joint posterior distribution of $K_{D,i}^{\text{app}}$ and A_i for all patient sera i and predicted the resulting HI titer to investigate the uncertainty in $K_{D,i}^{\text{app}}$ due to discretization of HI titer measurements and ELISA measurement error. On average, approximately 55% of samples resulted in the observed HI titer, whereas approximately 95% of samples also included HI titers one dilution step higher or lower than the actually observed HI titer.

3.4.12 Identification of patients with increase in avidity and increase in non-neutralizing IgG

For each inferred K_D^{app} value, we identified the uncertainty interval due to ELISA measurement error and dichotomization in HI titers by sampling from the joint posterior distribution (see above) and considered non-overlapping intervals as a significant change in K_D^{app} . To detect patients that produced non-neutralizing IgG after vaccination, we identified patients that showed no increase in HI titer while showing an increase in serum IgG that resulted in a significant decrease in avidity (**Figure S3.4a**).

3.4.13 Sensitivity analysis

Sobol sensitivity analysis attributes variance in model output to individual model input factors using variance decomposition (Saltelli et al., 2004). Given k model inputs, the total variance $V(y)$ in model output can be decomposed as:

$$V(y) = \sum_i V_i + \sum_i \sum_{j>i} V_{ij} + \dots + V_{12\dots k}, \quad (3.10)$$

where $V_i = V(E(Y|x_i))$ is the variance with respect to the distribution of input factor x_i . The second-order interaction term $V_{ij} = V(E(Y|x_i, x_j)) - V_i - V_j$ captures the part of the effect of x_i and x_j that is not described by the first order terms V_i, V_j and so on. The relative contribution of each term to the unconditional variance $V(y)$ serves as a measure of sensitivity. For instance, V_i will be large, if x_i is influential. The first order Sobol sensitivity index is defined as

$$S_i = \frac{V_i}{V(y)}. \quad (3.11)$$

To obtain the total contribution of x_i , that is the sum of all terms in the variance decomposition that include x_i , we compute the total contribution to variance $V(y)$ due to all factors but x_i , denoted by \mathbf{x}_{-1} . The total Sobol sensitivity index for x_i is then given by

$$S_i^T = \frac{V(y) - V(E(y|\mathbf{x}_{-1}))}{V(y)}. \quad (3.12)$$

We used Monte Carlo estimation to estimate Sobol indices (Jansen, 1999; Saltelli et al., 2010) implemented in the R package `sensitivity` (Iooss et al., 2019) with $n = 10000$ random samples of model input vector $\mathbf{x}^T = (x_1, x_2, \dots, x_k)$ and 10 bootstrap replicates to estimate confidence intervals. Input variables were assumed to be independent of each other. We considered $k = 12$ inputs sampled within a biologically reasonable range (**Table 3.1**).

3.4.14 Statistical analysis

Serum IgG and inferred K_D^{app} values were available for 43 patients at five time points ($t = 0, 7, 30, 60, 180$ days) with 197 observations in total. To estimate the effects of a patient's immune state on serum IgG and avidity ($1/K_D^{\text{app}}$), we used a linear mixed model with patient-specific random intercepts that takes the following general form:

$$\begin{aligned} y_{ij} &= \beta_0 + x_{ij}^T \beta_1 + \gamma_i + \epsilon_{ij}, \\ \gamma_i &\sim \mathcal{N}(0, \sigma_\gamma^2), \\ \epsilon_{ij} &\sim \mathcal{N}(0, \sigma_\epsilon^2), \end{aligned}$$

where y_{ij} is the log2-transformed IgG concentration or $1/K_D^{\text{app}}$ value, respectively, of patient i at time point j , x_{ij} is a p -dimensional vector of p covariates, β_0 is an intercept term, β_1 is a vector of fixed

effects, γ_i the random patient-specific intercept, and ϵ_{ij} models the within-patient measurement error. We modeled the observed rise and fall of serum IgG and $1/K_D^{\text{app}}$ value after vaccination using a second-degree polynomial. To distinguish time trends in avidity between neutralizing and non-neutralizing IgG responders, we added a dummy variable for neutralizing response when analysing response in avidity. Time post HSCT ≤ 2 years, cGVHD grade, and immunosuppression grade were added as fixed effects on intercept to investigate effects on baseline, and on slope to investigate effects on response. Time post HSCT ≤ 2 years was encoded as a binary variable (1 for ≤ 2 years, 0 for > 2 years). Both cGVHD and immunosuppression grade were encoded as numerical variables with values 0, 1, 2, 3, such that grade 0 is the reference level, and there is a linear increase in effect with increasing grade. To control for potential confounders, we corrected for sex and age. For model selection, the full model with fixed effects on slope and intercept was fitted using maximum likelihood estimation implemented in the `lmer4` package (Bates et al., 2015) and type II ANOVA by Satterthwaite's approximation provided by the `lmerTest` package (Kuznetsova et al., 2017).

We detected no significant effects on response for serum IgG and avidity. Therefore, we removed fixed effects on slope and refitted the final models using restricted maximum likelihood estimation to obtain unbiased estimates (Bates et al., 2015). Residuals indicated that the normality assumption was satisfied (**Figure S3.4b**). Confidence intervals were computed via the Wald method provided by `lme4`. To compare the results with HI titers, we estimated the effect of time post HSCT ≤ 2 years, cGVHD grade, and immunosuppression on HI titers controlling for age, sex, and time after vaccination using a generalized linear regression model for sequential ordered data (Tutz, 1991). The model was fitted using maximum likelihood estimation implemented in `VGAM` (Yee et al., 2010).

3.4.15 Data and software availability

The model is available in the R package `himodel` (<https://gitlab.com/csb.ethz/himodel>). Source files necessary to reproduce the results of this work are available on GitLab (<https://gitlab.com/csb.ethz/himodel-manuscript>).

3.4.16 Conflict of interests

None.

3.4.17 Author contributions

JL, JS, and AE designed the study. JL and JS developed the model. JL and MS designed and performed experiments. JL analysed data, implemented the model, and performed simulations. JH and YH recruited patients, collected patient samples, and patient information. YH, JH and AE consulted on medical questions. JS and AE supervised the project. JL and JS wrote the first draft of the manuscript, and all authors commented on the final version.

3.4.18 Acknowledgments

We thank our clinical collaborators Nathan Cantoni (Cantonal Hospital Aarau) and Sabine Ruosch-Girsberger (Cantonal Hospital Lucerne) for providing patient sera and supporting the cohort study. We thank Dominik Vogt and Lukas Kaufmann for technical support with patient samples and Fabian Rudolf for advice on the experimental design of avidity measurements.

3.5 SUPPLEMENTARY FIGURES

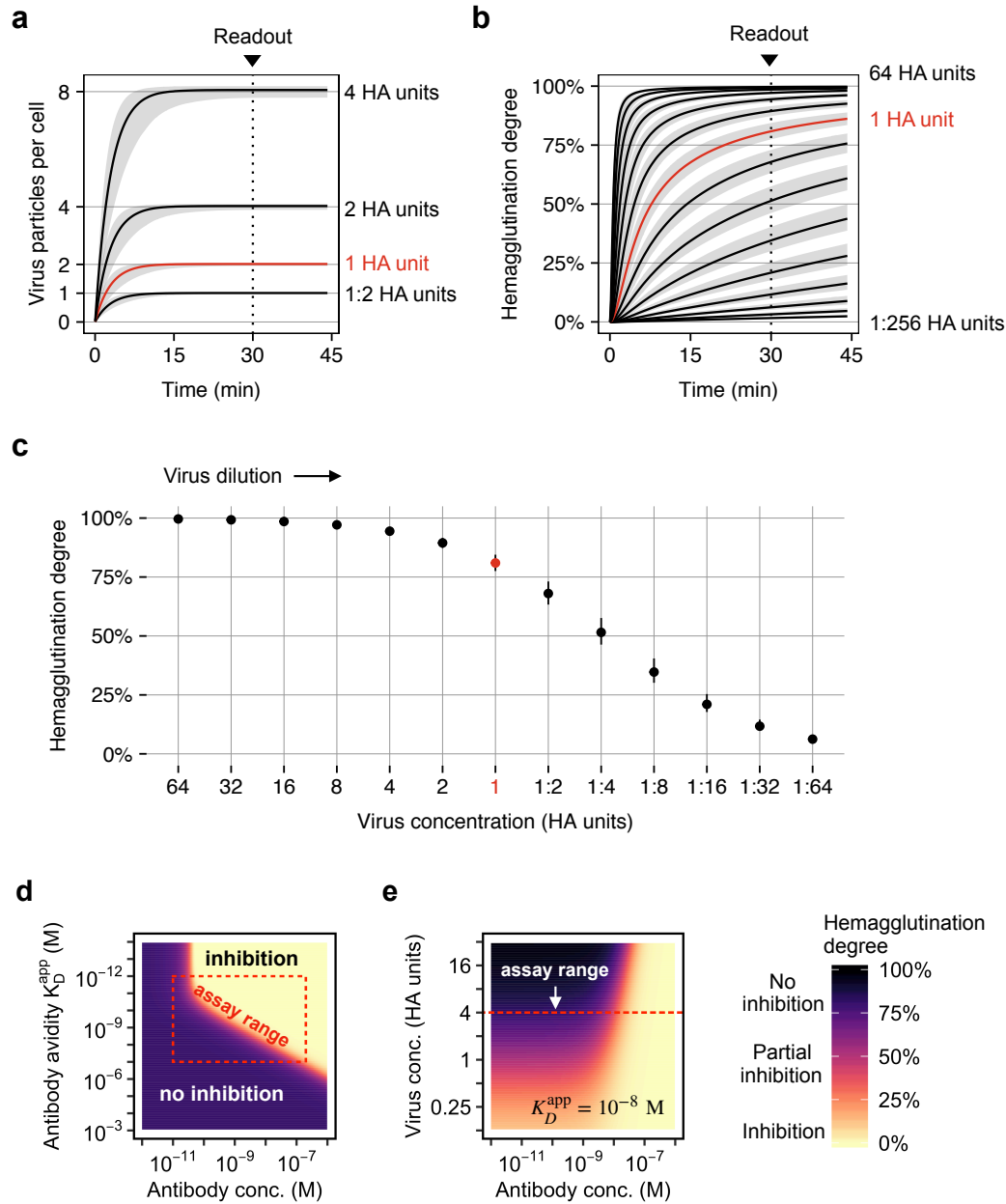


Figure S3.1. Simulation results for the HA titration assay with influenza H1N1pdm09 and model sensitivity. (a) Binding kinetics of virus particles to red blood cells. We assume that full hemagglutination requires at least two bound virus particles per cell. (b) Hemagglutination kinetics. (c) For HA units ≥ 1 , the hemagglutination degree is $> 75\%$, which is by definition interpreted as full hemagglutination. Gray areas and error bars indicate the uncertainty due to uncertainty in model parameters. (d) Performing the HI assay with 4 HA units balances sensitivity and robustness. There is a clear distinction between inhibition and no inhibition. (e) In addition, the assay detects with 4 HA units lower antibody concentrations than with ≥ 8 HA units.

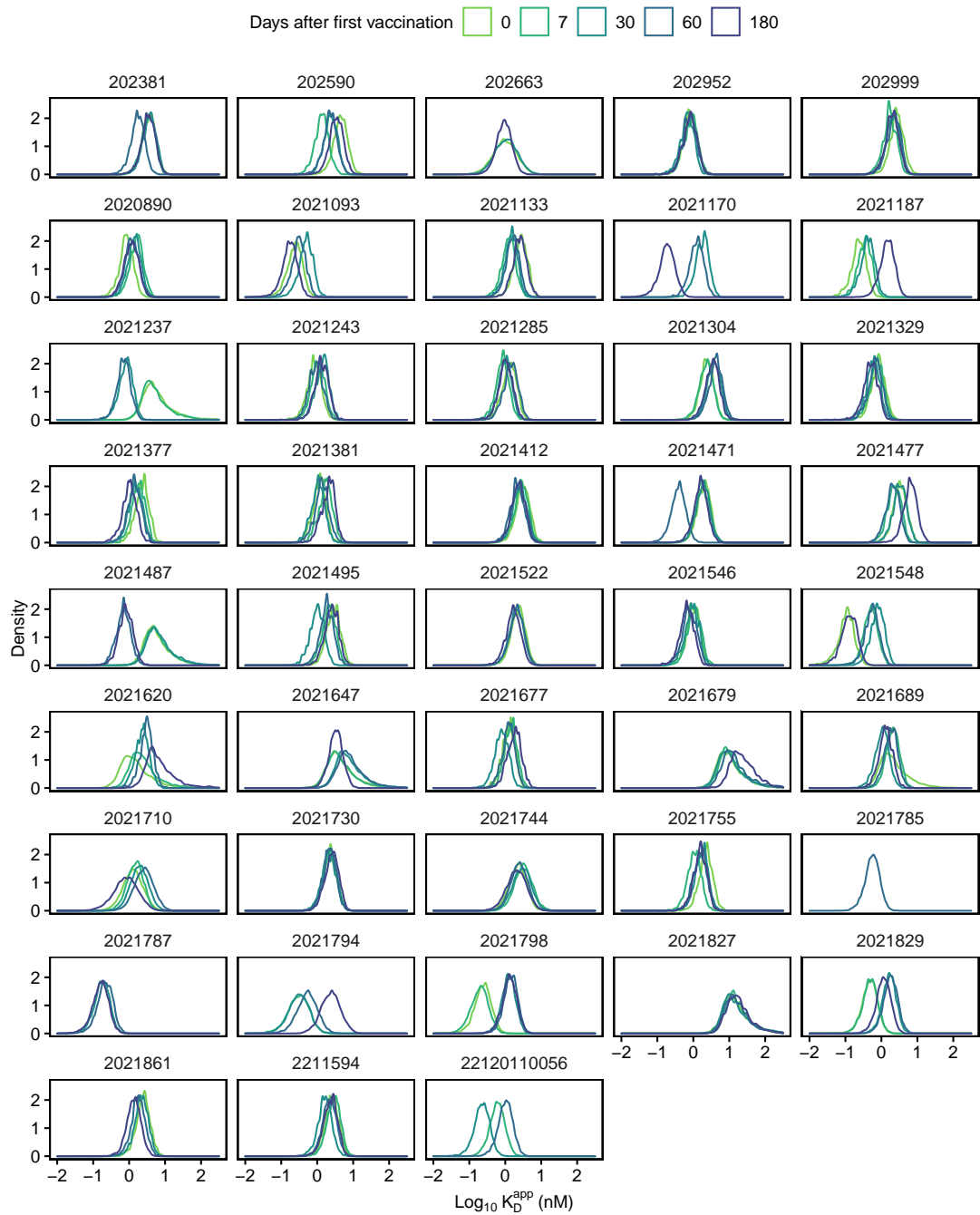


Figure S3.2. Marginal posterior distributions of the apparent dissociation constants in 43 patients (197 posteriors in total). Some posteriors show larger variance due to larger measurement error in ELISA-detected IgG concentration. Here, for samples with HI titer < 8, the shown posterior distributions correspond to the inferred avidity when assuming HI titer = 4 (affected 23 serum samples from seven patients)

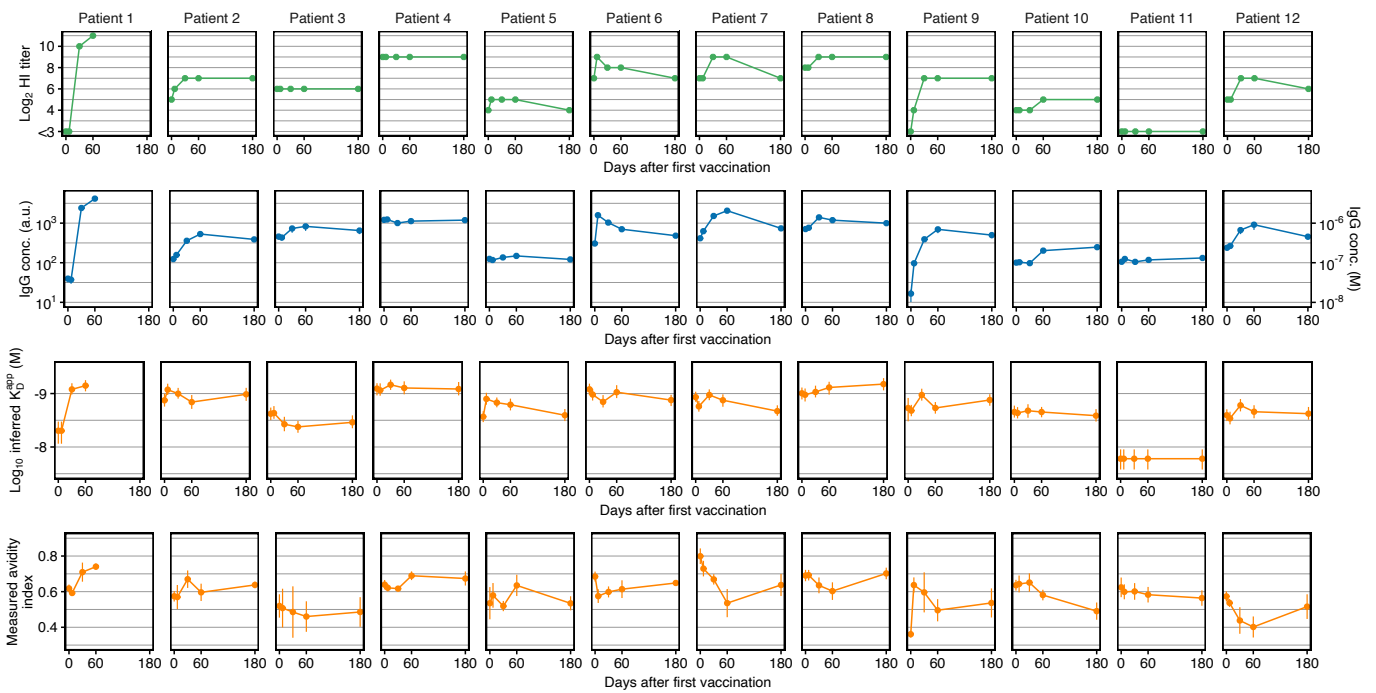


Figure S3.3. HI titer, ELISA-detected anti-H1N1pmd09 serum IgG concentration, inferred apparent dissociation constant and experimentally determined avidity index in twelve patients. Avidity indices correspond to the fraction of H1N1pmd09-specific serum IgG remaining bound after 4M urea treatment. Data shows mean and standard deviation for serum IgG and avidity indices and the median of the posterior distribution with the uncertainty range due to discretized HI titer measurements and ELISA measurement error for inferred apparent dissociation constants K_D^{app} . Most patients showed either little or no increase in avidity. In some patients, the measured avidity decreased and then returned back to baseline on d180, potentially because the vaccine-induced short-lived antibodies were sensitive to the urea treatment, resulting in antibody denaturation.

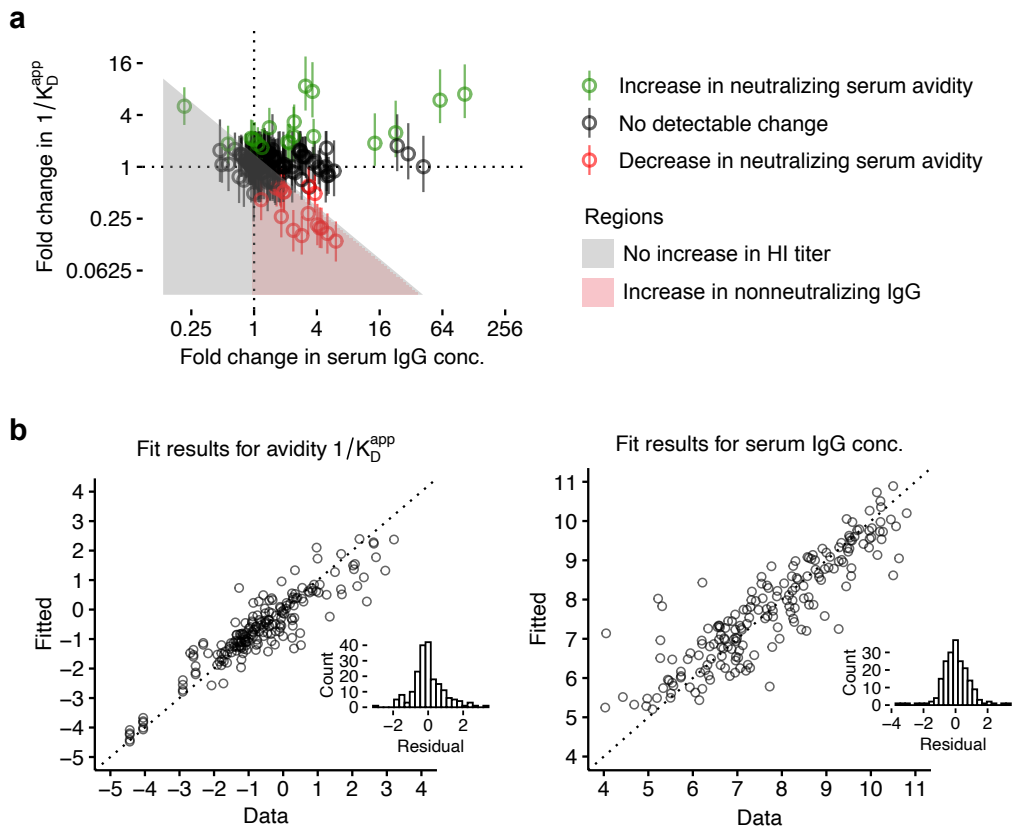


Figure S3.4. Vaccine response analysis in 43 patients (197 samples in total). (a) Fold change in inferred avidity and serum IgG concentration after vaccination. Error bars indicate uncertainty in fold change due to uncertainty in inferred K_D^{app} -values. Shading indicates regions with qualitatively different responses to vaccination. (b) Residual plots of the regression models used to investigate associations of criteria for compromised immune response with avidity and serum IgG concentration.

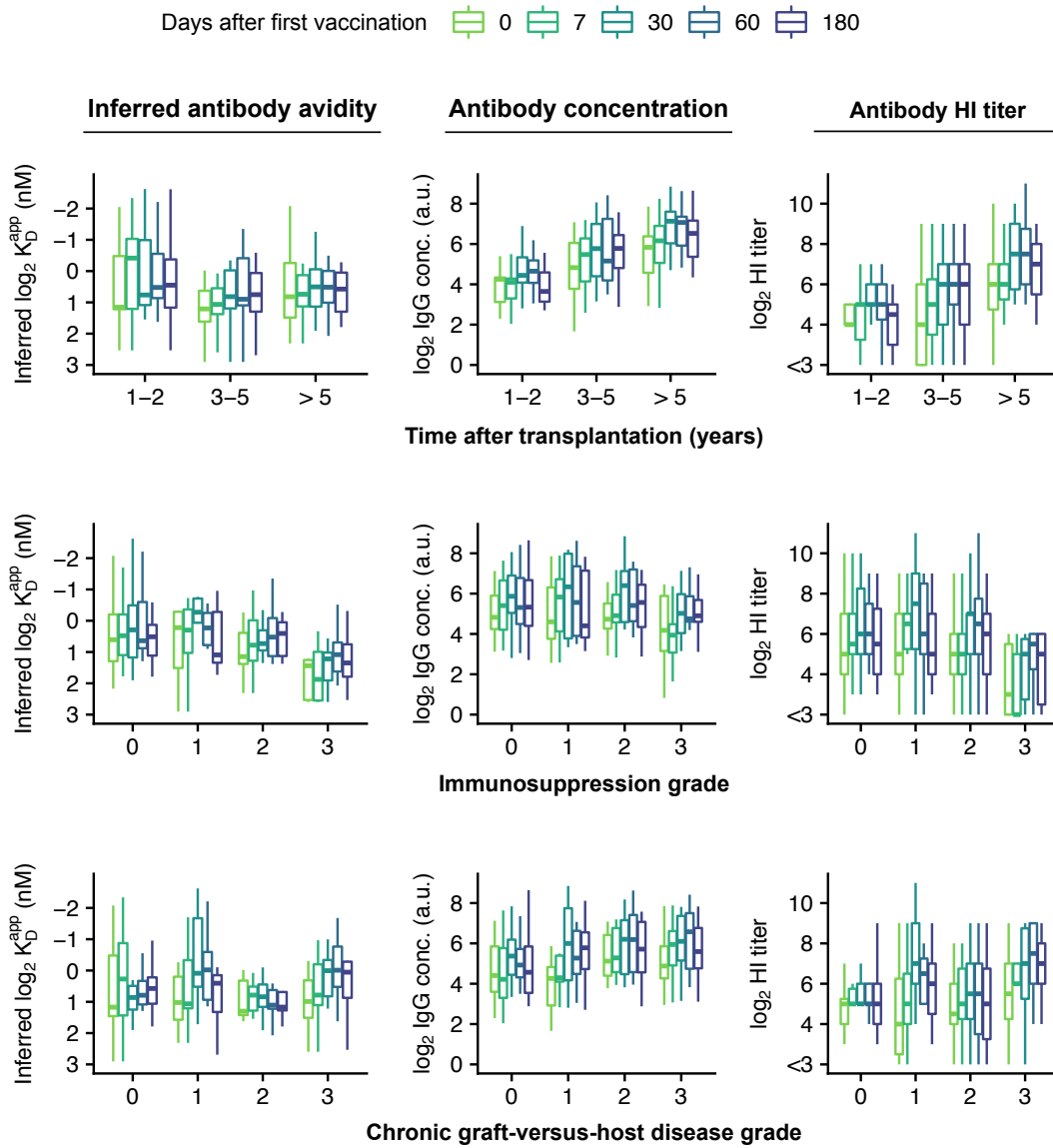


Figure S3.5. Inferred avidity, serum IgG concentration, and HI titers by time after transplantation, immunosuppression grade, and cGVHD grade in 43 patients (197 samples in total). Note that data show one-dimensional associations, whereas regression analysis was performed with a high-dimensional model simultaneously accounting for time after transplantation, immunosuppression/cGVHD grade, and correcting for sex and age.

INFERRING DIFFERENCES IN IMMUNE RESPONSE DYNAMICS FROM INFLUENZA VACCINE-INDUCED ANTIBODY TITERS IN IMMUNOCOMPROMISED PATIENTS

This chapter is to be submitted as: J. Linnik, A. Egli, and J. Stelling. "Inferring differences in immune response dynamics from influenza vaccine-induced titers in immunocompromised patients".

4.1 ABSTRACT

Vaccination aims at inducing high-levels of neutralizing antibodies and memory B cells that can protect the host from infection. Memory B cells and antibody-producing plasma cells evolve from germinal centers (GCs), where B cells compete for survival signals in a dynamic process, resulting in a rapid expansion of antigen-specific B cells. To which extent influenza vaccination induces GC reactions in immunocompromised patients is unknown and very difficult to study experimentally. Therefore, we asked whether our current understanding of GC dynamics captured by a mathematical model is able to explain the heterogeneous vaccine response in a population of hematopoietic stem cell transplant patients ($n = 102$). We integrated patient group-specific parameters into the classical GC reaction model according to mechanistic hypotheses on how these patient factors affect GC processes and inferred them from antibody titers. The model suggests that both reactivated memory B cells and GCs contribute to the observed vaccine response. The heterogeneity in antibody response was well described by only a few patient-specific variables, such as preexisting memory B cells, absolute lymphocyte count and IFN- λ genotype. Specifically, the model suggests that an increase in lymphocyte count increases the number of successfully formed GCs and potentially affects additional GC processes leading to higher antibody titers. This study demonstrates how dynamic modelling of the immune response can be combined with clinical patient information and statistical inference to investigate a heterogeneous antibody response from easily accessible measurements.

4.2 INTRODUCTION

The germinal center (GC) reaction is one of the most important processes of the human adaptive immunity (Victoria and Wilson, 2015; Mesin et al., 2016). GCs arise temporarily upon infection or vaccination in secondary lymphoid follicles (LFs) as densely packed, structured micro-environments, where resident follicular dendritic cells (FDCs) present antigen to B cells and fuel B cell proliferation (Gatto and Brink, 2010; Tam et al., 2016). Somatic hypermutation diversifies B cell receptors and mutated B cells that can bind the antigen compete for interaction with helper T cells to receive additional survival signals (Turner et al., 2018; Woodruff et al., 2018). As a result, antigen-specific B cells expand and differentiate to memory B cells or antibody-producing plasma cells ready to fight infection. The classical GC model distinguishes between two different GC B cell populations:

rapidly dividing centroblasts in the dark zone of the GC and non-proliferating centrocytes in the light zone that compete for T cell help (Allen et al., 2007a; Mesin et al., 2016).

Over the past decades, the investigation of the dynamic nature of the GC reaction has been accompanied by mathematical modelling to help data interpretation and suggest novel hypotheses (reviewed in Buchauer and Wardemann (2019)). In recent years, our understanding of the GC reaction to different types of antigens rapidly evolved thanks to novel sequencing and *in vivo* imaging techniques (Schwickert et al., 2007; Victora et al., 2010; Schwickert et al., 2011; Tas et al., 2016; Kuraoka et al., 2016; Firl et al., 2018). Mathematical models of a single GC helped to interpret the new wealth of data and to investigate mechanistic hypotheses on GC B cell selection, recycling, differentiation, and feedback mechanisms (Figge et al., 2008; Meyer-Hermann et al., 2012; Zhang et al., 2013; Papa et al., 2017; Hauser et al., 2007). Since activated GCs may respond in a coordinated manner, e. g., due to secreted antibodies that mask antigen in neighboring GCs (Schwickert et al., 2007; Zhang et al., 2013), models of GC populations have been developed to describe affinity maturation and antibody diversity during infection (Childs et al., 2015; Murugan et al., 2018). A model of several GC reactions in parallel has been successfully applied to explain affinity maturation during malaria infection in humans (Murugan et al., 2018). But how GC reactions may vary between individuals is not well characterized. An experimental study demonstrated recently that seasonal influenza vaccination can induce GC reactions in the draining lymph nodes (Turner et al., 2020). Therefore, we asked whether our current understanding of GC dynamics can explain the heterogeneous influenza vaccine-induced antibody in an immunocompromised patient population.

We combined the classical GC reaction model with a biophysical model of the hemagglutination inhibition (HI) assay to describe the vaccine-induced HI titer response against influenza A/California/7/2009 H1N1. We applied the model to a population of HSCT patients ($n = 102$) that received two doses of a seasonal influenza vaccine at a 30-day interval. HSCT patients are often immunocompromised due to graft-related comorbidities and immunosuppressive treatment, putting them at high risk for severe influenza infections (Ogonek et al., 2016; Schuster et al., 2017). They show a highly heterogeneous vaccine response, and a better understanding of why certain patient groups elicit a stronger antibody response than others could help to develop more targeted preventive strategies for vulnerable patient groups. We previously identified the most important patient factors associated with the antibody titer response in the investigated patient population (Chapter 2). We integrated these patient factors into the GC model based on mechanistic hypotheses about how these factors modulate crucial GC processes, such as B cell survival, selection, cycling between the light and the dark zone, and the number of activated GCs. Using a Bayesian inference approach, we inferred the patient factor-specific GC model parameters directly from measured antibody titers, taking the antibody response from preexisting memory B cells into account.

With the inferred parameters and initial memory B cell concentrations, the model could recapitulate different antibody responses over the full range of observed antibody titers. The model predicted that the observed heterogeneity in responses could be explained by previously acquired memory B cells and a few patient factors potentially modulating the GC reaction, such as absolute lymphocyte count and interferon (IFN)- λ genotype. Specifically, the model suggests that an increase in lymphocyte count increases the number of successfully formed GCs and potentially affects additional

GC processes leading to higher antibody titers. Moreover, the model suggests that the associations between antibody titers and chronic graft-versus-host-disease (cGVHD), immunosuppressive treatment with calcineurin inhibitors, and family relationship with the donor could be fully explained by differences in the amount of previously acquired memory B cells.

4.3 RESULTS

4.3.1 Vaccine response model

We combined published models of the humoral immune response and the GC reaction (Rundell et al., 1998; Iber and Maini, 2002) into a concise ordinary differential equation (ODE) model that describes with 35 parameters (**Table 4.1**) and ten model states (**Table 4.2**) the key processes of the GC-dependent IgG production: antigen uptake and presentation in lymph nodes, clonal expansion of centroblasts, selection and recycling of centrocytes, and bifurcation to plasma and memory B cells (**Figure 4.1a**). The model accounts for both the activation of naive B cells and the activation of memory B cells upon re-exposure to the antigen. Each key process of the GC reaction that determines GC B cell dynamics and B cell fate is captured by a single parameter: the duration of the GC reaction is determined by the fraction of absorbed antigen π_{abs} , GC B cell survival by the survival probability π_{surv} , the probability of non-fatal mutations is given by π_{mut} , the selection probability of centrocytes by π_{sel} , the recycling probability of centrocytes by π_{rec} , and the bifurcation into memory or plasma B cells by π_{mem} or $1 - \pi_{\text{mem}}$, respectively. The total number of activated GCs is restricted by the total volume of activated secondary LFs (V_{LF}), which defines a physical upper bound for the maximal total volume of activated GCs (**Figure 4.1b**). To link the IgG response to the observed HI antibody titers, we used a previously established biophysical model of the HI assay (Linnik et al. (2020), presented in Chapter 3).

The model captures the qualitative dynamics of B cells in GCs as well as the response in IgG and HI titers upon primary and secondary immunization (**Figure 4.1c**): Activated B cells (B_{act}) peak on approximately day 4 after vaccination (De Silva and Klein, 2015). Proliferation of GC B cells (B_{cb} and B_{cc}) is most active between d7 and d14 (Liu et al., 1991; De Silva and Klein, 2015). After two weeks, the GC begins to dissolve, and after three weeks the GC reaction is fully terminated. In general, the duration of the GC reaction depends on the amount of antigen retained in the GC and presented by FDCs (AG_{pr}) (Gatto and Brink, 2010; Tam et al., 2016), which is controlled in our model by the fraction of absorbed antigen π_{abs} (**Figure 4.6a**). The amount of centroblasts (B_{cb}) exceeds the amount of centrocytes (B_{cc}) as found *in vivo* (Victora et al., 2010). The $B_{\text{cb}}/B_{\text{cc}}$ ratio increases if the selection is less stringent (with $\pi_{\text{sel}} = 5\%$ shown in purple vs. $\pi_{\text{sel}} = 20\%$ in the other simulation scenarios, **Figure 4.1c**) as previously shown experimentally (Victora et al., 2010) and in simulation studies (Meyer-Hermann et al., 2012). Memory B cells appear on approximately d7 after vaccination. If high levels of previously acquired antigen-specific memory B cells are present, the model predicts a strong and rapid IgG response (Siegrist, 2008), which is already detectable on d7 in the HI assay (shown in green in **Figure 4.1c**). Without preexisting memory, plasma B cells and IgG antibodies begin to appear after one week and reach a maximum after approximately four weeks (Siegrist, 2008). The response to the second vaccination (injected on

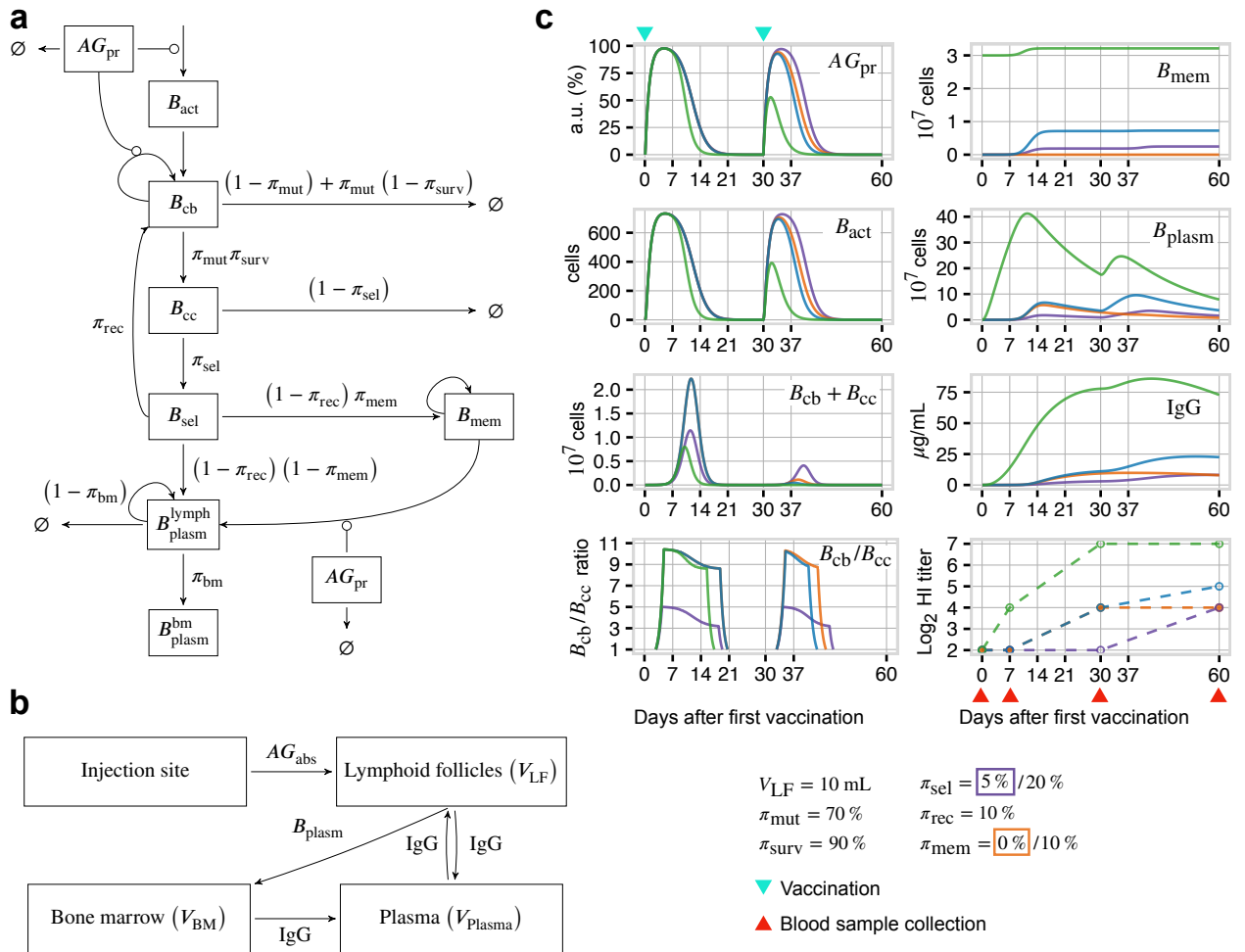


Figure 4.1. Overview of the vaccine response model. (a) Schematic overview of the germinal center reaction model. Arrows indicate transitions, edges on arrows indicate activations. Model states are summarized in **Table 4.2** and model parameters in **Table 4.1**. For a detailed model explanation with model equations, see **Methods**. (b) Model compartments. Injected vaccine antigen is transported from the subcutaneous tissue to the draining lymph nodes, where it is presented by antigen-presenting cells to initiate and fuel the GC reaction. IgG antibody-producing plasma B cells eventually migrate from the lymph nodes to the bone marrow, where they can survive for several months or even years. IgG antibodies are released into the plasma, where they are detected in HI assay experiments. High levels of secreted antibodies can block antigen presentation in lymph nodes and inhibit the GC reaction (Zhang et al., 2013). (c) Four different simulation scenarios of the response to two doses of seasonal influenza vaccination (first shot on d0, second shot on d30). The green line shows a response with high-levels of preexisting memory B cells. The other simulation scenarios assume no preexisting memory and show a strong vaccine response with vaccine-induced production of memory B cells (blue), a strong response without vaccine-induced production of memory B cells (orange), and a poor vaccine response which is only detectable in the HI assay after the second vaccination (purple). Simulations were performed with the parameter values summarized in **Table 4.1** and as indicated in the figure legend. Cell numbers refer to the total amount of the respective B cell population. IgG concentration refers to the concentration in plasma, which gives rise to the HI titer measured on d0, d7, d30, and d60 (here modelled for influenza A/California/7/2009).

d30) depends on the amount of memory B cells that can be reactivated and on the IgG level on d30 (high levels of neutralizing IgG block the antigen and inhibit the GC reaction) (Zhang et al., 2013; Andrews et al., 2019; Kil et al., 2019).

The actual number of activated GCs after influenza vaccination is unknown. Our model predicts that the maximal number of GC B cells is in the order of 10^7 for a strong immune response and 10^6 for a weaker response when neutralizing antibodies are already present. Assuming a fully activated GC consists of 10^4 – 10^5 cells (Liu et al., 1991; Küppers et al., 1993), this corresponds to approximately 100–1000 activated GCs for a strong, and 10–100 for a weak response. The maximal volume of one GC has been estimated to approximately 0.01 mL (Hollowood and Macartney, 1992). Given that the median volume of one lymph node is 10 mL (IQR 5–21 mL) (Agrawal et al., 2017), one lymph node might contain several hundred or up to 1000 GCs. Thus, our model predicts that influenza vaccination could induce on the order of 1–10 lymph nodes. This seems physiologically feasible as humans have about 20 axillary lymph nodes that drain the muscle of the upper arm in which the influenza vaccine is injected (Carati et al., 2010).

In summary, the model is able to recapitulate different types of vaccine responses consistent with our current understanding of the IgG-producing B cell response. Importantly, the model establishes a link between B cell dynamics and HI antibody titers.

4.3.2 Sensitivity to GC reaction parameters

We performed a Sobol sensitivity analysis to quantify the sensitivity of the plasma IgG level to the parameters modelling the key processes of the GC reaction (**Figure 4.2a**). Parameters were varied within a physiologically reasonable range (**Table S4.1**). Since the normal range of activated LFs after vaccination is unknown, we assume that at most ≈ 10 lymph nodes are activated as predicted by our model. The fraction of non-fatal mutations π_{mut} has been derived from mathematical modelling by Shlomchik et al. and has been estimated to $\approx 70\%$ (Shlomchik et al., 1998), which approximately matches with the number of non-apoptotic centroblasts (Liu et al., 1991; Hardie et al., 1993; Iber and Maini, 2002). Shlomchik et al. reported a very high sensitivity of their model outcome to the number of total mutations, concluding that the true value must be very close to this estimate. Consistent with their result, we observe a high sensitivity for π_{mut} assuming $\pi_{\text{mut}} = 50$ – 90% .

The sensitivity analysis suggests that processes involved in B cell proliferation dominate the IgG level, especially the survival probability π_{surv} (**Figure 4.2a**). The number of GC seeding B cells (β_{seed}) is only a minor contributor to the final IgG levels as it is probably compensated for in the subsequent clonal expansion. The migration of plasma B cells to the bone marrow (where B cells can survive over several months) is mostly relevant for the long-term antibody production (>d60 post vaccination). Interestingly, our model predicts a non-monotonic dependency of IgG on the recycling probability π_{mut} with an optimum at 45% (**Figure 4.2b**). Similarly, Oprea and Perelson predicted a non-monotonic dependency of the total affinity on the recycling probability with an optimum at 70% (Oprea and Perelson, 1997).

Table 4.1. Overview of model parameters. Most parameters were set to literature values or to estimated values as indicated below. The posterior distributions of estimated parameters are shown in **Figure 1.4**. Abbreviations: Ag, antigen; GC, germinal center; IgG, immunoglobulin G; LF, lymphoid follicle.

Description	Symbol	Value	Unit	Reference
Ag absorption	α_{abs}	1	d^{-1}	MacLean et al. (2001)
Ag decay	d_{ag}	0.012	d^{-1}	Tew and Mandel (1979)
Fraction of absorbed Ag	π_{abs}	Estimated	Unitless	(Figure 4.4)
Ag presentation	α_{pr}	1	d^{-1}	Set such that $AG_{\text{pr}}^{\text{max}} = 100\%$ reached on d4 (Liu et al., 1991; Hollowood and Macartney, 1992)
Decay of presented Ag	d_{pr}	1	d^{-1}	Set such that $AG_{\text{pr}}^{\text{max}} = 100\%$ reached on d4 (Liu et al., 1991; Hollowood and Macartney, 1992)
Activation and seeding of GC	β_{seed}	300	$\text{cells mL}^{-1} \text{d}^{-1}$	Set such that ≈ 100 cells seed GC (Tas et al., 2016)
Differentiation to centroblasts	β_{cb}	4	d^{-1}	Liu et al. (1991)
Maximal proliferation of centroblasts	$\beta_{\text{prol}}^{\text{cb}}$	4	d^{-1}	Liu et al. (1991)
Survival probability of centroblasts	π_{surv}	Estimated	Unitless	(Figure 4.4)
Probability of non-fatal mutations	π_{mut}	0.7	Unitless	Shlomchik et al. (1998)
Degradation of centroblasts	d_{cb}	0.8	d^{-1}	Liu et al. (1994)
Differentiation to centrocytes	β_{cc}	2	d^{-1}	Liu et al. (1991)
Selection of centrocytes	β_{sel}	48	d^{-1}	Meyer-Hermann et al. (2012)
Selection probability of centrocytes	π_{sel}	Estimated	Unitless	(Figure 4.4)
Recycling of centrocytes	β_{rec}	12	d^{-1}	Victoria et al. (2010)
Recycling probability of centrocytes	π_{rec}	Estimated	Unitless	(Figure 4.4)
Degradation of centrocytes	d_{cc}	3	d^{-1}	Cohen et al. (1992)
GC-limiting cell concentration	C_{gc}	$5 \cdot 10^7$	cells mL^{-1}	Rundell et al. (1998)

Differentiation to plasma B cells	β_{plasm}	4	d^{-1}	GC B cell differentiation rate (Liu et al., 1991)
Differentiation to memory B cells	β_{mem}	4	d^{-1}	GC B cell differentiation rate (Liu et al., 1991)
Bifurcation parameter for differentiation to memory/plasma B cells	π_{mem}	Estimated	Unitless	(Figure 4.4)
Proliferation of plasma B cells in lymph nodes	$\beta_{\text{prol}}^{\text{plasm}}$	$2.5 \cdot 10^{-4}$	d^{-1}	Rundell et al. (1998)
Degradation of plasma B cells in lymph nodes	$d_{\text{plasm}}^{\text{lymph}}$	0.05	d^{-1}	Estimated (corresponds to a half-life of 14d) (Macallan et al., 2005)
Degradation of plasma B cells in bone marrow	$d_{\text{plasm}}^{\text{bm}}$	0	d^{-1}	Given a half-live of several years, $d_{\text{plasm}}^{\text{bm}} \approx 0$ for our time scale (Hammarlund et al., 2017)
Activation of memory B cells	$\beta_{\text{act}}^{\text{mem}}$	2	d^{-1}	Estimated
Proliferation of activated memory B cells	$\beta_{\text{prol}}^{\text{mem}}$	2	d^{-1}	Assuming memory B cell pool is not depleted (Tangye and Hodgkin, 2004; Fearon et al., 2001)
Plasma B cell migration to bone marrow	β_{bm}	0.02	d^{-1}	Estimated
Probability of migration to bone marrow	π_{bm}	0.2	Unitless	Estimated
Production rate of IgG	p_{igg}	$4.3 \cdot 10^{-5}$	$\mu\text{g cell}^{-1} \text{d}^{-1}$	Rundell et al. (1998); Alberts et al. (2018)
Degradation of IgG	d_{igg}	0.033	d^{-1}	Half-life of 21d (Mankarious et al., 1988)
Neutralization factor on d0	κ_{init}	$1 \cdot 10^{-4}$	Unitless	Estimated
Increase in neutralization factor	α_{neutr}	Estimated	Unitless	(Figure 4.4)
Total volume of activated LFs	V_{LF}	Estimated	mL	(Figure 4.4)
Plasma volume	V_{plasm}	2800	mL	40 mL per Kg body weigth (Yiengst and Shock, 1962)
Bone marrow volume	V_{bm}	1750	mL	Hassan and El-Sheemy (2004)
Apparent IgG avidity (for predicting HI titers form IgG concentrations)	$K_{\text{D}}^{\text{app}}$	$2 \cdot 10^{-9}$	M	Estimated (Linnik et al., 2020)

Table 4.2. Overview of model states. Abbreviations: APCs, Antigen-presenting cells; GC, germinal center; IgG, immunoglobulin G

Description	Symbol	Initial value	Unit
Injected antigen	AG_{inj}	15	μg
Antigen presented by APCs	AG_{pr}	0	a.u. (%)
Activated naive B cells	B_{act}	0	cells/mL
GC centroblasts	B_{cb}	0	cells/mL
GC centrocytes	B_{cc}	0	cells/mL
Selected GC B cells	B_{sel}	0	cells/mL
Memory B cells	B_{mem}	0 / Patient-specific*	cells/mL
Long-lived plasma B cells in lymph nodes with a half-life of 14d	B_{plasm}^{lymph}	0	cells/mL
Long-lived plasma B cells in bone marrow with half-life $\gtrsim 1\text{y}$	B_{plasm}^{bm}	Patient-specific	cells/mL
IgG serum antibody	IgG	Patient-specific	$\mu\text{g/mL}$

* We compare two scenarios: with and without preexisting antigen-specific memory B cells.

As of today, the recycling probability of GC B cells remains unknown, in particular in immunocompromised patients. Modelling studies show that recycling is not necessary for GC establishment (Meyer-Hermann and Maini, 2005), and different models of GC populations suggest 30% recycling (Victora et al., 2010), or 90% recycling (Meyer-Hermann et al., 2012). In practice, the non-monotonic dependency of IgG production on π_{rec} makes this parameter non-identifiable. However, increased recycling has been linked to an increased affinity maturation (Oprea and Perelson, 1997). We previously observed in HSCT patients that the influenza vaccine-induced increase in HI titers is mostly explained by an increase in IgG concentrations (Linnik et al., 2020), indicating that the increase in affinity is low compared to the increase in IgG concentration. Therefore, we assume in the following estimation that the recycling probability is $\lesssim 50\%$ in our patient population (Oprea and Perelson, 1997).

4.3.3 Mapping of patient factors to GC reaction parameters

We previously identified the most important patient factors associated with the HI antibody titer response in the considered patient population in a multivariable regression analysis (Chapter 2). In the following, we summarize how we mapped each patient factor to a GC reaction process, accounting for mechanistic hypotheses reported in the literature on how these factors might affect the GC reaction. Specifically, we considered the following patient groups: grade of cGVHD (none, mild, moderate, severe), immunosuppressive treatment with calcineurin inhibitors (yes or no), IFN- λ genotype (rs8099917 TT or GT/GG), family relationship with the donor (related or unrelated), and the concentration of lymphocytes in the blood (continuous variable).

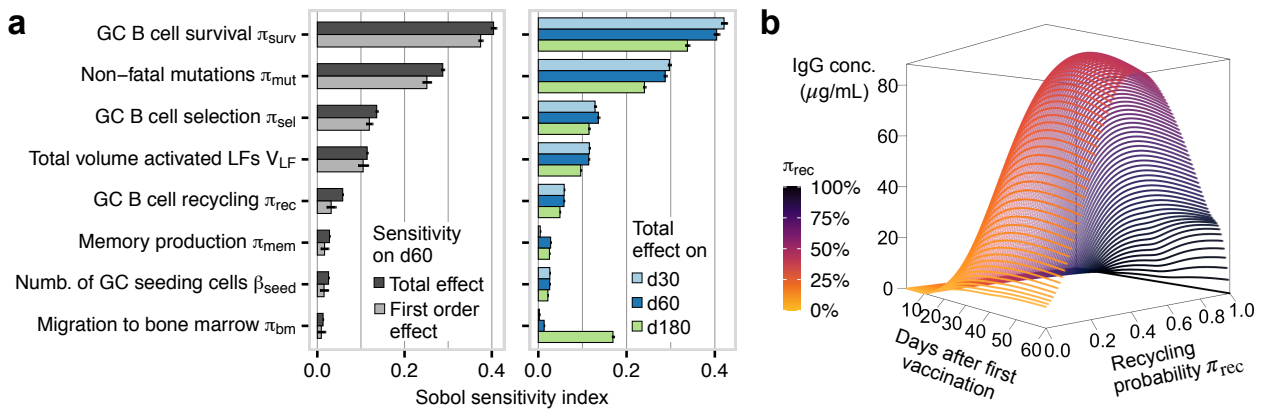


Figure 4.2. Sensitivity analysis. (a) Left: Sobol sensitivity index of the total and first order effect of parameters modelling the key processes of the germinal center reaction. The sensitivity refers to the log-transformed IgG concentration on d60 after the first vaccination. Right: Sobol sensitivity index of the total effect on d30, d60, and d180 after vaccination. (b) Local sensitivity of the IgG concentration over time to the recycling probability π_{rec} . Simulations were performed with two vaccine doses (vaccination on d0 and d30) with all initial concentrations set to 0 and model parameters $\pi_{abs} = 60\%$, $\pi_{surv} = 90\%$, $\pi_{sel} = 20\%$, $\pi_{mem} = 0\%$, $\pi_{bm} = 20\%$, $V_{LF} = 20$ mL. All other parameters were set to the values summarized in **Table 4.1**.

Chronic GVHD

We observed a positive association between cGVHD grade and antibody response in our HSCT patient population. Patients suffering from cGVHD show elevated levels of B-cell activating factor (BAFF), disturbed B cell homeostasis and persistent B cell activation (Sarantopoulos et al., 2007, 2009; Greinix et al., 2008; Jacobson et al., 2014). BAFF promotes survival of B cells (Mackay and Browning, 2002) and can increase the number of plasma B cells and enhance antibody response (Moore et al., 1999; Do et al., 2000). The role of BAFF in germinal centers remains unclear. However, experiments in mice suggest that BAFF inhibition has an inhibitory effect on GC formation and antibody production (Yan et al., 2000; Mackay and Browning, 2002), and that signalling through the BAFF receptor regulates the number of follicular B cells (Harless et al., 2001). Therefore, we hypothesized that the cGVHD grade might affect the survival probability of centroblasts π_{surv} and inferred this parameter for each cGVHD grade (π_{surv0} , π_{surv1} , π_{surv2} , π_{surv3} for none, mild, moderate and severe cGVHD).

Calcineurin inhibitors

Patients receiving calcineurin inhibitors, a frequently used immunosuppressive treatment to prevent graft rejection, showed a reduced antibody response. Calcineurin inhibitors block T cell proliferation (Hamawy, 2003) and have been shown to reduce the B cell antibody response by interfering with T cell help (Heidt et al., 2010). Centrocytes require signals from follicular helper T cells to survive the selection process (Turner et al., 2018). To investigate if calcineurin inhibitors could affect the selection process, we estimated the selection probability π_{sel} for the two patients groups (π_{sel0} for patients without calcineurin inhibitor treatment and π_{sel1} for patients with treatment).

IFN-λ genotype

Patients carrying the rs8099917 minor allele (GT/GG) in the IFN-λ gene *IFNL3* showed a stronger antibody response than patients carrying the major allele (TT). The same effect has been observed in vaccinated, immunocompromised solid organ transplant patients (Egli et al., 2014b). Both naive and memory B cells respond to IFN-λ. However, the role of IFN-λ in vaccine response remains unknown, and seemingly contradictory experimental results have been reported: IFN-λ boosts B cell differentiation to plasma B cells *in vitro* (de Groen et al., 2015; Syedbasha et al., 2020) and has adjuvant effects in mice vaccinated against influenza (Ye et al., 2019); yet, reduced IFN-λ expression has been observed in solid organ transplant patients carrying the minor allele and showing stronger antibody responses (Egli et al., 2014b). As a potential solution to this paradox, we hypothesized that patients carrying the minor allele might indeed have decreased plasma B cell differentiation (due to lower IFN-λ levels), causing fewer B cells exiting the GC reaction and a higher fraction of centrocytes cycling back to the dark zone to undergo additional rounds of proliferation and selection. Assuming $\pi_{\text{rec}} \lesssim 50\%$, this could explain why immunocompromised transplant patients show lower IgG levels despite a boosting effect of IFN-λ on B cell differentiation. We estimated the recycling probability π_{rec} for each genotype ($\pi_{\text{rec}0}$ for patients carrying the major allele TT and $\pi_{\text{rec}1}$ for patients with the minor allele GT/GG).

Lymphocyte count and family relationship with donor

We observed a strong positive effect of lymphocyte counts on antibody response, and a negative effect for an unrelated donor. We speculated that both lymphocyte count and a family relationship with the donor affect the number of activated GCs. The successful GC formation requires B cells to present antigen on their major histocompatibility (MHC) II complex to cognate helper T cells (Schwickert et al., 2011; Yeh et al., 2018). The disruption of the conjugate B-T cell interaction results in impaired GC formation and reduced humoral immunity (Crotty et al., 2003; Qi et al., 2008). Moreover, experimental results suggest that the MHCII-dependent selection of B cells is more stringent for B cells entering GCs than for B cells in already established GGc (Yeh et al., 2018). Therefore, we hypothesized that the number of lymphocytes is associated with the number of cognate T and B cells. Patients with an unrelated donor received blood stem cells that are potentially not well matched to their own human leukocyte antigen (HLA) gene that encodes the MHCII protein complex. Therefore, the number of cognate cells might be reduced in this patient group. In our model, the number of successfully formed GCs is restricted by the total volume of activated LFs (V_{LF}). We used the following linear model to investigate the dependency of V_{LF} to lymphocyte count and donor relationship:

$$\log_2(V_{\text{LF}}) = \log_2(V_{\text{LFref}}) + \gamma_{\text{lymph}} \log_2(x_{\text{lymph}}) - \gamma_{\text{donor}} x_{\text{donor}}. \quad (4.1)$$

Here, x_{lymph} is the absolute lymphocyte count in units 10^9 cells/L, such that $\log_2 x_{\text{lymph}} = 0$ if $x_{\text{lymph}} = 10^9$ cells/L (1000 cells/ μL), which corresponds to the lower limit of the normal range and is our reference value (normal counts range from 1000 – 4800 cells/ μL) (Valiathan et al., 2014). The patient's relationship with the donor is encoded by the dummy variable x_{donor} that takes the

value 1 if patient and donor are unrelated and 0 if they are related. We estimated $V_{L\text{Fref}}$, γ_{lymph} , and γ_{donor} .

4.3.4 Estimation and quality of fit

We estimated the patient-group specific GC reaction parameters presented above along with three unknown model parameters, i. e., the fraction of absorbed antigen π_{abs} , the increase in neutralization capacity at the injection site α_{neutr} and the bifurcation parameter π_{mem} by Bayesian inference (14 parameters in total, see **Methods** for details). All remaining model parameters were set to literature values or values previously estimated from the investigated patient data (**Table 4.1**). We performed the inference on antibody titers from 102 patients (**Table S4.2**) and four time points (d0, d7, d30, d60). All patients received two doses of a non-adjuvanted seasonal influenza vaccine (first dose on d0, second dose on d30, see **Methods**).

Importantly, patients' vaccination history was unknown, which prevented us from correcting for potential preexisting memory in a multivariable regression analysis (Chapter 2). The vaccine response model allows us to investigate the effect of preexisting memory by taking the initial memory B cell concentration ($B_{\text{mem,init}}$) into account. Therefore, we inferred $B_{\text{mem,init}}$ for each patient under the assumption that an increase in HI titer on d7 is due to an increase in IgG levels released by reactivated memory B cells. In addition, we performed an estimation where we set $B_{\text{mem,init}} = 0$ cells for all patients (no initial memory) to investigate to which extent antibody responses from preexisting memory B cells affect the results. In addition, we performed an inference where we estimated the number of activated LFs (V_{LF}) for each patient individually, not taking patient information into account (106 parameters in total, referred to as unconstrained estimation with initial memory, see **Methods** for details).

Posterior distributions were sampled using the No-U-Turn sampler (NUTS) (Hoffman and Gelman, 2014) implemented in Stan (Stan Development Team, 2020b) with 500 warm-up iterations, 1000 sampling iterations, and six chains. No divergences were detected in any of the estimation settings. All estimated parameters and initial concentrations had $\hat{R} = 1$, indicating that chains mixed well, with a Bulk Effective Sample Size and Tail Effective Sample Size >2000 , indicating that estimates from posterior quantiles are reliable (Vehtari et al., 2020).

The model is able describe different responses in our patient population over the full range of observed HI titers also when the inferred GC reaction parameters are constrained by patient factors (**Figure 4.3a** and **Figure S4.2**). Not taking initial memory B cells into account substantially impairs the model fit and the Bayesian information criterion (BIC) increased from 3136 to 3408 (**Figure 4.3b**). The difference $\Delta\text{BIC} = 272$ is strong evidence against the model without initial memory. In particular, the no-memory model underestimated the antibody titers in several patients, suggesting that the antibody response by preexisting memory B cells is necessary to fully explain the observed titer increase in these patients (**Figure S4.3**). The model with unconstrained parameters yielded a slightly better fit (**Figure 4.3c**). However, the BIC increased from 3136 to 3350 ($\Delta\text{BIC} = 214$) due to the larger number of estimated parameters, indicating that the model with patient factor-specific parameters explains the data best. Thus, adding patient-specific constraints to the model parameters substantially reduces the number of unknown parameters.

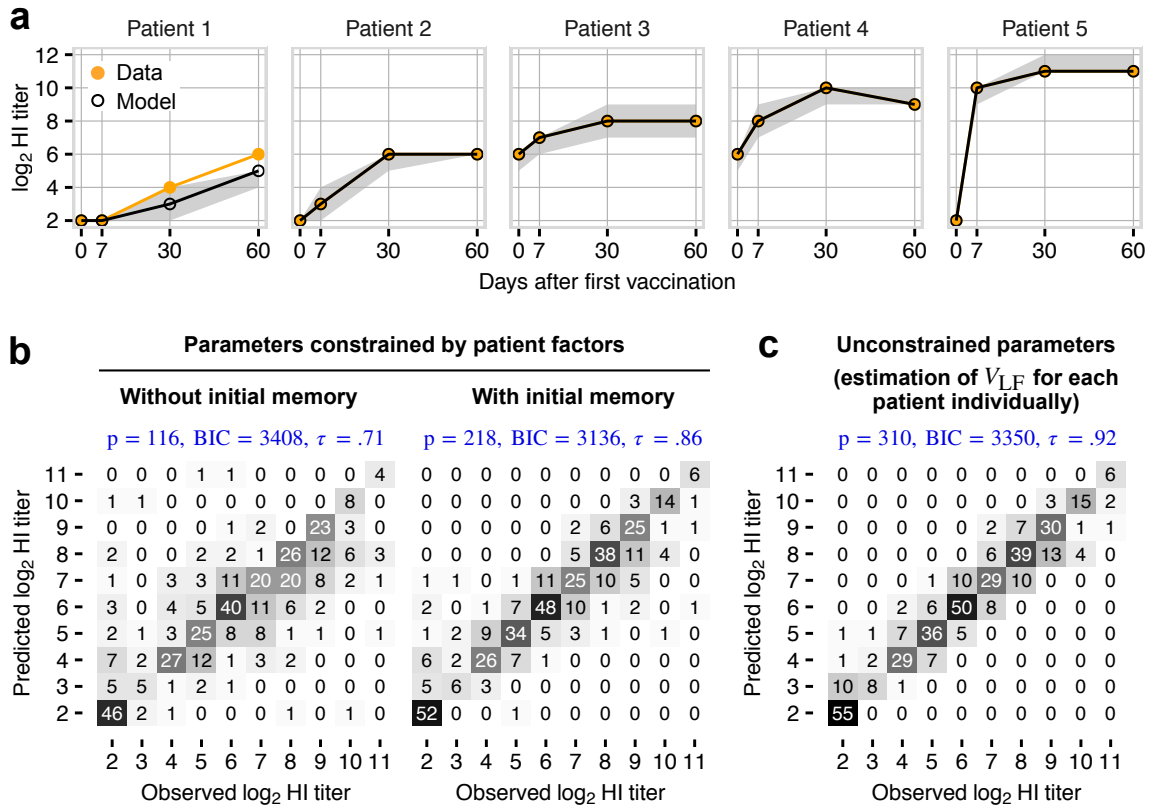


Figure 4.3. Model fits. (a) Predicted (black) and observed (orange) HI titers for five example patients showing different responses and antibody baseline levels (d0 titer). Predicted HI titers were obtained by setting estimated parameters to the median value of the posterior distributions obtained by the patient-factor constrained parameter estimation with initial memory. The gray area indicates 95% posterior predictive intervals. For all patients, see **Figure S4.2**. (b) Comparison of the quality of model fits for the patient-factor constrained parameter estimation without and with initial memory B cell estimation. Numbers indicate total counts; p indicates the total number of estimated model parameters and initial conditions in the respective estimation setting, BIC is the Bayesian information criterion for 4080 observations (102 patients, 4 time points, and 10 serum dilutions for HI titer determination), and τ indicates Kendall's correlation coefficient for observed and predicted titers. (c) As (b) but results show the predicted titers from an estimation where the patients factors were not taken into account and the number of activated LFs (V_{LF}) was estimated for each patient individually (unconstrained parameter estimation, see **Methods**).

In conclusion, the model can reflect the heterogeneous antibody titer response in our patient population by a few patient factors, but only when the antibody response from previously acquired memory B cells is taken into account.

4.3.5 Differences in vaccine responses can be explained by differences in GC reaction processes and differences in preexisting memory B cells

Finally, we compared the estimated GC reaction parameters between the investigated patient groups (**Figure 4.4a** and **Figure 4.4b**). In the estimation where we assume no initial memory for all patients, the results qualitatively agree with the previously observed associations inferred by the multivariable regression analysis: Patients with severe cGVHD show the highest survival probability π_{surv} , which could potentially explain the stronger antibody response. However, patients with mild or moderate cGVHD show similar π_{surv} as patients without cGVHD. Patients receiving calcineurin inhibitors show a lower selection probability π_{sel} , potentially explaining the weaker response. Patients carrying the IFN- λ minor allele show a higher recycling probability π_{rec} , potentially explaining a stronger antibody response despite lower IFN- λ expression (**Figure 4.4a**, left). The effect of an unrelated donor is $\gamma_{\text{donor}} = 1.4$ (1.0 – 1.9), which means that patients with an unrelated donor have 3- to 4-fold smaller V_{LF} . Increase in lymphocyte count increases the total volume of activated LFs (V_{LF}) with $\gamma_{\text{lymph}} = 2.3$ (95% credible interval 1.6 – 2.8), meaning that a doubling in lymphocyte count results in approximately 5-fold increase (3- to 7-fold) in V_{LF} . This result is unrealistic; given that the estimated reference value V_{LFref} is approximately 25 mL (**Figure 4.4b**), a patient with 4000 lymphocytes/ μL is predicted to have a total volume of activated LFs of 625 mL (225 – 1125 mL).

The results change substantially for some parameters when the antibody response by potentially preexisting memory B cells is taken into account (**Figure 4.4a** and **Figure 4.4b**). Then, the model predicts that patients without cGVHD and patients with severe cGVHD have similar survival probabilities ($\approx 80\%$), while patients with mild or moderate cGVHD have lower survival probabilities (around 75% and 50%, respectively). Thus, the strong response of patients with severe cGVHD could also be explained by previously acquired memory B cells. The difference in selection probabilities vanishes when initial memory is taken into account, as well as the donor effect ($\gamma_{\text{donor}} \approx 0$). This indicates that also these effects can also be explained by differences in memory B cells. The effect of lymphocyte counts decreases to $\gamma_{\text{lymph}} = 1.8$ (1.3 – 2.3), corresponding to a 3.5-fold (2.5- to 5-fold) increase in V_{GC} for a doubling in lymphocyte count. The reference value V_{LF} decreases to approximately 20 mL. Thus, a patient with 4000 lymphocytes/ μL is predicted to have $V_{\text{LF}} = 245$ mL (125 – 500 mL). This effect seems to be more realistic than the value estimated before but is still surprisingly high. Thus, the model proposes that the strong association between antibody response and lymphocyte counts can not be fully explained by an increase in the number of activated GCs. Taking initial memory B cells into account also affects the estimation of the other unknown model parameters that were estimated over all patients (**Figure 4.4c**), contributing to the better model fit. For instance, the parameter π_{abs} is estimated to be higher, resulting in a shorter duration of the vaccine-induced GC reaction compared to the estimation without initial memory. The estimated

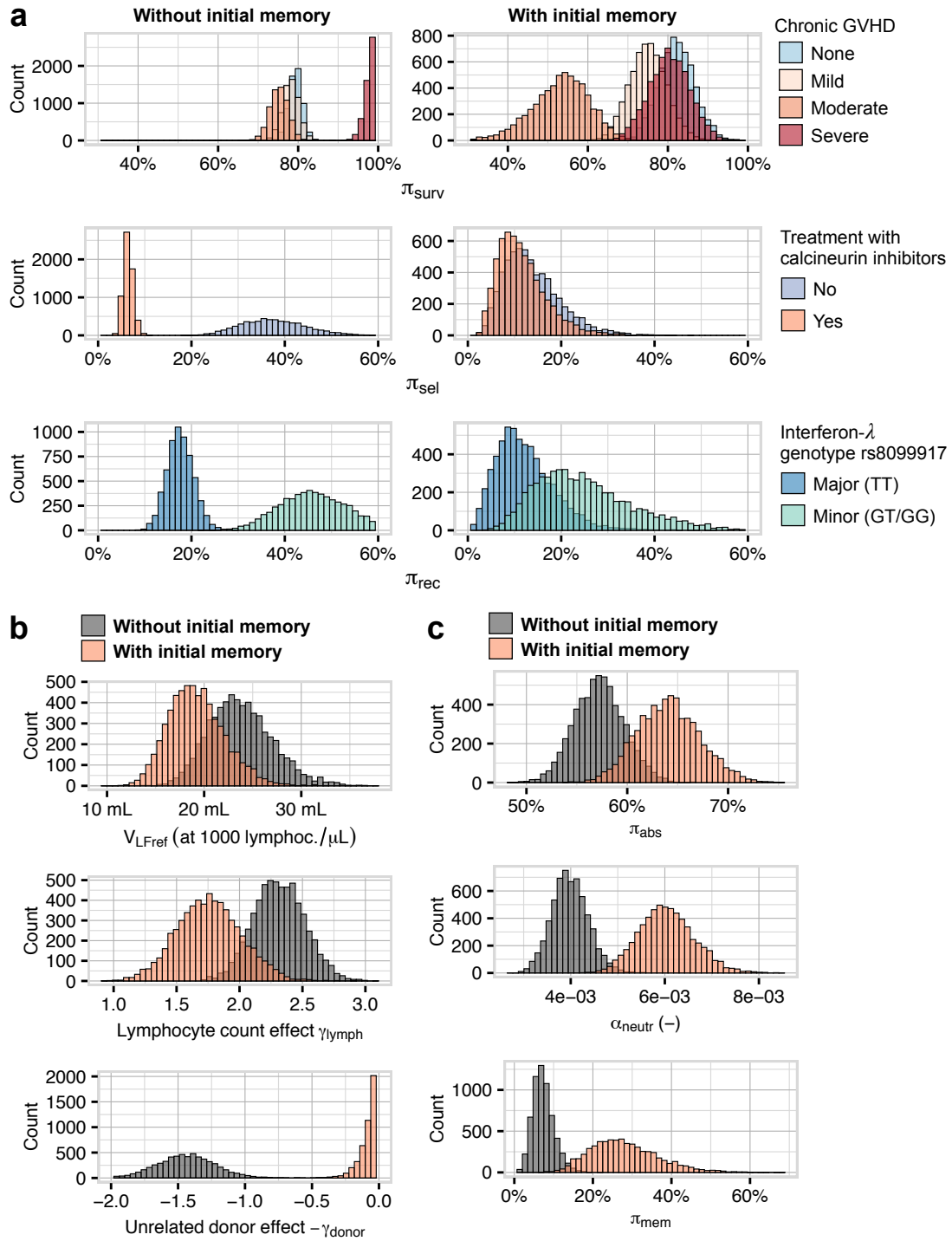


Figure 4.4. Marginal posterior distributions of estimated model parameters for two estimation settings: assuming no initial memory B cells for all patients (left) and with estimating patient-specific initial memory B cell concentrations from the d7 response (right). (a) Posterior distributions of the GC B cell survival probability π_{surv} by chronic graft-versus-host disease (GVHD) grade, selection probability π_{sel} by calcineurin inhibitor treatment, and recycling probability π_{rec} by IFN- λ genotype. (b) Posterior distributions for parameters affecting the total volume of activated lymphoid follicles (LFs) (V_{LF} , see Equation 4.1). (c) Posterior distributions of unknown model parameter that were estimated over all patients: fraction of absorbed antigen π_{abs} , increase in neutralization capacity at the injection site α_{neutr} , and bifurcation parameter for memory/plasma B cell differentiation π_{mem} .

value for π_{mem} of 30% (14 – 50%) suggests that the first vaccination induced the production of memory B cells that could be reactivated in the second vaccination (**Figure 4.4c**).

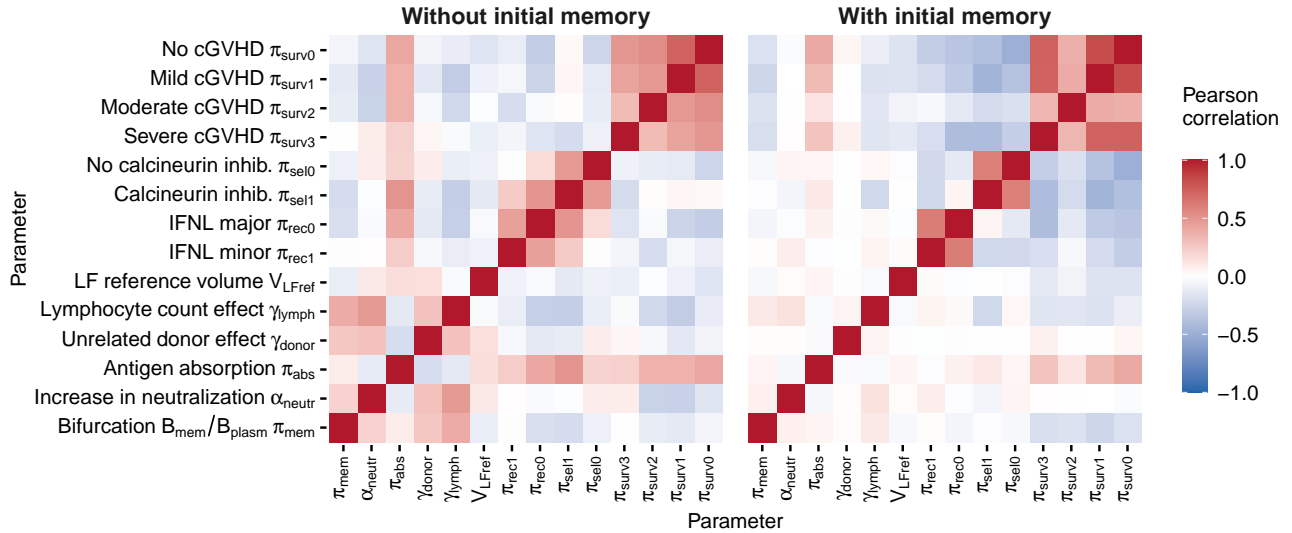


Figure 4.5. Pearson correlations of posterior draws. The chain-like model structure introduces correlations between π_{abs} , π_{surv} , π_{sel} , π_{rec} and V_{LF} . Because π_{surv} , π_{sel} , and π_{rec} are constrained by patient factors and the investigated patient groups highly overlap (**Figure S4.4**), the patient group-specific parameters also show a positive correlation between the groups. This allows to estimate differences between the groups (for instance between $\pi_{\text{rec}0}$ and $\pi_{\text{rec}1}$) more precisely than the absolute values of the estimated parameters.

The estimation allows to infer differences between patient groups more precisely than the marginal posterior distributions in **Figure 4.4** suggest. Due to the chain-like structure of the vaccine response model (**Figure 4.1a**), the absolute values of the GC model parameters π_{surv} , π_{sel} , π_{rec} , and V_{GC} depend on each other. For instance, an increase in π_{surv} could be compensated by a decrease in π_{sel} , π_{rec} , or V_{GC} , and thus have no effect on the final IgG concentration. By constraining these parameters by patient factors, we introduced additional correlations between the patient groups, i. e., between $\pi_{\text{surv}0}$, $\pi_{\text{surv}1}$, $\pi_{\text{surv}2}$, and $\pi_{\text{surv}3}$, as well as between $\pi_{\text{sel}0}$ and $\pi_{\text{sel}1}$, and $\pi_{\text{rec}0}$ and $\pi_{\text{rec}1}$ (**Figure 4.5**). These positive correlations occur because the patient groups highly overlap (**Figure S4.4**). This means that the relative differences in parameters between patient groups can be inferred more precisely than their absolute values. For instance, $\pi_{\text{rec}0}$ and $\pi_{\text{rec}1}$ show a broad marginal posterior distribution in **Figure 4.4b** (right). However, since both parameters are positively correlated (**Figure 4.5**), the shift between $\pi_{\text{rec}0}$ and $\pi_{\text{rec}1}$ is not affected by the absolute values of the other model parameters. Thus, although the marginal posterior distributions highly overlap, the model suggests that the recycling probability for patients carrying the IFN- λ minor allele is higher than for patients carrying the major allele also when taking antibody response by initial memory B cells into account.

In summary, the posterior distributions confirm that the increase in antibody titers can not be fully explained in some patients without the contribution of preexisting memory B cells. Not taking

initial memory B cells into account results in maximal survival probability for patients with severe cGVHD, maximal recycling probability for patients carrying the IFN- λ minor allele, very high selection probability for patients with calcineurin inhibitor treatment and a very high lymphocyte count effect γ_{lymph} . Therefore, we anticipate that (i) the heterogeneous antibody response in HSCT patients is mostly explained by previously acquired memory B cells, lymphocyte count and IFN- λ genotype, and (ii) the positive effect of cGVHD grade and the negative effects of calcineurin inhibitors and an unrelated donor are explained by differences in previously acquired memory B cells.

4.4 DISCUSSION

To the best of our knowledge, a study that infers GC reaction parameters and memory B cell responses directly from patient data to investigate differences in vaccine responses has not yet been reported. Our approach combines dynamic modelling of B cell populations and clinical patient information with statistical inference to describe the heterogeneous vaccine response in HSCT patients with minimal parameterization. We showed that the model can recapitulate the observed antibody titer kinetics and explain the observed differences between patient groups by previously acquired memory B cells and a few patient factors potentially modulating the GC reaction. The model predicts that an increase in lymphocyte count increases the number of successfully formed GCs and potentially affects additional GC processes. For instance, lymphocyte counts could additionally increase the selection probability; since patients with more lymphocytes have higher B and T cell diversity, more B cells might be able to acquire antigen from FDCs and receive T cell help. Our analysis also suggests that patients suffering from cGVHD do not have higher GC B cell survival probabilities than patients without cGVHD, as initially hypothesized. Furthermore, our results raise the question of whether cGVHD, treatment with calcineurin inhibitors, and a family relationship with the donor potentially affect memory B cell acquisition. Unfortunately, we were not able to investigate whether the differences in the amount of memory B cells can be explained by patients' immunization history (the annual influenza vaccine contained A/California/7/2009 already for five/six years, see **Table S4.2**).

How the GC reaction depends on its environment is by far not fully understood (Turner et al., 2018). The humoral immune response is a highly adaptive complex system and the observed differences in our patient population could also be explained by alternative mechanisms. The low survival probability for moderate cGVHD indicates a poor antibody response in this patient group when patients with preexisting memory B cells are excluded. This negative effect could also be explained by a mechanisms that were not taken into account in our model, e. g., by less antigen presentation in lymph nodes. Our analysis suggests that the observed association between IFN- λ genotype could be explained by different recycling probabilities, resolving the conflicting observations that IFN- λ boosts B cell differentiation and at the same time reduces vaccine-induced antibody production in immunocompromised transplant patients (Egli et al., 2014b; de Groen et al., 2015; Syedbasha et al., 2020). However, it is unknown how IFN- λ affects GC B cells. Due to the non-monotonic dependency of antibody production on recycling (**Figure 4.2b**), higher levels of IFN- λ and less recycling could also lead to a higher antibody production if recycling is more dominant than we

assumed in our immunocompromised population ($\tau_{\text{rec}} > 50\%$). The effect of IFN- λ in healthy and immunocompromised populations is poorly understood, and more studies on IFN- λ are needed to understand its role in vaccine response. And finally, the investigated patient factors could also influence several GC reaction processes in parallel.

In this study, only patients' antibody titers along with clinical patient information were included. In principle, the model can incorporate additional data on different B cell populations, for instance, memory B cells. However, detecting antigen-specific B cells is tedious, especially in larger studies, and we therefore inferred the amount of influenza-specific memory B cells indirectly from antibody titer kinetics. However, IgM antibodies released by short-lived plasmablasts could also influence the antibody titer on d7. Since IgM has a lower serum concentration than IgG (Gonzalez-Quintela et al., 2008), we assumed that its contribution is negligible compared to IgG. Longitudinal data of IgG concentrations with more time points (e.g., measured in ELISA experiments) could improve the estimation of initial memory B cells. In addition, patients' vaccination history could be included as a model variable determining the amount of previously acquired memory B cells similar to our implementation of a dependency between absolute lymphocyte count and total volume of activated LFs (Equation 4.1).

Our approach has several limitations. The total volume of activated LFs defines only an upper bound for the total number of activated GCs. Therefore, it does not accurately reflect the patients' ability to initiate the GC reaction. Furthermore, many parameters extracted from the literature were derived from mathematical models or experiments in mice and might not be directly applicable to influenza vaccination in humans. Another limitation is that we model the same GC dynamics in all activated GCs. GC processes could also vary within one patient, depending on the diversity and the number of GC seeding B cell clones. However, imaging and sequencing data show that early GCs are highly diverse (Tas et al., 2016). The homogeneous GC is the result of clonal expansion of a few clones, either randomly selected or based on their affinity (Tas et al., 2016). If most activated GCs were seeded by highly diverse B cells, we can assume that the estimated GC reaction model parameters are averages that represent the GC reaction in one patient.

We did not model affinity maturation and neglected the contribution of a potential increase in IgG avidity to the increase in HI titer. Reduced affinity maturation is likely in immunocompromised populations (Ogonek et al., 2016), and we previously observed in HSCT patients that an increase in influenza vaccine-induced HI titers is mostly explained by an increase in IgG concentrations (Linnik et al., 2020). Thus, we assumed that the vaccine-induced increase in affinity is low compared to the increase in IgG levels. Kuraoka et al. observed that GC B cell selection is more permissive in response to complex antigens, such as influenza hemagglutinin, compared to simple haptens, often used to study GC responses (Kuraoka et al., 2016). Moreover, simulation studies suggest that increased antigen complexity leads to reduced affinity maturation (Murugan et al., 2018). Whether the poor affinity maturation in HSCT patients is linked to the compromised immune system or to the antigen (or both) is unclear. Adding affinity maturation into the model (and taking its dependency on the recycling probability into account) could provide additional insights on affinity maturation in HSCT patients. However, additional data, either on patients' IgG concentration or IgG avidity, has to be included to disentangle their contributions to the HI titer.

As of today, little is known about the heterogeneity of GCs in vaccinated patient populations, since GC measurements are hardly accessible (Turner et al., 2020). Our approach that connects clinical patient data with B cell population dynamics via mechanistic hypothesis and checks their compatibility with observed HI titers could help to identify important differences between patient groups and to better understand the immune response to influenza vaccination in immunocompromised patients.

4.5 METHODS

4.5.1 Vaccine response model

Based on published work (Rundell et al., 1998; Iber and Maini, 2002), the model describes in eleven ordinary differential equations (ODEs) key processes of the vaccine-induced IgG antibody response, i. e., (i) antigen uptake and presentation in lymph nodes, (ii) antigen-dependent clonal expansion of centroblasts, (iii) T-cell dependent selection of centrocytes, and (iv) differentiation to plasma and memory B cells.

Injected antigen moves from the subcutaneous tissue to the draining lymph nodes in soluble form or through transportation by dendritic cells (Cavanagh and Von Andrian, 2002; Catron et al., 2004). In lymph nodes, the antigen is presented by antigen-presenting cells (APCs, here dendritic cells and follicular dendritic cells) to B cells (Itano et al., 2003). We model vaccine antigen absorption and antigen presentation by APCs phenomenologically. The injection site absorbs only a fraction of injected antigen (π_{abs}), the rest is slowly degraded (Tew and Mandel, 1979):

$$\frac{AG_{\text{inj}}}{dt} = - AG_{\text{inj}} \cdot [\pi_{\text{abs}}\alpha_{\text{abs}} + (1 - \pi_{\text{abs}})d_{\text{ag}}] \quad (4.2)$$

The antigen absorption by the injection site is much faster than the antigen processing and presentation by APCs. We can therefore assume quasi-steady state for the amount of absorbed antigen: $AG_{\text{abs}}^{\text{ss}} = \pi_{\text{abs}}AG_{\text{inj}}\frac{\alpha_{\text{abs}}}{d_{\text{ag}}}$, where α_{abs} is the absorption rate constant of the injected antigen and d_{ag} the degradation rate constant of absorbed antigen. Then, antigen processing and presentation by APCs can be modelled by the following Hill equation:

$$\frac{AG_{\text{pr}}}{dt} = \frac{\alpha_{\text{pr}}AG_{\text{abs}}^{\text{ss}}}{1 + (\kappa \cdot IgG)^2 + AG_{\text{abs}}^{\text{ss}}} - d_{\text{pr}}AG_{\text{pr}} \quad (4.3)$$

The term $(\kappa \cdot IgG)^2$ models the neutralization of antigen by IgG through competitive inhibition (Zhang et al., 2013). Here, κ is an unknown conversion factor estimated from data. Equations 4.2 and 4.3 are also known as the indirect response model often used to model drug uptake (Mager and Kimko, 2016). The advantage of this phenomenological model is that we can tune the duration of antigen presentation in germinal centers by only one parameter (π_{abs} , see **Figure 4.6a**).

To capture the observed response to the second vaccination (**Figure S4.2**), we had to include the contribution of other antibodies than IgG that can neutralize (or opsonize) the injected vaccine antigen at the injection site, such as IgA (Davis et al., 2020). We do not explicitly model the

production of IgA. Instead, we assume that the IgA concentration is correlated with IgG (Externe et al., 2000) and model its contribution by adding a time-dependent increase in κ : $\frac{\kappa}{dt} = \alpha_{\text{neutr}}$. The initial value for κ can be inferred from data based on the response to the first vaccination (d30) and α_{neutr} from the response to the second vaccination (d60).

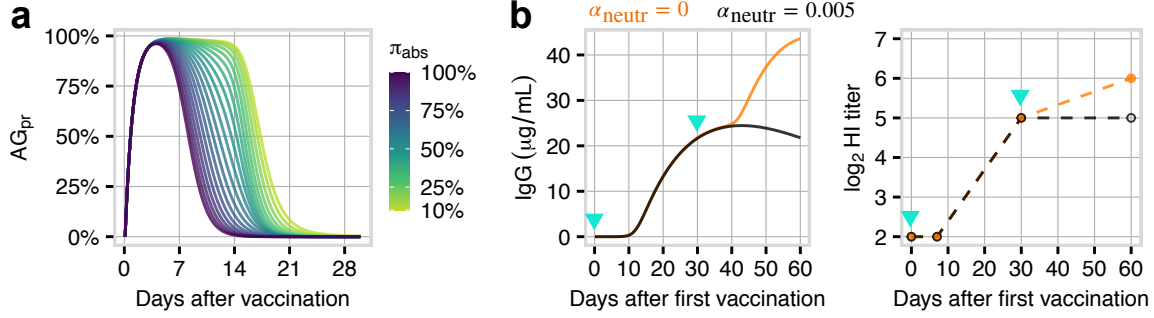


Figure 4.6. Antigen presentation in lymph nodes. (a) The model parameter π_{abs} controls the duration of antigen presentation in lymph nodes and thus the duration of the GC reaction. (b) The model parameter α_{neutr} models the contribution of IgA (and potentially other neutralizing factors) to the increase in the neutralization capacity after vaccination, that is not explained by the increase in IgG concentration. Arrows in cyan indicate the time point of vaccinations (d0 and d30). We estimate both π_{abs} and α_{neutr} .

Next, B cells are activated by APCs and helper T cells and eventually enter the GC reaction. We assume that the amount of B cells which recognize the vaccine antigen is not a limiting factor because 50 – 200 B cell clones suffice to seed a GC (Tas et al., 2016; Yeh et al., 2018). This corresponds to approximately $\beta_{\text{seed}} \in [100, 1000]$ cells $\text{mL}^{-1} \text{day}^{-1}$ in our model and our sensitivity analysis shows that the GC reaction is relatively insensitive to variability in this range (**Figure 4.1d**). We assume $\beta_{\text{seed}} = 300$ cells $\text{mL}^{-1} \text{day}^{-1}$ for all patients:

$$\frac{B_{\text{act}}}{dt} = \beta_{\text{seed}} AG_{\text{pr}} - \beta_{\text{enter}} B_{\text{act}} \quad (4.4)$$

When activated B cells enter the GC reaction (with rate constant β_{enter}), they differentiate to centroblasts (B_{cb}), which proliferate, undergo somatic hypermutation, and differentiate to centrocytes (B_{cc}). Only centroblasts with non-fatal mutations (π_{mut}) and that receive survival signals through their BAFF receptor (π_{surv}) clonally expand with maximal proliferation rate $\beta_{\text{prol}}^{\text{cb}}$, and differentiate further to centrocytes with differentiation rate constant β_{cc} ; all other cells undergo apoptosis (Mackay and Browning, 2002). Centroblasts require restimulation with antigen to continue proliferation; when no antigen is present anymore, the GC dissolves (Gatto and Brink, 2010; Tam et al., 2016; Pikor et al., 2020). Therefore, the proliferation rate depends on the amount of presented antigen AG_{pr} . The maximal proliferation $\beta_{\text{prol}}^{\text{cb}}$ is only reached when $AG_{\text{pr}} = 100\%$ (**Figure 4.6a**). The differentiation rate constant β_{cc} remains constant over the course of the GC reaction. In summary, the dynamics of centroblasts is given by:

$$\begin{aligned}
\frac{B_{cb}}{dt} = & \beta_{\text{enter}} B_{\text{act}} + \beta_{\text{prol}}^{\text{cb}} B_{\text{cb}} \pi_{\text{mut}} \pi_{\text{surv}} A G_{\text{pr}} \left(1 - \frac{B_{\text{cb}} + B_{\text{cc}}}{C_{\text{gc}}} \right) \\
& - d_{\text{cb}} B_{\text{cb}} \left[(1 - \pi_{\text{mut}}) + \pi_{\text{mut}} (1 - \pi_{\text{surv}}) \right] \\
& - \beta_{\text{cc}} B_{\text{cb}} \pi_{\text{mut}} \pi_{\text{surv}} \\
& + \beta_{\text{rec}} B_{\text{sel}} \pi_{\text{rec}}
\end{aligned} \tag{4.5}$$

The parameter C_{gc} accounts for the physical size constrain of the GC (Rundell et al., 1998) and β_{rec} is the recycling rate constant of positively selected centrocytes that return to the dark zone (Victora et al., 2010).

After capturing antigen from FDCs, centrocytes compete for interaction with follicular helper T cells to receive additional survival signals (Turner et al., 2018; Woodruff et al., 2018). Only a fraction of centrocytes survive this selection process (π_{sel}), the rest is degraded:

$$\frac{B_{\text{cc}}}{dt} = \beta_{\text{cc}} B_{\text{cb}} \pi_{\text{mut}} \pi_{\text{surv}} - B_{\text{cc}} \left[\beta_{\text{sel}} \pi_{\text{sel}} + d_{\text{cc}} (1 - \pi_{\text{sel}}) \right] \tag{4.6}$$

One fraction of selected B cells return to the dark zone of the GC and undergo additional rounds of proliferation (π_{rec}), the other fraction differentiate further to either memory B cells (π_{mem}) or plasma cells ($1 - \pi_{\text{mem}}$):

$$\begin{aligned}
\frac{B_{\text{sel}}}{dt} = & \beta_{\text{sel}} B_{\text{cc}} \pi_{\text{sel}} - \beta_{\text{rec}} B_{\text{sel}} \pi_{\text{rec}} \\
& - B_{\text{sel}} \left[\beta_{\text{mem}} (1 - \pi_{\text{rec}}) \pi_{\text{mem}} + \beta_{\text{plasm}} (1 - \pi_{\text{rec}}) (1 - \pi_{\text{mem}}) \right]
\end{aligned} \tag{4.7}$$

Memory B cells that are activated by presented antigen differentiate directly to plasma cells, inducing a rapid antibody response:

$$\frac{B_{\text{mem}}}{dt} = \beta_{\text{mem}} B_{\text{sel}} (1 - \pi_{\text{rec}}) \pi_{\text{mem}} + B_{\text{mem}} A G_{\text{pr}} \left(\beta_{\text{prol}}^{\text{mem}} - \beta_{\text{act}}^{\text{mem}} \right) \tag{4.8}$$

Given our time-scale of 60 days post vaccination, we assume that, once established, the memory B cell pool remains constant (Tangye and Hodgkin, 2004; Fearon et al., 2001). Thus, activated memory B cells proliferate with proliferation rate constant $\beta_{\text{prol}}^{\text{mem}} = \beta_{\text{act}}^{\text{mem}}$ to ensure that the memory B cell pool is not depleted.

IgG-producing plasma B cells in the lymph nodes ($B_{\text{plasm}}^{\text{lymph}}$) proliferate with rate constant $\beta_{\text{prol}}^{\text{plasm}}$ or eventually migrate to the bone marrow ($B_{\text{plasm}}^{\text{bm}}$) with migration probability π_{bm} and migration rate constant β_{bm} (Davis et al., 2020):

$$\begin{aligned} \frac{B_{\text{plasm}}^{\text{lymph}}}{dt} = & \beta_{\text{act}}^{\text{mem}} B_{\text{mem}} A G_{\text{pr}} + \beta_{\text{plasm}} B_{\text{sel}} (1 - \pi_{\text{rec}}) (1 - \pi_{\text{mem}}) \\ & + \beta_{\text{prol}}^{\text{plasm}} B_{\text{plasm}}^{\text{lymph}} (1 - \pi_{\text{bm}}) \\ & - B_{\text{plasm}}^{\text{lymph}} \left[\beta_{\text{bm}} \pi_{\text{bm}} + d_{\text{plasm}}^{\text{lymph}} (1 - \pi_{\text{bm}}) \right] \end{aligned} \quad (4.9)$$

$$\frac{B_{\text{plasm}}^{\text{bm}}}{dt} = \beta_{\text{bm}} B_{\text{plasm}}^{\text{lymph}} \pi_{\text{bm}} \frac{V_{\text{LF}}}{V_{\text{BM}}} - d_{\text{plasm}}^{\text{bm}} B_{\text{plasm}}^{\text{bm}} \quad (4.10)$$

We assume that only the environment of the plasma B cell determines its half-life ($d_{\text{plasm}}^{\text{lymph}}$ and $d_{\text{plasm}}^{\text{bm}}$). B cells resident in the lymph node or blood have a half-life in the order of several weeks (Macallan et al., 2005), while bone marrow B cells ($B_{\text{plasm}}^{\text{bm}}$) can have half-lives in the order of months or even years and are thus responsible for the long-term antibody production (Hammarlund et al., 2017).

Finally, IgG is released into the plasma, where it is quantified in HI assay experiments:

$$\frac{IgG}{dt} = \frac{p_{\text{igg}}}{V_{\text{Plasma}}} \left(B_{\text{plasm}}^{\text{lymph}} V_{\text{LF}} + B_{\text{plasm}}^{\text{bm}} V_{\text{BM}} \right) - d_{\text{igg}} IgG \quad (4.11)$$

Here, p_{igg} is the IgG production rate in units $\mu\text{g cell}^{-1} \text{day}^{-1}$, d_{igg} the IgG degradation rate constant, $B_{\text{plasm}}^{\text{lymph}} V_{\text{LF}}$ the total number of plasma cells in the lymph nodes, $B_{\text{plasm}}^{\text{bm}} V_{\text{BM}}$ the total number of plasma cells in the bone marrow and V_{Plasma} the plasma volume. An illustrative simulation showing the influence of the parameters modelling the key processes of the GC reaction on the plasma IgG concentration is shown in **Figure S4.1**.

4.5.2 Sobol sensitivity analysis

We analysed the global sensitivity of the IgG response to the key processes of the GC reaction (summarized in **Table S4.1**) using a Sobol sensitivity analysis (Saltelli et al., 2004). The Sobol sensitivity analysis quantifies the contribution of model inputs on a model output using the following variance decomposition: Given p model inputs (here the investigated model parameters), the total variance $V(\log(IgG))$ in model output (here the log-transformed IgG concentration) can be decomposed as:

$$V(\log(IgG)) = \sum_i V_i + \sum_i \sum_{j>i} V_{ij} + \dots + V_{12\dots p},$$

where $V_i = V(E(\log(IgG)|x_i))$ is the variance with respect to the distribution of parameter x_i , $V_{ij} = V(E(\log(IgG)|x_i, x_j)) - V_i - V_j$ is the second order interaction term describing the effect of x_i and x_j not captured by the first order terms V_i, V_j , and so on. The relative contribution of each term to the unconditional variance $V(\log(IgG))$ quantifies the sensitivity of the considered parameter. The first order Sobol sensitivity index is defined as:

$$S_i = \frac{V_i}{V(\log(IgG))}.$$

The total contribution of x_i is the sum of all terms in the variance decomposition that include x_i . The total contribution to variance $V(\log(IgG))$ due to all factors but x_i is denoted by \mathbf{x}_{-1} . Then, the total Sobol sensitivity index for x_i is given by:

$$S_i^T = \frac{V(\log(IgG)) - V(E(\log(IgG)|\mathbf{x}_{-1}))}{V(\log(IgG))}.$$

Sobol sensitivity indices were determined using a Monte Carlo estimation (Jansen, 1999; Saltelli et al., 2010) implemented in the R package sensitivity (Iooss et al., 2019) with $n = 10000$ samples and 10 bootstrap replicates for estimating confidence intervals. We considered $p = 7$ model parameters sampled within a physiologically reasonable range (**Table S4.1**). All initial concentrations were set to 0 (no preexisting plasma/memory B cells). All other model parameters were set to values summarized in **Table 4.1**.

4.5.3 Patient data

We performed the inference on HI titers measured against influenza A/California/7/2009 from 102 HSCT patients and four time points (d0, d7, d30, d60) (data set presented in Chapter 2). All patients were vaccinated with a non-adjuvanted, subunit seasonal influenza vaccine on d0 and d30 by intramuscular injection. The original data set contained 135 HSCT patients; however, we had to exclude 33 patients due to missing values (4 patients with missing cGVHD grade, 6 patients with missing HI titers, 12 patients with missing lymphocyte count). We choose the complete case analysis instead of missing value imputation because the investigated associations showed robust results on random data subsamples (**Figure S2.7** in Chapter 2), and pooling posterior distributions from a couple of imputed data sets does not guarantee reliable posteriors (Zhou and Reiter, 2010). For patients' characteristics, see **Table S4.2**.

4.5.4 Linking IgG antibody concentrations to HI antibody titers

To link the IgG concentrations predicted from the vaccine response model to the observed HI titers, we used a previously established biophysical model of the HI assay (Linnik et al., 2020) (presented in Chapter 3). In brief, the HI titer is determined as follows: a serum sample with an unknown antibody concentration is serially diluted, and a constant amount of influenza virus and animal red blood cells (RBCs) is added to each dilution. If no influenza-specific antibodies are present (or not enough), the virus cross-links RBCs to macroscopic aggregates (hemagglutination) (Hirst, 1941). However, if antibodies recognize the influenza virus and block the binding, hemagglutination is prevented (hemagglutination inhibition). The dilution factor of the last serum dilution that can still fully inhibit hemagglutination is the HI titer (WHO, 2002).

The HI assay model predicts the inhibition probability for each dilution from a given serum IgG concentrations and apparent IgG avidity K_D^{app} . Since we previously inferred for a subset of the

investigated HSCT patient population ($n = 43$) that the vaccine-induced increase in HI titers is mostly explained by an increase in IgG concentrations (Linnik et al., 2020), we assumed that the increase in avidity is small compared to the increase in IgG and set the apparent IgG avidity to the estimated median value of 2 nM for all patients and time points (Linnik et al., 2020).

To speed up computation, we approximated the solution of the HI model by a superposition of two generalized logistic functions:

$$y = \frac{p_1}{(1 + p_2 \exp(-p_3 x))^{1/p_4}} + \frac{1 - p_1}{(1 + p_5 \exp(-p_6 x))^{1/p_7}}. \quad (4.12)$$

Here, $x = \log(IgG) - \log(K_D^{app})$ and y is the log-transformed and normalized inhibition probability predicted by the HI model. Approximation and model show excellent agreement over all IgG concentrations and a range of IgG avidities (**Figure 4.7**).

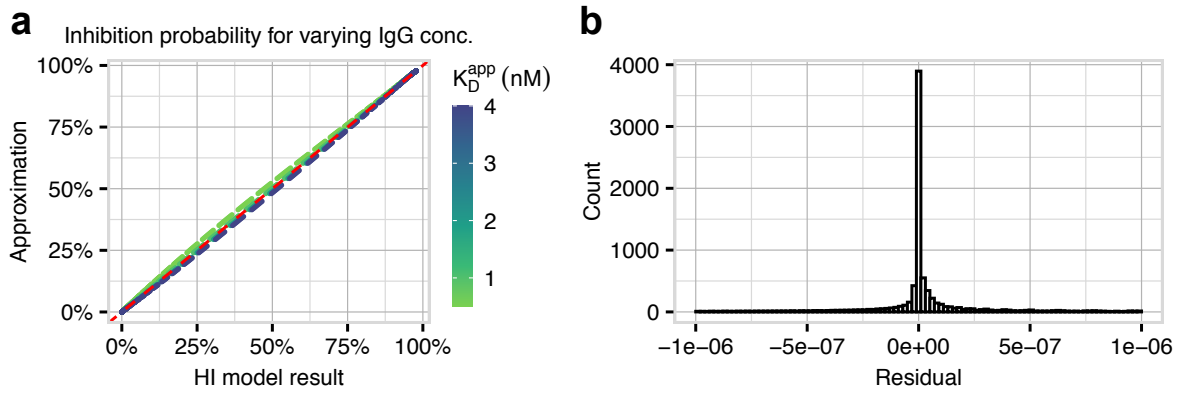


Figure 4.7. Approximation of the biophysical model of the HI assay. (a) Inhibition probabilities obtained by the HI model vs by approximation (Equation 4.12) for a large range of IgG concentrations ($0 - 4 \cdot 10^4$ $\mu\text{g/mL}$). (b) Histogram of the residuals for the results shown in (a).

4.5.5 Inference

We estimated the initial concentrations for antigen-specific IgG (IgG_{init}), long-lived plasma B cells in bone marrow ($B_{plasm,init}^{bm}$) and memory B cells ($B_{mem,init}$) for each patient along with 14 parameters (summarized in **Figure 4.4**). All other initial concentrations were set to 0 cells/mL and all remaining parameters were set to the values summarized in **Table 4.1**.

For each patient i , $IgG_{init,i}$ was estimated using a log-normal prior centered at $\mu_{igg,i}$, which is the IgG value predicted by the HI assay model from the patient's prevaccination titer (d0 titer) for an

apparent IgG avidity of 2 nM. The log standard deviation $\sigma_{\text{igg}} = 0.1$ accounts for the uncertainty in IgG concentration due to the discretization in HI titer measurements:

$$\text{IgG}_{\text{init},i} \sim \text{Lognormal}(\mu_{\text{igg},i}, \sigma_{\text{igg}}^2).$$

Then, $B_{\text{plasm},\text{init}}^{\text{bm}}$ is simply given by the steady-state solution:

$$B_{\text{plasm},\text{init},i}^{\text{bm}} = \frac{d_{\text{igg}} \text{IgG}_{\text{init},i} V_{\text{Plasma}}}{p_{\text{igg}} V_{\text{BM}}}$$

The estimation of $B_{\text{mem},\text{init}}$ is based on the assumption that the observed HI titer response on d7 is determined by IgG released by memory B cells, while IgM released by short-lived plasmablasts is neglectable. We used a long-normal prior with a large log standard deviation ($\sigma_{\text{mem}} = 1$):

$$B_{\text{mem},\text{init},i} \sim \text{Lognormal}(\mu_{\text{mem},i}, \sigma_{\text{mem}}^2),$$

where $\mu_{\text{mem},i}$ is the number of plasma cells needed to achieve the observed increase in HI titer on d7 in patient i ($\mu_{\text{mem},i} = 0$ cells, if no increase from d0 to d7 is observed).

To take into account that survival probabilities $\pi_{\text{surv},n}$ ($n = 0, 1, 2, 3$) are most likely above 50% (Liu et al., 1991; Hardie et al., 1993), while selection probabilities $\pi_{\text{sel},m}$ and recycling probabilities $\pi_{\text{rec},m}$ ($m = 0, 1$) are below 50% (Tas et al., 2016; Oprea and Perelson, 1997), we used appropriate Beta priors. We further assumed that the absolute volume of activated LFs at a lymphocyte count of 1000 cells/ μL corresponds to approximately 1–2 activated lymph nodes (Agrawal et al., 2017), and used a log-normal prior centered at 20 mL for V_{LRef} . For the effect of lymphocyte counts and donor family relationship, we used broad uniform priors. Finally, given patient's cGVHD grade (encoded by the 4-dimensional design vector $x_{\text{gvhd},i}$), calcineurin inhibitor treatment (encoded by the dummy variable $x_{\text{inh},i} \in \{0, 1\}$), IFN- λ genotype ($x_{\text{lambda},i} \in \{0, 1\}$), and donor family relationship (dummy variable $x_{\text{donor},i} \in \{0, 1\}$), as well as patient's absolute lymphocyte count $x_{\text{lymph},i}$ (continuous variable), the generative model is given by:

$$\begin{aligned} \pi_{\text{surv},n} &\sim \text{Beta}(10, 2), \quad n = 0, 1, 2, 3 \\ \pi_{\text{sel},m} &\sim \text{Beta}(4, 20), \quad m = 0, 1 \\ \pi_{\text{rec},m} &\sim \text{Beta}(3, 10), \quad m = 0, 1 \\ V_{\text{GCreff}} &\sim \text{Lognormal}(\log(20), 0.15^2) \\ \gamma_{\text{lymph}} &\sim \text{Uniform}(1, 10) \\ \gamma_{\text{donor}} &\sim \text{Uniform}(1, 10) \\ \pi_{\text{abs}} &\sim \text{Lognormal}(\log(0.6), 0.05^2) \\ \alpha_{\text{neutr}} &\sim \text{Lognormal}(\log(5 \cdot 10^{-3}), 0.1^2) \\ \pi_{\text{mem}} &\sim \text{Beta}(2, 10) \end{aligned}$$

$$\begin{aligned}
\pi_{\text{surv},i} &= x_{\text{gvhd},i}^T \left(\pi_{\text{surv}0} \quad \pi_{\text{surv}1} \quad \pi_{\text{surv}2} \quad \pi_{\text{surv}3} \right)^T \\
\pi_{\text{sel},i} &= (1 - x_{\text{inh},i}) \pi_{\text{sel}0} + x_{\text{inh},i} \pi_{\text{sel}1} \\
\pi_{\text{rec},i} &= (1 - x_{\text{lambda},i}) \pi_{\text{rec}0} + x_{\text{lambda},i} \pi_{\text{rec}1} \\
\log_2(V_{\text{LF},i}) &= \log_2(V_{\text{LFref}}) + \gamma_{\text{lymph}} \log_2(x_{\text{lymph},i}) - \gamma_{\text{donor}} x_{\text{donor},i} \\
\text{IgG}_{ij} &= f(\text{IgG}_{\text{init},i}, B_{\text{plasm},\text{init},i}^{\text{bm}}, B_{\text{mem},\text{init},i}, \pi_{\text{surv},i}, \pi_{\text{sel},i}, \pi_{\text{rec},i}, V_{\text{LF},i}, \pi_{\text{abs}}, \alpha_{\text{neutr}}, \pi_{\text{mem}}, t_j) \\
P_{ijk} &= g(\text{IgG}_{ij}, K_{\text{D}}^{\text{app}}, \text{dilution}_k) \\
Y_{ijk} &\sim \text{Bernoulli}(P_{ijk})
\end{aligned}$$

Here, IgG_{ij} is the plasma IgG concentration of patient i at time point j predicted by the vaccine response model (denoted by f), P_{ijk} is the corresponding hemagglutination inhibition probability for serum dilution step k and $K_{\text{D}}^{\text{app}} = 2$ nM predicted by the HI assay model (denoted by g), and Y_{ijk} is an indicator variable which takes the value $Y_{ijk} = 1$ if hemagglutination inhibition has been observed and $Y_{ijk} = 0$ otherwise. The full likelihood is given by the product of Bernoulli likelihoods over all patients, time points, and dilution steps:

$$\prod_{ijk} P_{ijk}^{Y_{ijk}} \cdot (1 - P_{ijk})^{(1 - Y_{ijk})}$$

We refer to the estimation described above as the *constrained estimation with initial memory* as model parameters are constrained by patient factors, and we estimate $B_{\text{mem},\text{init},i}$ for each patient. For comparison, we performed the same estimation but with $B_{\text{mem},\text{init},i} = 0$ cells (i. e., assuming no initial memory B cells) for all patients. In addition, to compare the model fits from the constrained estimation to model fits where parameters are not constrained by patient factors (*unconstrained estimation with initial memory*), we performed a slightly modified estimation using the following priors and parameters:

$$\begin{aligned}
V_{\text{GC},i} &\sim \text{Lognormal}(\log(20), 2^2) \\
\pi_{\text{rec}} &\sim \text{Beta}(3, 10) \\
\pi_{\text{abs}} &\sim \text{Lognormal}(\log(0.6), 0.05^2) \\
\alpha_{\text{neutr}} &\sim \text{Lognormal}(\log(5 \cdot 10^{-3}), 0.1^2) \\
\pi_{\text{mem}} &\sim \text{Beta}(2, 10) \\
\pi_{\text{surv}} &= 0.9 \\
\pi_{\text{sel}} &= 0.2
\end{aligned}$$

In this setting, the total volume of activated LFs is estimated for each patient individually, π_{rec} is estimated over all patients, and π_{surv} and π_{sel} are set to constant values to ensure convergence. The rest is identical to the constrained estimation.

Posterior distributions were sampled using the No-U-Turn sampler (NUTS) (Hoffman and Gelman, 2014) implemented in Stan (Stan Development Team, 2020b) with 500 warm-up iterations, 1000 sampling iterations, and six chains. Processing of results was performed in R (R Core Team, 2019) using the packages CmdStanR (Gabry and Češnovar, 2020) and RStan (Stan Development Team, 2020a).

4.5.6 *Data and code availability*

The model is implemented in R and Stan. All source files used in this study are available on GitLab (<https://gitlab.com/csb.ethz/bcell-model>). The patient data are available at <https://gitlab.com/csb.ethz/hsct-study>. (Both repositories will be made public upon publication.)

4.6 AUTHOR CONTRIBUTIONS

JL, JS and AE designed the study. JL and JS developed the model. JL implemented the model and performed the analysis. JS and AE acquired funding and supervised the project. JL wrote the first draft of the manuscript, and JS commented on the final version.

4.7 ACKNOWLEDGMENTS

We thank Simon Dirmeier for helping with the initial implementation of the model in Stan and Hans-Michael Kaltenbach for valuable discussions. AE, JS and JL acknowledge support by an iPhD fellowship of the SystemsX program evaluated by the Swiss National Science Foundation (9th call).

4.8 SUPPLEMENTARY TABLES

Table S4.1. Model parameters and parameter distributions considered in the Sobol sensitivity analysis.

Description	Symbol	Sampling distr.	Reference
Activation and seeding of GC	β_{seed}	Uniform(100, 1000) cells mL ⁻¹ d ⁻¹	$\approx 50 - 200$ cells seed GC (Tas et al., 2016)
Total volume of activated LFs	V_{LF}	Uniform(0.1, 200) mL	Hollowood and Macartney (1992); Agrawal et al. (2017)
Survival probability of centroblasts	π_{surv}	Uniform(0.5, 1)	(Mackay and Browning, 2002)
Selection probability of centrocytes	π_{sel}	Uniform(0.01, 0.5)	(Woodruff et al., 2018)
Recycling probability of centrocytes	π_{rec}	Uniform(0.01, 0.99)	(Victoria et al., 2010)
Bifurcation parameter for differentiation to plasma/memory B cell	π_{mem}	Uniform(0, 0.5)	
Migration probability to bone marrow	π_{bm}	Uniform(0, 1)	

Table S4.2. Characteristics of hematopoietic stem cell transplant patients. Abbreviations: IQR, interquartile range; cGVHD, chronic graft-versus-host-disease; IFN, interferon; HI, hemagglutination inhibition.

Variable	Count (%) or median (IQR) [range]
Male	58 (57%)
Female	44 (43%)
Age in years	55 (46, 63) [22, 74]
Time after transplantation in years	4 (2, 7) [1, 25]
Recruited in influenza season 2014/15	42 (41%)
Recruited in influenza season 2015/16	60 (59%)
No cGVHD	44 (43%)
Mild cGVHD	21 (21%)
Moderate cGVHD	17 (17%)
Severe cGVHD	20 (20%)
No treatment with calcineurin inhibitors	63 (62%)
Treatment with calcineurin inhibitors	39 (38%)
IFN- λ genotype rs8099917 (TT)	64 (63%)
IFN- λ genotype rs8099917 (GT/GG)	38 (37%)
Absolute lymphocyte count (10^9 cells/L)	1.7 (1.1, 2.3) [0.3, 7.5]
Related donor	54 (53%)
Unrelated donor	48 (47%)
No HI titer increase on d7	63 (62%)
HI titer increase on d7	39 (38%)
with inferred B_{mem} on d0 (10^7 cells)	5.1 (1.4, 13.0) [0.2, 131.4]

4.9 SUPPLEMENTARY FIGURES

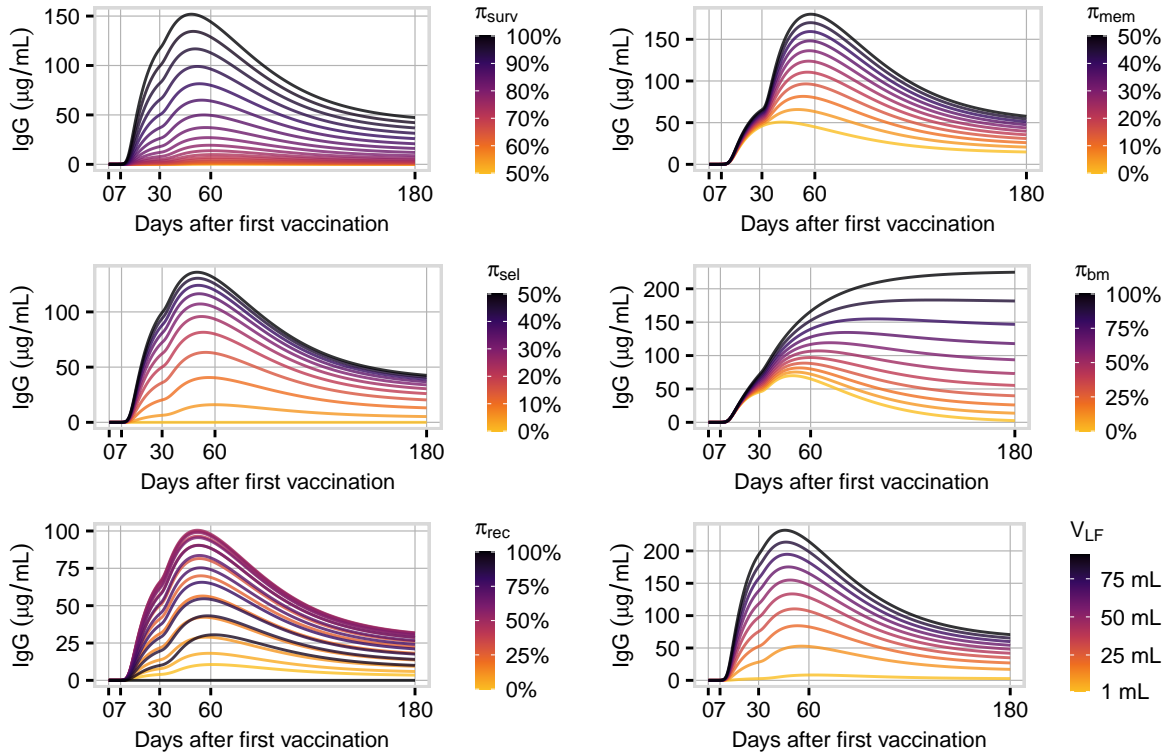


Figure S4.1. Effect of parameters modelling the key processes of the GC reaction on plasma IgG concentration. Simulations were performed with two vaccine doses (vaccination on d0 and d30) and model parameters $\pi_{\text{abs}} = 65\%$, $\pi_{\text{surv}} = 90\%$, $\pi_{\text{sel}} = 20\%$, $\pi_{\text{rec}} = 30\%$, $\pi_{\text{mem}} = 10\%$, $\pi_{\text{bm}} = 20\%$, $V_{\text{GC}} = 20$ mL or as indicated in the figure legends. All other parameters were set to the values summarized in **Table 4.1**.

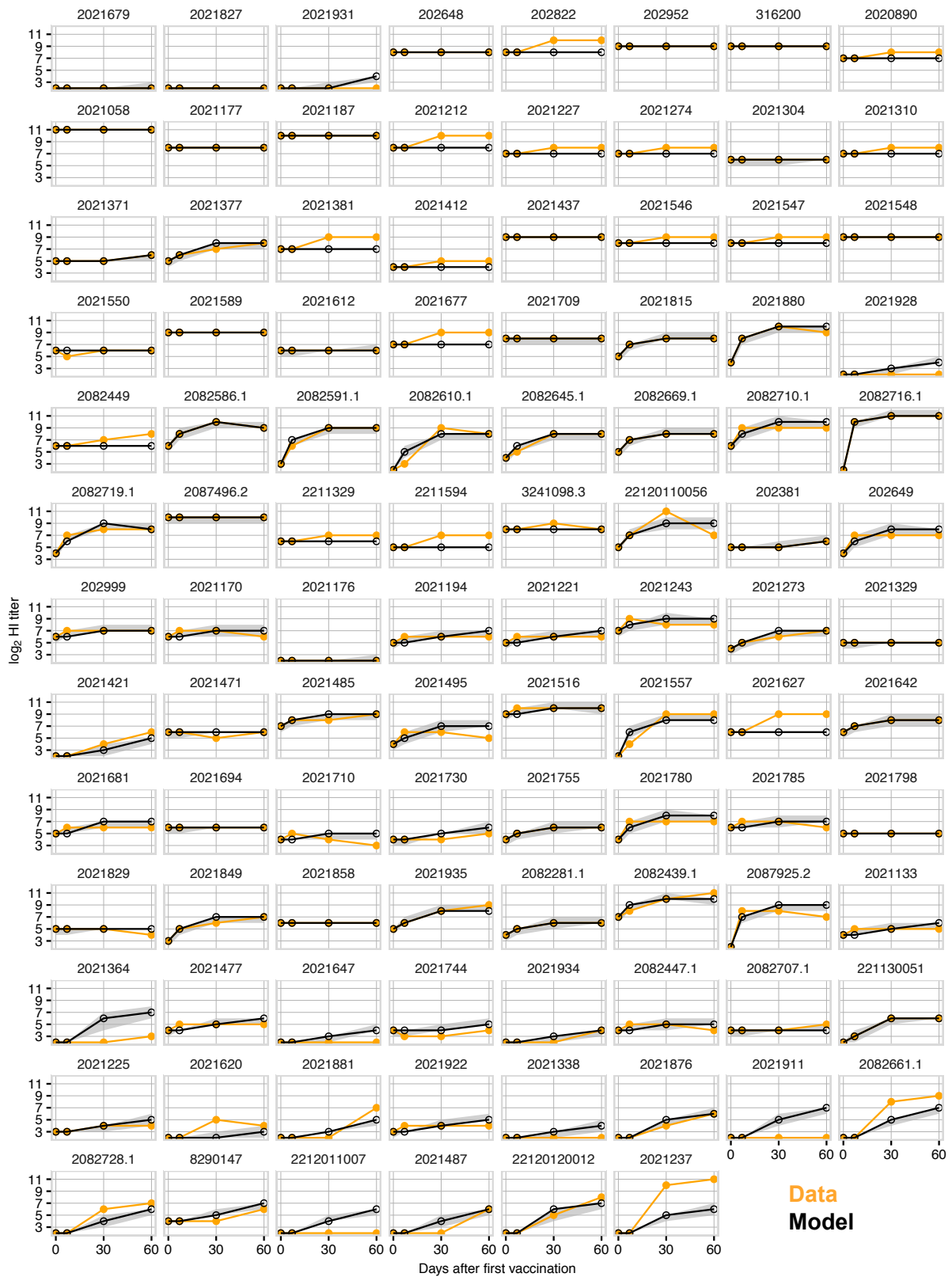


Figure S4.2. Model fit for the patient-factor constrained estimation with initial memory. Data show predicted (black) and observed (orange) HI antibody titers in 102 HSCT. The gray area indicates 95% posterior predictive intervals.

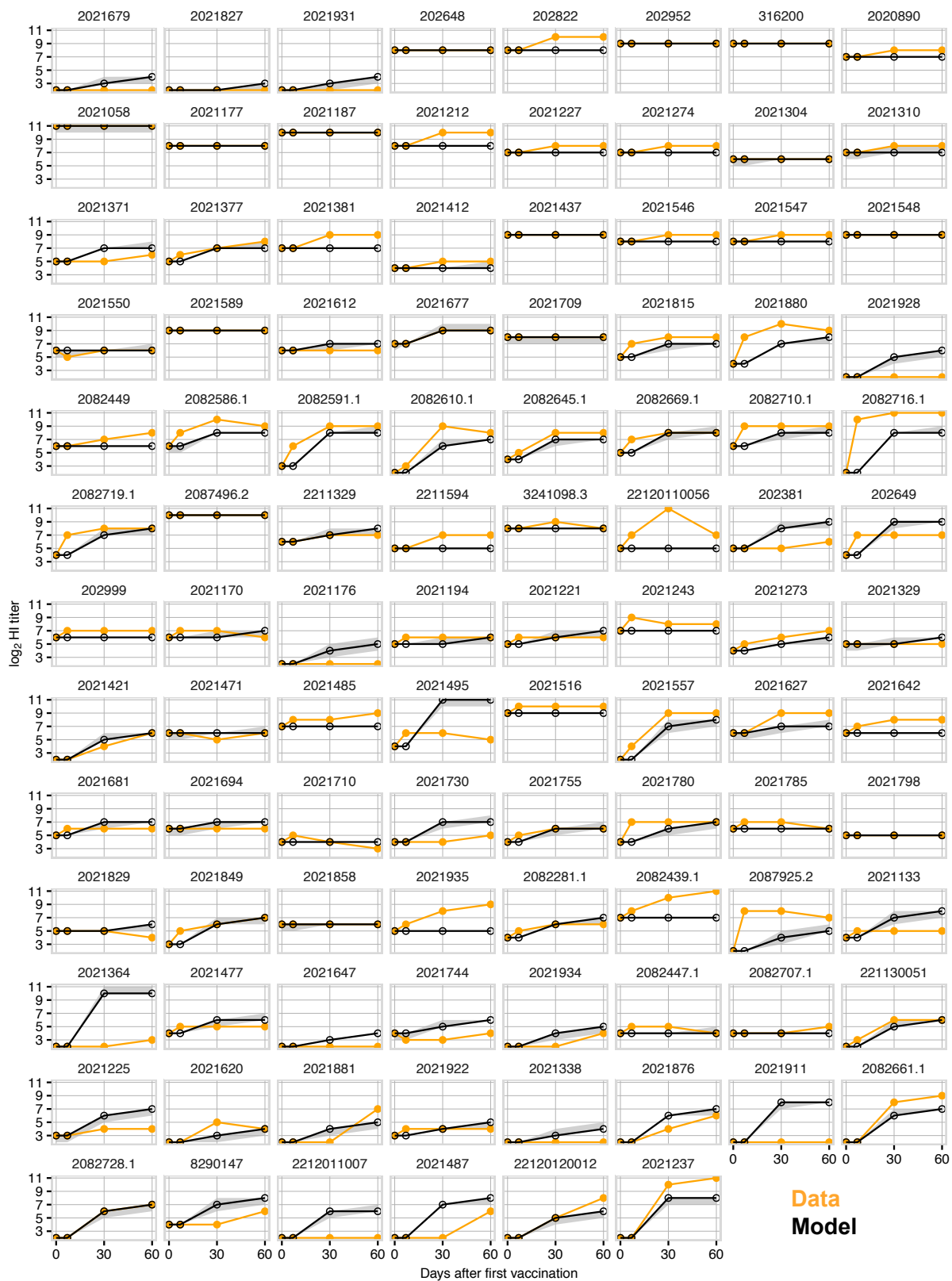


Figure S4.3. Model fit for the patient-factor constrained estimation without initial memory. Data show predicted (black) and observed (orange) HI antibody titers in 102 HSCT. The gray area indicates 95% posterior predictive intervals. The model poorly describes the observed titer responses.

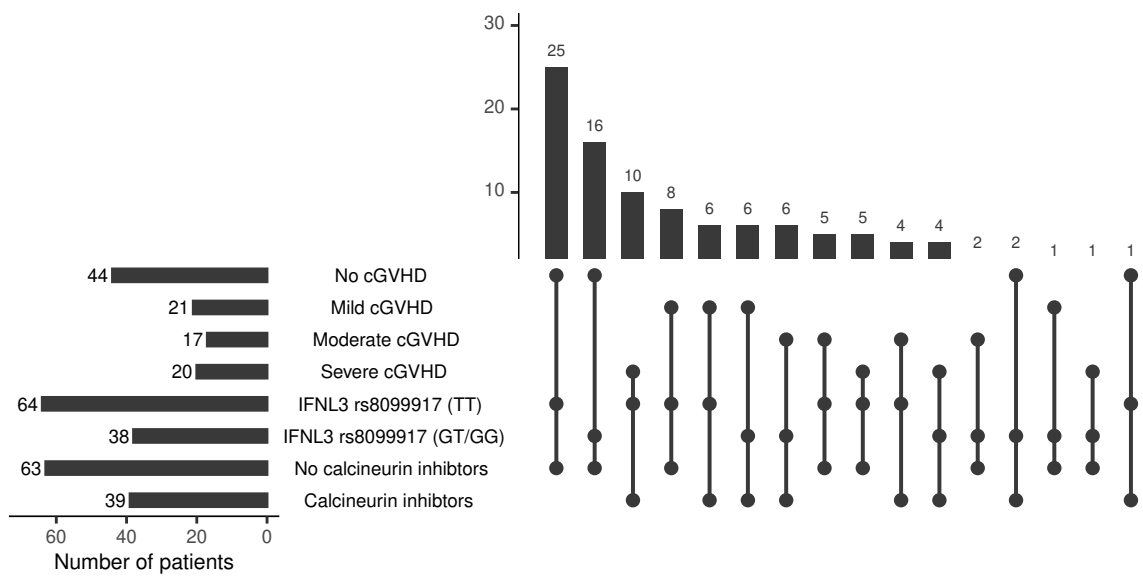


Figure S4.4. Co-occurrence of patient factors in the investigated patient groups. The horizontal barplot on the left shows the total number of patients in each group and the barplot on top the number of patients in the respective intersection/subset that is specified by the diagram below.

CONCLUDING REMARKS AND OUTLOOK

We presented three mathematical models for analysing the immune response to influenza vaccination and how they can be applied in combination to characterize the vaccine response in a patient population based on easily accessible measurements and clinical record information. We especially focused on overcoming limitations in the evaluation of HI titers: their analysis for inferring associations with patient factors, their relationship to antibody concentration and avidity, and how the gap between immunobiological models and clinical observations could be addressed. However, some important aspects of vaccine-induced immunity were not covered, and several open questions remain to be answered in further studies.

5.1 SEQUENTIAL MODELS FOR TITER REGRESSION

In Chapter 2, we showed that the common approach to dichotomize HI titers based on seroconversion and seroprotection cut-offs unnecessarily neglects the full range of observed HI titers when comparing patient groups. Effects inferred by sequential logistic regression and binary logistic regression can be both interpreted as a shift in the unobserved antibody concentration (or, more precisely, in neutralizing activity if a shift in antibody avidity also contributes to the difference in HI titers). Consistent with this interpretation, they yielded qualitatively similar results but regression on HI titers increased the precision in estimated effects due to the higher resolution in patients' underlying antibody concentration. However, the proportional odds assumption, i. e., that the inferred effects (β in Equation 2.2) do not depend on the HI titer level, could be violated if saturation effects in antibody responses decrease the difference in concentrations between compared patient groups with increasing HI titer. In this case, the general sequential model that accounts for category-specific effects (β_k) would be more appropriate (Fahrmeir et al., 2007). We presented only a first case study on the application of sequential models to HI titers. Sequential models are not yet established in seroepidemiological studies in humans, and additional studies investigating their limitations and applicability to different HI titer data sets are needed. Of particular interest would be to investigate when the proportional odds assumption is violated, whether the model can be further simplified by assuming that all threshold parameters (θ_k , Equation 2.2) must have the same distance between each other (because the serum samples are serially diluted), or whether the thresholds show a nonlinear behavior due to a detection limit that could be eventually accounted for. In addition, future studies could investigate sequential models in a systematic manner, e.g., in simulation studies, to evaluate their performance with respect to power, bias and precision (Morris et al., 2019), and how they perform in comparison to ordinal regression models that have been previously proposed for analysing HI titers (Capuano et al., 2007).

5.2 A MECHANISTIC MODEL FOR HI ASSAYS

The biophysical model of the HI assay presented in Chapter 3 establishes the first reported quantitative relationship between IgG concentration, avidity, and HI titer. The model explains why \log_2 HI titers >13 are seldom observed as such high titers would require avidities in the fM range (<0.01 nM), and predicts a yet unknown property of the HI assay: for very high avidities (<0.03 nM), the assay only detects changes in IgG concentration. We further showed that the model can be applied to infer avidities from IgG concentrations and HI titers and thereby refine the analysis of antibody responses. We focused on IgGs due to their major role in immunity against influenza and because they constitute the majority of serum antibodies (Schroeder and Cavacini, 2010). However, early no-memory antibody responses are dominated by IgMs, and when basal IgG levels are low, they could contribute to the observed HI titer. Since IgGs released by reactivated memory B cells and IgMs released by short-lived plasmablasts peak both approximately at the same time (one week after antigen exposure) (Krammer et al., 2018), accounting for IgMs in serum might be necessary in some cases to properly infer memory B cell responses from HI titer response kinetics. Therefore, it would be useful to investigate if the neutralizing activity of IgMs could be integrated into the model. Furthermore, we focused on influenza H1N1 as this influenza subtype is well characterized in the literature. Since we do not know which influenza strain might become the next pandemic strain, it is worth exploring whether the HI model could be extended to influenza H3N2 and B viruses. Although these influenza viruses are less well characterized, our model could serve as a starting point and perhaps be calibrated based on antibody concentration, avidity and HI titer measurements for H3N2 and B strains.

5.3 TOWARDS A BETTER UNDERSTANDING OF IMMUNE RESPONSE DYNAMICS IN PATIENT POPULATIONS

The HI model closes the gap between immunological models describing B cell dynamics and HI titers obtained in vaccine studies. This enabled us to directly infer differences in memory B cell responses and GC processes from measured HI titers (Chapter 4). An important result of this chapter is that the previously inferred associations between cGVHD, calcineurin inhibitors, and donor family relationship with antibody response could be explained by differences in previously acquired memory B cells, either due to (i) differences in vaccination history or (ii) differences in memory B cell production. In both cases, previous vaccinations or vaccination outcomes would be the main determinant of the vaccine response in the investigated influenza season. Specifically, it suggests that either (i) repeated seasonal vaccinations can induce memory and boost the antibody response in HSCT patients, or (ii) some patient groups respond differently to repeated vaccination. This is a clinically relevant aspect that should be further investigated. For instance, previous vaccine studies in HSCT patients reported no significant effect of cGVHD on vaccine response (Pauksen et al., 2000; Issa et al., 2011; Engelhard et al., 2011; Gueller et al., 2011; Fukatsu et al., 2017), or a negative effect (Mohty et al., 2011; Dhédin et al., 2014; Roll et al., 2012). If the positive effect of cGVHD in our patient cohort is linked to a greater number of previous vaccinations in patients with cGVHD (especially with severe cGVHD), similar vaccination schedules could potentially improve

vaccine responses also in other cGHVD patients. Effective vaccination strategies for cGVHD patients are not sufficiently explored and not well established, mostly because of the low number of patients in most vaccine studies (Hilgendorf et al., 2011).

Another interesting finding is that clinical patient information, pre-filtered by statistical inference of associations between patient factors and HI titers (Chapter 2), and integrated into a dynamic B cell model via mechanistic hypotheses, is able to explain the heterogeneous HI titer response with minimal model parameterization (Chapter 4). Next, it would be relevant to quantify the contribution of newly generated plasma cells vs. reactivated memory B cells to the observed HI titer responses. We also want to test how well the model describes the data *only* by reactivated memory B cells (setting $V_{LF} = 0$ for all patients, Equation 4.1). Furthermore, the strong association between lymphocyte count and antibody response has to be investigated in more detail. A lymphocyte count dependency could be implemented for additional GC reaction processes, e.g., T-cell dependent selection, to investigate whether the inferred differences in GC reaction processes lie within a physiologically reasonable range or whether the strong association between lymphocyte count and HI titers must be explained by alternative mechanisms not captured by our model structure. We also did not further investigate the correlations between the inferred parameters and whether some patient groups exhibit stronger compensatory effects than others.

Importantly, we did not investigate the long-term antibody production (>60d post vaccination) determined by bone marrow plasma cells (BMPCs). The migration kinetics of plasma cells to the bone marrow is not well characterized, and until recently, it was unclear with which magnitude and what half-life BMPCs occur after influenza vaccination; Davis et al. detected at four weeks after influenza vaccination an increase in influenza-specific BMPCs in healthy individuals (Davis et al., 2020). The newly-generated BMPCs were derived from preexisting memory cells, showing that vaccination did not induce new BMPC clones. The BMPC levels mostly returned to pre-vaccination levels after one year. Therefore, we would like to examine how long-term immunity is associated with patient factors and preexisting memory B cells.

To better understand the vaccine response in a patient population in general, it is essential to identify which processes can be assumed to be very similar in the investigated population (population parameters), which processes are modulated by patient factors (group-specific parameters), and which processes have to be inferred for each patient individually (patient-specific parameters), such as the reactivation of previously acquired memory B cells. More data on influenza vaccine-induced GC and B cell dynamics is needed to identify sources of heterogeneity. Since GCs are hardly accessible in experiments, little is known about their variability in humans. Mathematical models could help to identify the most sensitive parameters for the research question at hand. Experimentalists could then decide which parameters could be established by measurement and which parameters would need to be inferred statistically.

5.4 NEW CORRELATES OF PROTECTION

A critical aspect of vaccine-mediated protection that we have not covered is the vaccine-induced memory B cell and antibody *diversity*. The inferred avidity by the HI model (Chapter 3) refers to the *apparent* dissociation constant over all neutralizing IgGs and we do not know whether the

neutralization activity arises from only a few influenza-specific B cell clones (oligoclonal), or whether vaccination induced a broad response with antibodies targeting different epitopes with different HA-binding avidities (polyclonal). Since narrow vaccine responses can lead to poor vaccine effectiveness, understanding how broad vaccine responses emerge is of great importance. In recent years, promising high-throughput methods for measuring antibody affinities have been developed, enabling to characterize antigen binding of thousand of antibody variants in parallel (Fowler et al., 2014; Adams et al., 2016). More sophisticated models of GC populations have been proposed to explain how antigen dosage, antigen complexity, and vaccine composition (monovalent vs. polyvalent) affect affinity maturation and clonal diversity (Chaudhury et al., 2014; Childs et al., 2015; Wang et al., 2015; Wang, 2017; Papa et al., 2017; Murugan et al., 2018; Molari et al., 2020). These models distinguish between naive and memory B cells recruited to GCs, account for stochastic events during somatic hypermutation and selection, and consider B cell competition for antigen across neighboring GCs (Schwickert et al., 2007). A simulation study on malaria vaccination proposed that the administration of polyvalent vaccines favors cross-reactive antibodies (Chaudhury et al., 2014). However, modelling studies and experiments in mice on vaccination with HIV (human immunodeficiency virus) envelope proteins suggest that sequential immunization with one antigen type at a time (at a 2-week interval) induces cross-reactive antibody more effectively than the polyvalent cocktail approach (Wang et al., 2015). Several aspects of clonal diversity in GCs are not yet understood, for instance, how GCs respond to several antigen variants at once, to which extent preexisting memory B cells contribute to the GC seeding B cell population, and how re-engaged memory B cells influence the GC reaction outcome. To better understand vaccine-induced diversity and identify optimal influenza vaccination schedules and formulations (especially in repeatedly vaccinated patients), we have to complement measurements of antibody concentration and avidity with a measure of antibody diversity that could be assessed in larger vaccine studies. Single-cell technologies and monoclonal antibody production in mice lead to the discovery of broadly-neutralizing *monoclonal* antibodies that target the HA stem domain, which is more conserved across influenza strains than the HA globular domain (Okuno et al., 1993; Cho and Wrammert, 2016). This discovery raised the question about the possibility of an universal influenza vaccine (Paules et al., 2017). New vaccination approaches have been proposed for inducing broadly-neutralizing antibodies against influenza (Wei et al., 2010; Nabel and Fauci, 2010). However, the HA stem domain is usually not targeted in influenza vaccine-induced immune responses and B cells recognizing the HA head domain dominate the vaccine response (Andrews et al., 2015). How to overcome this immunodominance of the HA head domain and how to boost stem-reactive B cells is focus of ongoing research (Krammer, 2016). The current understanding is that stem-reactive memory B cells constitute a small part of the B cell repertoire, while head-reactive memory B cells dominate (Altman et al., 2015; Cho and Wrammert, 2016). Only if a new influenza strain lacks the immunodominant epitopes recognized by preexisting memory B cells, stem-reactive memory B cells are reactivated and boosted (Wrammert et al., 2011; Pica et al., 2012). Since reactivated memory B cells respond faster than naive B cells, they will dominate the immune response. This is consistent with studies showing that re-exposure to the same influenza strains boosts head-reactive responses, while exposure to more diverse influenza strains can boost stem-reactive antibodies (Miller et al., 2013; Andrews et al., 2015). The distinction between head- vs. stem-reactive anti-

bodies will be important for developing such next-generation influenza vaccines. However, the HI assay mostly detects head-reactive antibodies; stem-reactive antibodies often show low or even no hemagglutination activity at all (Andrews et al., 2015; Krammer, 2016). Therefore, novel correlates of protection are currently explored, e.g., based on ELISAs or cell responses (Ng et al., 2019; Krammer et al., 2020). In the future, additional correlates of protection could be integrated into immune response models and not only improve influenza vaccine development but also enhance our understanding of vaccine-mediated immunity.

The SARS-CoV-2 pandemic in 2020 revealed that our society is not as robust to pandemics as we would wish. Climate change and the emergence of new viral reservoirs due to deforestation could accelerate the emergence and spread of new pathogens in future decades (Lindgren et al., 2012; Afelt et al., 2018). The success story of vaccines leading to the eradication of smallpox and control of several dangerous infectious diseases over the last century demonstrates that vaccines are the key to protect against rapidly evolving pathogens (Hinman, 1998; Andre et al., 2008). Hence, a better understanding of how vaccination shapes adaptive immunity and how vaccination strategies can be optimized to their full potential is of fundamental importance and will require the joint effort of multiple disciplines.

BIBLIOGRAPHY

- M. Abdullah, P.-S. Chai, M.-Y. Chong, E. R. M. Tohit, R. Ramasamy, C. P. Pei, and S. Vidyadaran. Gender effect on in vitro lymphocyte subset levels of healthy individuals. *Cellular Immunology*, 272(2):214–219, 2012.
- R. M. Adams, T. Mora, A. M. Walczak, and J. B. Kinney. Measuring the sequence-affinity landscape of antibodies with massively parallel titration curves. *eLife*, 5:e23156, 2016.
- A. Afelt, R. Frutos, and C. Devaux. Bats, coronaviruses, and deforestation: Toward the emergence of novel infectious diseases? *Frontiers in Microbiology*, 9:702, 2018.
- V. Agrawal, T. P. Coroller, Y. Hou, S. W. Lee, J. L. Romano, E. H. Baldini, A. B. Chen, D. Kozono, S. J. Swanson, J. O. Wee, et al. Lymph node volume predicts survival but not nodal clearance in Stage IIIA-IIIB NSCLC. *PLOS One*, 12(4):e0174268, 2017.
- A. Agresti. *Categorical Data Analysis*, volume 482. John Wiley & Sons, 2003.
- U. Aich, N. Beckley, Z. Shriver, R. Raman, K. Viswanathan, S. Hobbie, and R. Sasisekharan. Glycomics-based analysis of chicken red blood cells provides insight into the selectivity of the viral agglutination assay. *The FEBS journal*, 278(10):1699–1712, 2011.
- M. Akkaya, K. Kwak, and S. K. Pierce. B cell memory: building two walls of protection against pathogens. *Nature Reviews Immunology*, 20(4):229–238, 2020.
- B. Alberts, A. Johnson, J. Lewis, D. Morgan, M. Raff, P. W. Keith Roberts, et al. *Molecular biology of the cell*. 2018.
- C. D. Allen, T. Okada, and J. G. Cyster. Germinal-center organization and cellular dynamics. *Immunity*, 27(2):190–202, 2007a.
- C. D. Allen, T. Okada, H. L. Tang, and J. G. Cyster. Imaging of germinal center selection events during affinity maturation. *Science*, 315(5811):528–531, 2007b.
- A. C. Allison and E. M. Eugui. Mechanisms of action of mycophenolate mofetil in preventing acute and chronic allograft rejection. *Transplantation*, 80(2S):S181–S190, 2005.
- M. O. Altman, J. R. Bennink, J. W. Yewdell, and B. R. Herrin. Lamprey VLRB response to influenza virus supports universal rules of immunogenicity and antigenicity. *eLife*, 4:e07467, 2015.
- F. E. Andre, R. Booy, H. L. Bock, J. Clemens, S. K. Datta, T. J. John, B. W. Lee, S. Lolekha, H. Peltola, T. Ruff, et al. Vaccination greatly reduces disease, disability, death and inequity worldwide. *Bulletin of the World Health Organization*, 86:140–146, 2008.

- S. F. Andrews, Y. Huang, K. Kaur, L. I. Popova, I. Y. Ho, N. T. Pauli, C. J. H. Dunand, W. M. Taylor, S. Lim, M. Huang, et al. Immune history profoundly affects broadly protective b cell responses to influenza. *Science Translational Medicine*, 7(316):316ra192–316ra192, 2015.
- S. F. Andrews, M. J. Chambers, C. A. Schramm, J. Plyler, J. E. Raab, M. Kanekiyo, R. A. Gillespie, A. Ransier, S. Darko, J. Hu, et al. Activation dynamics and immunoglobulin evolution of pre-existing and newly generated human memory B cell responses to influenza hemagglutinin. *Immunity*, 51(2):398–410, 2019.
- D. Angeletti, J. S. Gibbs, M. Angel, I. Kosik, H. D. Hickman, G. M. Frank, S. R. Das, A. K. Wheatley, M. Prabhakaran, D. J. Leggat, et al. Defining B cell immunodominance to viruses. *Nature Immunology*, 18(4):456, 2017.
- T. Aoki. A comprehensive review of our current understanding of red blood cell (RBC) glycoproteins. *Membranes*, 7(4):56, 2017.
- Y. Arai, K. Yamashita, K. Mizugishi, T. Kondo, T. Kitano, M. Hishizawa, N. Kadowaki, and A. Takaori-Kondo. Risk factors for hypogammaglobulinemia after allo-SCT. *Bone Marrow Transplantation*, 49(6):859–862, 2014.
- P. Arevalo, H. Q. McLean, E. A. Belongia, and S. Cobey. Earliest infections predict the age distribution of seasonal influenza a cases. *eLife*, 9:e50060, 2020.
- B. G. Armstrong and M. Sloan. Ordinal regression models for epidemiologic data. *American Journal of Epidemiology*, 129(1):191–204, 1989.
- A. D. Association et al. Influenza and pneumococcal immunization in diabetes. *Diabetes Care*, 27 (suppl 1):s111–s113, 2004.
- G. Avetisyan, J. Aschan, M. Hassan, and P. Ljungman. Evaluation of immune responses to seasonal influenza vaccination in healthy volunteers and in patients after stem cell transplantation. *Transplantation*, 86(2):257–263, 2008.
- D. Aw, A. B. Silva, and D. B. Palmer. Immunosenescence: emerging challenges for an ageing population. *Immunology*, 120(4):435–446, 2007.
- S. K. Ballas. Erythrocyte concentration and volume are inversely related. *Clinica chimica acta; international journal of clinical chemistry*, 164(2):243–244, 1987.
- D. Bates, M. Mächler, B. Bolker, and S. Walker. Fitting linear mixed-effects models using lme4. *Journal of Statistical Software*, 67(1):1–48, 2015. doi: 10.18637/jss.v067.i01.
- A. L. Bauer, C. A. Beauchemin, and A. S. Perelson. Agent-based modeling of host–pathogen systems: The successes and challenges. *Information sciences*, 179(10):1379–1389, 2009.
- C. R. Beck, B. C. McKenzie, A. B. Hashim, R. C. Harris, U. of Nottingham Influenza, a. the ImmunoCompromised (UNIIC) Study Group, and J. S. Nguyen-Van-Tam. Influenza vaccination for immunocompromised patients: systematic review and meta-analysis by etiology. *The Journal of Infectious Diseases*, 206(8):1250–1259, 2012.

- G. I. Bell. Mathematical model of clonal selection and antibody production. *Journal of Theoretical Biology*, 29(2):191–232, 1970.
- E. A. Belongia, D. M. Skowronski, H. Q. McLean, C. Chambers, M. E. Sundaram, and G. De Serres. Repeated annual influenza vaccination and vaccine effectiveness: review of evidence. *Expert Review of Vaccines*, 16(7):723–736, 2017.
- A. Benoit, J. Beran, J.-M. Devaster, M. Esen, O. Launay, G. Leroux-Roels, J. E. McElhaney, L. Oostvogels, G. A. van Essen, M. Gaglani, et al. Hemagglutination inhibition antibody titers as a correlate of protection against seasonal A/H3N2 influenza disease. In *Open Forum Infectious Diseases*, volume 2, page ofv067. Oxford University Press, 2015.
- S.-E. Bentebibel, S. Lopez, G. Obermoser, N. Schmitt, C. Mueller, C. Harrod, E. Flano, A. Mejias, R. A. Albrecht, D. Blankenship, et al. Induction of ICOS+ CXCR3+ CXCR5+ TH cells correlates with antibody responses to influenza vaccination. *Science Translational Medicine*, 5(176):176ra32–176ra32, 2013.
- W. Beyer, A. Palache, G. Lüchters, J. Nauta, and A. Osterhaus. Seroprotection rate, mean fold increase, seroconversion rate: which parameter adequately expresses seroresponse to influenza vaccination? *Virus Research*, 103(1-2):125–132, 2004.
- M. F. Boni. Vaccination and antigenic drift in influenza. *Vaccine*, 26:C8–C14, 2008.
- N. M. Bouvier and P. Palese. The biology of influenza viruses. *Vaccine*, 26:D49–D53, 2008.
- S. Brooks, A. Gelman, G. Jones, and X.-L. Meng. *Handbook of Markov Chain Monte Carlo*. CRC press, 2011.
- J. Bruening, B. Weigel, and G. Gerold. The role of type III interferons in hepatitis C virus infection and therapy. *Journal of Immunology Research*, 2017, 2017.
- G. W. Brunette, P. E. Kozarsky, and N. J. Cohen. *CDC health information for international travel 2016: the yellow book*. Oxford University Press, USA, 2015.
- L. Buchauer and H. Wardemann. Calculating germinal centre reactions. *Current Opinion in Systems Biology*, 18:1–8, 2019.
- A. Buisman, C. De Rond, K. Öztürk, H. Ten Hulscher, and R. Van Binnendijk. Long-term presence of memory B-cells specific for different vaccine components. *Vaccine*, 28(1):179–186, 2009.
- A. Cagigi, N. Cotugno, S. Rinaldi, V. Santilli, P. Rossi, and P. Palma. Downfall of the current antibody correlates of influenza vaccine response in yearly vaccinated subjects: Toward qualitative rather than quantitative assays. *Pediatric Allergy and Immunology*, 27(1):22–27, 2016.
- A. W. Capuano, J. D. Dawson, and G. C. Gray. Maximizing power in seroepidemiological studies through the use of the proportional odds model. *Influenza and Other Respiratory Viruses*, 1(3):87–93, 2007.

- C. Carati, B. Gannon, and N. Piller. Anatomy and physiology in relation to compression of the upper limb and thorax. *J Lymph*, 5(1):58–67, 2010.
- D. M. Catron, A. A. Itano, K. A. Pape, D. L. Mueller, and M. K. Jenkins. Visualizing the first 50 hr of the primary immune response to a soluble antigen. *Immunity*, 21(3):341–347, 2004.
- L. L. Cavanagh and U. H. Von Andrian. Travellers in many guises: the origins and destinations of dendritic cells. *Immunology and Cell Biology*, 80(5):448–462, 2002.
- B. S. Chambers, K. Parkhouse, T. M. Ross, K. Alby, and S. E. Hensley. Identification of hemagglutinin residues responsible for H3N2 antigenic drift during the 2014–2015 influenza season. *Cell Reports*, 12(1):1–6, 2015.
- S. Chaudhury, J. Reifman, and A. Wallqvist. Simulation of B cell affinity maturation explains enhanced antibody cross-reactivity induced by the polyvalent malaria vaccine AMA1. *The Journal of Immunology*, 193(5):2073–2086, 2014.
- L. Chen and D. B. Flies. Molecular mechanisms of T cell co-stimulation and co-inhibition. *Nature Reviews Immunology*, 13(4):227–242, 2013.
- L. M. Childs, E. B. Baskerville, and S. Cobey. Trade-offs in antibody repertoires to complex antigens. *Philosophical Transactions of the Royal Society B: Biological Sciences*, 370(1676):20140245, 2015.
- C. Chiu, A. H. Ellebedy, J. Wrammert, and R. Ahmed. B cell responses to influenza infection and vaccination. In *Influenza Pathogenesis and Control-Volume II*, pages 381–398. Springer, 2014.
- A. Cho and J. Wrammert. Implications of broadly neutralizing antibodies in the development of a universal influenza vaccine. *Current Opinion in Virology*, 17:110–115, 2016.
- J. J. Cohen, R. C. Duke, V. A. Fadok, and K. S. Sellins. Apoptosis and programmed cell death in immunity. *Annual review of immunology*, 10(1):267–293, 1992.
- E. A. Copelan. Hematopoietic stem-cell transplantation. *New England Journal of Medicine*, 354(17):1813–1826, 2006.
- R. B. Couch, R. L. Atmar, L. M. Franco, J. M. Quarles, J. Wells, N. Arden, D. Niño, and J. W. Belmont. Antibody correlates and predictors of immunity to naturally occurring influenza in humans and the importance of antibody to the neuraminidase. *The Journal of Infectious Diseases*, 207(6):974–981, 2013.
- C. Cox. Multinomial regression models based on continuation ratios. *Statistics in Medicine*, 7(3):435–441, 1988.
- S. Crotty, E. N. Kersh, J. Cannons, P. L. Schwartzberg, and R. Ahmed. SAP is required for generating long-term humoral immunity. *Nature*, 421(6920):282–287, 2003.

- S. R. S. da Silva Conde, L. L. Rocha, V. M. Ferreira, J. C. M. Soares Monteiro, N. K. Fonseca Filgueiras, P. A. d. Almeida Lins, B. T. Silva dos Santos, F. Bonfim Freitas, E. da Silva Graça, S. Demachki, et al. Absence of correlation between IL-28B gene polymorphisms and the clinical presentation of chronic hepatitis B in an Amazon Brazilian population. *Disease markers*, 2014, 2014.
- C. W. Davis, K. J. Jackson, M. M. McCausland, J. Darce, C. Chang, S. L. Linderman, C. Chennareddy, R. Gerkin, S. J. Brown, J. Wrammert, et al. Influenza vaccine-induced human bone marrow plasma cells decline within a year after vaccination. *Science*, 370(6513): 237–241, 2020.
- R. A. de Groen, Z. M. Groothuisink, B.-S. Liu, and A. Boonstra. IFN- λ is able to augment TLR-mediated activation and subsequent function of primary human B cells. *Journal of Leukocyte Biology*, 98(4):623–630, 2015.
- H. de Lavallade, P. Garland, T. Sekine, K. Hoschler, D. Marin, K. Stringaris, E. Loucaides, K. Howe, R. Szydlo, E. Kanfer, et al. Repeated vaccination is required to optimize seroprotection against h1n1 in the immunocompromised host. *Haematologica*, 96(2):307–314, 2011.
- N. S. De Silva and U. Klein. Dynamics of B cells in germinal centres. *Nature Reviews Immunology*, 15(3):137–148, 2015.
- N. Dhédin, A. Krivine, N. Le Corre, A. Mallet, B. Lioure, J.-O. Bay, M.-T. Rubio, P. Agape, A. Thiébaud, J. Le Goff, et al. Comparable humoral response after two doses of adjuvanted influenza A/H1N1pdm2009 vaccine or natural infection in allogeneic stem cell transplant recipients. *Vaccine*, 32(5):585–591, 2014.
- R. K. Do, E. Hatada, H. Lee, M. R. Tourigny, D. Hilbert, and S. Chen-Kiang. Attenuation of apoptosis underlies B lymphocyte stimulator enhancement of humoral immune response. *Journal of Experimental Medicine*, 192(7):953–964, 2000.
- I. Dogan, B. Bertocci, V. Vilmont, F. Delbos, J. Mégret, S. Storck, C.-A. Reynaud, and J.-C. Weill. Multiple layers of B cell memory with different effector functions. *Nature Immunology*, 10(12): 1292–1299, 2009.
- E. B. Dolgosheina, A. Y. Karulin, and A. V. Bobylev. A kinetic model of the agglutination process. *Mathematical Biosciences*, 109(1):1–10, 1992.
- M. Duk, H. Krotkiewski, T. V. Stasyk, M. Lutsik-Kordovsky, D. Syper, and E. Lisowska. Isolation and characterization of glycophorin from nucleated (chicken) erythrocytes. *Archives of Biochemistry and Biophysics*, 375(1):111–118, 2000.
- T. D’Mello, L. Brammer, L. Blanton, K. Kniss, S. Smith, D. Mustaquim, C. Steffens, R. Dhara, J. Cohen, S. S. Chaves, et al. Update: influenza activity — United States, September 28, 2014–February 21, 2015. *MMWR. Morbidity and mortality weekly report*, 64(8):206, 2015.

- M. Edwards and N. Dimmock. Two influenza A virus-specific Fabs neutralize by inhibiting virus attachment to target cells, while neutralization by their IgGs is complex and occurs simultaneously through fusion inhibition and attachment inhibition. *Virology*, 278(2):423–435, 2000.
- A. Egli, A. Levin, D. M. Santer, M. Joyce, D. O’Shea, B. S. Thomas, L. F. Lisboa, K. Barakat, R. Bhat, K. P. Fischer, et al. Immunomodulatory function of interleukin 28B during primary infection with cytomegalovirus. *The Journal of Infectious Diseases*, 210(5):717–727, 2014a.
- A. Egli, D. M. Santer, D. O’Shea, K. Barakat, M. Syedbasha, M. Vollmer, A. Baluch, R. Bhat, J. Groenendyk, M. A. Joyce, et al. IL-28B is a key regulator of B-and T-cell vaccine responses against influenza. *PLOS Pathogens*, 10(12):e1004556, 2014b.
- S. Eidem, S. M. Tete, Å. Jul-Larsen, K. Hoschler, E. Montomoli, K. A. Brokstad, and R. J. Cox. Persistence and avidity maturation of antibodies to A (H1N1) pdm09 in healthcare workers following repeated annual vaccinations. *Vaccine*, 33(33):4146–4154, 2015.
- A. H. Ellebedy. Immunizing the immune: Can we overcome influenza’s most formidable challenge? *Vaccines*, 6(4):68, 2018.
- D. Engelhard, A. Nagler, I. Hardan, A. Morag, M. Aker, H. Baciú, N. Strauss, G. Parag, E. Naparstek, Z. Ravid, et al. Antibody response to a two-dose regimen of influenza vaccine in allogeneic T cell-depleted and autologous BMT recipients. *Bone Marrow Transplantation*, 11:1–1, 1993.
- D. Engelhard, Z. Zakay-Rones, M. Y. Shapira, I. Resnick, D. Averbuch, S. Grisariu, L. Dray, E. Djian, N. Strauss-Liviatan, I. Grotto, et al. The humoral immune response of hematopoietic stem cell transplantation recipients to AS03-adjuvanted A/California/7/2009 (H1N1) v-like virus vaccine during the 2009 pandemic. *Vaccine*, 29(9):1777–1782, 2011.
- European Centre for Disease Prevention and Control. Seasonal influenza - Annual Epidemiological Report for 2014-15 season, 2016.
URL <https://www.ecdc.europa.eu/en/publications-data/seasonal-influenza-annual-epidemiological-report-2014-15-season>.
- D. Externest, B. Meckelein, M. A. Schmidt, and A. Frey. Correlations between antibody immune responses at different mucosal effector sites are controlled by antigen type and dosage. *Infection and Immunity*, 68(7):3830–3839, 2000.
- L. Fahrmeir, T. Kneib, S. Lang, and B. Marx. *Regression*. Springer, 2007.
- A. N. Faucette, B. L. Unger, B. Gonik, and K. Chen. Maternal vaccination: moving the science forward. *Human Reproduction Update*, 21(1):119–135, 2015.
- D. T. Fearon, P. Manders, and S. D. Wagner. Arrested differentiation, the self-renewing memory lymphocyte, and vaccination. *Science*, 293(5528):248–250, 2001.
- V. Fedorov, F. Mannino, and R. Zhang. Consequences of dichotomization. *Pharmaceutical Statistics: The Journal of Applied Statistics in the Pharmaceutical Industry*, 8(1):50–61, 2009.

- F. Fenner, D. A. Henderson, I. Arita, Z. Jezek, I. D. Ladnyi, et al. *Smallpox and its eradication*, volume 6. World Health Organization Geneva, 1988.
- M. T. Figge, A. Garin, M. Gunzer, M. Kosco-Vilbois, K.-M. Toellner, and M. Meyer-Hermann. Deriving a germinal center lymphocyte migration model from two-photon data. *The Journal of Experimental Medicine*, 205(13):3019–3029, 2008.
- A. H. Filipovich, D. Weisdorf, S. Pavletic, G. Socie, J. R. Wingard, S. J. Lee, P. Martin, J. Chien, D. Przepioraka, D. Couriel, et al. National Institutes of Health consensus development project on criteria for clinical trials in chronic graft-versus-host disease: I. Diagnosis and staging working group report. *Biology of Blood and Marrow Transplantation*, 11(12):945–956, 2005.
- D. J. Firl, S. E. Degn, T. Padera, and M. C. Carroll. Capturing change in clonal composition amongst single mouse germinal centers. *eLife*, 7:e33051, 2018.
- J. Fonville, S. Wilks, S. James, A. Fox, M. Ventresca, M. Aban, L. Xue, T. Jones, N. Le, Q. Pham, et al. Antibody landscapes after influenza virus infection or vaccination. *Science*, 346(6212):996–1000, 2014.
- D. M. Fowler, J. J. Stephany, and S. Fields. Measuring the activity of protein variants on a large scale using deep mutational scanning. *Nature protocols*, 9(9):2267–2284, 2014.
- T. Francis. On the doctrine of original antigenic sin. *Proceedings of the American Philosophical Society*, 104(6):572–578, 1960.
- L. M. Franco, K. L. Bucasas, J. M. Wells, D. Niño, X. Wang, G. E. Zapata, N. Arden, A. Renwick, P. Yu, J. M. Quarles, et al. Integrative genomic analysis of the human immune response to influenza vaccination. *eLife*, 2:e00299, 2013.
- G. M. Frank, D. Angeletti, W. L. Ince, J. S. Gibbs, S. Khurana, A. K. Wheatley, E. E. Max, A. B. McDermott, H. Golding, J. Stevens, et al. A simple flow-cytometric method measuring B cell surface immunoglobulin avidity enables characterization of affinity maturation to influenza A virus. *MBio*, 6(4):e01156–15, 2015.
- Y. Fukatsu, Y. Nagata, M. Adachi, T. Yagyu, and T. Ono. Serum IgM levels independently predict immune response to influenza vaccine in long-term survivors vaccinated at > 1 year after undergoing allogeneic hematopoietic stem cell transplantation. *International Journal of Hematology*, 105(5):638–645, 2017.
- D. Furman, B. P. Hejblum, N. Simon, V. Jojic, C. L. Dekker, R. Thiébaud, R. J. Tibshirani, and M. M. Davis. Systems analysis of sex differences reveals an immunosuppressive role for testosterone in the response to influenza vaccination. *Proceedings of the National Academy of Sciences*, 111(2):869–874, 2014.
- D. Fürst, C. Müller, V. Vucinic, D. Bunjes, W. Herr, M. Gramatzki, R. Schwerdtfeger, R. Arnold, H. Einsele, G. Wulf, et al. High-resolution HLA matching in hematopoietic stem cell transplantation: a retrospective collaborative analysis. *Blood, The Journal of the American Society of Hematology*, 122(18):3220–3229, 2013.

- J. Gabry and R. Češnovar. *cmdstanr: R Interface to 'CmdStan'*, 2020. <https://mc-stan.org/cmdstanr>, <https://discourse.mc-stan.org>.
- D. Gatto and R. Brink. The germinal center reaction. *Journal of Allergy and Clinical Immunology*, 126(5):898–907, 2010.
- B. M. Gavillet, C. S. Eberhardt, F. Auderset, F. Castellino, A. Seubert, J. S. Tregoning, P.-H. Lambert, E. de Gregorio, G. Del Giudice, and C.-A. Siegrist. MF59 mediates its B cell adjuvanticity by promoting T follicular helper cells and thus germinal center responses in adult and early life. *The Journal of Immunology*, 194(10):4836–4845, 2015.
- D. Ge, J. Fellay, A. J. Thompson, J. S. Simon, K. V. Shianna, T. J. Urban, E. L. Heinzen, P. Qiu, A. H. Bertelsen, A. J. Muir, et al. Genetic variation in IL28B predicts hepatitis C treatment-induced viral clearance. *Nature*, 461(7262):399–401, 2009.
- L. Gelinck, Y. Teng, G. Rimmelzwaan, B. Van Den Bemt, F. Kroon, and J. Van Laar. Poor serological responses upon influenza vaccination in patients with rheumatoid arthritis treated with rituximab. *Annals of the Rheumatic Diseases*, 66(10):1402–1403, 2007.
- W. Gerhard, J. Yewdell, M. E. Frankel, and R. Webster. Antigenic structure of influenza virus haemagglutinin defined by hybridoma antibodies. *Nature*, 290(5808):713, 1981.
- R. N. Germain. Vaccines and the future of human immunology. *Immunity*, 33(4):441–450, 2010.
- A. Gonzalez-Quintela, R. Alende, F. Gude, J. Campos, J. Rey, L. Meijide, C. Fernandez-Merino, and C. Vidal. Serum levels of immunoglobulins (IgG, IgA, IgM) in a general adult population and their relationship with alcohol consumption, smoking and common metabolic abnormalities. *Clinical & Experimental Immunology*, 151(1):42–50, 2008.
- K. Goodwin, C. Viboud, and L. Simonsen. Antibody response to influenza vaccination in the elderly: a quantitative review. *Vaccine*, 24(8):1159–1169, 2006.
- K. M. Gostic, M. Ambrose, M. Worobey, and J. O. Lloyd-Smith. Potent protection against H5N1 and H7N9 influenza via childhood hemagglutinin imprinting. *Science*, 354(6313):722–726, 2016.
- S. Greenland, M. A. Mansournia, and D. G. Altman. Sparse data bias: a problem hiding in plain sight. *bmj*, 352:i1981, 2016.
- H. T. Greinix, D. Pohlreich, M. Kouba, U. Körmöcz, I. Lohmann, K. Feldmann, C. Zielinski, and W. F. Pickl. Elevated numbers of immature/transitional CD21- B lymphocytes and deficiency of memory CD27+ B cells identify patients with active chronic graft-versus-host disease. *Biology of Blood and Marrow Transplantation*, 14(2):208–219, 2008.
- L. A. Grohskopf, S. J. Olsen, L. Z. Sokolow, J. S. Bresee, N. J. Cox, K. R. Broder, R. A. Karron, and E. B. Walter. Prevention and control of seasonal influenza with vaccines: recommendations of the Advisory Committee on Immunization Practices (ACIP)—United States, 2014–15 influenza season. *MMWR. Morbidity and mortality weekly report*, 63(32):691, 2014.

- C. P. Gross and K. A. Sepkowitz. The myth of the medical breakthrough: smallpox, vaccination, and Jenner reconsidered. *International Journal of Infectious Diseases*, 3(1):54–60, 1998.
- S. F. d. S. Groth. The neutralization of viruses. In *Advances in Virus Research*, volume 9, pages 1–125. Elsevier, 1963.
- S. Gueller, R. Allwinn, S. Mousset, H. Martin, I. Wieters, E. Herrmann, H. Serve, M. Bickel, and G. Bug. Enhanced immune response after a second dose of an AS03-adjuvanted H1N1 influenza A vaccine in patients after hematopoietic stem cell transplantation. *Biology of Blood and Marrow Transplantation*, 17(10):1546–1550, 2011.
- L. R. Haaheim and J. M. Katz. Immune correlates of protection against influenza: challenges for licensure of seasonal and pandemic influenza vaccines. *Influenza and Other Respiratory Viruses*, 5(4):288–295, 2011.
- T. Hagan, H. I. Nakaya, S. Subramaniam, and B. Pulendran. Systems vaccinology: enabling rational vaccine design with systems biological approaches. *Vaccine*, 33(40):5294–5301, 2015.
- M. M. Hamawy. Molecular actions of calcineurin inhibitors. *Drug news & perspectives*, 16(5):277, 2003.
- E. Hammarlund, A. Thomas, I. J. Amanna, L. A. Holden, O. D. Slayden, B. Park, L. Gao, and M. K. Slifka. Plasma cell survival in the absence of B cell memory. *Nature Communications*, 8(1):1–11, 2017.
- I. H. Haralambieva, I. G. Ovsyannikova, R. B. Kennedy, R. A. Vierkant, V. S. Pankratz, R. M. Jacobson, and G. A. Poland. Associations between single nucleotide polymorphisms and haplotypes in cytokine and cytokine receptor genes and immunity to measles vaccination. *Vaccine*, 29(45):7883–7895, 2011.
- D. L. Hardie, G. D. Johnson, M. Khan, and I. C. MacLennan. Quantitative analysis of molecules which distinguish functional compartments within germinal centers. *European Journal of Immunology*, 23(5):997–1004, 1993.
- S. M. Harless, V. M. Lentz, A. P. Sah, B. L. Hsu, K. Clise-Dwyer, D. M. Hilbert, C. E. Hayes, and M. P. Cancro. Competition for BlyS-mediated signaling through Bcmd/BR3 regulates peripheral B lymphocyte numbers. *Current Biology*, 11(24):1986–1989, 2001.
- F. E. Harrell Jr, with contributions from Charles Dupont, and many others. *Hmisc: Harrell Miscellaneous*, 2019. URL <https://CRAN.R-project.org/package=Hmisc>. R package version 4.2-0.
- A. Harris, G. Cardone, D. C. Winkler, J. B. Heymann, M. Brecher, J. M. White, and A. C. Steven. Influenza virus pleiomorphy characterized by cryoelectron tomography. *Proceedings of the National Academy of Sciences*, 103(50):19123–19127, 2006.

- A. K. Harris, J. R. Meyerson, Y. Matsuoka, O. Kuybeda, A. Moran, D. Bliss, S. R. Das, J. W. Yewdell, G. Sapiro, K. Subbarao, et al. Structure and accessibility of HA trimers on intact 2009 H1N1 pandemic influenza virus to stem region-specific neutralizing antibodies. *Proceedings of the National Academy of Sciences*, 110(12):4592–4597, 2013.
- H. Hassan and M. El-Sheemy. Adult bone-marrow stem cells and their potential in medicine. *Journal of the Royal Society of Medicine*, 97(10):465–471, 2004.
- A. E. Hauser, T. Junt, T. R. Mempel, M. W. Sneddon, S. H. Kleinstei, S. E. Henrickson, U. H. von Andrian, M. J. Shlomchik, and A. M. Haberman. Definition of germinal-center B cell migration in vivo reveals predominant intrazonal circulation patterns. *Immunity*, 26(5):655–667, 2007.
- B. A. Heesters, R. C. Myers, and M. C. Carroll. Follicular dendritic cells: dynamic antigen libraries. *Nature Reviews Immunology*, 14(7):495–504, 2014.
- S. Heidt, D. L. Roelen, C. Eijnsink, M. Eikmans, C. Van Kooten, F. H. Claas, and A. Mulder. Calcineurin inhibitors affect B cell antibody responses indirectly by interfering with T cell help. *Clinical & Experimental Immunology*, 159(2):199–207, 2010.
- I. Hilgendorf, M. Freund, W. Jilg, H. Einsele, J. Gea-Banacloche, H. Greinix, J. Halter, A. Lawitschka, D. Wolff, and R. Meisel. Vaccination of allogeneic haematopoietic stem cell transplant recipients: report from the international consensus conference on clinical practice in chronic GVHD. *Vaccine*, 29(16):2825–2833, 2011.
- A. R. Hinman. Global progress in infectious disease control. *Vaccine*, 16(11-12):1116–1121, 1998.
- G. K. Hirst. The agglutination of red cells by allantoic fluid of chick embryos infected with influenza virus. *Science*, 94(2427):22–23, 1941.
- D. Hobson, R. Curry, A. Beare, and A. Ward-Gardner. The role of serum haemagglutination-inhibiting antibody in protection against challenge infection with influenza a2 and b viruses. *Epidemiology & Infection*, 70(4):767–777, 1972.
- M. D. Hoffman and A. Gelman. The No-U-Turn sampler: adaptively setting path lengths in Hamiltonian Monte Carlo. *J. Mach. Learn. Res.*, 15(1):1593–1623, 2014.
- K. Hollowood and J. Macartney. Cell kinetics of the germinal center reaction—a stathmokinetic study. *European Journal of Immunology*, 22(1):261–266, 1992.
- K. Honda and T. Taniguchi. IRFs: master regulators of signalling by Toll-like receptors and cytosolic pattern-recognition receptors. *Nature Reviews Immunology*, 6(9):644–658, 2006.
- K. Houser and K. Subbarao. Influenza vaccines: challenges and solutions. *Cell Host & Microbe*, 17(3):295–300, 2015.
- I. F. Hung, K. K. To, C.-K. Lee, C.-K. Lin, J. F. Chan, H. Tse, V. C. Cheng, H. Chen, P.-L. Ho, C. W. Tse, et al. Effect of clinical and virological parameters on the level of neutralizing antibody against pandemic influenza A virus H1N1 2009. *Clinical Infectious Diseases*, 51(3):274–279, 2010.

- D. Iber and P. K. Maini. A mathematical model for germinal centre kinetics and affinity maturation. *Journal of Theoretical Biology*, 219(2):153–175, 2002.
- B. Iooss, A. Janon, G. Pujol, with contributions from Baptiste Broto, K. Boumhaout, S. D. Veiga, T. Delage, J. Fruth, L. Gilquin, J. Guillaume, L. Le Gratiet, P. Lemaitre, A. Marrel, A. Meynaoui, B. L. Nelson, F. Monari, R. Oomen, O. Rakovec, B. Ramos, O. Roustant, E. Song, J. Staum, R. Sueur, T. Touati, and F. Weber. *sensitivity: Global Sensitivity Analysis of Model Outputs*, 2019. URL <https://CRAN.R-project.org/package=sensitivity>. R package version 1.16.2.
- N. C. Issa, F. M. Marty, L. S. Gagne, S. Koo, K. A. Verrill, E. P. Alyea, C. S. Cutler, J. Koreth, P. Armand, V. T. Ho, et al. Seroprotective titers against 2009 H1N1 influenza A virus after vaccination in allogeneic hematopoietic stem cell transplantation recipients. *Biology of Blood and Marrow Transplantation*, 17(3):434–438, 2011.
- A. A. Itano, S. J. McSorley, R. L. Reinhardt, B. D. Ehst, E. Ingulli, A. Y. Rudensky, and M. K. Jenkins. Distinct dendritic cell populations sequentially present antigen to CD4 T cells and stimulate different aspects of cell-mediated immunity. *Immunity*, 19(1):47–57, 2003.
- D. Jackson, B. Crabb, P. Pountourios, W. Tulip, and W. Laver. Three antibody molecules can bind simultaneously to each monomer of the tetramer of influenza virus neuraminidase and the trimer of influenza virus hemagglutinin. *Archives of Virology*, 116(1-4):45–56, 1991.
- C. A. Jacobson, L. Sun, H. T. Kim, S. M. McDonough, C. G. Reynolds, M. Schowalter, J. Koreth, C. S. Cutler, V. T. Ho, E. P. Alyea, et al. Post-transplantation B cell activating factor and B cell recovery before onset of chronic graft-versus-host disease. *Biology of Blood and Marrow Transplantation*, 20(5):668–675, 2014.
- M. J. Jansen. Analysis of variance designs for model output. *Computer Physics Communications*, 117(1-2):35–43, 1999.
- E. Jenner. *An inquiry into the causes and effects of the variolae vaccinae, a disease discovered in some of the western counties of England, particularly Gloucestershire, and known by the name of the cow pox*. 1800.
- M. Jiménez-Sousa, J. Berenguer, N. Rallon, M. Guzmán-Fulgencio, J. Lopez, V. Soriano, A. Fernández-Rodríguez, J. Cosin, C. Restrepo, M. García-Álvarez, et al. IL28RA polymorphism is associated with early hepatitis C virus (HCV) treatment failure in human immunodeficiency virus-/HCV-coinfected patients. *Journal of Viral Hepatitis*, 20(5):358–366, 2013.
- N. A. Karras, M. Weeres, W. Sessions, X. Xu, T. DeFor, J.-A. H. Young, H. Stefanski, C. Brunstein, S. Cooley, J. S. Miller, et al. A randomized trial of one versus two doses of influenza vaccine after allogeneic transplantation. *Biology of Blood and Marrow Transplantation*, 19(1):109–116, 2013.
- D. S. Katikaneni and L. Jin. B cell MHC class II signaling: A story of life and death. *Human immunology*, 80(1):37–43, 2019.

- L. Kaufmann, M. Syedbasha, D. Vogt, Y. Hollenstein, J. Hartmann, J. E. Linnik, and A. Egli. An Optimized Hemagglutination Inhibition (HI) Assay to Quantify Influenza-specific Antibody Titers. *JoVE (Journal of Visualized Experiments)*, (130):e55833, 2017.
- T. Kawai and S. Akira. The role of pattern-recognition receptors in innate immunity: update on Toll-like receptors. *Nature Immunology*, 11(5):373, 2010.
- R. B. Kennedy, I. G. Ovsyannikova, I. H. Haralambieva, M. M. O’Byrne, R. M. Jacobson, V. S. Pankratz, and G. A. Poland. Multigenic control of measles vaccine immunity mediated by polymorphisms in measles receptor, innate pathway, and cytokine genes. *Vaccine*, 30(12): 2159–2167, 2012.
- T. B. Kepler and A. S. Perelson. Cyclic re-entry of germinal center B cells and the efficiency of affinity maturation. *Immunology Today*, 14(8):412–415, 1993.
- S. Khurana, N. Verma, J. W. Yewdell, A. K. Hilbert, F. Castellino, M. Lattanzi, G. Del Giudice, R. Rappuoli, and H. Golding. MF59 adjuvant enhances diversity and affinity of antibody-mediated immune response to pandemic influenza vaccines. *Science Translational Medicine*, 3(85):85ra48–85ra48, 2011.
- S. Khurana, D. Frasca, B. Blomberg, and H. Golding. AID activity in B cells strongly correlates with polyclonal antibody affinity maturation in-vivo following pandemic 2009-H1N1 vaccination in humans. *PLOS Pathogens*, 8(9), 2012.
- S. Khurana, M. Hahn, E. M. Coyle, L. R. King, T.-L. Lin, J. Treanor, A. Sant, and H. Golding. Repeat vaccination reduces antibody affinity maturation across different influenza vaccine platforms in humans. *Nature Communications*, 10(1):3338, 2019.
- L. P. Kil, J. Vaneman, J. E. van der Lubbe, D. Czapska-Casey, J. T. Tolboom, R. Roozendaal, R. C. Zahn, H. Kuipers, and L. Solfrosi. Restrained expansion of the recall germinal center response as biomarker of protection for influenza vaccination in mice. *PLOS One*, 14(11):e0225063, 2019.
- S. L. Klein and K. L. Flanagan. Sex differences in immune responses. *Nature Reviews Immunology*, 16(10):626, 2016.
- B. F. Koel, D. F. Burke, T. M. Bestebroer, S. van der Vliet, G. C. Zondag, G. Vervaet, E. Skepner, N. S. Lewis, M. I. Spronken, C. A. Russell, et al. Substitutions near the receptor binding site determine major antigenic change during influenza virus evolution. *Science*, 342(6161):976–979, 2013.
- C. Kollman, S. R. Spellman, M.-J. Zhang, A. Hassebroek, C. Anasetti, J. H. Antin, R. E. Champlin, D. L. Confer, J. F. DiPersio, M. Fernandez-Viña, et al. The effect of donor characteristics on survival after unrelated donor transplantation for hematologic malignancy. *Blood, The Journal of the American Society of Hematology*, 127(2):260–267, 2016.
- F. Krammer. Novel universal influenza virus vaccine approaches. *Current Opinion in Virology*, 17: 95–103, 2016.

- F. Krammer. The human antibody response to influenza a virus infection and vaccination. *Nature Reviews Immunology*, 19(6):383–397, 2019.
- F. Krammer, G. J. Smith, R. A. Fouchier, M. Peiris, K. Kedzierska, P. C. Doherty, P. Palese, M. L. Shaw, J. Treanor, R. G. Webster, et al. Influenza (Primer). *Nature Reviews: Disease Primers*, 2018.
- F. Krammer, J. P. Weir, O. Engelhardt, J. M. Katz, and R. J. Cox. Meeting report and review: Immunological assays and correlates of protection for next-generation influenza vaccines. *Influenza and Other Respiratory Viruses*, 14(2):237–243, 2020.
- K. M. Kunisaki and E. N. Janoff. Influenza in immunosuppressed populations: a review of infection frequency, morbidity, mortality, and vaccine responses. *The Lancet Infectious Diseases*, 9(8):493–504, 2009.
- R. Küppers, M. Zhao, M. Hansmann, and K. Rajewsky. Tracing B cell development in human germinal centres by molecular analysis of single cells picked from histological sections. *The EMBO journal*, 12(13):4955–4967, 1993.
- M. Kuraoka, A. G. Schmidt, T. Nojima, F. Feng, A. Watanabe, D. Kitamura, S. C. Harrison, T. B. Kepler, and G. Kelsoe. Complex antigens drive permissive clonal selection in germinal centers. *Immunity*, 44(3):542–552, 2016.
- A. Kuznetsova, P. B. Brockhoff, and R. H. B. Christensen. lmerTest package: Tests in linear mixed effects models. *Journal of Statistical Software*, 82(13):1–26, 2017. doi: 10.18637/jss.v082.i13.
- N. Kylilis, P. Riangrunroj, H.-E. Lai, V. Salema, L. A. Fernandez, G.-B. V. Stan, P. S. Freemont, and K. M. Polizzi. Whole-cell biosensor with tunable limit of detection enables low-cost agglutination assays for medical diagnostic applications. *ACS sensors*, 4(2):370–378, 2019.
- D. Lau, L. Y.-L. Lan, S. F. Andrews, C. Henry, K. T. Rojas, K. E. Neu, M. Huang, Y. Huang, B. DeKosky, A.-K. E. Palm, et al. Low CD21 expression defines a population of recent germinal center graduates primed for plasma cell differentiation. *Science Immunology*, 2(7), 2017.
- J. Lee, D. R. Boutz, V. Chromikova, M. G. Joyce, C. Vollmers, K. Leung, A. P. Horton, B. J. DeKosky, C.-H. Lee, J. J. Lavinder, et al. Molecular-level analysis of the serum antibody repertoire in young adults before and after seasonal influenza vaccination. *Nature Medicine*, 22(12):1456, 2016.
- J. K. Lee, G. K. Lam, T. Shin, J. Kim, A. Krishnan, D. P. Greenberg, and A. Chit. Efficacy and effectiveness of high-dose versus standard-dose influenza vaccination for older adults: a systematic review and meta-analysis. *Expert Review of Vaccines*, 17(5):435–443, 2018.
- J. A. Lewnard and S. Cobey. Immune history and influenza vaccine effectiveness. *Vaccines*, 6(2):28, 2018.
- Y. Li, J. L. Myers, D. L. Bostick, C. B. Sullivan, J. Madara, S. L. Linderman, Q. Liu, D. M. Carter, J. Wrammert, S. Esposito, et al. Immune history shapes specificity of pandemic H1N1 influenza antibody responses. *Journal of Experimental Medicine*, 210(8):1493–1500, 2013.

- Z.-N. Li, S.-C. Lin, P. J. Carney, J. Li, F. Liu, X. Lu, M. Liu, J. Stevens, M. Levine, J. M. Katz, et al. IgM, IgG, and IgA antibody responses to influenza A (H1N1) pdm09 hemagglutinin in infected persons during the first wave of the 2009 pandemic in the United States. *Clin. Vaccine Immunol.*, 21(8):1054–1060, 2014.
- E. Lindgren, Y. Andersson, J. E. Suk, B. Sudre, and J. C. Semenza. Monitoring EU emerging infectious disease risk due to climate change. *Science*, 336(6080):418–419, 2012.
- J. Linnik, M. Syedbasha, Y. Hollenstein, J. Halter, A. Egli, and J. Stelling. Model-based inference of neutralizing antibody avidities against influenza virus. *bioRxiv*, 2020.
- J. Linnik, M. Syedbasha, H.-M. Kaltenbach, D. Vogt, Y. Hollenstein, L. Kaufmann, N. Cantoni, S. Ruosch-Girsberger, A. M. S. Müller, U. Schanz, T. Pabst, G. Stüssi, M. Weisser, J. Halter, J. Stelling, and A. Egli. Association of host factors with antibody response to seasonal influenza vaccination in allogeneic hematopoietic stem cell transplant (HSCT) patients. *The Journal of Infectious Diseases*, 08 2021.
- J. E. Linnik and A. Egli. Impact of host genetic polymorphisms on vaccine induced antibody response. *Human Vaccines & Immunotherapeutics*, 12(4):907–915, 2016.
- R. J. Little and D. B. Rubin. *Statistical analysis with missing data*, volume 793. John Wiley & Sons, 2019.
- X. Liu, A. A. O’Connell, and H. Koirala. Ordinal regression analysis: Predicting mathematics proficiency using the continuation ratio model. *Journal of Modern Applied Statistical Methods*, 10(2):11, 2011.
- Y.-J. Liu, J. Zhang, P. J. Lane, E. Y.-T. Chan, and I. C. MacLennan. Sites of specific B cell activation in primary and secondary responses to T cell-dependent and T cell-independent antigens. *European Journal of Immunology*, 21(12):2951–2962, 1991.
- Y.-J. Liu, C. Barthelemy, O. de Bouteiller, and J. Banchereau. The differences in survival and phenotype between centroblasts and centrocytes. In *In Vivo Immunology*, pages 213–218. Springer, 1994.
- P. Ljungman. Vaccination of immunocompromised patients. *Clinical Microbiology and Infection*, 18:93–99, 2012.
- P. Ljungman and G. Avetisyan. Influenza vaccination in hematopoietic SCT recipients. *Bone Marrow Transplantation*, 42(10):637–641, 2008.
- P. Ljungman, R. de la Camara, L. Perez-Bercoff, M. Abecasis, J. B. N. Campuzano, M. J. Cannata-Ortiz, C. Cordonnier, H. Einsele, M. Gonzalez-Vicent, I. Espigado, et al. Outcome of pandemic H1N1 infections in hematopoietic stem cell transplant recipients. *Haematologica*, 96(8):1231–1235, 2011.
- D. C. Macallan, D. L. Wallace, Y. Zhang, H. Ghattas, B. Asquith, C. de Lara, A. Worth, G. Panayiotakopoulos, G. E. Griffin, D. F. Tough, et al. B-cell kinetics in humans: rapid turnover of peripheral blood memory cells. *Blood*, 105(9):3633–3640, 2005.

- C. Machado, M. Cardoso, I. Da Rocha, L. Boas, F. Dullely, and C. Pannuti. The benefit of influenza vaccination after bone marrow transplantation. *Bone Marrow Transplantation*, 36(10):897–900, 2005.
- C. Mackall, T. Fry, R. Gress, K. Peggs, J. Storek, and A. Toubert. Background to hematopoietic cell transplantation, including post transplant immune recovery. *Bone Marrow Transplantation*, 44(8):457–462, 2009.
- F. Mackay and J. L. Browning. BAFF: a fundamental survival factor for B cells. *Nature Reviews Immunology*, 2(7):465–475, 2002.
- D. S. MacLean, J. D. Robertson, and M. Jay. Monitoring the retention of a protein antigen in complete Freund’s adjuvant, alum, and pluronic F-127 gel formulations by X-ray fluorescence. *Pharmaceutical development and technology*, 6(2):241–246, 2001.
- D. E. Mager and H. H. Kimko. *Systems Pharmacology and Pharmacodynamics*, volume 23. Springer, 2016.
- S. Mankarious, M. Lee, S. Fischer, K. Pyun, H. Ochs, V. Oxelius, and R. Wedgwood. The half-lives of IgG subclasses and specific antibodies in patients with primary immunodeficiency who are receiving intravenously administered immunoglobulin. *The Journal of Laboratory and Clinical Medicine*, 112(5):634–640, 1988.
- M. A. Mansournia, A. Geroldinger, S. Greenland, and G. Heinze. Separation in logistic regression: causes, consequences, and control. *American Journal of Epidemiology*, 187(4):864–870, 2018.
- O. Manuel, M. Pascual, K. Hoschler, S. Giulieri, D. Alves, K. Ellefsen, P.-A. Bart, J.-P. Venetz, T. Calandra, and M. Cavassini. Humoral response to the influenza A H1N1/09 monovalent AS03-adjuvanted vaccine in immunocompromised patients. *Clinical Infectious Diseases*, 52(2): 248–256, 2011.
- A. Martin and M. D. Scharff. AID and mismatch repair in antibody diversification. *Nature Reviews Immunology*, 2(8):605–614, 2002.
- I. Martínez-Baz, I. Casado, A. Navascués, J. Díaz-González, A. Aguinaga, L. Barrado, J. Delfrade, C. Ezpeleta, and J. Castilla. Effect of repeated vaccination with the same vaccine component against 2009 pandemic influenza A (H1N1) virus. *The Journal of Infectious Diseases*, 215(6): 847–855, 2017.
- P. McCullagh. Regression models for ordinal data. *Journal of the Royal Statistical Society: Series B (Methodological)*, 42(2):109–127, 1980.
- P. McCullagh. *Generalized linear models*. Routledge, 2018.
- L. Mesin, J. Ersching, and G. D. Victora. Germinal center B cell dynamics. *Immunity*, 45(3): 471–482, 2016.

- L. Mesin, A. Schiepers, J. Ersching, A. Barbulescu, C. B. Cavazzoni, A. Angelini, T. Okada, T. Kurosaki, and G. D. Victora. Restricted clonality and limited germinal center reentry characterize memory b cell reactivation by boosting. *Cell*, 180(1):92–106, 2020.
- M. Meyer-Hermann. Injection of antibodies against immunodominant epitopes tunes germinal centers to generate broadly neutralizing antibodies. *Cell Reports*, 29(5):1066–1073, 2019.
- M. Meyer-Hermann, E. Mohr, N. Pelletier, Y. Zhang, G. D. Victora, and K.-M. Toellner. A theory of germinal center B cell selection, division, and exit. *Cell Reports*, 2(1):162–174, 2012.
- M. E. Meyer-Hermann and P. K. Maini. Cutting edge: back to “one-way” germinal centers. *The Journal of Immunology*, 174(5):2489–2493, 2005.
- M. E. Meyer-Hermann, P. K. Maini, and D. Iber. An analysis of B cell selection mechanisms in germinal centers. *Mathematical medicine and biology: a journal of the IMA*, 23(3):255–277, 2006.
- M. S. Miller, T. J. Gardner, F. Krammer, L. C. Aguado, D. Tortorella, C. F. Basler, and P. Palese. Neutralizing antibodies against previously encountered influenza virus strains increase over time: a longitudinal analysis. *Science Translational Medicine*, 5(198):198ra107–198ra107, 2013.
- T. K. Ming, H. S. Goodman, and B. BROWN. Mathematical model for the process of aggregation in immune agglutination. *Nature*, 208(5005):84, 1965.
- B. Mohty, M. Bel, M. Vukicevic, M. Nagy, E. Levrat, S. Meier, S. Grillet, C. Combescure, L. Kaiser, Y. Chalandon, et al. Graft-versus-host disease is the major determinant of humoral responses to the AS03-adjuvanted influenza A/09/H1N1 vaccine in allogeneic hematopoietic stem cell transplant recipients. *Haematologica*, 96(6):896–904, 2011.
- M. Molari, K. Eyer, J. Baudry, S. Cocco, and R. Monasson. Quantitative modeling of the effect of antigen dosage on B-cell affinity distributions in maturing germinal centers. *bioRxiv*, 2020.
- P. A. Moore, O. Belvedere, A. Orr, K. Pieri, D. W. LaFleur, P. Feng, D. Soppet, M. Charters, R. Gentz, D. Parmelee, et al. BLYS: member of the tumor necrosis factor family and B lymphocyte stimulator. *Science*, 285(5425):260–263, 1999.
- I. Moran, A. Nguyen, W. H. Khoo, D. Butt, K. Bourne, C. Young, J. R. Hermes, M. Biro, G. Gracie, C. S. Ma, et al. Memory B cells are reactivated in subcapsular proliferative foci of lymph nodes. *Nature Communications*, 9(1):1–14, 2018.
- T. P. Morris, I. R. White, and M. J. Crowther. Using simulation studies to evaluate statistical methods. *Statistics in Medicine*, 38(11):2074–2102, 2019.
- S. Movassaghian and V. P. Torchilin. Long-circulating therapies for cancer treatment. In *Novel Approaches and Strategies for Biologics, Vaccines and Cancer Therapies*, pages 433–462. Elsevier, 2015.
- K. Murphy and C. Weaver. *Janeway’s immunobiology*. Garland Science, 2016.

- R. Murugan, L. Buchauer, G. Triller, C. Kreschel, G. Costa, G. P. Martí, K. Imkeller, C. E. Busse, S. Chakravarty, B. K. L. Sim, et al. Clonal selection drives protective memory B cell responses in controlled human malaria infection. *Science Immunology*, 3(20), 2018.
- G. J. Nabel and A. S. Fauci. Induction of unnatural immunity: prospects for a broadly protective universal influenza vaccine. *Nature Medicine*, 16(12):1389–1391, 2010.
- I. Nazi, J. G. Kelton, M. Larché, D. P. Snider, N. M. Heddle, M. A. Crowther, R. J. Cook, A. T. Tinmouth, J. Mangel, and D. M. Arnold. The effect of rituximab on vaccine responses in patients with immune thrombocytopenia. *Blood*, 122(11):1946–1953, 2013.
- G. Neumann and Y. Kawaoka. Predicting the next influenza pandemics. *The Journal of Infectious Diseases*, 219(Supplement_1):S14–S20, 2019.
- S. Ng, R. Nachbagauer, A. Balmaseda, D. Stadlbauer, S. Ojeda, M. Patel, A. Rajabhathor, R. Lopez, A. F. Guglia, N. Sanchez, et al. Novel correlates of protection against pandemic h1n1 influenza a virus infection. *Nature Medicine*, 25(6):962–967, 2019.
- W. G. Nichols, K. A. Guthrie, L. Corey, and M. Boeckh. Influenza infections after hematopoietic stem cell transplantation: risk factors, mortality, and the effect of antiviral therapy. *Clinical Infectious Diseases*, 39(9):1300–1306, 2004.
- J. Ogonek, M. Kralj Juric, S. Ghimire, P. R. Varanasi, E. Holler, H. Greinix, and E. Weissinger. Immune reconstitution after allogeneic hematopoietic stem cell transplantation. *Frontiers in Immunology*, 7:507, 2016.
- S. E. Ohmit, J. G. Petrie, R. T. Cross, E. Johnson, and A. S. Monto. Influenza hemagglutination-inhibition antibody titer as a correlate of vaccine-induced protection. *The Journal of Infectious Diseases*, 204(12):1879–1885, 2011.
- Y. Okuno, Y. Isegawa, F. Sasao, and S. Ueda. A common neutralizing epitope conserved between the hemagglutinins of influenza a virus h1 and h2 strains. *Journal of Virology*, 67(5):2552–2558, 1993.
- J. Olsson, J. Johansson, E. Honkala, B. Blomqvist, E. Kok, B. Weidung, H. Lövheim, and F. Elgh. Urea dilution of serum for reproducible anti-HSV1 IgG avidity index. *BMC Infectious Diseases*, 19(1):164, 2019.
- W. Olszewska, O. E. Obeid, and M. W. Steward. Protection against measles virus-induced encephalitis by anti-mimotope antibodies: the role of antibody affinity. *Virology*, 272(1):98–105, 2000.
- M. Oprea and A. S. Perelson. Somatic mutation leads to efficient affinity maturation when centrocytes recycle back to centroblasts. *The Journal of Immunology*, 158(11):5155–5162, 1997.
- M. T. Osterholm, N. S. Kelley, A. Sommer, and E. A. Belongia. Efficacy and effectiveness of influenza vaccines: a systematic review and meta-analysis. *The Lancet Infectious Diseases*, 12(1):36–44, 2012.

- J. J. Otterstrom, B. Brandenburg, M. H. Koldijk, J. Juraszek, C. Tang, S. Mashaghi, T. Kwaks, J. Goudsmit, R. Vogels, R. H. Friesen, et al. Relating influenza virus membrane fusion kinetics to stoichiometry of neutralizing antibodies at the single-particle level. *Proceedings of the National Academy of Sciences*, 111(48):E5143–E5148, 2014.
- J. Paget, P. Spreeuwenberg, V. Charu, R. J. Taylor, A. D. Iuliano, J. Bresee, L. Simonsen, C. Viboud, et al. Global mortality associated with seasonal influenza epidemics: New burden estimates and predictors from the GLaMOR Project. *Journal of Global Health*, 9(2), 2019.
- A. Palache, W. Beyer, G. Rimmelzwaan, A. Boon, A. Osterhaus, et al. Haemagglutination-inhibiting antibody to influenza virus. *Developments in Biologicals*, 115:63–73, 2003.
- I. Papa, D. Saliba, M. Ponzoni, S. Bustamante, P. F. Canete, P. Gonzalez-Figueroa, H. A. McNamara, S. Valvo, M. Grimbaldston, R. A. Sweet, et al. T_{FH}-derived dopamine accelerates productive synapses in germinal centres. *Nature*, 547(7663):318–323, 2017.
- K. A. Pape, D. M. Catron, A. A. Itano, and M. K. Jenkins. The humoral immune response is initiated in lymph nodes by B cells that acquire soluble antigen directly in the follicles. *Immunity*, 26(4):491–502, 2007.
- K. A. Pape, J. J. Taylor, R. W. Maul, P. J. Gearhart, and M. K. Jenkins. Different B cell populations mediate early and late memory during an endogenous immune response. *Science*, 331(6021):1203–1207, 2011.
- J. Passweg, U. Schanz, Y. Chalandon, T. Güngör, H. Baldomero, D. Heim, G. Nair, M. Medinger, S. Masouridi-Levrat, G. De Faveri, et al. High-resolution HLA matching in unrelated donor transplantation in Switzerland: differential impact of class I and class II mismatches may reflect selection of nonimmunogenic or weakly immunogenic DRB1/DQB1 disparities. *Bone Marrow Transplantation*, 50(9):1201–1205, 2015.
- K. Pauksen, A. Linde, V. Hammarström, J. Sjölin, J. Carneskog, G. Jonsson, G. Öberga, H. Engelman, and P. Ljungman. Granulocyte-macrophage colony-stimulating factor as immunomodulating factor together with influenza vaccination in stem cell transplant patients. *Clinical Infectious Diseases*, 30(2):342–348, 2000.
- C. Paules and K. Subbarao. Influenza, 2017.
- C. I. Paules and A. S. Fauci. Influenza vaccines: good, but we can do better. *The Journal of Infectious Diseases*, 219(Supplement_1):S1–S4, 2019.
- C. I. Paules, H. D. Marston, R. W. Eisinger, D. Baltimore, and A. S. Fauci. The pathway to a universal influenza vaccine. *Immunity*, 47(4):599–603, 2017.
- E. W. Petersdorf. Genetics of graft-versus-host disease: the major histocompatibility complex. *Blood Reviews*, 27(1):1–12, 2013.
- E. W. Petersdorf, M. Malkki, M. M. Horowitz, S. R. Spellman, M. D. Haagenon, and T. Wang. Mapping MHC haplotype effects in unrelated donor hematopoietic cell transplantation. *Blood*, 121(10):1896–1905, 2013.

- N. Pica, R. Hai, F. Krammer, T. T. Wang, J. Maamary, D. Eggink, G. S. Tan, J. C. Krause, T. Moran, C. R. Stein, et al. Hemagglutinin stalk antibodies elicited by the 2009 pandemic influenza virus as a mechanism for the extinction of seasonal H1N1 viruses. *Proceedings of the National Academy of Sciences*, 109(7):2573–2578, 2012.
- N. B. Pikor, U. Mörbe, M. Lütge, C. Gil-Cruz, C. Perez-Shibayama, M. Novkovic, H.-W. Cheng, C. Nombela-Arrieta, T. Nagasawa, M. A. Linterman, et al. Remodeling of light and dark zone follicular dendritic cells governs germinal center responses. *Nature Immunology*, pages 1–11, 2020.
- S. Plotkin, W. Orenstein, and P. Offit. *Vaccines 6th Edition*. Elsevier, 2012.
- F. P. Polack, S. J. Hoffman, G. Crujeiras, and D. E. Griffin. A role for nonprotective complement-fixing antibodies with low avidity for measles virus in atypical measles. *Nature Medicine*, 9(9): 1209–1213, 2003.
- P. Pountourios, L. E. Brown, D. O. White, and D. C. Jackson. The stoichiometry of binding between monoclonal antibody molecules and the hemagglutinin of influenza virus. *Virology*, 179 (2):768–776, 1990.
- B. Pulendran. Systems vaccinology: probing humanity’s diverse immune systems with vaccines. *Proceedings of the National Academy of Sciences*, 111(34):12300–12306, 2014.
- H. Qi, J. L. Cannons, F. Klauschen, P. L. Schwartzberg, and R. N. Germain. SAP-controlled T–B cell interactions underlie germinal centre formation. *Nature*, 455(7214):764–769, 2008.
- R Core Team. *R: A Language and Environment for Statistical Computing*. R Foundation for Statistical Computing, Vienna, Austria, 2019. URL <https://www.R-project.org/>.
- D. A. Randolph, G. Huang, C. J. Carruthers, L. E. Bromley, and D. D. Chaplin. The role of CCR7 in TH1 and TH2 cell localization and delivery of B cell help in vivo. *Science*, 286(5447):2159–2162, 1999.
- S. Riedel. Edward Jenner and the history of smallpox and vaccination. In *Baylor University Medical Center Proceedings*, volume 18, pages 21–25. Taylor & Francis, 2005.
- G. N. Rogers and B. L. D’Souza. Receptor binding properties of human and animal H1 influenza virus isolates. *Virology*, 173(1):317–322, 1989.
- D. Roll, J. Ammer, B. Holler, B. Salzberger, B. Schweiger, W. Jilg, R. Andreesen, M. Edinger, D. Wolff, and E. Holler. Vaccination against pandemic H1N1 (2009) in patients after allogeneic hematopoietic stem cell transplantation: a retrospective analysis. *Infection*, 40(2):153–161, 2012.
- R. Ruigrok, P. Andree, R. H. Van Huysduynen, and J. Mellema. Characterization of three highly purified influenza virus strains by electron microscopy. *Journal of General Virology*, 65(4): 799–802, 1984.

- A. Rundell, R. DeCarlo, H. HogenEsch, and P. Doerschuk. The Humoral Immune Response to Haemophilus influenzae Type b: a Mathematical Model Based on T-zone and Germinal Center B-cell Dynamics. *Journal of Theoretical Biology*, 194(3):341–381, 1998.
- A. Saltelli, S. Tarantola, F. Campolongo, and M. Ratto. *Sensitivity analysis in practice: a guide to assessing scientific models*, volume 1. Wiley Online Library, 2004.
- A. Saltelli, P. Annoni, I. Azzini, F. Campolongo, M. Ratto, and S. Tarantola. Variance based sensitivity analysis of model output. design and estimator for the total sensitivity index. *Computer Physics Communications*, 181(2):259–270, 2010.
- S. Sarantopoulos, K. E. Stevenson, H. T. Kim, N. S. Bhuiya, C. S. Cutler, R. J. Soiffer, J. H. Antin, and J. Ritz. High levels of B-cell activating factor in patients with active chronic graft-versus-host disease. *Clinical Cancer Research*, 13(20):6107–6114, 2007.
- S. Sarantopoulos, K. E. Stevenson, H. T. Kim, C. S. Cutler, N. S. Bhuiya, M. Schowalter, V. T. Ho, E. P. Alyea, J. Koreth, B. R. Blazar, et al. Altered B-cell homeostasis and excess BAFF in human chronic graft-versus-host disease. *Blood, The Journal of the American Society of Hematology*, 113(16):3865–3874, 2009.
- N. K. Sauter, M. D. Bednarski, B. A. Wurzburg, J. E. Hanson, G. M. Whitesides, J. J. Skehel, and D. C. Wiley. Hemagglutinins from two influenza virus variants bind to sialic acid derivatives with millimolar dissociation constants: a 500-MHz proton nuclear magnetic resonance study. *Biochemistry*, 28(21):8388–8396, 1989.
- N. K. Sauter, J. E. Hanson, G. D. Glick, J. H. Brown, R. L. Crowther, S. J. Park, J. J. Skehel, and D. C. Wiley. Binding of influenza virus hemagglutinin to analogs of its cell-surface receptor, sialic acid: analysis by proton nuclear magnetic resonance spectroscopy and X-ray crystallography. *Biochemistry*, 31(40):9609–9621, 1992.
- H. W. Schroeder and L. Cavacini. Structure and function of immunoglobulins. *Journal of Allergy and Clinical Immunology*, 125(2):S41–S52, 2010.
- M. G. Schuster, A. A. Cleveland, E. R. Dubberke, C. A. Kauffman, R. K. Avery, S. Husain, D. L. Paterson, F. P. Silveira, T. M. Chiller, K. Benedict, et al. Infections in hematopoietic cell transplant recipients: results from the organ transplant infection project, a multicenter, prospective, cohort study. In *Open Forum Infectious Diseases*, volume 4, page ofx050. Oxford University Press US, 2017.
- T. A. Schwickert, R. L. Lindquist, G. Shakhar, G. Livshits, D. Skokos, M. H. Kosco-Vilbois, M. L. Dustin, and M. C. Nussenzweig. In vivo imaging of germinal centres reveals a dynamic open structure. *Nature*, 446(7131):83–87, 2007.
- T. A. Schwickert, G. D. Victora, D. R. Fooksman, A. O. Kamphorst, M. R. Mugnier, A. D. Gitlin, M. L. Dustin, and M. C. Nussenzweig. A dynamic T cell-limited checkpoint regulates affinity-dependent B cell entry into the germinal center. *Journal of Experimental Medicine*, 208(6):1243–1252, 2011.

- S. C. Scott, M. S. Goldberg, and N. E. Mayo. Statistical assessment of ordinal outcomes in comparative studies. *Journal of Clinical Epidemiology*, 50(1):45–55, 1997.
- T. Sheahan, N. Imanaka, S. Marukian, M. Dorner, P. Liu, A. Ploss, and C. M. Rice. Interferon lambda alleles predict innate antiviral immune responses and hepatitis C virus permissiveness. *Cell Host & Microbe*, 15(2):190–202, 2014.
- M. Shlomchik, P. Watts, M. Weigert, and S. Litwin. Clone: a Monte-Carlo computer simulation of B cell clonal expansion, somatic mutation, and antigen-driven selection. In *Somatic Diversification of Immune Responses*, pages 173–197. Springer, 1998.
- M. J. Shlomchik and F. Weisel. Germinal center selection and the development of memory B and plasma cells. *Immunological Reviews*, 247(1):52–63, 2012.
- L. D. Shultz, M. A. Brehm, J. V. Garcia-Martinez, and D. L. Greiner. Humanized mice for immune system investigation: progress, promise and challenges. *Nature Reviews Immunology*, 12(11):786–798, 2012.
- C.-A. Siegrist. Vaccine immunology. *Vaccines*, 5(1):17–36, 2008.
- C.-A. Siegrist and R. Aspinall. B-cell responses to vaccination at the extremes of age. *Nature Reviews Immunology*, 9(3):185–194, 2009.
- J. J. Skehel and D. C. Wiley. Receptor binding and membrane fusion in virus entry: the influenza hemagglutinin. *Annual Review of Biochemistry*, 69(1):531–569, 2000.
- J. Smetana, R. Chlibek, J. Shaw, M. Splino, and R. Prymula. Influenza vaccination in the elderly. *Human Vaccines & Immunotherapeutics*, 14(3):540–549, 2018.
- W. Smith, C. H. Andrewes, P. P. Laidlaw, et al. A virus obtained from influenza patients. *Lancet*, pages 66–8, 1933.
- F. Spensieri, E. Borgogni, L. Zedda, M. Bardelli, F. Buricchi, G. Volpini, E. Fragapane, S. Tavarini, O. Finco, R. Rappuoli, et al. Human circulating influenza-CD4+ ICOS1+ IL-21+ T cells expand after vaccination, exert helper function, and predict antibody responses. *Proceedings of the National Academy of Sciences*, 110(35):14330–14335, 2013.
- Stan Development Team. RStan: the R interface to Stan, 2020a. URL <http://mc-stan.org/>. R package version 2.21.2.
- Stan Development Team. Stan Modeling Language Users Guide and Reference Manual 2.25, 2020b. URL <https://mc-stan.org>.
- J. Storek, M. Geddes, F. Khan, B. Huard, C. Helg, Y. Chalandon, J. Passweg, and E. Roosnek. Reconstitution of the immune system after hematopoietic stem cell transplantation in humans. In *Seminars in Immunopathology*, volume 30, page 425. Springer, 2008.

- V. Suppiah, M. Moldovan, G. Ahlenstiel, T. Berg, M. Weltman, M. L. Abate, M. Bassendine, U. Spengler, G. J. Dore, E. Powell, et al. IL28B is associated with response to chronic hepatitis C interferon- α and ribavirin therapy. *Nature Genetics*, 41(10):1100, 2009.
- M. Syedbasha and A. Egli. Interferon lambda: modulating immunity in infectious diseases. *Frontiers in Immunology*, 8:119, 2017.
- M. Syedbasha, F. Bonfiglio, J. Linnik, C. Stuehler, D. Wüthrich, and A. Egli. Interferon- λ Enhances the Differentiation of Naive B Cells into Plasmablasts via the mTORC1 Pathway. *Cell Reports*, 33(1):108211, 2020.
- D. K. Takemoto, J. J. Skehel, and D. C. Wiley. A surface plasmon resonance assay for the binding of influenza virus hemagglutinin to its sialic acid receptor. *Virology*, 217(2):452–458, 1996.
- H. H. Tam, M. B. Melo, M. Kang, J. M. Pelet, V. M. Ruda, M. H. Foley, J. K. Hu, S. Kumari, J. Crampton, A. D. Baldeon, et al. Sustained antigen availability during germinal center initiation enhances antibody responses to vaccination. *Proceedings of the National Academy of Sciences*, 113(43):E6639–E6648, 2016.
- Y. Tanaka, N. Nishida, M. Sugiyama, M. Kurosaki, K. Matsuura, N. Sakamoto, M. Nakagawa, M. Korenaga, K. Hino, S. Hige, et al. Genome-wide association of IL28B with response to pegylated interferon- α and ribavirin therapy for chronic hepatitis C. *Nature Genetics*, 41(10):1105, 2009.
- S. G. Tangye and P. D. Hodgkin. Divide and conquer: the importance of cell division in regulating B-cell responses. *Immunology*, 112(4):509–520, 2004.
- L. Tao and T. A. Reese. Making mouse models that reflect human immune responses. *Trends in Immunology*, 38(3):181–193, 2017.
- J. M. Tas, L. Mesin, G. Pasqual, S. Targ, J. T. Jacobsen, Y. M. Mano, C. S. Chen, J.-C. Weill, C.-A. Reynaud, E. P. Browne, et al. Visualizing antibody affinity maturation in germinal centers. *Science*, 351(6277):1048–1054, 2016.
- H. Taylor, S. Armstrong, and N. Dimmock. Quantitative relationships between an influenza virus and neutralizing antibody. *Virology*, 159(2):288–298, 1987.
- J. Tew and T. Mandel. Prolonged antigen half-life in the lymphoid follicles of specifically immunized mice. *Immunology*, 37(1):69, 1979.
- B. S. Thomas, M. A. Joyce, A. Levin, and D. L. J. Tyrrell. Validation of TaqMan® SNP genotyping specificity for rs12979860 of IL-28B: Modeling primer specificity in vitro. *Disease Markers*, 203:39–47, 2014.
- D. L. Thomas, C. L. Thio, M. P. Martin, Y. Qi, D. Ge, C. O’huigin, J. Kidd, K. Kidd, S. I. Khakoo, G. Alexander, et al. Genetic variation in IL28B and spontaneous clearance of hepatitis C virus. *Nature*, 461(7265):798–801, 2009.

- M. G. Thompson, A. Naleway, A. M. Fry, S. Ball, S. M. Spencer, S. Reynolds, S. Bozeman, M. Levine, J. M. Katz, and M. Gaglani. Effects of repeated annual inactivated influenza vaccination among healthcare personnel on serum hemagglutinin inhibition antibody response to A/Perth/16/2009 (H3N2)-like virus during 2010-11. *Vaccine*, 34(7):981–988, 2016.
- J.-M. Tiercy. How to select the best available related or unrelated donor of hematopoietic stem cells? *Haematologica*, 101(6):680–687, 2016.
- S. Tong, X. Zhu, Y. Li, M. Shi, J. Zhang, M. Bourgeois, H. Yang, X. Chen, S. Recuenco, J. Gomez, et al. New world bats harbor diverse influenza A viruses. *PLoS Pathogens*, 9(10):e1003657, 2013.
- J. S. Tregoning, R. F. Russell, and E. Kinnear. Adjuvanted influenza vaccines. *Human Vaccines & Immunotherapeutics*, 14(3):550–564, 2018.
- C. M. Trombetta, E. J. Remarque, D. Mortier, and E. Montomoli. Comparison of hemagglutination inhibition, single radial hemolysis, virus neutralization assays, and ELISA to detect antibody levels against seasonal influenza viruses. *Influenza and Other Respiratory Viruses*, 12(6):675–686, 2018.
- J. S. Turner, F. Ke, and I. L. Grigorova. B cell receptor crosslinking augments germinal center B cell selection when T cell help is limiting. *Cell Reports*, 25(6):1395–1403, 2018.
- J. S. Turner, J. Q. Zhou, J. Han, A. J. Schmitz, A. A. Rizk, W. B. Alsoussi, T. Lei, M. Amor, K. M. McIntire, P. Meade, et al. Human germinal centres engage memory and naive B cells after influenza vaccination. *Nature*, 586(7827):127–132, 2020.
- G. Tutz. Sequential models in categorical regression. *Computational Statistics & Data Analysis*, 11(3):275–295, 1991.
- D. Tyrrell and R. Valentine. The assay of influenza virus particles by haemagglutination and electron microscopy. *Microbiology*, 16(3):668–675, 1957.
- P. A. Underwood. Problems and pitfalls with measurement of antibody affinity using solid phase binding in the ELISA. *Journal of Immunological Methods*, 164(1):119–130, 1993.
- R. Valiathan, K. Deeb, M. Diamante, M. Ashman, N. Sachdeva, and D. Asthana. Reference ranges of lymphocyte subsets in healthy adults and adolescents with special mention of T cell maturation subsets in adults of South Florida. *Immunobiology*, 219(7):487–496, 2014.
- S. van Assen, A. Holvast, C. A. Benne, M. D. Posthumus, M. A. van Leeuwen, A. E. Voskuyl, M. Blom, A. P. Risselada, A. de Haan, J. Westra, et al. Humoral responses after influenza vaccination are severely reduced in patients with rheumatoid arthritis treated with rituximab. *Arthritis & Rheumatism: Official Journal of the American College of Rheumatology*, 62(1):75–81, 2010.
- A. Vehtari, A. Gelman, D. Simpson, B. Carpenter, P.-C. Bürkner, et al. Rank-normalization, folding, and localization: An improved \hat{R} for assessing convergence of MCMC. *Bayesian Analysis*, 2020.

- G. D. Victora and M. C. Nussenzweig. Germinal centers. *Annual review of immunology*, 30: 429–457, 2012.
- G. D. Victora and P. C. Wilson. Germinal center selection and the antibody response to influenza. *Cell*, 163(3):545–548, 2015.
- G. D. Victora, T. A. Schwickert, D. R. Fooksman, A. O. Kamphorst, M. Meyer-Hermann, M. L. Dustin, and M. C. Nussenzweig. Germinal center dynamics revealed by multiphoton microscopy with a photoactivatable fluorescent reporter. *Cell*, 143(4):592–605, 2010.
- M. Von Smoluchowski. Mathematical theory of the kinetics of the coagulation of colloidal solutions. *Z. Phys. Chem*, 92(129):129–68, 1917.
- A. Wack, E. Terczyńska-Dyla, and R. Hartmann. Guarding the frontiers: the biology of type III interferons. *Nature Immunology*, 16(8):802–809, 2015.
- S. Wang. Optimal sequential immunization can focus antibody responses against diversity loss and distraction. *PLOS Computational Biology*, 13(1):e1005336, 2017.
- S. Wang, J. Mata-Fink, B. Kriegsman, M. Hanson, D. J. Irvine, H. N. Eisen, D. R. Burton, K. D. Wittrup, M. Kardar, and A. K. Chakraborty. Manipulating the selection forces during affinity maturation to generate cross-reactive HIV antibodies. *Cell*, 160(4):785–797, 2015.
- R. Webby. Understanding immune responses to the influenza vaccine. *Nature Medicine*, 22(12): 1387–1388, 2016.
- C.-J. Wei, J. C. Boyington, P. M. McTamney, W.-P. Kong, M. B. Pearce, L. Xu, H. Andersen, S. Rao, T. M. Tumpey, Z.-Y. Yang, et al. Induction of broadly neutralizing h1n1 influenza antibodies by vaccination. *Science*, 329(5995):1060–1064, 2010.
- E. G. Weinhold and J. R. Knowles. Design and evaluation of a tightly binding fluorescent ligand for influenza A hemagglutinin. *Journal of the American Chemical Society*, 114(24):9270–9275, 1992.
- WHO. WHO manual on animal influenza diagnosis and surveillance. 2002.
- J. A. Williams, L. Gui, N. Hom, A. Mileant, and K. K. Lee. Dissection of epitope-specific mechanisms of neutralization of influenza virus by intact IgG and Fab fragments. *Journal of Virology*, 92(6):e02006–17, 2018.
- K. M. Williams and R. E. Gress. Immune Reconstitution and Implications for Immunotherapy Following Hematopoietic Stem Cell Transplantation. In *Allogeneic stem cell transplantation*, pages 545–564. Springer, 2010.
- I. A. Wilson, J. J. Skehel, and D. Wiley. Structure of the haemagglutinin membrane glycoprotein of influenza virus at 3 Å resolution. *Nature*, 289(5796):366–373, 1981.

- S. L. Wooden and W. C. Koff. The Human Vaccines Project: Towards a comprehensive understanding of the human immune response to immunization. *Human Vaccines & Immunotherapeutics*, 14(9):2214–2216, 2018.
- M. C. Woodruff, E. H. Kim, W. Luo, and B. Pulendran. B cell competition for restricted T cell help suppresses rare-epitope responses. *Cell Reports*, 25(2):321–327, 2018.
- A. Woolfrey, J. P. Klein, M. Haagensohn, S. Spellman, E. Petersdorf, M. Oudshoorn, J. Gajewski, G. A. Hale, J. Horan, M. Battiwalla, et al. HLA-C antigen mismatch is associated with worse outcome in unrelated donor peripheral blood stem cell transplantation. *Biology of Blood and Marrow Transplantation*, 17(6):885–892, 2011.
- J. Wrammert, D. Koutsonanos, G.-M. Li, S. Edupuganti, J. Sui, M. Morrissey, M. McCausland, I. Skountzou, M. Hornig, W. I. Lipkin, et al. Broadly cross-reactive antibodies dominate the human B cell response against 2009 pandemic H1N1 influenza virus infection. *Journal of Experimental Medicine*, 208(1):181–193, 2011.
- M. Yan, S. A. Marsters, I. S. Grewal, H. Wang, A. Ashkenazi, and V. M. Dixit. Identification of a receptor for BLYS demonstrates a crucial role in humoral immunity. *Nature Immunology*, 1(1):37–41, 2000.
- L. Ye, A. Ohnemus, L. C. Ong, H. H. Gad, R. Hartmann, N. Lycke, and P. Staeheli. Type I and type III interferons differ in their adjuvant activities for influenza vaccines. *Journal of Virology*, 93(23), 2019.
- T. W. Yee et al. The VGAM package for categorical data analysis. *Journal of Statistical Software*, 32(10):1–34, 2010.
- C.-H. Yeh, T. Nojima, M. Kuraoka, and G. Kelsoe. Germinal center entry not selection of B cells is controlled by peptide-MHCII complex density. *Nature Communications*, 9(1):1–11, 2018.
- M. J. Yiengst and N. W. Shock. Blood and plasma volume in adult males. *Journal of Applied Physiology*, 17(2):195–198, 1962.
- Y. Zhang, M. Meyer-Hermann, L. A. George, M. T. Figge, M. Khan, M. Goodall, S. P. Young, A. Reynolds, F. Falciani, A. Waisman, et al. Germinal center B cells govern their own fate via antibody feedback. *Journal of Experimental Medicine*, 210(3):457–464, 2013.
- X. Zhou and J. P. Reiter. A note on Bayesian inference after multiple imputation. *The American Statistician*, 64(2):159–163, 2010.
- G. V. Zuccarino-Catania, S. Sadanand, F. J. Weisel, M. M. Tomayko, H. Meng, S. H. Kleinstein, K. L. Good-Jacobson, and M. J. Shlomchik. CD80 and PD-L2 define functionally distinct memory B cell subsets that are independent of antibody isotype. *Nature Immunology*, 15(7):631–637, 2014.